UNIVERSITI TEKNOLOGI MARA

DEVELOPMENT AND MECHANICAL EVALUATION OF INTERLOCKING BLOCKS INCOR – PORATING EGGSHELL POWDER AND RECYCLED CONCRETE AGGREGATE

NUR SYAHIRAH BINTI OTHMAN

MSc

February 2026

UNIVERSITI TEKNOLOGI MARA

DEVELOPMENT AND MECHANICAL EVALUATION OF INTERLOCKING BLOCKS INCOR – PORATING EGGSHELL POWDER AND RECYCLED CONCRETE AGGREGATE

NUR SYAHIRAH BINTI OTHMAN

Thesis submitted in fulfilment
of the requirements for the degree of
Master of Science
(Civil Engineering)

Faculty of Civil Engineering

February 2026

CONFIRMATION BY PANEL OF EXAMINERS

I certify that a Panel of Examiners has met on 21 October 2025 to conduct the final examination of Nur Syahirah Binti Othman on her Masters of Science thesis entitled "Development and Mechanical Evaluation of Interlocking Blocks Incorporating Eggshell Powder and Recycled Concrete Aggregate" in accordance with Universiti Teknologi MARA Act 1976 (Akta 173). The Panel of Examiner recommends that the student be awarded the relevant degree. The Panel of Examiners was as follows:

Tey Li Sian, PhD
Associate Professor
Faculty of Civil Engineering
Universiti Teknologi MARA
(Chairperson)

Yee Hooi Min, PhD
Professor
Faculty of Civil Engineering
Universiti Teknologi MARA
(Internal Examiner)

Noor Sheena Herayani Harith, PhD
Associate Professor
Faculty of Engineering
Universiti Malaysia Sabah
(External Examiner)

PROFESSOR DR HJH ZURAEDA IBRAHIM
Dean
Institute of Postgraduates Studies
Universiti Teknologi MARA

Date: 27 February 2026

AUTHOR'S DECLARATION

I declare that the work in this thesis was carried out in accordance with the regulations of Universiti Teknologi MARA. It is original and is the results of my own work, unless otherwise indicated or acknowledged as referenced work. This thesis has not been submitted to any other academic institution or non-academic institution for any degree or qualification.

I, hereby, acknowledge that I have been supplied with the Academic Rules and Regulations for Postgraduate, Universiti Teknologi MARA, regulating the conduct of my study and research.

Name of Student	:	Nur Syahirah Binti Othman
Student ID. No.	:	2023267672
Programme	:	Master of Science (Civil Engineering) – CEEC750
Faculty	:	Faculty of Civil Engineering
Thesis Title	:	Development and Mechanical Evaluation of Interlocking Block Incorporating Eggshell Powder and Recycled Concrete Aggregate
Signature of Student	:	…….
Date	:	27 February 2026

ABSTRACT

In response to the growing environmental concerns surrounding the depletion of natural resources and the accumulation of construction waste. The increasing demand for sustainable construction materials has driven research into alternative binders and aggregates, such as Eggshell Powder (ESP) and Recycled Concrete Aggregates (RCA), to minimize environmental impact and reduce reliance on natural resources. There is insufficient research on the combined effect of ESP and RCA in interlocking blocks. Although eggshell powder and recycled concrete aggregates show potential impact individually, their combined effect on the reliability of interlocking blocks remains underexplored. This research addresses the challenge of designing eco-friendly masonry units by pursuing three main objectives. First, it aims to determine the salient mix design incorporating ESP and RCA that balances strength and durability requirements. Second, it involves the design and fabrication of interlocking blocks using the selected mixtures, ensuring structural performance and practical applicability. Third, the research evaluates the predictive capability of an Artificial Neural Network (ANN) model trained on experimental data from the first two objectives, enabling accurate estimation of mechanical properties and generalization beyond the tested samples. The research incorporated Ordinary Portland Cement (OPC) and Natural Aggregate (NA) as the main constituents, while ESP and RCA served as sustainable substitutes, together with Silica Fume (SF) and a superplasticiser in a 1:4 mortar mix (w/r = 0.65). Cube and prism specimens were prepared to identify the best mix proportions before applying them to interlocking blocks cured for 3, 7, 28, and 56 days. Three block configurations SIB, SICIB, and DTIIB were designed and assessed. Experimental procedures covered particle size distribution, flowability, water absorption, compression, and flexural performance, with the final blocks measuring 280 mm × 125 mm × 100 mm and cured for 7, 14, and 28 days. Based JKR Standards, compressive strength (28 days) is 34.69 MPa (Control), and flexural strength (28 days) of SIB is 4.623 N/mm^2 (5EPRCA0), and 5.162 N/mm^2 (5EPRCA30) were exceed minimum required strength as reliable baseline. Results of compression strength of cubes, flexural strength of prisms, and flexural strength of interlocking blocks were used to evaluate the experimental results by using ANN. ANN in MATLAB are used to evaluate experimental data of flexural strength, providing a cost-effective alternative to physical testing that potentially achieved the third objective of evaluating the experiment results. This approach accelerates the evaluation process and supports large-scale implementation. The 5EPERCA30 mix yielded the best mechanical performance in sustainable interlocking blocks, validated by ANN (R = 0.99701). The SICIB design proved structurally viable, confirming the potential of eggshell powder and recycled aggregates in eco-friendly construction. It promotes green building practices, contributing to sustainable construction and responsible resource management, paving the way for more environmentally friendly infrastructure development.

ACKNOWLEDGEMENT

I would like to extend my deepest appreciation to all individuals and institutions whose support made this research possible. Foremost, I am profoundly grateful to my supervisor, Dr. Soffian Noor Mat Saliah, for his unwavering guidance, insightful expertise, and exceptional patience throughout the course of this study. His mentorship was instrumental in shaping the direction and clarity of this research.

I also wish to express my sincere thanks to my co-supervisor, Dr. Masyitah Md Nujid, for her invaluable assistance in navigating the complexities of the Artificial Neural Network (ANN) analysis. Her technical support and thoughtful feedback were critical to the success of this work. My heartfelt gratitude goes to the research team led by Assoc. Prof. Dr. Noorsuhada Md Nor, whose steadfast support, constructive insights, and generous patience have been a source of strength throughout this academic journey.

I am also thankful to Universiti Teknologi MARA, Cawangan Pulau Pinang, for providing the necessary resources and facilities that enabled the completion of this study. Special appreciation is extended to the laboratory team for their consistent assistance during extensive testing and data collection phases. To my family and friends, thank you for your unwavering encouragement and emotional support. Your belief in me sustained my motivation during the most challenging moments of this journey.

Finally, I acknowledge the pioneering researchers in sustainable construction whose foundational work inspired and informed this study. It is my hope that this research contributes meaningfully to the advancement of environmentally responsible construction practices. Above all, I am grateful for the personal resilience and dedication that carried me through this process. This journey has been a testament to perseverance, and I am proud to have remained committed to its completion.

TABLE OF CONTENTS

LIST OF TABLES

LIST OF FIGURES

LIST OF SYMBOLS

Symbols

A	Loaded area (mm^2 or m^2)
b	Width of the specimen (mm)
CO_2	Carbon dioxide
$CaCO_3$	Calcium carbonate
CaO	Calcium oxide
d	Depth (height) of the specimen (mm)
D	Final spread diameter after flow table test
D_o	Mold base diameter
f_c	Compressive strength (MPa or N/mm^2)
f_r	Flexural strength (MPa or N/mm^2)
L	Span length (mm)
n	Number of observations
P	Maximum load (N or kN)
Wd	Initial dry weight of the material (in grams or kilograms)
Ww	Weight of the material after saturation (in grams or kilograms)
y_i	Actual (target) value for observation i
$\hat{y}_i$	Predicted value for observation i

LIST OF ABBREVIATIONS

Abbreviations

ANN	Artificial Neutral Network
CDW	Construction and Demolition Waste
DTIIB	Dual Tongue Inclined Interlocking Block
ESP	Eggshell Powder
ESA	Eggshell Ash
FA	Fly Ash
IB	Interlocking Block
MSE	Mean Squared Error
NA	Natural Fine Aggregates – Sand
OPC	Ordinary Portland Cement
R^2	Coefficient of Determination
RCA	Recycled Concrete Aggregate
RHA	Rice Husk Ash
SIB	Solid Interlocking Block
SICIB	Single Inclined Connection Interlocking Block
SF	Silica Fume
SCM	Supplementary Cementitious Materials

CHAPTER 1
INTRODUCTION

1.1 Introduction

Over the past few years, there has been an upsurge in the need by countries to find viable waste recycling mechanisms, whereby Ordinary Portland Cement (OPC) has proven to be an important but costly and environmental intensive material in the manufacture of concrete. The cement sector is the second-largest industrial carbon dioxide (CO2) emitter in the world; hence, there is need to partially replace the materials used to manufacture high-performance concrete. Utilization of Ordinary Portland Cement (OPC) with other materials such as Fly Ash (FA), Rice Husk Ash (RHA), Bottom Ash (BA) and Eggshell Powder (ESP) can improve mortar and concrete density and uniformity without compromising workability. It is interesting to note that eggshells are also a serious waste source that estimated at approximately 8,400 tonnes each year (Young et al., 2022; Pachideh et al., 2020). When combined with other additives such as SF, ESP is a more sustainable alternative to OPC that increases the compressive strength of the concrete mix and decreases porosity. The construction industry's push for innovative and efficient solutions has encouraged the integration of ESP and other sustainable materials into interlocking concrete block applications. This shift reflects a growing commitment to environmental stewardship and social responsibility, supported by the blocks' versatility, reliability, and cost-effectiveness.

Rising shortage of natural sand and the high prices of disposing solid waste has encouraged the construction sector to find long-term solutions to use concrete production. Utilization of RCA can be considered one of such working solutions since it involves recreating the previously left-over construction materials and demolished concrete structures in a process that can be used as an aggregate. It not only enhances environmental issues through disposal fewer waste in landfills, but it preserves the natural resources thus meeting the global trend to implement sustainable buildings. Currently, there is a lot of creditability has been given to the use of RCA in concrete mixtures, especially in the manufacturing of what has come to be known as Interlocking Blocks (IB) and is used extensively in new and existing construction projects. In

Malaysia, interlocking block systems have been actively implemented in various construction projects, particularly in affordable housing and sustainable development initiatives. Universiti Teknologi Malaysia introduced the Interlocking Hollow Block System (IHBS), which has been applied in low-cost housing to reduce construction time and labor dependency. Proven Engineering Block Sdn Bhd's interlocking brick system has also seen widespread use in residential and infrastructure projects, with validation from CIDB Malaysia for its structural performance and innovation. Universiti Malaysia Pahang (UMP) conducted a case study on single-storey house construction using interlocking blocks, demonstrating their cost-effectiveness and practicality for budget-conscious housing. These implementations reflect Malaysia's growing commitment to modular, eco-friendly, and efficient construction technologies. According to Awoyera et al. (2021), concrete composed of alternative material, including RCA, can achieve mechanical performances equal to those made using conventional aggregates. This adds weight to the possibility of RCA as a viable substitute to coming up with reliable and durable building materials.

Nonetheless, implementing RCA also poses some obstacles that have to be overcome so that it works effectively. There is a difference in density between recycled and natural aggregates because residual cement paste of the original concrete is likely to be present in recycled aggregates; this renders them less dense and more porous than aggregates. These properties may cause the alkali-silica reaction, the effect on the long-term concrete strength of structures (Hoai-Bao et al., 2020). To counter these challenges, continuous studies have been done to improve the optimization of proportioning RCA in the concrete mix and the optional additional treatment or additives that will improve the characteristics of recycled aggregates.

The determination of the flexural strength of IB manufactured using partial replacement of natural sand with RCA is important to understand the applicability of both in the structural element. Other methods such as three-point bending tests are used where sampling pieces are placed on the loading at the centre of the sampling whilst being held at the ends until it breaks. The tests supply vital information regarding the capacity of material to resist bending bars, which is especially significant in case of load bearing wall panels structures.

In addition, the experimental results are checked and supported using MATLAB's Artificial Neural Network (ANN). MATLAB stands for Matrix Laboratory and is a programming language used by many researchers for doing calculations, analysing data, making graphs, and building algorithms. Created by a company called MathWorks, MATLAB has many useful tools for modelling, simulation, and scientific studies. MATLAB provides a comprehensive environment with powerful built-in functions and toolboxes specifically designed for developing, training, and validating neural networks (Chapra, 2008). Its intuitive graphical interface and extensive documentation simplify the process of designing complex network architectures and experimenting with different configurations (Wang et al., 2024). Additionally, the measured experiment and predicted values can be integrated to enhance the accuracy of key parameter validation (Guo et al., 2022).

The primary objective of this study is to determine the flexural strength of interlocking blocks with partial substitution of OPC by ESP and fine aggregates by RCA under three-point loading conditions, confirmed by ANN verification. Achieving positive results will reinforce the effectiveness of using recycled materials in green building practices, promoting sustainable resource management and encouraging wider adoption of eco-friendly materials in the construction industry.

1.2 Research Background

According to the Department of Statistics Malaysia, the country's population was estimated at 33.4 million in 2023, reflecting an increase from 32.7 million in 2022. This population growth will intensify the demand for housing, putting pressure on the government to meet the residential needs of society. To keep up with this demand, the adoption of prefabricated construction methods must accelerate in line with population growth (OpenDOSM, 2023), Department of Statistics Malaysia that total population is 34.1 million with 2% of population growth of Malaysia.

Global aggregate demand is also on the rise, with the most recent forecasts estimating it at 3.8 tonnes per capita (Chandru et al., 2023). This demand places significant strain on the planet's resources, as construction projects continue to deplete them at an unsustainable rate. The need for concrete is growing rapidly, driven by the expanding economies of both developed and developing nations. However, not all

countries have easy access to natural resources like sand, which is in high demand for new construction. As a result, the supply of natural aggregates is dwindling, creating long-term challenges for the industry.

Additionally, the disposal of Construction and Demolition Waste (CDW) has become a significant problem (Sanjay et al., 2022). As nations strive for development, resource consumption is rising, which is a major concern in today's world (Potentiallysam et al., 2022). According to Statista Market Insights, egg production in Malaysia is projected to increase from 145.10 million kilograms in 2018 to 205.60 million kilograms by 2026. Alongside this, food waste and construction demolition waste are also increasing, driven by the high demand for these products. This growing demand highlights the urgent need for sustainable construction practices that can balance the needs of a growing population with the preservation of our natural resources.

1.3 Problem Statement

The rapid increase in eggshell consumption (Statista Market Insight, 2023), combined with the continuous growth of concrete production, has resulted in uncontrolled waste generation that poses significant environmental risks (Our World in Data, 2024). Economic expansion has accelerated solid waste accumulation, much of which is traditionally disposed of in landfills (Prodhan et al., 2024). This situation has triggered a global reassessment of recycling technologies, driven by limited landfill capacity, industrial growth, and stricter environmental regulations. In response to these challenges, eggshells composed of approximately 95% calcium carbonate, share chemical similarity with limestone used in cement production, making them a sustainable substitute that reduces reliance on non-renewable raw materials (Gowsika et al., 2024; Muthusamy et al., 2023).

In the construction sector, aggregate production nearly doubled between 2007 and 2014, reaching 40 billion tonnes (Vivian et al., 2018). This alarming growth underscores the urgent need for sustainable waste management and recycling practices. The depletion of natural resources further highlights the importance of reusing construction and demolition wastes, including Recycled Concrete Aggregates (RCA), in civil engineering applications.

Although RCA can be incorporated into interlocking blocks to support sustainable infrastructure, conventional solid blocks present several limitations. They are heavy, difficult to modify, and pose challenges for utility installations. Their weight complicates transportation and handling, while also exerting additional pressure on supporting structures. Furthermore, solid blocks often lack adequate ventilation, making them unsuitable for certain applications. These shortcomings emphasize the necessity of redesigning interlocking blocks to be lighter, more adaptable, and more practical.

To address these challenges, the present study proposes the development of innovative interlocking bricks that integrate sustainable materials such as eggshell powder. This approach not only reduces the environmental burden of eggshell waste but also enhances the sustainability of construction materials by partially replacing cement with a renewable, calcium-rich alternative.

1.4 Research Objectives

The objectives of this research:

a) To determine the salient proportions of eggshell powder and recycled concrete aggregates for the production of sustainable products.

b) To analyse the flexural performance characteristics of the interlocking block incorporating eggshell powder and recycled concrete aggregates in various forms.

c) To evaluate the results of experimental testing by using Artificial Neural Network (ANN) by MATLAB.

1.5 Research Scope

The scope of this study is organized into three main methodological phases to fulfil the research objectives. The first phase was to be achieved first objective that focuses on optimizing the proportions of sustainable materials in mortar mixtures. Materials used include Ordinary Portland Cement (OPC), Eggshell Powder (ESP), Silica Fume (SF), Natural Aggregates (NA), Recycled Coarse Aggregates (RCA), superplasticizer (Sika ViscoCrete-2192), and water. Experimental samples were

prepared in the form of cubes (50 mm x 50 mm x 50 mm), and prisms (160 mm x 40 mm x 40 mm). These samples were used for knowing the strength of the trial materials mixture percentage. The main materials to observed in this study were the waste materials replacement which are ESP and RCA. The ESP has 3 different percentages which are 5%, 10% and 15%, meanwhile RCA had consistency percentage replacement which is 30%. Considering the curing ages of the samples at 3, 7, 28, and 56 days, there are three samples for each curing age and seven different compositions, resulting in a total of 168 samples.

A series of standardized tests were conducted to evaluate the physical and mechanical properties of the mixtures, including particle size distribution (ASTM C430 for cement and ASTM C144-18 for sand), flowability of fresh mortar (ASTM C1437), water absorption (ASTM C642), compressive strength (ASTM C109), and flexural strength (ASTM C78). These tests provided essential data for assessing the performance of each mixture, with particular emphasis on the effects of replacement materials on strength and workability.

The second phase (objective 2) involves the design and fabrication of Interlocking Blocks (IBs) using the salient of 3 mortar mixtures. Three distinct IB configurations were proposed: Solid Interlocking Block (SIB), Single Inclined Connection Interlocking Block (SICIB), and Dual Tongue Inclined Interlocking Block (DTIIB). Each IB with dimensions of 280 mm x 125 mm x 100 mm (length x width x height). The samples underwent curing at 7, 14, and 28 days, with three samples for each curing age and three different compositions, totaling 81 samples. The testing was flexural testing which is three-point bending test (ASTM C78) and visual crack pattern analysis to investigate load distribution and structural behaviour under applied stress.

The integration of Eggshell Powder (ESP) and Recycled Concrete Aggregates (RCA) in mortar and interlocking block production directly advances several Sustainable Development Goals (SDGs) through measurable outcomes. By partially replacing cement with ESP, which contains ~95% calcium carbonate, the study reduces reliance on virgin limestone and lowers CO_2 emissions from cement manufacturing, contributing to SDG 13 (Climate Action). The consistent 30% RCA replacement minimizes quarrying activities and landfill disposal, aligning with SDG 12 (Responsible Consumption and Production) by promoting recycling and circular economy practices.

The design and testing of innovative interlocking blocks (SIB, SICIB, DTIIB) enhance structural efficiency, adaptability, and affordability, supporting SDG 11 (Sustainable Cities and Communities). Furthermore, the application of waste materials in interlocking block fulfilling SDG 9 (Industry, Innovation, and Infrastructure) by fostering sustainable industrialization and resilient infrastructure development.

In the final phase, the phase to achieved objective 3 was data collected from the flexural testing of cubes, prisms, and IBs. Three mixtures; OPCNA, and selected proportions from the EPRCA0 and EPRCA30 series were evaluated using Artificial Neural Network (ANN) in MATLAB. The Neural Network Fitting tool (nftool) was employed, utilizing the Levenberg–Marquardt algorithm (trainlm) for training. The ANN generated outputs were compared with experimental results through graphical analysis, confirming the reliability and predictive accuracy of the computational model.

1.6 Research Significance

This study aims to reduce construction waste by repurposing it into other materials, contributing to environmental protection and minimizing pollution. The transformation of construction and demolition waste into RCA is facilitated by widely available and cost-effective mechanical crushing equipment (Vivian et al., 2018). Both developed and developing nations can utilize this approach to recycle demolition waste into aggregates. The importance of this study lies in its potential to convert waste materials into valuable construction resources. Incorporating RCA into mortar helps reduce landfill waste while promoting sustainable construction practices. Additionally, using ESP and SF as partial OPC replacements enhances the mechanical properties of mortar and provides an eco-friendly solution for managing agricultural and industrial byproducts.

The expectation to reduce eggshell and concrete waste through their integration into mortar and interlocking block production highlights the environmental and economic benefits of sustainable material innovation. Rather than limiting eggshells to fertilizer use, this research demonstrates their potential as a cement substitute, enhancing environmental quality, promoting knowledge transfer, and contributing to national economic growth. By the action, it is indirect supporting SDG 13 (Climate Action). Similarly, the replacement of natural aggregates with RCA minimizes

quarrying activities and landfill disposal, advancing SDG 12 (Responsible Consumption and Production) through recycling and circular economy practices.

The research also anticipates presenting novel interlocking block designs (SIB, SICIB, DTIIB) that match or surpass the strength of existing blocks while serving as eco-friendly alternatives. These blocks are adaptable, and practical, offering affordable solutions for sustainable housing and infrastructure. This aligns with SDG 11 (Sustainable Cities and Communities) by promoting resilient and inclusive urban development. Finally, the application of ESP and RCA in interlocking block production reflects SDG 9 (Industry, Innovation, and Infrastructure), as it fosters industrial innovation, sustainable construction technologies, and resilient infrastructure development

The validation procedure will give the early prediction of the interlocking block behaviour that the ANN achieved an R^2 value of ≥ 0.977 for the training set and ≥ 0.972 for the test sets, indicating high predictive accuracy (Tamimi et al., 2023). Besides, it will give a good perspective in society to used and believing the production of the interlocking block.

1.7 Summary

There have a lot of waste that produced of different industrial market in Malaysia or worldwide. With the problem that world facing now, there will have alternative idea to create a solution and solve the problem. In this study, it is focused on eggshell waste that come from food waste and concrete waste that refined as the recycled concrete aggregates from construction waste. Thus, the idea of creating a sustainable interlocking block is the alternative way to save environment, community, and country.

CHAPTER 2
LITERATURE REVIEW

2.1 Introduction

This chapter is specifically interested in the addition of other materials to concrete and to find out the mechanical performance of ESP, SF and recycled concrete aggregate and the environmental advantages associated with ESP, SF and recycled concrete aggregates. Their prospective merits and shortcomings are evaluated in the review and can be used as an experiment design basis and to analyse their effect on the mortar strength.

2.2 Review on The Optimum Percentage of Eggshell Powder, Silica Fume and Recycled Concrete Aggregates

The review on the optimum percentage of Eggshell Powder (ESP), Silica Fume (SF), and Recycled Concrete Aggregates (RCA) focuses on identifying the ideal combination of these materials in concrete to enhance its properties. ESP, a sustainable byproduct, can partially replace cement due to its calcium content, while SF improves strength and durability by enhancing the bonding matrix. RCA, as a substitute for natural aggregates, promote environmental sustainability. The review examines how varying proportions of these components affect concrete's compressive strength, flexural strength, workability, and durability, aiming to determine the most effective blend for both performance and sustainability in construction.

2.2.1 Cement

Figure 2.1 depicts the publication trends for three materials consisted of OPC, SF, and ESP, spanning from 1970 to 2023. The comparative publication trend graph illustrates a significant disparity in research focus among Ordinary Portland Cement (OPC), Silica Fume (SF), and Eggshell Powder (ESP). OPC, represented by the blue scatter as the highest number of publications because it is the primary binder in concrete

worldwide (Sutar et al., 2021). It has long been the cornerstone of cementitious materials in construction. Its widespread use in infrastructure and industrial applications has led to extensive research on its hydration chemistry, durability, and environmental impact. Silica Fume (SF), shown in orange, shows a substantial number of publications, though lower than OPC because it is an emerged in the 1980s as a high-performance Supplementary Cementitious Material (SCM) (Alengaram et al., 2023). Its pozzolanic reactivity and ability to enhance concrete strength and impermeability have made it a staple in high-strength and durable concrete applications, with consistent research output over the decades (Siddiqi et al., 2023). The relatively high publication count reflects its industrial availability, proven performance, and integration into mainstream construction practices.

In contrast, Eggshell Powder (ESP), represented by the red scatter, has only 101 publications between 1970 and 2023. This limited count reflects its status as an emerging material in sustainable cement technology. Several factors contribute to this low visibility. First, ESP is derived from agro waste, which historically received less attention than industrial by-products like SF (Paruthi et al., 2023). Second, the variability in eggshell composition affected by regional diets, species, and processing methods raised concerns about consistency in mix design and performance (Bhardwaj et al., 2025). Third, ESP lacks standardized processing protocols and certification, making it less attractive for large-scale adoption and regulatory inclusion (Prodhan et al., 2024).

Despite the lower publication count, ESP is gaining traction because it is rich in calcium carbonate ($CaCO_3$), chemically like limestone used in cement production (Zhang et al., 2024). Notably, Chong et al. (2020) identified a suitable composition for OPC was having in ESP chemical properties. Additionally, Alsharari et al. (2022) highlighted ESP as a promising binder, while Juyu Xi et al. (2022) emphasized the suitability of SF.

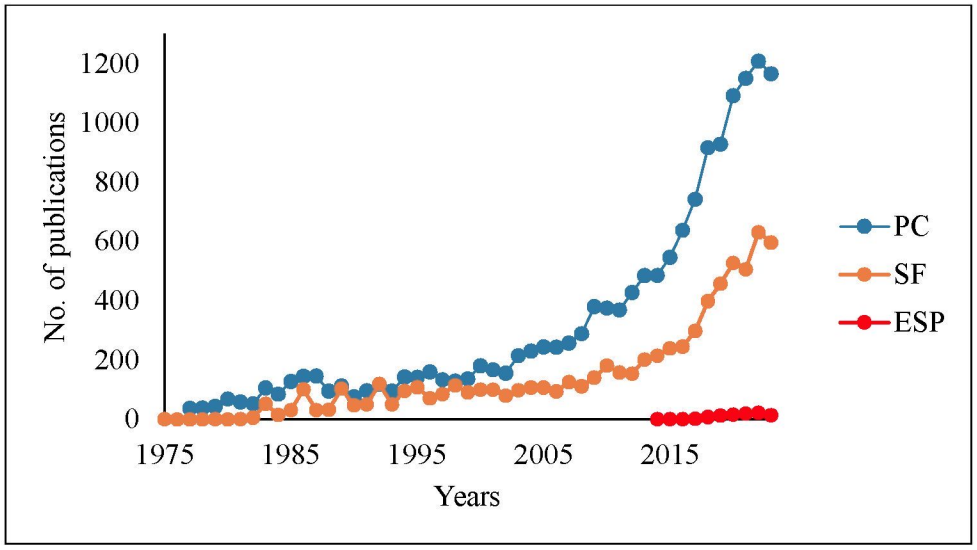

Figure 2.1 The Paper Publications of Ordinary Portland Cement (OPC), Eggshell Powder (ESP), and Silica Fume (SF)

2.2.2 Eggshell Powder

Malaysia is among the world's largest consumers of eggs, with an estimated 20 million eggs consumed daily (Lee, 2014). Eggshells (ES) are a major agricultural waste generated from bakeries, fast-food chains, and hatcheries. Meanwhile, rapid urbanization and large-scale infrastructure projects are continuously expanding worldwide. Given the widespread availability of raw materials for cement production, significantly reducing cement consumption soon remains a challenge. Research suggests that ESP, which is rich in calcium, can be effectively combined with low calcium pozzolanic materials such as fly ash (FA) (Hamada et al., 2020).

The cement industry is recognized as one of the largest contributors to global carbon emissions, accounting for approximately 6% of total CO_2 output, which translates to nearly 2.4 billion metric tons released annually (Statista, 2023; IEA, 2023; Net Zero Industry Tracker, 2024). Most of these emissions originate from the calcination of limestone, a chemical process that releases carbon dioxide as calcium carbonate decomposes into calcium oxide (≈60%), while the remainder is generated through fuel combustion in high-temperature kilns (≈40%) (Cong et al., 2024; Benhelal et al., 2013, Gibbs et al., 1996).

With the rapid growth of construction activities worldwide, the environmental

burden of cement production has become increasingly critical, driving the urgent need for sustainable alternatives and innovative solutions. One promising approach is the incorporation of ESP as a partial cement replacement. Eggshells, being rich in calcium carbonate, offer chemical compatibility with cementitious systems while simultaneously addressing waste management challenges. Moreover, ESP is inexpensive, abundantly available, and capable of maintaining concrete performance, making it a cost-effective substitute that can reduce overall construction expenses while supporting sustainability goals (Bhardwaj et al., 2025; Ngayakamo, 2025).

In Figure 2.2 shows the red cluster, which includes terms like eggshell powder, compressive strength, tensile strength, and sustainable development, indicates a focused but relatively small body of research centred on ESP's mechanical and environmental performance. The network graph highlights the growing but still limited research on ESP in cement applications, with a focus on mechanical properties and sustainability. ESP shows interdisciplinary relevance, connecting to biomaterials and powder processing techniques like SEM and ball milling. Studies by Dezfouli (2020) and Othman et al. (2026) confirm ESP's compatibility with cement systems and its rising appeal as a sustainable alternative, despite fewer publications compared to silica fume.

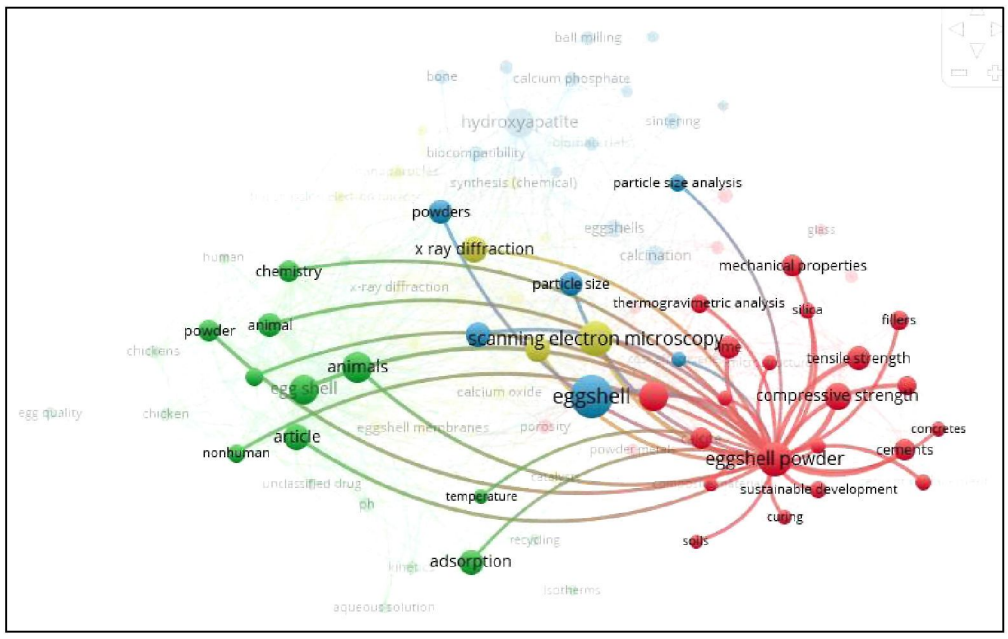

Figure 2.2 Relation of Keywords in Paper Publications of Eggshell Powder

2.2.2.1 Background of Eggshell Powder

The growing consumption of OPC each year for producing concrete and other mixtures contributes to the depletion of natural resources and the emission of CO_2 into the atmosphere, significantly impacting climate change and global warming. According to Teara et al. (2020), an increasing number of waste materials, such as slag, FA, RHA, ESP, and palm oil fuel ash (POFA), are being used to partially replace cement. However, there is generally a limit typically no more than 50% to how much FA can substitute for OPC. Exceeding this proportion potentially weaken the mortar or concrete, making it unsuitable for construction, as FA contains less calcium oxide (CaO) than cement, which can reduce concrete strength. In contrast, ESP is rich in CaO, making up about 60% of its composition (Teara et al., 2020; Murthi et al., 2022). Consequently, Teara et al. (2020) explored using FA and ESP as partial cement replacements to create high-strength concrete.

Figures 2.3(a), 2.3(b), and 2.3(c) present a bibliographic mapping analysis centred on three key materials in concrete research: Ordinary Portland Cement (OPC), Silica Fume (SF), and Eggshell Powder (ESP). Each diagram places its respective keyword at the centre, surrounded by colour-coded clusters that represent dominant research themes. For OPC, the green cluster highlights material inputs and durability enhancers such as lime, fillers, and agricultural wastes, while the yellow bubble reflects structural performance through bearing capacity. Chemical interactions and additives like slags and alkali activators are grouped in cyan, with environmental degradation and silica fume effects shown in pink. Mechanical properties and industrial relevance appear in orange, sustainability in purple, and infrastructure links such as asphalt in violet collectively illustrating the broad scope of OPC-related studies.

In contrast, the SF map emphasizes its central role in enhancing compressive strength and high-performance concrete, with brown bubbles at the core. Surrounding clusters include green (durability and abrasion resistance), red (chemical interactions with aggregates and alkaline agents), purple (specialized infrastructure applications), yellow (sustainability via nano-silica), orange (structural toughness with steel fibres), and cyan/blue (advanced technologies like 3D printing and machine learning). Meanwhile, the ESP diagram showcases its emerging role in sustainable concrete innovation. Blue bubbles represent cement chemistry and hydration, green bubbles

highlight mechanical properties, orange bubbles link ESP to high-performance applications and eco-friendly glass, pink bubbles address carbon reduction and sustainability, and grey bubbles reflect technical processes such as calcination and grinding. Together, these bibliometric maps provide a comparative overview of how OPC, SF, and ESP are positioned within the research landscape, helping to structure the bibliography according to material function, performance, and sustainability impact.

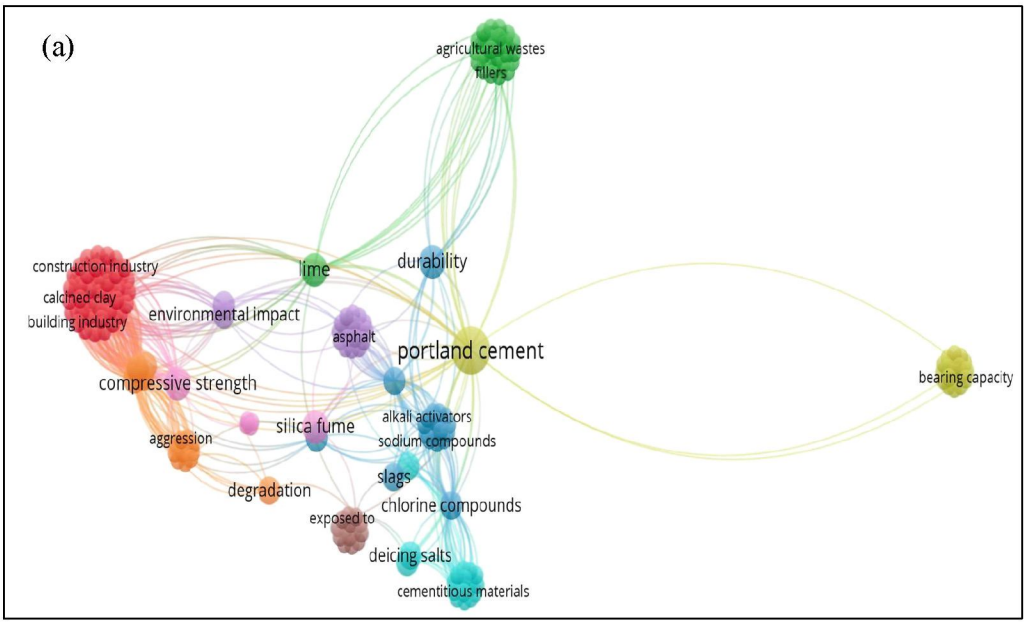

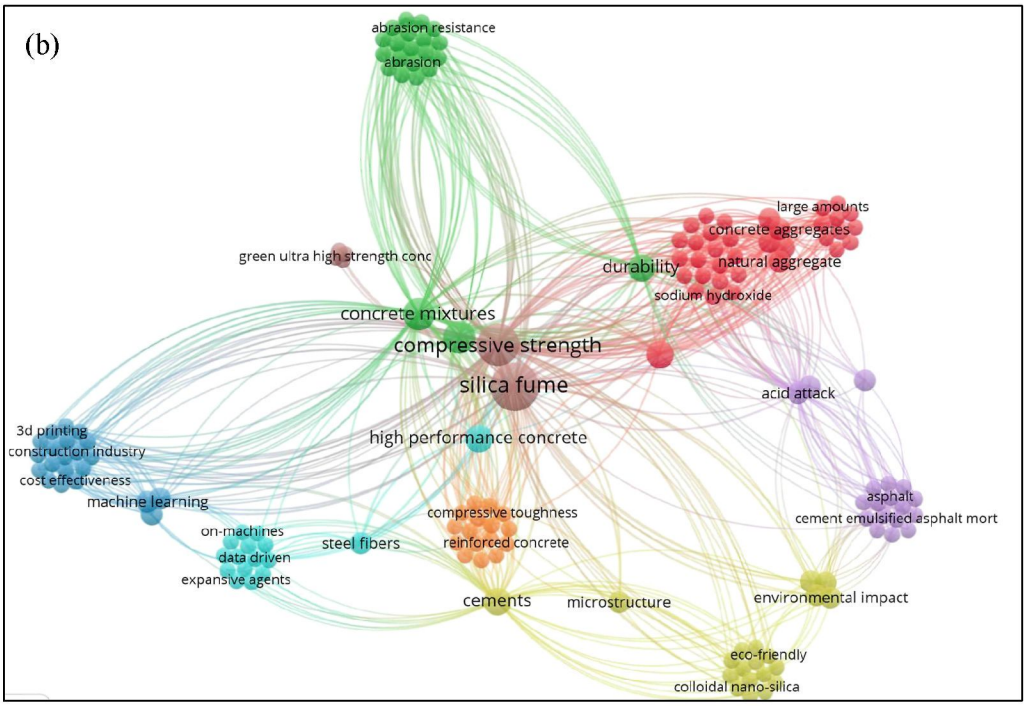

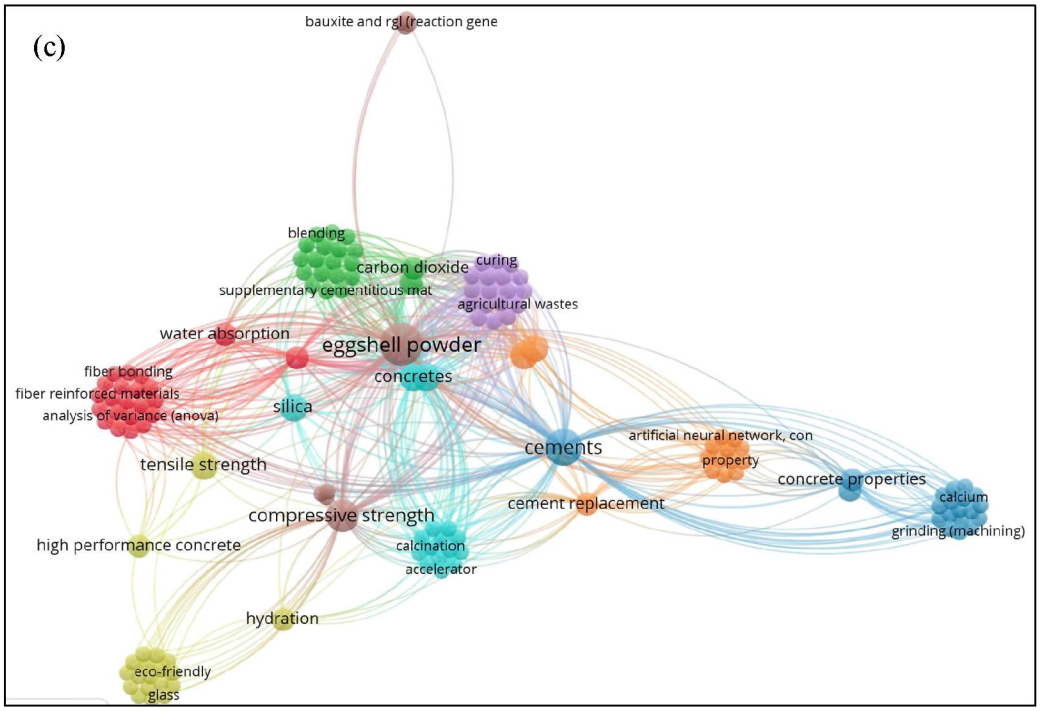

Figure 2.3 Bibliographic Mapping of Cement in Relation to Concrete: (a) Portland Cement; (b) Silica Fume; (c) Eggshell Powder

2.2.2.2 Percentage and Properties of Eggshell Powder

According to Rivera et al. (1999), 94% calcium carbonate, 1% calcium phosphate, 4% organic matter, and 1% magnesium carbonate make up most eggshells, which make up 11% of an egg's overall weight. ESP has been shown to improve compressive, flexural, and tensile strength when used in place of some of the cement. However, a decrease in strength is frequently noted when the ESP content above 10%.

The chemical composition of OPC, as shown in Table 2.1, has similarities with the substitute material ESP. Thus, when researchers consider replacing a certain percentage of cement with alternative materials, it is important to understand the chemical properties through experimentation or literature review. The main component of ESP is CaO, which significantly improves the properties of cementitious materials (Teara et al., 2020; Chong et al., 2020; Yang et al., 2022; Hakeem et al., 2023; Paruthi et al., 2023). With a high calcium content (about 85–95% in the form of calcium carbonate), ESP is suitable as a cement replacement in concrete (Chong et al., 2020; Paruthi et al., 2023). ESP with a CaO content above 90% improves the performance of

the composite, while a lower CaO content deteriorates the performance of the composite (Yang et al., 2022; Hakeem et al., 2023), possibly due to the lower CaO content (52.15%) of the chemical composition.

Table 2.1
Chemical Properties of Cement by Previous Studies.

Chemical Compound (%)	Range OPC	OPC [Chong et al., 2020]	OPC [Amin et al., 2023]	OPC [Hakeem et al., 2023]	OPC [Adamu et al., 2024]	OPC [Teara et al., 2020]
Calcium Oxide (CaO)	60 – 67	60.1	62.02	62.15	65.18	60.1
Magnesium Oxide (MgO)	0.1 – 3.0	2.1	-	2.78	0.91	0.5
Silica Dioxide (SiO_2)	17 – 25	21.8	25.37	20.54	19.17	21.8
Aluminium (Al_2O_3)	3.0 – 8.0	6.6	4.87	5.21	5.39	6.66
Iron Oxide (Fe_2O_3)	0.5 – 6.0	4.1	2.93	3.83	3.40	4.1
Chloride (Cl)	-	-	-	0.07	-	-
Sulphur Trioxide (SO_3)	1.3 – 3.0	2.2	3.14	2.67	3.51	2.5
Potassium Oxide (K_2O)	0.4 – 1.3	0.4	0.81	0.82	1.22	0.25
Sodium Oxide (Na_2O)	0.4 – 1.3	0.4	-	0.94	0.17	-
Phosphorus Pentoxide (P_2O_5)	-	-	0.54	-	0.09	-
Strontium Oxide (SrO)	-	-	-	0.05	-	-
Titanium Dioxide (TiO_2)	-		0.19	0.15	-	-
Manganese (II) Oxide (MnO)	-		0.02	0.09	0.18	
Loss on Ignition (LOI)	1 - 5	2.4	-	0.88	-	

Replacing cement with ESP in the range of 5 to 10 % is optimal and does not affect the mechanical behaviour of concrete. Nevertheless, replacement more than 10 % reduces these properties. Addition of 6.50% ESP has been reported to improve the early age strength of blended cement concrete (Murthi et al., 2022). Also, Hasan et al. (2021), published in the Journal of Materials Research and Technology. This study confirmed that combining silica fume (SF) and eggshell ash (ESA) as soil stabilizers significantly improved the undrained shear strength of kaolin clay soils, with optimum performance achieved at a mixture of 6% SF and 6% ESA, resulting in a strength increase of up to 68.8%. The greater value of the coefficient of determination (R^2) indicator indicates that the observed parameters are likely to change, and the occurrence of such changes can be predicted with high confidence with the application of SF and ESA as soil stabilizers, and the observed approach to soil enhancement is likely to be cost-efficient and environmentally sustainable (Hasan et al., 2021). Accordingly, this research explores the incorporation of eggshell powder (ESP) at replacement levels of 5%, 10%, and 15% in mortar mixtures.

Moreover, Yerramala (2014) emphasized that the waste of shells of eggs is calcareous and chemically closely resembles limestone. Use of eggshell waste as a natural substitute of lime in the manufacturing process of cement has its environmental benefits such as using less cement in the manufacturing of cement and it also encourages green building practices. This radical method does not only reduce wastes but also helps to bring eco-friendly and resource-differentiated building solutions.

It was also established by Hamada et al. (2020) that incorporation of ESP instead of cement, in addition to other materials, improves mechanical properties of concrete. But just like in the former studies, their results showed that performance suffers when ESP replacement is beyond 10 %. Conversely, Yerramala (2014) found that adding an SPB made of 5% cement and ESP lead to superior strength than the presence of ordinary concrete, and that 5 % was the most effective level of cementing substitution to ensure optimal mechanical rates. In the meantime,

Table 2.2 reveals the results that the stable chemical proportions for replacement materials ESP as their content with the same chemical as OPC. However, for these both of chemical which are Titanium Dioxide (TiO2), and Manganese (II) Oxide (MnO) are not found in the ESP. Both can influence cement and concrete performance, though their roles differ. TiO_2 is often studied for strength enhancement and photocatalytic properties (Vishnusankar et al., 2023; Pandey & Singh, 2025), while MnO affects clinker chemistry and hydration behaviour (Yang et al., 2023; Jasim et al., 2025). Their absence in Eggshell Powder (ESP) means ESP does not provide these specific effects, but ESP contributes through its calcium carbonate content instead which supports cement hydration and strength development, making it a sustainable replacement for part of OPC. The results demonstrate the promise of ESP as an environmentally friendly sustainable alternative to traditional soil stabilizers such as lime and provided a less expensive solution to cement-based soil strength improvements.

Chemical Compound (%)	Range ESP [Paruthi et al., 2023]	ESP [Chong et al., 2020]	ESP [Alsharari et al., 2022]	ESP [Amin et al., 2023]	ESP [Adamu et al., 2024]	ESP [Teara et al., 2020]	Burned ESP [Teara et al., 2020]
Calcium Oxide (CaO)	33.1 – 99.8	52.15	83.2	83.2	97.46	62.35	97.25
Magnesium Oxide (MgO)	< 1	0.6	0.1	0.1	0.69	0.36	1.03
Silica Dioxide (SiO_2)	< 1	1.22	0.15	0.15	0.03	0.61	0.14
Aluminium (Al_2O_3)	< 1	0.28	0.28	0.28	0.02	0.07	0.07
Iron Oxide (Fe_2O_3)	< 1	0.16	0.18	0.18	-	0.63	0.02
Chloride (Cl)		0.011			-	-	-
Sulphur Trioxide (SO_3)	0 – 1.3	-	0.25	0.25	0.35	0.61	0.14
Potassium Oxide (K_2O)	< 1	-	0.06	0.06	0.07	0.22	0.07
Sodium Oxide (Na_2O)	0 – 2.9	-	0.11	0.11	0.17	-	0.25
Phosphorus Pentoxide (P_2O_5)		-	0.55	0.55	0.47	-	0.77
Strontium Oxide (SrO)		-	0.38	0.38	-	-	0.05
Titanium Dioxide (TiO_2)				-	-	-	-
Manganese (II) Oxide (MnO)				-	-		
Loss on Ignition (LOI)	0.1 – 47.8	-	14.5	14.5	-		

Table 2.2
Chemical Properties of Eggshell Powder by Previous Studies.

2.2.2.3 Application of Eggshell Powder

There are numerous uses of eggshells that go beyond agriculture such as in the pharmaceutical field and eggshells have been processed into tablet dosage forms as ESP. These were the tablets that were subjected to various tests to determine their effectiveness and bioavailability as compared to commercially available calcium supplements as in the case of CIPCAL-500 (Gaonkar et al., 2016). In building, ESP has also been used to partially replace cement in lightweight foamed concrete providing large increases in initial surface absorption, sorptivity and total water absorption. This paper advocates the viability of the eggshell waste to mitigate boron contamination in desalinated water (Tiong, 2020). In addition to the technical advantages, the use of this agricultural by-product facilitates environmental

sustainability by recycling waste and still providing a cheaper alternative, which exhibits its economic and ecological savings.

The research by Teara et al. (2020) conducted previously used locally accessible raw materials that were OPC (concrete), river sand as a fine aggregate, crushed granite as a coarse aggregate, tap water, eggshells, and FA class F. The said raw materials were used in lieu of cement as part replacements where ESP was used at 5 and 10 %, and FA at 20, 30, 40, and 50 % respectively. In a nutshell, using ESP combined with FA in concrete fund solution of replaced cement by at least 5 %, and 30 to 40 % can provide significant advantages in producing a high-strength concrete with compressive strength greater than 40 MPa 28 days when water is cured (Teara et al., 2020). Previous study of Shi & Shui, (2023) has found that about 10% ESP substitution benefit not only the addition of CO2 in pastes but also the strength development of cement pastes in the first phases of the early ages after accelerated carbonation. Thus, the initial CO2 curing was not appropriate in enhancing strength in 20% of ESP replacements in cement.

Agricultural by-product like the eggshell waste has demonstrated the possibility of being used to stabilize soil because it contains high levels of lime, calcium, and proteins (Kumar et al., 2015). Its chemistry is almost similar to the lime; hence, it can be used as an alternative in soil stabilization (Anoop et al., 2017). According to Johns et al. (2017) research, the 12 % ESP combined with soil stabilization can substitute 4 % lime since they show comparable strength in terms of California Bearing Ratio (CBR) due to their similarity in strength when used in clay soils. In addition, studies show an optimal percentage of ESP being 13 % as revealed by Ahmed et al. in the year 2016 in maximizing the value of CBR in clay soil (Ahmed et al., 2016).

Holistically, the preceding research foresees the exemplary flexibility in the use of eggshell wastes. Besides being used to enhance soil quality and create a better growth of plants, its products also show imminent results compared to their conventional uses in the pharmaceutical formulations. The fact that they have high ca-bioavailability, better performance than conventional sources, and environmentally friendly areas like boron in contaminating the water, point to their wide-ranging importance. This combination of environmental, economic, and practical advantages

highlights the essentiality of eggshell-based innovations in the enhancement of resource-efficient and sustainability.

2.2.3 Silica Fume

Silica fume (SF), an industrial by-product often incorporated in concrete, does bear a little resemblance in chemical composition to SF as depicted in Table 2.3. Since the SF is by-product of OPC it is perfect mixer with these 3 materials in mortar or concrete. Previous studies have shown that eggshell powder (ESP), especially when rich in CaO, has been utilized to compensate for the low calcium content in concrete and cement mortars (Hakeem et al., 2023). Furthermore, the fine particle size of ESP can act as a pore filler within the concrete matrix, thereby enhancing its mechanical strength (Adamu et al., 2024).

Table 2.3
Chemical Properties of Silica Fume by Previous Studies.

Chemical Compound (%)	Range SF [Sathparan et al., 2021]	SF [Amin et al., 2023]	SF [Hakeem et al., 2023]	SF [Xi et al., 2022]	SF [Sharma et al., 2022]	SF [Mohamed et al., 2023]
Calcium Oxide (CaO)	< 1	1.76	0.10	0.19	0.45	0.2
Magnesium Oxide (MgO)	0 – 4.5	0.001	-	0.34	1.85	0.2
Silica Dioxide (SiO_2)	> 85.0	86.75	98.75	96.76	92.4	97
Aluminium (Al_2O_3)	0 – 1.1	1.12	0.08	0.28	0.84	0.2
Iron Oxide (Fe_2O_3)	0 – 2.0	1.78	0.04	0.25	1.25	0.5
Chloride (C_1)	-	-	0.03	-	-	0.01
Sulphur Trioxide (SO_3)	0 – 1.3	0.394	0.67	1.29	-	0.15
Potassium Oxide (K_2O)	0 – 1.3	3.02	-	0.23	1.26	0.5
Sodium Oxide (Na_2O)	< 1	1.05	-	-	0.78	0.2
Phosphorus Pentoxide (P_2O_5)		0.615	-	0.24	-	-
Strontium Oxide (SrO)		-	0.02	-	-	-
Titanium Dioxide (TiO_2)		0.018	0.08	-	-	-
Manganese (II) Oxide (MnO)		0.021	0.04	-	-	-
Chromic Oxide (Cr_2O_3)			0.03	-	-	-
Loss on Ignition (LOI)	0 – 2.8	3.12	0.53	2.61	-	-

The findings agree with the study of Adamu et al. (2024) where a combination of SF and ESP in concrete resulted in higher eco-strength (Adamu et al., 2024). The weight of the binder materials in a typical Ultra High Portland Cement (UHPC) range between 800 and 1300 kg/m^3 and are composed mainly of SF and OPC that enhances

the use of silica-based materials (Hakeem et al., 2023). Taking into consideration the beneficial impact of SF, particularly when used with pozzolanic materials, it can be said that it is suitable in enhancing the behaviour of cementitious materials that rely on ESP (Alsharari et al., 2022). The strength of the material is a positive impact of the addition of SF (Amin et al., 2023).

2.2.3.1 Background of Silica Fume

Silica fume is an ultra-fine pozzolanic material with physical and chemical properties that significantly enhance concrete performance (Mohamed et al., 2011). Also referred to as micro-silica or silica dust, it is a byproduct of silicon and ferrosilicon alloy production (Khedr, 1994). During manufacturing, filters capture SF vapours from outgoing gases as part of environmental protection measures. It primarily consists of 85 – 97% silicon dioxide and is made up of tiny, spherical glassy siliceous particles. When mixed with cement, it reacts with calcium hydroxide ($Ca(OH)_2$) to form calcium silicate hydrate (C-S-H), which strengthens the concrete matrix while reducing porosity and permeability (Hamada et al., 2023).

It was only in 1987 that the American Concrete Institute (ACI) Committee 226 dedicated to condensed SF practically made it a pozzolan. It comprises very small particles in the form of vitreous that weighs between 13,000 and 30,000 m 2/kg (Shanmugapriya & Uma, 2013; Robayo-Salazar et al., 2018), which is 100 times lighter than the standard cement particles. SF is a fine silica rich material, which could be used as a good pozzolanic strength in concrete works (Mohanaselvan & Ravinchandran, 2015). There was a lot of research to determine suitable renewable sources that can replace aggregate and cement (Hamada et al., 2023). SCM, including FA, GGBS, POFA, SF, RHA, and ESP, have a positive effect on the properties of concrete (Samad & Shah, 2017; Givi et al., 2010; Aprianti, 2017; Das et al., 2020; Hamada et al., 2023).

SF improves a number of properties in concrete such as compressive strength and bond strength, as well as abrasion resistance. It also decreases permeability and acts as a corrosion shield in the structure of reinforcement (Senhadji et al., 2014), which determines its efficiency as an additive to increase the durability and life span of concrete building materials.

2.2.3.2 Percentage and Properties of Silica Fume

Silica fume is usually composed of the substitute of partial cement in concrete, with replacements often chosen at levels of about 5 to 15%, however, in high-performance concretes (HPC), levels as high as 25% may be utilized. Since it was concluded by Pachideh et al. (2020) and Juyu Xi et al. (2022), the percentage distribution is dependent on the desired characteristics, with smaller percentages of the addition (5 to 10%) giving better early strength, and decreased permeability, moderate additions (10 to 15%) giving improved strength compressive and improved durability, and higher percentages (15 to 25%) used in ultra-high-performance concrete (UHPC) in instances where extreme levels of strength are needed.

Addition of SF to concrete replaces several mechanical advantages, such as 30 to 40% increase of compressive strength, a stronger bond between aggregates and cement paste, and abrasion and sulphate resistance (Antoni et al., 2015). It also aids in decreasing permeability, which makes concrete less prone to attack by the elements, in particular to water ingress and chemical assault. Another of its primary benefits is the fact that it can avoid reinforcement corrosion by reducing penetration of chloride. With such features, SF finds great application in high-performance and green building to enhance strength and durability in new forms of concrete and construction. According to Pachideh et al. (2020), there would be little difference in water absorption at older ages since 56 and 90-day water absorption changes by less than 10 % against 28 days.

A number of research have revealed flexural strength of concrete to increase appreciably when supplemented with SF. As an example, Karthikeyan and Dhinakaran (2018) found that the addition of 10% SF resulted in an increase in flexural strength over the rest of concrete mixtures, which indicates that the given proportion is balanced. Likewise, Liu et al., (2020) concluded that flexural strength increased steadily as the proportion of SF increased to 17.2 MPa at 20% and to 23.1 MPa at 30%. These findings mean that increased volumes of SF could increase the bending resistance of a material.

Amin et al., (2022) observed that the corresponding increase in flexural strength, despite being low in UHPC, may be due to the fine particles being exceptionally small in SF. The extreme fineness contributes towards ensuring that the voids are filled better and the bond between the cement is also strengthened. In the meantime, Chen et al., (2022) noted that the improvement in the flexural strength of 8.48 % was achieved when

7% SF was added to the control sample, demonstrating that even minor quantities of SF have a positive effect.

Generally, it can be concluded that the flexural strength has significantly increased due to use of SF in various studies which demonstrates the utility of this ingredient to optimize the microstructure of concrete and improve its capacity to withstand the tensile stresses particularly when used in mixtures subjected to strain due to bending or flexural forces.

2.2.3.3 Application of Silica Fume

Silica fume, a modern pozzolanic material, has become increasingly popular in concrete applications. First introduced in Norway in 1969, its use expanded to North America and Europe in the early 1980s, and its application in concrete has grown significantly since then. Researchers are paying more attention to the use of SF in building materials. For example, in HPC and UHPC, SF can be utilised as a primary additive. Because SF could repair columns, marine piles, and deteriorating bridges, it was utilised as a main constituent in many significant infrastructures, including parking decks, tunnels, and highway bridges (Siddique, 2011). Additionally, the SF can be utilised to produce UHPC for significant infrastructure, including highway bridges, maritime constructions, and high-rise skyscrapers (Azmee & Shafiq, 2018; Nodehi & Nodehi, 2022).

Toutanji, et al. (1995) research has shown that SF as a partial cement replacement when used together with super-plasticizers, is very effective in improving concrete strength. The strengthening is the consequence of the lower amount of water in the fresh concrete and the creation of a compressed-like matrix in the interfacial region that led to an increase in the strength and durability. Cong et al., (1990) observed a similar phenomenon finding that SF together with 15 oz/cwt of superplasticizer contributed to cement paste strength at any curing condition, with the least strength variation occurring at three days. This high strength gain is mainly attributed to ultra-small particle size of SF (enables it to fill gaps between cement particles, minimizing space but does not change overall porosity).

Moreover, Singh et al. (2015) proved that addition of 5 to 15% SF to mortar can show a 30 to 40% increase in compressive strength. This increase is done by substituting

some, but not all, cement/sand by SF, with the most marked strength gain occurring in a 1:3 mix ratio. The maximum strength development is reported in 15 % SF replacing sand thereby signifying that a richer mix is more comfortable to use when incorporating SF. In summary, SF significantly improves concrete strength by reducing water content and creating a denser matrix, especially when combined with superplasticizers. Studies by Toutanji et al. (1995) and Cong et al. (1990) confirm that SF enhances cement paste strength across all curing stages, while Singh et al. (2015) reported a 30 to 40% increase in compressive strength with 5 to 15% SF, with 15% replacement of sand yielding the highest strength gain. Generally, the compressive strength is impacted when 14% pozzolanic waste is added to cementitious mortars (Pachideh et al., 2020).

2.2.4 Natural Aggregate (NA)

Based on study made by Singh et al. (2015), adding 5 to 15% SF to mortar increases its compressive strength by 30 to 40%. This is achieved by replacing some of the cement or sand with SF. For all SF percentages, the greatest increases are shown in the 1:3 mix proportion; this suggests that a richer mix is more amenable to the addition of SF. The greatest strength gain happens when 15% SF is substituted for sand. In summary, SF has significantly improved concrete strength by reducing water content and creating a denser matrix when combined with superplasticizers. Study by Toutanji et al. (1995) and Cong et al. (1990) found that SF enhances cement paste strength at all curing stages. Singh et al. (2015) observed a 30 to 40% increase in compressive strength with 5 to 15% SF in mortar, with the highest strength gain seen with 15% SF replacing sand.

Indrajit et al. (2022) reported a water-to-cement ratio of 0.56, with recycled aggregates replacing natural coarse aggregates at rates of 0%, 20%, 30%, 40%, and 60%. Compressive, tensile, and flexural strength tests were conducted after processing periods of seven and twenty-eight days. Table 2.5 summarizes the properties of the aggregates used, while Figure 2.5 illustrates the grain size and distribution. The study found that recycled aggregates are weaker than natural aggregates due to the mortar that remains bonded to them, as well as their higher water absorption and porosity. Additionally, the effectiveness and compressive strength of recycled concrete tend to decrease as the percentage of recycled aggregates increases. Therefore, minimal use of

RCA enhances workability. However, with the right mix design and proportions, it is possible to maintain workability comparable to that of natural aggregates.

Table 2.4
Natural and Recycled Aggregate Have Different Physical Properties

Aggregate specifications	Relevant standards	Aggregate type		
		Natural coarse grains	Recycled coarse grain	Natural fine grains
Maximum nominal size (mm)	ASTM C136	21	21	2.85
Bulk specific gravity	ASTM C127	2660	2600	2620
Percentage of water absorption with dry surface in a saturated state	ASTM C127	1.35	6.45	2.7
Modulus of softness	ASTM C136	-	-	3.10

Source: (Indrajit et al., 2022)

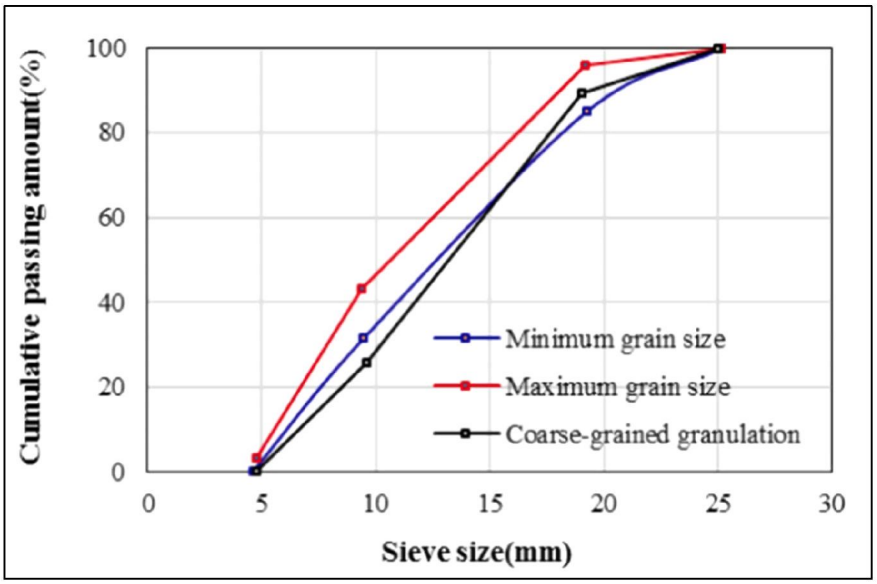

Figure 2.4 Granulation Lines of Natural and Recyclable Materials with A Coarse Grain Size
(Source: Indrajit et al., 2022)

In addition, Mirjana et al. (2010) identified other characteristics of RCA in their study. They evaluated RCA for properties such as crushing resistance, chemical composition, water absorption, and bulk density. The properties of both natural and RCA were tested according to Serbian standards for natural aggregates. The quality requirements outlined in Tables 2.6 and 2.7 also adhere to these Serbian standards. The

aggregates tested meet all quality standards, showing adequate strength, excellent freeze thaw durability, very low water absorption, and acceptable bulk density. These results confirm their reliability and sustainability for use in concrete and mortar production.

Table 2.5
Results of Natural Aggregate Testing

Tested property	Measured value	Grain size				Quality requirement
		0/4	4/8	8/16	16/32	
Crushing resistance (in cylinder)	mass loss (%)	-	14.0	18.6	23.8	<30
Freezing resistance test	mass loss (%)	1.8	1.6	1.4	1.5	<12
Water absorption after	(%)	0.7	0.4	0.4	0.3	-
Bulk density, uncompacted	(kg/m^3)	1,611	1,490	1,470	1,460	-
Bulk density, compacted	(kg/m^3)	1,729	1,590	1,570	1,560	-

Source: (Mirjana et al., 2010)

Table 2.6
Results of Recycled Concrete Aggregate Testing

Tested property	Measured value	Grain size			Quality requirement
		4/8	8/16	16/32	
Crushing resistance (in cylinder)	mass loss (%)	18.3	26.7	30.7	<30
Freezing resistance test	mass loss (%)	2.0	1.4	1.0	<12
Chemical testing (mortar part of recycled aggregate)	chloride content	0	0	0	<0.1
	sulphate content	in traces	in traces	in traces	<1.0
	pH	9.85	9.85	9.85	-

Source: (Mirjana et al., 2010)

2.2.5 Recycled Concrete Aggregate (RCA)

Replacing natural aggregates with RCA is becoming more popular. Figure 2.6 shows that there are more study papers about recycled concrete aggregates from 1999 to 2022. This means that more people are interested in studying this and doing study on it over the years. So, researchers are looking into it more deeply, as shown in Figure 2.7 They are studying how strong structures made from recycled concrete aggregates are getting better each year. The constrained availability of conventional construction materials poses significant risks to structural integrity, thereby reinforcing the

imperative to adopt sustainable alternatives. Incorporating waste-derived resources offers a viable pathway to enhance resilience and ensure the long-term sustainability of the construction industry.

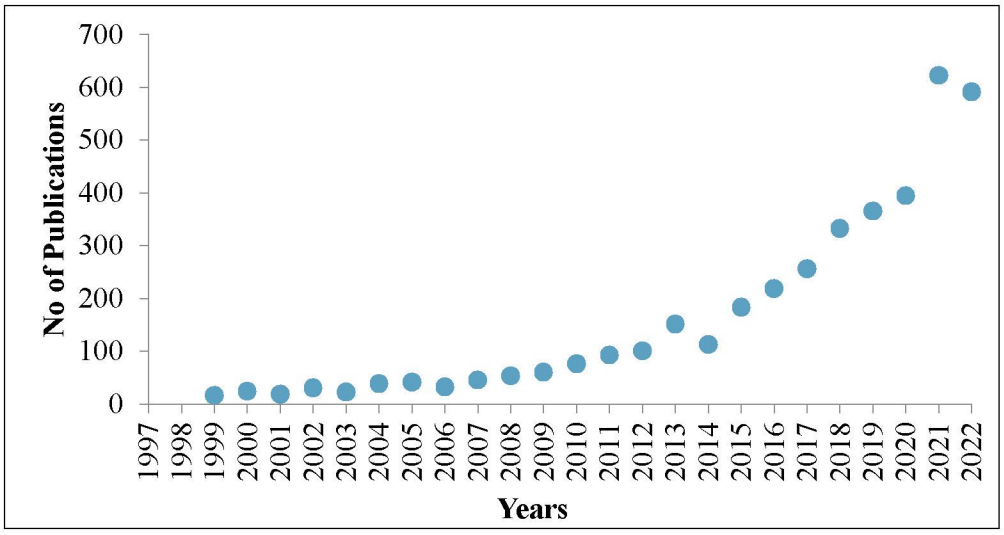

Figure 2.5 Recycled Concrete Aggregate Research Trend

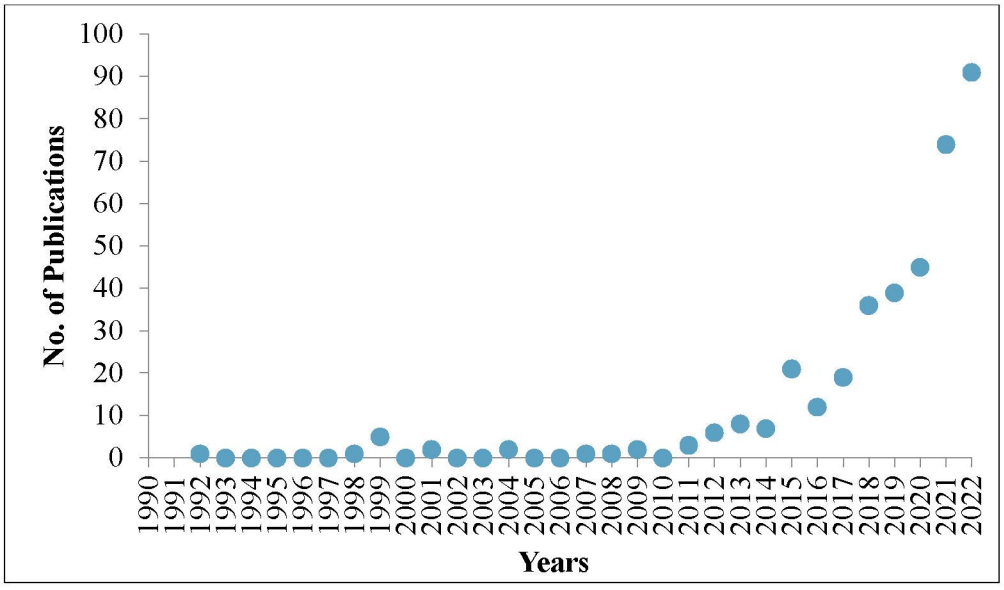

Figure 2.6 Flexural Strength Behaviour of Recycled Concrete Aggregates (RCA) Structure Elements Research Trend

2.2.5.1 Background of Recycled Concrete Aggregate (RCA)

The use of Recycled Concrete Aggregates (RCA) is gaining attention as a sustainable alternative to conventional construction materials. Incorporating recycled aggregates into construction aligns with circular economy principles and promotes environmental conservation. Over the past two decades, global cement production has increased dramatically, rising from 1.10 billion tons to 3.27 billion tons (Verein Deutscher, 2019), reflecting rapid expansion in the construction sector. Projections suggest that cement production could reach 4.83 billion tons by 2030, highlighting the growing demand for construction materials.

The rising cement production also drives an increased need for Natural Aggregates (NA), which are primarily derived from natural stone. Sinoh et al. (2022) predict the demand for Natural Aggregates (NA) is expected to rise significantly in the coming decades, creating risks of resource depletion and environmental strain from quarrying. Research highlights that sustainable construction must incorporate both improved quarrying practices and the use of alternative materials. Studies show that industrial by-products and RCA can effectively replace natural sand and stone, supporting circular economy principles (Mohammed et al., 2024). In Malaysia, recycled aggregates are emphasized as a sustainable solution, though wider adoption requires stronger policy and industry awareness (Ismail et al., 2018). Technical reviews further confirm that recycled concrete aggregates, when used at optimized replacement rates, can maintain structural performance while reducing environmental impact (Folorunso et al. (2023). Collectively, these findings reinforce the importance of balancing growing aggregate demand with innovative material strategies to ensure long-term sustainability.

According to Nedeljković et al. (2021), concrete recycling plays a crucial role in ensuring sustainable development in concrete structures. Construction and Demolition Waste (CDW) serve as the primary source of RCA, contributing significantly to sustainable material management. The vast scale of global aggregate production, estimated at 40 billion tons annually (Vivian et al., 2018), underscores the immense infrastructure development occurring worldwide.

Replacing Natural Aggregates (NA) with Recycled Aggregates (RA) in concrete production presents economic and environmental benefits. Study by Zheng et al. (2017) suggests that using RA in concrete could reduce material costs by 10–20%.

Furthermore, a life cycle assessment conducted in Hong Kong demonstrated that utilizing recycled aggregates from CDW significantly reduces environmental impact. Compared to conventional concrete made with natural aggregates, recycled aggregate concrete can achieve a 65% reduction in greenhouse gas emissions and conserve 58% of non-renewable energy resources (Hossain et al., 2016). These findings highlight both the economic viability and environmental advantages of incorporating recycled materials into concrete production, promoting sustainable construction practices for the future.

In Figure 2.7, the bibliometric graph shows rising research on recycled concrete aggregate (RCA) as fine aggregate replacement. The diagram illustrates the relationships among keywords in study publications focusing on the use of RCA in mortar. Numerous publications have been recorded from 1987 to 2024, exceeding a thousand. Upon closer examination and narrowing the scope, the publications specifically addressing fine aggregates that incorporate RCA as replacements in mortar mix total 439 from 1987 to 2024. By clusters highlighting different focus areas, the green cluster links RCA to recycling and resource recovery. The red cluster emphasizes concrete performance and mechanical strength, the blue cluster connects RCA to construction and demolition waste management, and the yellow cluster focuses on recycled fine aggregates and particle characterization. Together, these clusters reveal RCA's interdisciplinary role in sustainable construction, where studies confirm its ability to reduce natural resource use, improve waste management, and support eco-efficient concrete practices (Mahmoud & Omar, 2024; Folorunso, 2023; Yao & Hong, 2024). Notably, there is an absence of publications on the combination of eggshells powder and RCA, indicating that study on this combination is relatively novel and warrants further in-depth exploration.

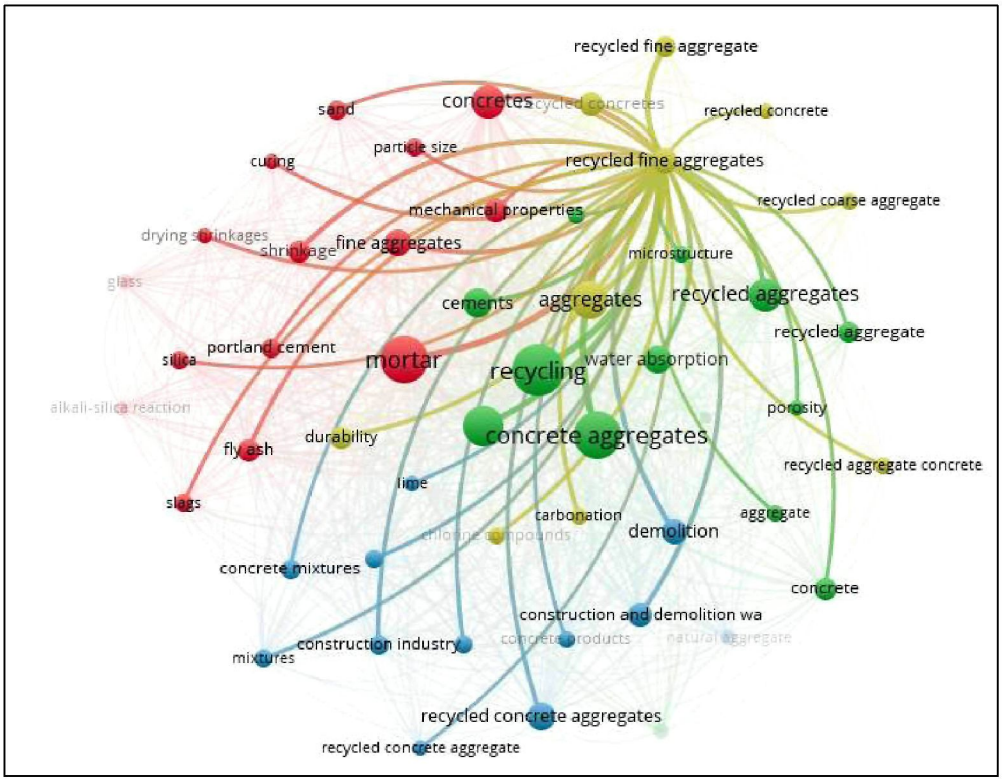

Figure 2.7 Relation of Keywords in Paper Publications of Fine Aggregates Containing Recycled Concrete Aggregates

Natural resources have been steadily depleting, a concern that has been prevalent since the 1970s. According to Enric et al. (2016), formal and systematic study into the use of CDW in construction projects began during this time, with laboratory experiments and demonstration projects exploring its potential applications. In 1978, Nixon PJ published a key review titled "Recycled Concrete as an Aggregate for Concrete," which significantly contributed to the growing body of literature on this subject. Sanjay et al. (2022) noted that using recycled materials in concrete production could reduce costs, benefiting both society and the economy. Vivian et al. (2018) further explained that recycled aggregate is widely used in various applications, including bulk backfill, sub-base, base, and surface material in road construction, lean concrete bases, hydraulically bound materials, and even in the production of new concrete.

When quality standards are met, then recycled aggregate can either be employed in hydraulically bound material or it can also be used in the manufacture of new concrete. Nonetheless, the most important thing is to make sure whether the recycled aggregate has no dangerous contaminants. In most cases, the contaminants mostly are

confined to old concrete surface, and therefore there is minimal contamination of the harmful substances in bulk of recycled construction materials. Also in other situations, a potentially harmful contaminant could be found but they could be potentially insoluble by water, and as such they will be harmless within recycled aggregate concrete.

2.2.5.2 Percentage and Properties of Recycle Concrete Aggregates

In view of possible large dissimilarity in the properties between Recycled Aggregates (RA) and Natural Aggregates (NA), the use of waste concrete-derived aggregates to form new concretes mixtures implies a thorough knowledge of the properties of the aggregates. The quantity and quality of cement mortar applied to the recycled aggregate grains is one of the main factors that impact these variations (Malešev et al., 2014). According to the study by Maleev et al. (2014), recyclable coarse aggregate tends to match the desired gradual need of natural aggregates, but the recycled fine aggregate may likely need corrective measures in composition since usually, it contains oversized grains which could not conform to the standards set to natural aggregates standards.

RCA tends to consume a greater amount of water in mix design to obtain comparable workability to normal concrete due to the propensity of RCA to absorb large amounts of water (Shima et al., 2005). Also, recycled aggregates are likely to enhance drying shrinkage, creep and water permeability and decrease compressive strength relative to natural aggregate concrete. The magnitude of such effects depends on the percentage of recycled aggregates incorporated, and both the strength losses can reach between 10 and 30 % (Malešev et al., 2014). These trade-offs are important to be considered when amending mix designs in order to attain an optimum performance and durability.

The mixture with recycled aggregates is placed in fresh mixture in a wet but not in a saturated form to control the characteristics of materials and maintain consistencies. The method allows regulating the effective water-to-cement (w/c) ratio and minimizes strength variation as well as improves concrete performance (Zhu et al., 2013). Although recycling aggregates is an environmentally sustainable construction practice, desired outcomes can only be achieved through profile balancing of the mix design and stringent quality requirements to ensure the sound structure of the end product.

Velay-Lizancos et al. (2018) addressed the issue of fine aggregate replacement in mixtures containing RCA at concentrations of 0%, 20%, 35% and 50%, and Tables 2.8 and 2.9 summarized the process particle size to concrete mix design. This confirms the notion that RCA are a perfect option to come up with concrete that is of a standard quality and environmentally friendly. Chandru et al. (2023) also pointed out that fine natural aggregates include 30 % reduced embodied energy and 60 % reduced carbon emissions. However, using recycled fine concrete aggregates offers several environmental advantages and additional benefits.

Table 2.7
Particle Size Distribution, Particle Density and Water Absorption

Property	NA 0/2.5	NA 0/5	NA 6/12	RA 0/12
% passing 0.063 mm (%)	1.94	1.49	0.43	3.61
% passing 4 mm (%)	100	100	3.72	40.64
Apparent particle density (Mg/m^3)	2.79	2.90	2.62	2.55
Oven dried particle density (Mg/m^3)	2.74	2.88	2.55	2.21
Saturated surface dried particle density (Mg/m^3)	2.76	2.88	2.58	2.34
Water absorption (%)	0.67	0.30	1.04	6.06

Source: (Velay - Lizancos et al., 2018)

Table 2.8
Mix design for Mortar Concrete

Component	M-0	M-20	M-35	M-50
Cement (kg)	335	335	335	335
Filler (kg)	320	320	320	320
NA 0/2.5 (kg)	370	370	370	370
NA 0/5 (kg)	510	375	273	172
NA 6/12 (kg)	810	607	455	303
RA 0/12 (kg)	-	338	592	845
Superplasticizer (kg)	5.4	5.4	6	6
Effective water / cement ratio (m^3)	0.5	0.5	0.5	0.5
Volume (m^3)	1.000	1.009	1.015	1.022

Source: (Velay - Lizancos et al., 2018)

Meanwhile, Quanmin et al. (2018) investigated the RCA percentages of 0%, 30%, 50%, 70% and 100% in production of mortar. Mix proportions are listed Table 2.10 and the basic properties are list in Table 2.11. In Mirjana et al. (2010), have different view in distribution of the RCA and focus on the differentiation between the 0%, 50%, and 100%. Table 2.12 to Table 2.13 are the compilation of the process for the

mix design for materials that be need in mixture concrete and end with the design of the amount of the aggregate fractions. Table 2.14 indicated the design mixture of the study from Mirjana et al. (2010) as the percentages of the replacement RCA into natural fine aggregates.

Table 2.9
Basic Properties of Coarse Aggregate

Coarse aggregate type	Size (mm)	Apparent Density (kg/m^3)	Bulk Density (kg/m^3)	Crushing Value (%)	Water Absorption (%)
Natural coarse aggregate	5-31.5	2857	1430	4.21	0.47
Recycled coarse aggregate	5-3.15	2500	1290	16.46	3.96

Source: (Quanmin et al.,2018)

Table 2.10
Mix Proportion of NCA and RCA

Replacement percentage	w/c	Amount of material (kg/m^3)				
		Cement	Sand	NCA	RCA	Water
0	0.45	411	631	1173	0	185
30%	0.45	411	631	821	352	199
50%	0.45	411	631	587	586	208
70%	0.45	411	631	352	821	218
100%	0.45	411	631	0	1173	231

Source: (Quanmin et al., 2018)

Table 2.11
Design Quantities of Component Materials

Concrete mixture	Cement (kg/m^3)	Effective water (kg/m^3)	Aggregate (kg/m^3)	Additional water (kg/m^3)	Effective water cement ratio	Total water cement ratio	Bulk density (kg/m^3)
R0	350	180	1857	0	0.514	0.514	2,387
R50	350	180	1816	19	0.514	0.569	2,365
R100	350	180	1775	37	0.514	0.620	2,343

Source: (Mirjana et al., 2010)

Table 2.12
Percentage Participation of Each Aggregate Fraction in Aggregate Mixture

Concrete type	Natural river aggregate (kg/m^3)				Recycled concrete aggregate (kg/m^3)		
	0/4	4/8	8/16	16/32	4/8	8/16	16/32
R0	33	16	21	30	0	0	0
R50	33	8	10.5	15	6.5	7.5	19.5
R100	33	0	0	0	13	15	39

Source: (Mirjana et al., 2010)

Table 2.13
Design Amounts of Different Aggregate Fractions

Concrete mixture	Content of natural river aggregate (kg/m^3)				Content of recycled aggregate (kg/m^3)		
	0/4	4/8	8/16	16/32	4/8	8/16	16/32
R0	612	298	390	556	0	0	0
R50	600	145	191	272	118	136	354
R100	586	0	0	0	231	266	693

Source: (Mirjana et al., 2010)

This chapter provides a concise overview of the key properties of RCA and concrete produced using RCA, based on findings from Mirjana et al. (2010) and available experimental data. When concrete is demolished and crushed, some of the original mortar and cement paste remains adhered to the stone particles within the recycled aggregate. This residual mortar largely contributes to the lower quality of RCA compared to Natural Aggregate (NA).

In a separate study by Prakash et al. (2022), the impact of partially replacing natural coarse aggregate with RCA in high-strength concrete was examined. A total of eighteen concrete mixes were prepared with varying RCA replacement levels of 0%, 20%, 40%, 60%, 80%, and 100%, while maintaining water-to-cement (w/c) ratios of 0.45 and 0.50. The specific mix proportions for these trials are presented in Tables 2.15 and 2.16. Drawing inspiration from Prakash et al. (2022), two experimental series were developed: EPRCA0 and EPRCA30. Both series incorporated Ordinary Portland Cement (OPC), eggshell powder (ESP), and silica fume (SF), while the inclusion of recycled concrete aggregate (RCA) was varied to isolate and evaluate the strength and performance contributions of ESP.

Table 2.14
Mix Proportions (kg/m^3) Series I

Mix-ID	Water	Cement	w/c	NFA	NCA	RCA	Super-Plasticizer
A_0	197.00	366.00	0.50	665.00	1140.00	00.00	1.50
A_{20}	197.00	366.00	0.50	665.00	912.00	228.00	1.50
A_{40}	197.00	366.00	0.50	665.00	684.00	456.00	1.50
A_{60}	197.00	366.00	0.50	665.00	456.00	684.00	1.50
A_{80}	197.00	366.00	0.50	665.00	228.00	912.00	1.50
A_{100}	197.00	366.00	0.50	665.00	0.00	1140.00	1.50

Source: (Prakash et al., 2022)

Table 2.15
Mix Proportions (kg/m^3) Series II

Mix-ID	Water	Cement	w/c	NFA	NCA	RCA	Super-Plasticizer
B_0	184.50	381.00	0.55	670.00	1132.00	00.00	1.50
B_{20}	184.50	381.00	0.55	670.00	905.60	226.40	1.50
B_{40}	184.50	381.00	0.55	670.00	679.20	452.80	1.50
B_{60}	184.50	381.00	0.55	670.00	452.80	679.20	1.50
B_{80}	184.50	381.00	0.55	670.00	226.40	905.60	1.50
B_{100}	184.50	381.00	0.55	670.00	0.00	1132.00	1.50

Source: (Prakash et al., 2022)

Numerous study papers have highlighted that replacing fine aggregates in concrete with a percentage of RCA tends to reduce the strength of structural elements. However, studies focusing on the behaviour of recycled fine aggregates from CDW as a substitute for natural fine aggregates are relatively limited, especially when compared to those on recycled coarse aggregates (Chandru et al., 2023). As a result, there are restrictions on its use, and the construction industry has been cautious about adopting RFA. Upon replacing the natural sand by about 30% in crushed rock incorporated concrete, the percentage increase in the compressive strength was around 6.2%. Further increasing the replacement level of sand by 50, 70, and 100% resulted in declined compressive strength of crushed rock incorporated concrete by roughly 0.17, 16.87, and 24.51%, respectively (Chandwani et al., 2016).

Although individual elements or concrete cubes can be tested in controlled experiments, applying such replacements in real-world construction carries significant risks. Compared to NA, RCA exhibit several distinct properties: higher water absorption, lower bulk density, reduced specific gravity, greater abrasion loss, increased crushability, more dust particles, and potentially higher levels of organic impurities especially if the concrete was mixed with soil during demolition. Additionally, the RCA potentially contain harmful chemical substances depending on the conditions of the building from which it was sourced.

As RCA had different of percentages, the suitable of the study RCA percentage is 30%. Since, the materials that were used in the study is combination of organic waste from eggshell powder replaced cement and inorganic waste from RCA replaced fine aggregates.

2.2.5.3 Application of Recycled Concrete Aggregate (RCA)

A study by Kawai et al. (2014) highlighted Japan's advancements in developing cutting-edge production technologies for manufacturing high-quality Recycled Concrete Aggregate (RCA). These innovations have facilitated the integration of RCA into construction applications, promoting sustainability in the industry. Two key technologies have emerged in this sector. The first enables the use of mid-quality recycled fine aggregate in building superstructures. While its quality potentially not match that of conventional fine aggregate, it has been successfully incorporated into RCA. To assess its viability, a trial application was conducted where this mid-quality recycled fine aggregate was used in an upper building structure.

Further developments were also recorded by Yoda et al. (2014) who developed a technology tailored towards high quality production of recycled fine aggregate. This high-quality recycled aggregate, unlike mid-quality that is used in ordinary buildings, matches the tough demands that are required in nuclear power plants so that the facility is safe and long lasting even in highly specialized areas.

In Canada, RCA use has been acceptable in most of the sectors in construction. The RCA finding common use is in pavements, granular and lean concrete subbases and soil-cement mixtures. As it has become clear that it has great potential, the Canadian Standards Association (2014) update its standards to allow the use of RCA in unrestructured contexts, including sidewalks, curbs, gutters, and fill materials not shrinkable, which makes it a possible alternative to construction projects of low risk. Japan and Canada have gone a long way by implementing the RCA method in their constructions, and this is indicative of the trend of the world that is reducing it practices in construction to building sustainably. By focusing on the technologies required in mining mid- and high quality recycled fine aggregates, Japan has already taken the lead in applying them not only to conventional buildings but nuclear plants as well (Hideo et al., 2019). In the meantime, Canada has incorporated RCA in different areas of construction revising the regulations to assist in non-structural applications. The same gains in these advancements demonstrate the further embrace and use of recycled materials that solidify their environmental and structural advantage in contemporary infrastructure development in different parts of the world.

2.2.6 Summary on The Use of Eggshell Powder, Silica Fume and Recycled Concrete Aggregate (RCA) in Mortar.

The study of sustainable building techniques has resulted in new approaches to material development. One possible involves the use of RCA and ESP in ICB. Mechanical performance is an important factor to consider when choosing materials for ICBs. When treated and integrated properly, RCA increases the total compressive strength of the concrete. In addition, because of their high calcium carbonate concentration, ESP has the potential to increase strength and durability, providing a synergistic impact. Kumar and Vasanthi (2022) conducted compressive testing using ESP as one of materials for paver blocks and find out the result of the compressive strength was improved with the increasing amount of ESP in the blocks. The combined impact of RCA and ESP potentially go beyond strength, positively improving the structural integrity of interlocking blocks and promising increased robustness and durability. The synergy of RCA and ESP enables mix design optimization, which is essential in generating a balanced and effective construction material. Many researchers also found out that careful balance of cement, water, and aggregates creates a harmonious combination that takes advantage of the mechanical advantages of both materials.

2.3 Review on The Design of Interlocking Block (IB)

Figure 2.8 depicts the connections between keywords in study publications centring on the utilization of interlocking block. A substantial number of publications, totalling 367, have been documented from 1969 to 2023. The network graph highlights growing research on interlocking concrete blocks (ICBs), showing how they connect to various themes in construction. The green cluster focuses on material properties like compressive strength, water absorption, and aggregates, reflecting performance optimization. The red cluster links ICBs to construction techniques, grouting, and structural partitions, emphasizing practical applications. The blue cluster relates to pavement, infiltration, and runoff, showing ICBs' role in environmental and drainage systems. The yellow cluster includes structural design and concrete pavements, pointing

to engineering and layout considerations. Thus, these clusters confirm ICBs' interdisciplinary relevance in sustainable, structural, and hydrological research.

Upon closer scrutiny and focusing on a narrower context, as demonstrated in Figure 2.9, the publications specifically addressing interlocking blocks in structural building amount to 119 from 1983 to 2024. The directed graph illustrates the complex and interdisciplinary nature of concrete systems research, with color-coded clusters representing distinct thematic areas. The red cluster focuses on construction techniques and structural applications such as grouting and partition walls, while the orange and yellow clusters highlight structural design and pavement engineering, reflecting the integration of concrete into infrastructure planning. The green cluster centres on material properties like compressive strength, water absorption, and aggregate behaviour, indicating ongoing efforts to optimize mix performance. Meanwhile, the blue cluster connects concrete to environmental aspects such as infiltration and runoff, showing its role in hydrological systems. These interconnected nodes and directional links reveal how concrete research has evolved to encompass sustainability, performance, and multifunctional design. Bibliometric studies by Zhou et al. (2020), Mohamed et al. (2025), and Benaicha et al. (2024) support this visualization, confirming that concrete innovation spans civil engineering, materials science, and environmental design. Despite being beyond the scope of structural building, the number of publications related to interlocking blocks is relatively low. Therefore, there is an opportunity for further study and the development of new designs for commercialization.

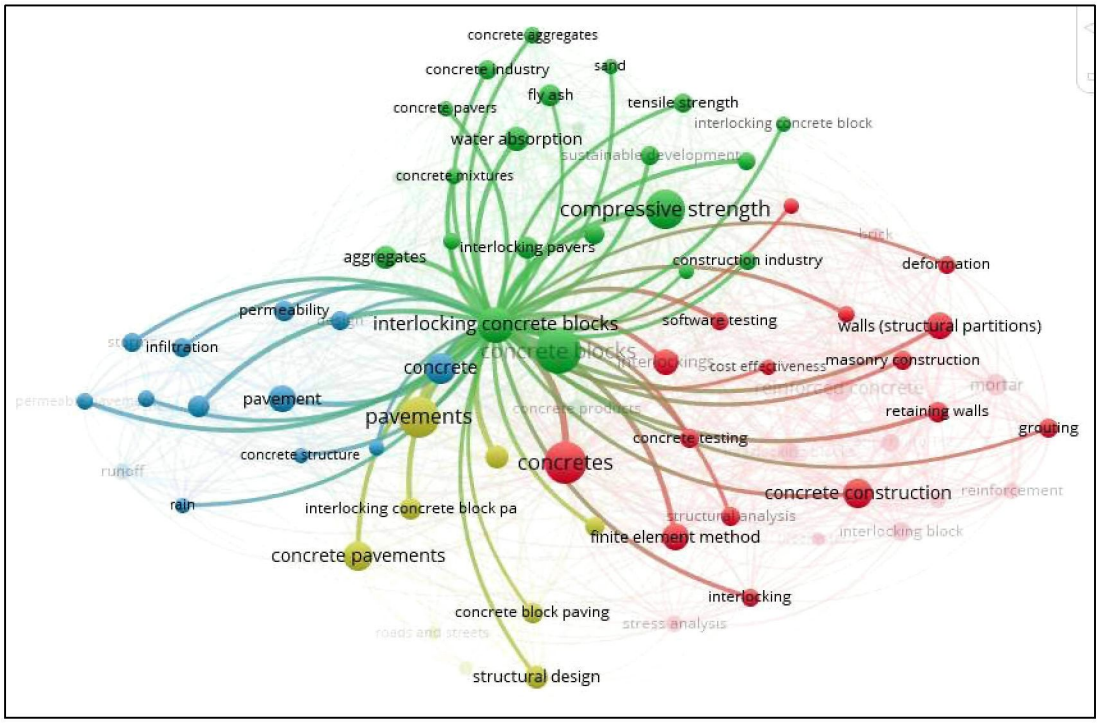

Figure 2.8 Relation of Keywords in Paper Publications of Interlocking Block

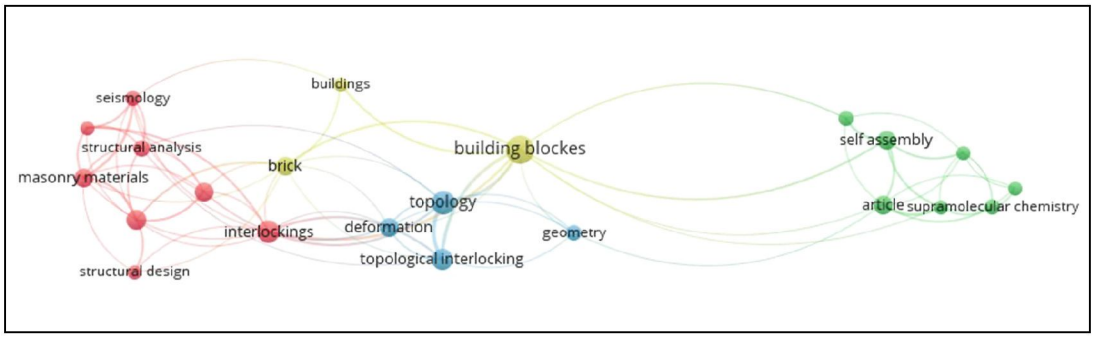

Figure 2.9 Relation of Keywords in Paper Publications of Interlocking Block of Structure Building

2.3.1 Background of Interlocking Block (IB)

Study from Tang et al. (2014) about said that the residual compressive and shear strengths of innovative "Coconut Fiber Reinforced Concrete" (CFRC) interlocking blocks were tested under dynamic loading. The investigation found that the CFRC interlocking bricks have appropriate residual capacity after being subjected to dynamic stresses and storing them for 15 months.

Furthermore, Nanang et al. (2017) mentioned Indonesia, in a nation experiencing ongoing population growth and economic advancement, there is a significant rate of resource consumption. According to the Central Bureau of Statistics, the value of completed construction projects in 2015 surpassed Rp. 635 trillion. A recent projection by PT Semen Indonesia (Persero) TBK suggests that national cement consumption in 2017 will reach 68 million tonnes, marking an 8.04% increase from the previous year's consumption of 62.94 million tonnes.

In Indonesia, red bricks are widely utilized in construction due to their prevalence and suitability for earthquake-prone regions. However, in response to environmental concerns and the imperative for sustainable resource management, there is growing demand for alternative brick types. One potential solution being explored is hollow core concrete bricks manufactured from a blend of sand and stone ash. These bricks are being assessed as alternative wall materials, with considerations including weight, load capacity, installation duration, and cost (Azizi et al., 2017).

2.3.2 Design of Interlocking Block (IB)

Interlocking blocks will usually be single item, that is the concrete block itself, often precast and produced in a particular shape and size to interlock. Nonetheless, not all interlocking concrete block systems are guaranteed to include any extra parts to expand functionality or make installation easier. The different materials and designs consist of these blocks that can be prepared in solid or hollow configuration and enable better performance and functionality.

The choice of constituents of the production of interlocking concrete blocks also depends upon the purpose and the necessity generated in it. This paper looks at the new design, which is characterized by appropriate joint and is interconnected to compose walls or structures. The block will consist of vacuums or ethers in the material and was made such that it is interlocking on both the top and the bottom so that they can fit firmly. There are many variations in the interlocking blocks design and concrete used to construct them.

The hollow inside the blocks serves multiple purposes, such as reducing block weight, providing insulation, accommodating reinforcement bars or utilities (e.g., electrical or plumbing conduits), or allowing for grout or concrete fill to enhance

strength and stability. The interlocking design ensures a tight and secure connection between blocks, minimizing the need for mortar or other binding agents during construction. This design offers easy installation, flexibility, and potential for rapid construction.

Additionally, various patented interlocking systems are already available in the masonry brick market. Solid block systems include, to name a few, hydra-form interlocking blocks. Figure 2.10 and Figure 2.11 provide examples of the interlocking blocks. Bricks with an interlocking design were found to be less expensive to make than ordinary bricks, as well as less expensive to build with, taking less time to complete.

Additionally, an advantage of utilizing interlocking masonry blocks is the ability to construct lined walls through dry stacking. The study examined the faster construction process and cost-effective materials. According to findings, it takes only 9 minutes and 50 seconds to build a 1 m by 1 m wall panel using pulverized EPS interlocking blocks, compared to 28 minutes and 5 seconds for conventional bricks without an interlocking system. This significant reduction in construction time offers a substantial advantage in reducing workload and expediting project completion (Harries et al., 2016).

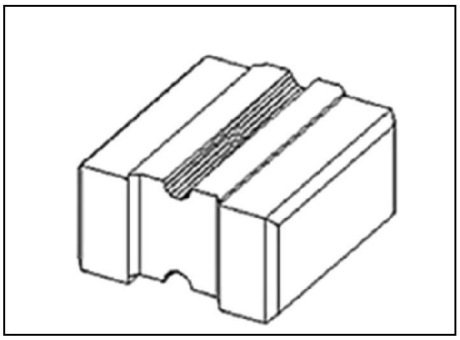

Figure 2.10 Hydraform Interlocking Block
(Source: Chen et al., 2022)

Figure 2.11 Azar Interlocking Block Model
(Source: Chen et al., 2022)

2.3.2.1 Design of Solid Block

Figure 2.12 illustrates the shape and geometry of our innovative interlocking brick, which is 25 mm thick and 50 mm x 50 mm in size. The plate made from the new bricks has the dimensions 400 mm x 400 mm x 25 mm and is depicted in Figure 2.13(a). In the new design, each brick's out-of-plane movement is limited by its four adjacent bricks through the bricks' four lined side surfaces. The brick's symmetrical arrangement could result in identical mechanical behaviour on all four sides (Javan et al., 2016).

Javan et al. (2016) proposed a novel orthomorphic brick design with the objective of surpassing conventional brick configurations in terms of dynamic energy absorption. The term orthomorphic is derived from ortho (meaning straight, correct, or aligned) and morphic (meaning form or shape), suggesting a structural geometry that maintains orthogonal alignment such as straight edges and right angles while being modified to achieve enhanced performance. Within engineering applications, orthomorphic designs are often developed to balance symmetry and load distribution, which served as the primary inspiration for this research in advancing interlocking block innovation.

Building upon recent developments in interlocking brick technologies, this work introduces a revised orthomorphic configuration intended to improve structural resilience under impact and vibration conditions. In this design, the brick's four sides are interconnected, while two additional lined surfaces are incorporated to facilitate load transfer. Unlike conventional rectangular bricks, orthomorphic bricks are engineered to optimize stress distribution and maximize dynamic energy absorption, particularly when subjected to external loading.

This approach studies on innovative brick geometries. For example, Rao and Chandar (2021) explored energy-efficient organic bricks incorporating industrial by-products, demonstrating how alternative geometries and sustainable materials can enhance both mechanical strength and environmental performance. Inspired by these advances, the present research emphasizes the integration of balanced symmetry and load distribution in the orthomorphic brick design, while simultaneously promoting sustainability using waste derived materials.

In addition, a comparative assessment was carried out between the newly developed brick, and the conventional brick. Figure 2.13(b) illustrates the top and bottom surface configurations of both the new and old interlocking assembly plates from Javan et al. (2016). The plate formed with the new brick design features identical patterns on both faces, whereas the plate constructed with the older brick design exhibits distinctly different surface arrangements.

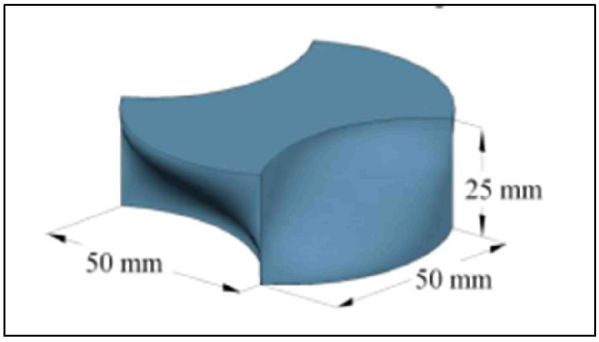

Figure 2.12 Sketch of The Proposed New Brick with Four Lined Side Surface (Source: Javan et al., 2016)

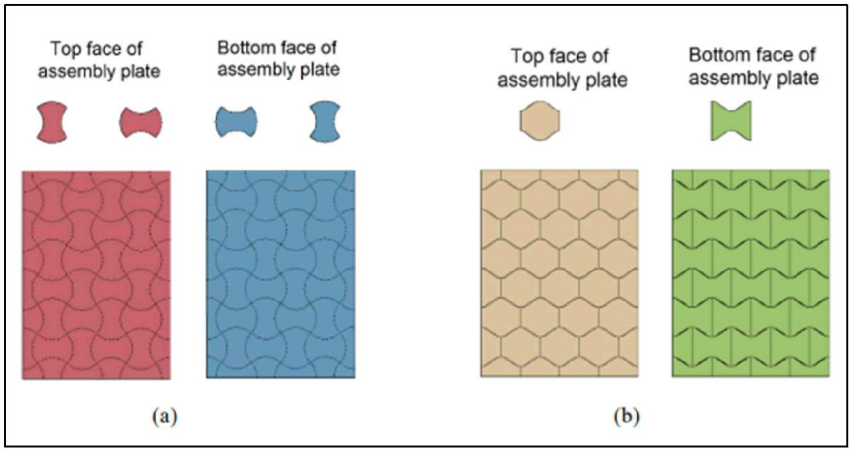

Figure 2.13 Top and Bottom Patterns of The Design; (a) New Interlocking Assembly Plate, and (b) Existing Interlocking Assembly Plate.
(Source: Javan et al., 2016)

2.3.2.2 Design of One Hollow Interlocking Brick

Over the years, a variety of interlocking block and brick types have been developed, each featuring differences in material composition, size, and shape tailored to specific strength requirements and applications. These variations encompass considerations such as weight, load-bearing capacity, shear resistance, shape, manufacturability, integration of vertical and horizontal reinforcement stabilizing ties, and effectiveness of the interlocking mechanism under imposed loads.

In Malaysia, the Putra Block was developed, an interlocking hollow block designed for load-bearing masonry systems. These blocks are stacked vertically and feature 3D projections to facilitate interconnection. A total of twenty-one various block models were constructed and tested, factors such as weight, load-bearing capacity shear area, shape and simplicity in production, compatibility with vertical and horizontal reinforcing ties, and the usefulness of the interlocking mechanism when under loaded were considered during the experiment. This methodology led to a prompt, efficient and an accurate construction process.

Not in the least, another two interlocking blocks in Malaysia (based on the LEGO design) have been created by Al-Fakih et al. (2017) (Figure 2.14). At Universiti Putra Malaysia, the individual units and wall panels under different loads have been experimentally tested, which demonstrate that the blocks have the compressive strength, which is compliant with the Malaysian standards. This new type of block system is effective to build strong and secure two-level building (Al-Fakih et al., 2017).

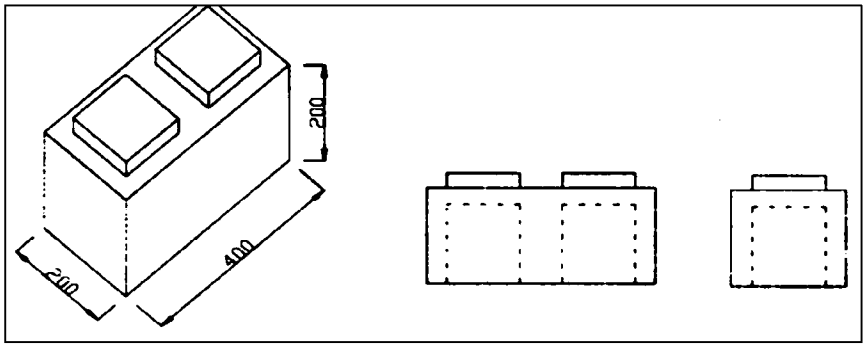

Figure 2.14 Interlocking Hollow Block System
(Source: Al-Fakih et al., 2017)

Nanang et al. (2017) tested these bricks as an alternative to the walls in terms of weight load, time installation, and cost. Figure 2.15 modified the 2-cm trapezoidal notch model to also include a 2-cm rectangular notch model and 3- and 3.5-cm trapezoidal notch models. The mix proportion was: 25:75 sand and stone ash. Existing studies underline the reference of the mentioned wall specimens that have been tested in both out-of- and in-plane load factors 90 x 45 cm 2 and 60 x 60 cm 2, respectively (Nanang et al., 2017).

The design of interlocking mechanism in hollow core concrete bricks as shown in Figure 2.16 will need further research in terms of flexural strength and wall failure mode. Research by Akhtar and Malkawi (2025) explored the incorporation of composite waste as a partial material replacement in the production of concrete hollow blocks, while Tañedo et al. (2023) examined the use of bamboo fibre and recycled concrete fine grains as alternatives to natural sand. Building on these studies, previous work has evaluated hollow core concrete bricks made from sand and stone ash mixtures, particularly in terms of weight, load-bearing capacity, construction efficiency, and overall cost. In continuation of this research direction, the present study focuses on refining the notch configuration to enhance the performance of the interlocking mechanism.

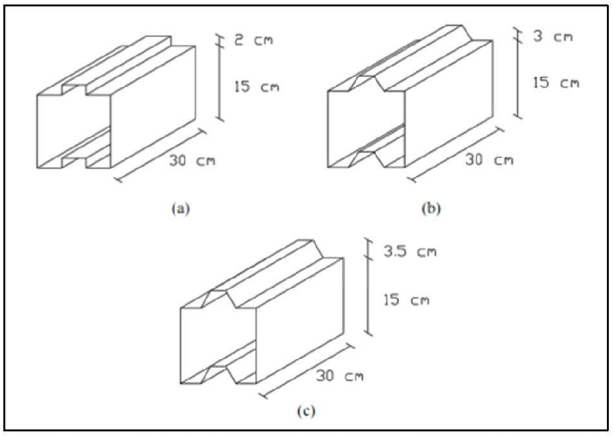

Figure 2.15 Hollow Core Brick Mould; (a) 2-cm Square Notch, (b) 3-cm Trapezoid Notch, (c) 3.5-cm Trapezoid Notch
(Source: Nanang et al., 2017)

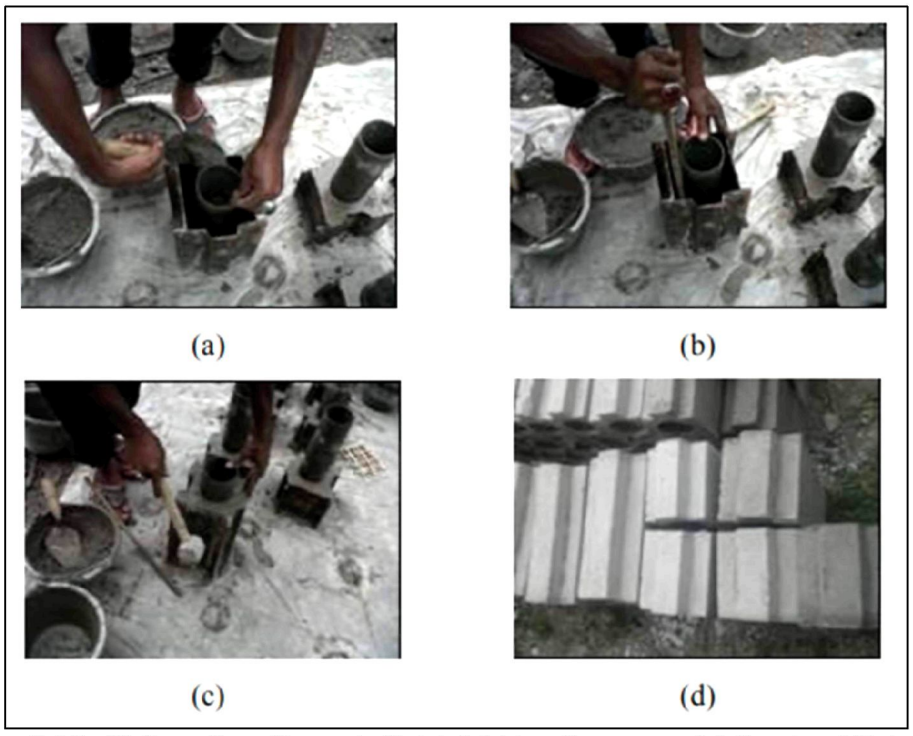

Figure 2.16 Hollow Core Concrete Brick Making Processes; (a) Pouring Mixture to The Mould, (b) Solidifying the Mixture, (c) Hitting the Surrounding Outer Part of The Mould, (d) Hollow Core Concrete Bricks
(Source: Nanang et al., 2017)

2.3.2.3 Design of Two – Hollow Interlocking Concrete Blocks

In according to Calderon et al. (2020), the strength and width of the blocks, the aspect ratio of the wall, the proportion of vertical and horizontal reinforcement, and the presence of flanges (transversal edge features) were the design variables that were examined. Masonry wall panels with a height of 2270 mm were constructed using Hollow Concrete Blocks (HCB) that were 390 mm long, 190 mm high, and 140 mm thick (Figure 2.17(a)). The majority of the wall panels were vertically reinforced with four 22 mm steel rebars and horizontally reinforced with ladder-type reinforcement made of two longitudinal steel bars of 4.2 mm in diameter in every mortar bed-joint.

To ensure uniform displacement at the top of the specimens and proper anchorage for the vertical reinforcement, capping beams measuring 350 mm thick and 600 mm tall were cast. These design specifications were consistent across the other walls, except for the specific design variable being studied in each case. Figure 2.17(b) illustrates a block that exhibited greater compressive and tensile strength than the base blocks, although the external dimensions remained the same, with slight variations in internal geometry between blocks B14 and G14.

Further details on the material properties of the units are provided in the following sections. Edge elements, which were 190 mm thick and 615 mm long, were created using the same HCBs of 190 mm width (Figure 2.17(c)) as those used in Wall HCBW3. A running bond, along with horizontal reinforcement extended into the edge elements, was employed to securely connect the in-plane masonry panel to the edge components.

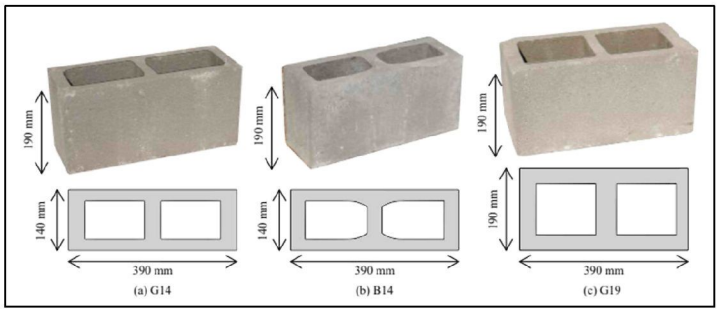

Figure 2.17 Top and Bottom Patterns of; (a) New Interlocking Assembly Plate, and (b) Existing Interlocking Assembly Plate.
(Source: Calderon et al., 2020)

Other than that, Chen et al. (2022) outlined a process for making concrete where sand and cement are first mixed in a concrete mixer, followed by the addition of water until a cohesive cement mortar is achieved. Recycled Expanded Polystyrene (EPS) beads and kenaf fiber are then gradually added to the mixture, ensuring thorough integration for a uniformly distributed cement mortar. The remaining sand and water are incorporated and blended to create a homogeneous slurry.

To enhance the mixture's workability while reducing the water requirement, a superplasticizing additive is included. The leftover recycled EPS beads and pre-treated kenaf fiber are mixed in until fully integrated. Once the mixture is uniform, it is poured into a selected mold and manually compacted to prevent the EPS beads from rising to the surface. Figure 2.18 illustrates the conceptual design of the interlocking block proposed by Chen et al. (2022).

After 24 hours, the concrete samples are demoulded and placed in a water curing tank, following the guidelines of ASTM C192. In total, 15 cube specimens (100 x 100 x 100 mm) are prepared for compression testing, 15 cylindrical specimens (100 mm diameter x 200 mm length) for tensile testing, and 15 beam specimens (100 x 100 x 500 mm) for flexural strength testing.

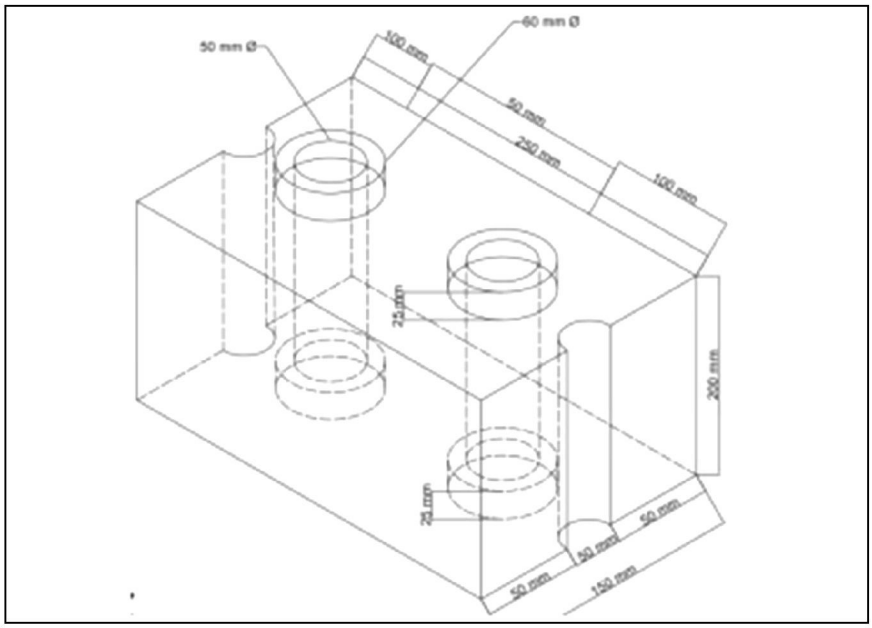

Figure 2.18 Conceptional Design of Interlocking Block
(Source: Chen et al., 2022)

2.3.3 Application of Interlocking Block (IB)

The masonry systems date as far back as 8000 B.C. when sun-dried clay bricks were used in constructions revealing the timeless relevance of the systems in the history of constructions. Despite their structural potential, there is a necessity to continue implementations and upgrading to modernize such systems. Changing design principles and revised building regulations have also supported the use of masonry into greater variety of structural constructions in many countries. The change has given a rise to new construction methods like the Interlocking Loadbearing Hollow Block (ILHB) method (Bosro et al., 2018). Several innovative interlocking load-bearing brick (ILHB) configurations have emerged, including Interlocking Stabilized Soil Blocks (ISSB), Hydraform, Auram, Haener, Sparlock, Mecano, and Sparfil (Al-Fakih et al., 2018). These designs were introduced by researchers as alternative solutions aimed at addressing limitations and challenges identified in earlier interlocking brick systems.

The use of masonry techniques has been used so broadly and at different levels of scale over the span of centuries, beyond buildings and in the case of monuments and infrastructure construction. With both structural functionality and beauty, masonry has frequently led to heritage building. Hollow block technology became popular in Malaysia during the 1970s 80s in Taman Sri Kemuning in Jitra, Setapak Jaya in Kuala Lumpur and Selayang Utara/Selatan (Hendry and Khalaf, 2001; Ahmad et al., 2014). There exist numerous buildings made in the traditional masonry techniques and many of those structures still survive and have been put under national heritage status. Due to their performance and their conformance to international standards, masonry systems became approved and codified into the Uniform Building By- Laws in 1989.

The past decades witnessed the striving to perfect ILHB systems around the world. In Canada, Juan Haener established the Haener block system in 1994 using concrete in building load bearing walls (Cetholic 1988 Mortarless Masonry, 1988; Oh, 1994). More innovation was witnessed with Mecano block that was developed by Cetholic in Peru in 1988 and lacked the interlocking concept and employed sand-lime as its primary material (Jaafar et al., 2006). These masonry blocks are placed in dry stack, to create walls, using varied structural methodologies.

The ISSB system was introduced in 1967 in Thailand by the Thailand Institute of Scientific and Technological Research (TISTR) which is a long-term solution to

house construction. Such blocks consist of the local soil, loam, or earth that is modified with low cement content and then pressed by equipment that is not complicated (Bredenoord et al., 2019). They are used to encourage green construction procedures instead of fired clay or standard concrete blocks. Homes constructed through simple procedures, with local raw materials accessible, can be constructed by community members themselves (Bredenoord, 2017) further minimizing the building cost and building time.

ISSB technology meets a wide variety of housing requirements- low-cost/high income (Janbunjong, 2019). Since Thailand needs affordable housing, ISSB can be applicable to the social programs of encouraging self-build projects. According to Kokkamhaeng (2019), ISSB has substantial potential in the rural areas and in small towns and provides sustainable and durable community infrastructure products. The technology was successfully implemented in building homes, schools, and other buildings and now SMEs have risen to implement the use of the technology in the areas it is most required.

Fabrication of Interlocking Recycled Concrete Blocks (IRCB) using RCA as an alternative to the conventional concrete systems is a viable knot that can underscore the management of concrete waste (Aswad et al., 2022). IRCBs are made to be affordable and within reach of the populations in developing regions, therefore, reducing the level of labor force, as well as the duration of installation. These blocks are very flexible both in structural and non-structural applications, can be used in pavements, in temporary roads, and in such structures as columns and walls. IRCBs have a dry-lay system, it has utility channels embedded in it, and dual-directional design beauty, and it has better insulation and earth resistance.

According to a study by Sabai et al. (2013) on the possible use of 100 recycled aggregate in concrete blocks in Tanzania and the results were similar and lower than the natural aggregate mixes with findings similar to those of a study in Hong Kong. Ganesh & Lokeshwaran (2017) experienced the idea of enhancing the performance of loadbearing walls with the help of new designs of interlocking blocks. In their study, three important approaches were brought up: First, 20-35% RCA replacement ratios will maximize the strength of any structural application. Second, incorporating pozzolanic materials containing silica can boost strength by approximately 23% after

28 days. Third, advanced treatments like calcium carbonate bio-deposition may increase strength by up to 40%, though such methods may be cost-prohibitive and unsuitable for large-scale deployment (Shaban et al., 2019).

2.3.4 Material for Production of Interlocking Block (IB)

Interlocking bricks, traditionally made from clay, are designed to fit together without the use of mortar by employing a shear key and lock mechanism, resembling puzzle pieces in assembly. These bricks commonly consist of a blend of cement, sand, and stone dust, measured and mixed in precise ratios to ensure material uniformity. Various types of interlocking blocks have been developed based on raw material availability, such as soil-cement blocks, rice husk ash cement blocks, and concrete blocks. For soil-cement blocks, the cement-to-soil volumetric ratio typically ranges from 1:6 to 1:10, whereas rice husk ash cement blocks use a 1:4 ratio. Concrete block mixes conventionally follow a 1:5:3 ratio for cement, sand, and gravel, respectively. In current formulations, interlocking bricks contain 29% sand, 2% water, 12% cement, and 57% subsoil.

To enhance environmental sustainability, several manufacturers incorporate recycled materials into the production of interlocking concrete blocks. For example, recycled concrete rubble is used instead of virgin stone aggregates, thereby minimizing material consumption and reducing construction waste. These blocks are versatile and can be utilized for retaining walls, walkways, and erosion control structures, with modularity allowing flexible adaptation for diverse construction needs.

In laboratory settings, concrete batching is performed using weight-based measures. A mix ratio of 1:2 was employed, where 20% of the sand content was substituted with crushed ceramic waste, and variable amounts of waste plastic fibres were randomly incorporated. A control batch, which excluded ceramic waste and plastic fibre, was prepared for comparison. All mixes complied with ASTM C94/C94M-20a standards to ensure methodological consistency.

Chen et al. (2022) stated that interlocking concrete blocks should consist of minimum performance standards that demand the compressive strength of no more than 5 N/mm² and 7.5 N/mm² of cubes established in construction-grade uses. Lately in the developments, materials used to give desirable strength and thermal conductivity have

included Expanded Polystyrene (EPS), Rice Husk Ash (RHA) and natural fibers to the interlocking blocks.

Ferriz-Papi & Thomas (2020) divide CDW management into downcycling (e.g., backfilling) and upcycling that can be defined as supporting the production of new constructional materials. Rubble recycling has burgeoned in recent decades and provides alternate sustainable products like the Interlocking Recycled Concrete Blocks (IRCB). IRCBs can be used in structural constructions, such as retaining and bearing walls and do not require mortar. Their nucleuses can be intertwined using the steel rods, consequently increasing tensile, lateral, and shear resistance. Performance outcomes could be improved by the inclusion of additive materials and industrial by-products.

Several studies that covered the mechanical behaviour of RCA-made blocks were reviewed by Guo et al. (2018). Kumar and Vigneshvar (2014) suggested new innovative patterns of masonry building units with the elements of tongue-and-groove and projection, which permitted perfect arriving and structural strength. In their blocks, fly ash (FA) was partially replaced by cement as a support of mortarless construction resistant to earthquakes, which is argued to help save up to 65 % in time, cost, manpower, and material consumption (Aswad et al., 2022).

Recycling of rubble is an increasingly popular phenomenon, where RCA replenishment ranges between 20 to 35%, all in concrete block cases. When there are additives, these rates may reach 25 to 50 % (Lee et al., 2017; Manasa et al., 2019). Mirasa & Chong (2020) and Nagaraja et al. (2017) found out that the compressive strength increased over time since it changed under the influence of block geometry and RCA source. Nonetheless, past testing data indicated that interlocking concrete blocks using RCA and additives tend to achieve a 10 – 25% decrease in compressive strength compared to a similar block produced using natural aggregates.

2.3.5 Properties of The Interlocking Block (IB)

The three-point load test is one of the tests conducted to evaluate this property so as to provide important data on the ability of the material to resist bending stresses that is essential when applying it in pavements, masonry and other structural materials. It is the standardized way of measuring the flexural strength of concrete in this three-point load test. In such a test, a concrete specimen is supported at two points and then a

load is applied in a third point in the centre of the two support points. This type of set up causes bending stress and the highest stress before the specimen breaks is measured as flexural strength.

After casting the interlocking blocks, they were immersed in an alkaline curing tank of water at 7, 28 and 90 days. This enabled the concrete to cement and become stronger because of continuous hydration. Wet weighed was difference in the dry weight which determined water absorption. Awoyera et al. (2021) point at the emerging trend of using materials derived out of wastes in the production of concrete as one method of encouraging more sustainable practices in this respect. They found out that the concrete produced with unconventional ingredients can be like conventional mixes in respect of mechanical properties as Figure 2.19 demonstrates. Considering that interlocking concrete blocks are likely to support vehicular loads, it is critical that they retain sufficient compressive strength that supports structural behaviour in the future.

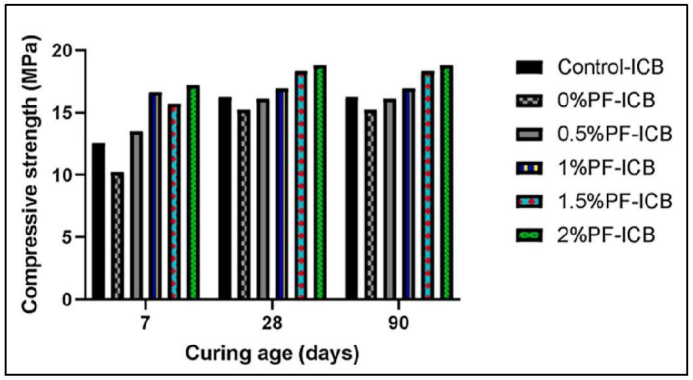

Figure 2.19 Result for Compressive Strength Test for The Curing Age (Source: Awoyera et al., 2021)

As another differentiation, the study distinguishes soil-cement blocks, Rice Husk Ash (RHA) cement blocks, and concrete blocks among various types of interlocking blocks, by material used. The cement to soil ratios in the soil-cement and RHA cement blocks all differ dependent on the properties of the soil and the cement. The ratios of the soil-cement block usually vary within 1 to 6 or 1 to 10 volumes to 1 cement volume and the RHA cement blocks have a ratio of 1 to 4 volumes. Concrete blocks, in their turn, are guided by the ratio between the dry cement, sand, and gravel of 1:5:3 (Al-Fakih et al., 2017).

Flexural strength was determined under a three-point bend in which samples have been supported at the ends with a load centred on them. The maximum uniaxial stress on the tension face at failure is the ultimate flexural strength of the material. An evaluation of RCA performance is conducted, encompassing the analysis of concrete properties in both fresh and hardened states (Kim, 2022; Şimşek et al., 2022). The experimental design consisted of two block types Two Hollow Interlocking Concrete Block (THICB) with size 360 mm x 100 mm x 100 mm and Solid Interlocking Concrete Block (SICB) that were water-cured on 7, 14 and 28 days. Testing was in accordance with BS EN 13523-7: 2001 and was carried out at a 100 kN Universal Testing Machine (UTM) with fixed support span of 270mm under each sample.

As detailed by Othman et al. (2025), the UTM was calibrated and operated under displacement control at a constant rate of 0.2 mm/min. The THICB specimens featured two 50 mm surface recesses, and deformation measurements were recorded via Linear Variable Differential Transformers (LVDTs). Based on Figure 2.20, the average maximum load recorded for 7-day cured THICB samples was 6437.26 N, corresponding to a flexural strength of 3.186 N/mm². This early performance highlights strong initial mechanical response. For 14-day curing, flexural strength assessment was repeated with three samples, yielding an increased average maximum force of 9353.01 N and a flexural strength of 3.788 N/mm², reflecting consistent progression from the 7-day results. Similar procedures were applied to samples cured for 28 days, producing an average force of 14058.63 N and a peak flexural strength of 6.062 N/mm². These findings collectively demonstrate a gradual and positive trend in flexural strength development throughout the curing timeline.

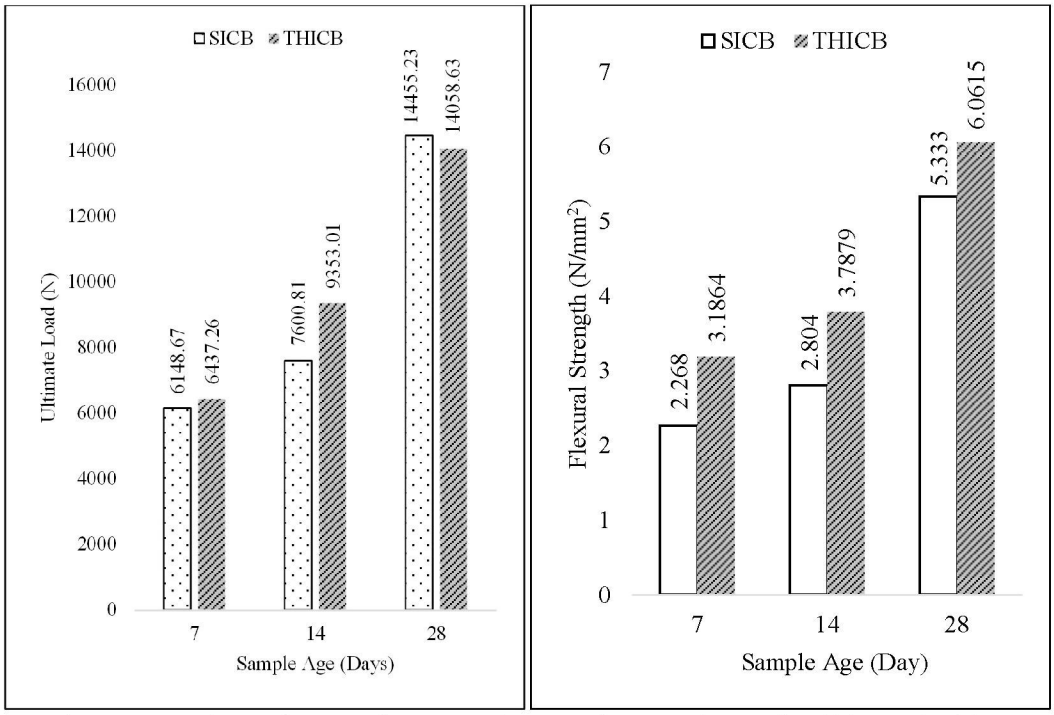

Figure 2.20 Flexural strength vs sample age of comparison of Solid Interlocking Concrete Block (SICB) and Two Hollow Interlocking Concrete Block (THICB). (Source: Othman et al., 2025)

2.3.6 Summary on The Design of Interlocking Block (IB)

Traditional fired brick production poses significant environmental concerns due to the emission of greenhouse gases during the burning process (Arif et al., 2023). Although its application in the construction sector remains substantial, the extent to which professionals are willing to implement it depends largely on their evaluation of its suitability for structural purposes (Omoregie & Imuetinyan, 2015). In alignment with the United Nations Sustainable Development Goals (SDG), particularly Goal 9, there is an emphasis on developing resilient infrastructure, advancing sustainable industrial practices, and fostering innovation. Robust and adaptable infrastructure is recognized as a cornerstone of thriving societies. Addressing future demands necessitates the modernization of industrial systems and built environments by embracing sustainable technological solutions and ensuring inclusive access to financial resources and information (UNDP, 2023). With current advancements in technology, simulation platforms and digital applications are increasingly utilized to facilitate early prediction

and validation of experimental findings (Murray-Smith, 2019; Casas, 2023; Oberkampf et al., 2022).

2.4 Artificial Neural Network (ANN) by MATLAB

The rapid expansion of the social economy has introduced new requirements and technological hurdles in the field of materials engineering, compelling the development of advanced materials with superior mechanical properties for structural applications (Ye et al., 2016; Slobodyan et al., 2023; Nagarjuna et al., 2023). Creating high-performance materials tailored to specific property requirements poses a significant challenge for metallurgical scientists, driven by escalating industrial demands and continuous technological evolution (Dewangan et al., 2023).

Moreover, various simulation approaches each with their own advantages and limitations play a vital role in the progress of materials study (refer to Table 2.19). Techniques such as First Principles Calculations, CALPHAD, and the Finite Element Method (FEM) offer detailed insights at the atomic level and enable accurate predictions rooted in fundamental science (Liu, 2009; Dewangan et al., 2023). These methods provide valuable data regarding electrical behaviour, energy profiles, and essential physical attributes. Additionally, machine learning has made a substantial impact on the field of material design by enhancing the prediction of material properties.

Table 2.16
The List of Advantages, Drawbacks, and Application Areas of Different Simulation Techniques

Simulation Method	Advantages	Drawback / Limits	Application Area
First Principles Calculation	Based on fundamental physical principles and offers precise and trustworthy forecasts.	Costly in terms of computation, especially for big systems and complicated events.	1. Included in the category of electronic properties are electronic structure, band structure, and density of states. 2. Theoretical information acquired from first principles calculations on the lattice constants, binding energy, and mixing enthalpy can aid CALPHAD modelling.

Finite Element (FEM) Simulation	Allows for the correct representation of the system by enabling the modelling of boundary conditions and macroscopic complicated geometries.	Model complexity leads to a rise in computational cost, and improving accuracy necessitates a significant investment in computing power.	1. Stress and strain distribution reveal details about the system's deformation characteristics. 2. Mechanical characteristics provide quantitative measurements of material strength, such as Young's modulus and yield strength.
Machine Learning (ML)	Machine learning accelerates the search for novel materials by using mathematical and statistical models to anticipate material qualities based on historical data. It offers forecasting models for a range of traits and occurrences.	Depends on the availability of varied and high-quality training data.	1. Phase stability prediction. 2. Thermal, electrical, magnetic, and optical qualities, as well as mechanical properties including strength and elasticity.
CALPHAD Calculation of Phase Diagram	For multi component systems, predict phase diagrams and thermodynamic features, such as solidification sequence and diffusion behaviour. Enables the alloy compositions to be optimized to attain the necessary attributes.	Relies on assumptions and empirical databases, which might cause uncertainties.	Phase diagrams and thermodynamic characteristics for multi-component systems, such as diffusion behaviour and the order of solidification.

(Source: Dewangan et al., 2023)

An Artificial Neural Network (ANN) can be fine-tuned through adequate training to become a specialized model for specific applications. Once trained, ANNs demonstrate strong predictive capabilities by learning from data sets (Hasan et al., 2024). In this study, MATLAB software is used alongside an ANN to develop predictive models. As shown in Figures 2.21, a neural network is composed of an input layer, an output layer, and multiple intermediate hidden neurons. These components are systematically connected to form a network, designed to process specific inputs efficiently, showcasing the intricate operations of neural networks (Ding et al., 2013).

Input data is relayed to the hidden layer neurons, which then pass the activated values to the output layer. One point in training a neural network with back-propagation is to minimize the error function which is implemented by a procedure referred to as the gradient descent (Amari et al., 1993). This is done by optimization of the weights to obtain least error. A supervised learning algorithm called back-propagation plays a very important role in mathematically training neural networks because the backpropagation minimizes the loss function, because of which the accuracy and efficiency of the networks are enhanced.

Normally Mean Square Error (MSE) is applied as a squared loss measure in error equation (C). MSE is a common measure used to evaluate how much error exists in a neural network. A higher MSE indicates more error, while an MSE of zero means the model has no error (Benyekhlef et al., 2021). Also, the correlation coefficient (R) will be employed to evaluate the validity of a given model on different data sets. The closer R-value is near one, the more similar is the correlation between the experimental and the data produced by the ANN model.

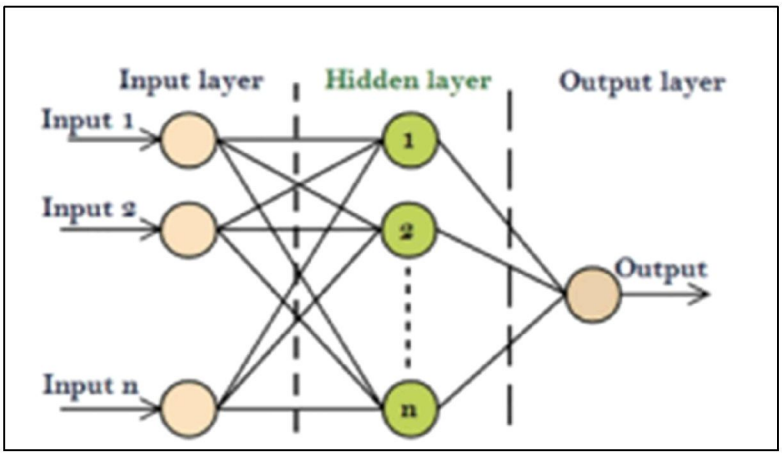

Figure 2.21 An Artificial Neural Network Architecture
(Source: Amari et al., 1993)

2.4.1 Background of Artificial Neural Network (ANN) by MATLAB

New developments in osmotically driven membrane processes like Forward Osmosis (FO) and Pressure-Retarded Osmosis (PRO) have given them an additional standing as the future candidate processes that could offer the clean energy, food, wastewater treatment processes, and desalination (Singh et al., 2024). Parallel to these

technological advancements, a model of Artificial Neural Network (ANN) has also been applied by Singh et al. (2024) to forecast permeate flux in a laboratory-scale FO membrane. ANN was based on input parameters that were congruent to the training data and had a coefficient of determination (R^2) above 0.91 indicative of high level of accuracy in prediction. Further, economic analysis was conducted to predict the cost of membrane which is very significant in determining the viability of such membrane systems.

Although in simple forms, a single functioning layer can be sufficient, most of them involving daily uses involve the construction of three different layers viz. input level, the hidden layer, and the output level to ensure complicated interpretation and processing of data (Dewangan et al., 2023). These layers of the structure have been universally agreed upon and have been characterized by broader levels of terminologies that fits all forms of networks. In real time applications the input neurons gather information via external sensors, or computer files, and the output neurons forward processed data to other external systems, or processors or devices e.g. mechanical controllers. Above the input and output layers, networks can also include many hidden layers with layers consisting of many neurons that are put in the form of interconnected networks (Paliwal et al., 2009). Each hidden unit normally receives inputs, as shown in Figure 2.22, on each unit in the previous layer. None of the neurons in some network models are found at the surface but rather in hidden layers in that they provide feedback tracks where signals are sent to both the previous and the following layer in the iterative learning and precision of the predictions.

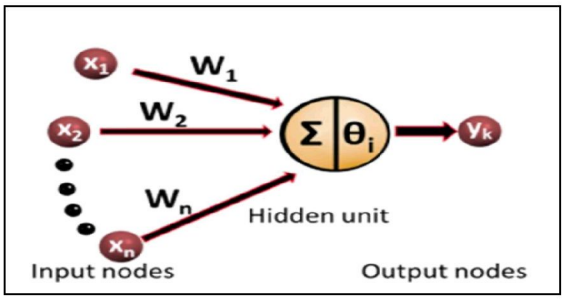

Figure 2.22 Fundamental Model of Artificial Neural Network
(Source: Dewangan et al., 2023)

Neural network models can be loosely classified as either a traditional neural network (including Multi-Layer Perceptron Neural Networks (MLPNNs)) or of higher

complexity Deep Neural Networks (DNNs). MLPNNs are feed forward structures usually consisting of one input layer, two or one hidden layer and one output layer. They can be implemented as standalone application or can be combined with genetic algorithms or fuzzy logic systems to tackle problems such as making predictions, approximations and binary classification (Kim et al., 2004; Grima et al., 2000; Golafshani et al., 2015). DNNs further elaborate on this constellation by the presence of at least three hidden layers and many different variants of subtypes within the like of Recurrent Neural Networks (RNN), Convolutional Neural Networks (CNN), Auto-Encoders (AE), and Restricted Boltzmann Machines (RBM). The RNNs are known to be especially effective at working with time-based data, whereas the CNNs excel at feature and shape identification on two-dimensional data, mainly an image (Akinosho et al., 2020; Khallaf & Khallaf, 2021). They use AEs on tasks such as data denoising and dimensionality reduction and use RBMs to learn probabilistic representations of input dataset (Yang et al., 2021; Marzouk & Zaher, 2020).

In the current study, ANN model was developed as part of the data distribution, where 70 % of data was used as the training, 15% utilized to validate, and 15% utilized to predict. The LM-BP algorithm was used in training because it has been found to converge and fine tune the weights and biases of the network fast and quite accurately minimizing the errors of prediction. The algorithm has been considered very accurate and very efficient in ANN optimization applications (Madaeni et al., 2015; Barello et al., 2014).

To observe the optimal performance, hidden layers neurons variably (systematically) ranged between 5 and 45. Optimal performance was achieved with a network with 30 of the neurons in the hidden layer. This result demonstrates the importance of the number of neurons to the accuracy of the model, where the incorrect setting, either under or over-abundance of neurons, may destroy the performance. It is therefore very important to determine the right number of neurons to have a properly functioning neural network.

2.4.2 Properties of Artificial Neural Network (ANN) by MATLAB

More than 80 predictions were done with the aim of determining the best ANN architecture and the performance was measured in the coefficient of determination (R^2)

and the Sum of Squared Errors (SSE). As epochs increased, there was an improvement in the performance of the model viewed in terms of training, validation and prediction data sets. The optimal validation performance, with a mean squared error (MSE) of 65.83, was observed at the 27th epoch. The high R^2 value of 0.91 during the training phase indicates the model's effectiveness in predicting the desired outcomes (Singh et al., 2024).

For the validation dataset, the ANN model achieved an R^2 value better than 0.80 (see Figure 2.23(a)), demonstrating good performance. The generalization capability of the trained network was also strong, with an R^2 value of 0.76 as shown in Figure 2.24(c) for various study scenarios. However, the model's efficiency was somewhat reduced during the validation (Figure 2.23(b)) and test phases compared to the training phase, likely due to the test dataset not being included in the training process, which may have led to extrapolation. Overall, the ANN model performed well, as evidenced by the R^2 value surpassing 0.87 when considering all data, as shown in Figure 2.23(d).

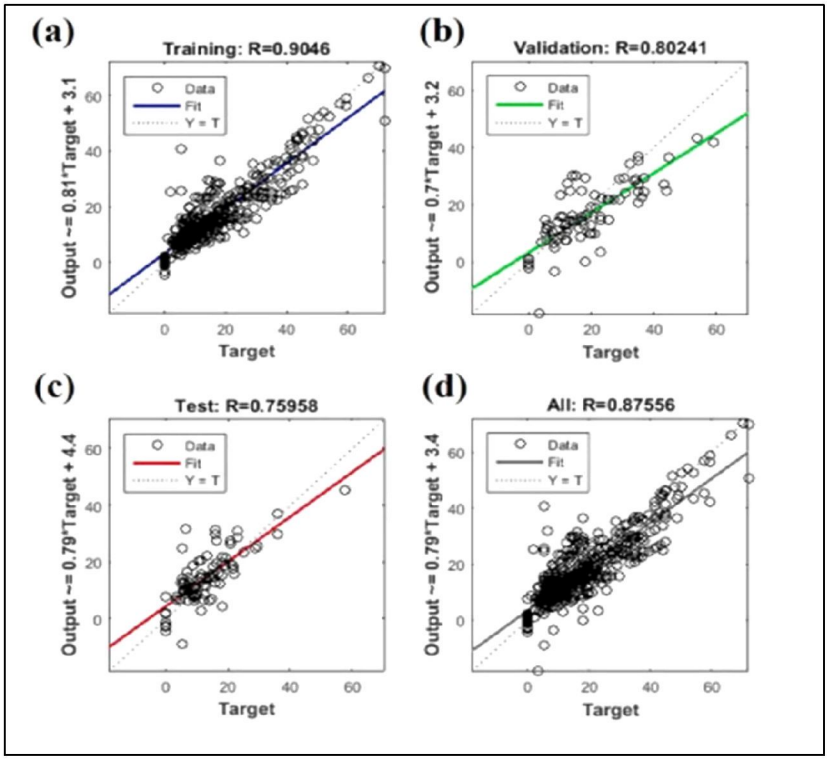

Figure 2.23 Evaluation of Trained ANN Network Performance Through Regression Analysis of Predicted vs. Targeted Output, With R^2 Scores for Different Phases: (a) R^2 score for the training phase; (b) R^2 score for the validation phase; (c) R^2 score for the prediction/test phase; and (d) R^2 score for the overall dataset
(Source: Singh et al., 2024)

Hasan et al. (2024) employed an ANN to predict the thermal conductivity of EG/water mixtures with incorporated CNC. Analysis reveals that the network achieves peak performance in error reduction when using the Tansig activation function. As the learning process advances, a plateau is observed around the epoch threshold, signifying the transition to a final phase that extends to the 46th epoch, marking the completion of the training period. At this point, the model reaches a high level of precision, as evidenced by an MSE of $3.7959 \times 10{-}8$, demonstrating optimized learning.

In this study, a significant portion of the data set, specifically 60%, is allocated to network training, with smaller portions reserved for testing and validation. Figures 2.24 presents a scatter plot showing accuracy metrics for training, testing, validation, and the overall performance of the ANN model. The results clearly demonstrate a strong alignment between the output and target data, with the training dataset exhibiting an exceptionally high correlation coefficient of 0.99904. This high correlation extends to the other datasets as well, with the test, validation, and overall datasets achieving correlation coefficients of 0.99885, 0.99918, and 0.99903, respectively.

These findings highlight the model's remarkable consistency and precision across different evaluation phases, indicating a strong convergence between the predicted values and the experimental data. The results confirm the ANN's effectiveness in accurately predicting outcomes, underscoring its reliability and predictive power.

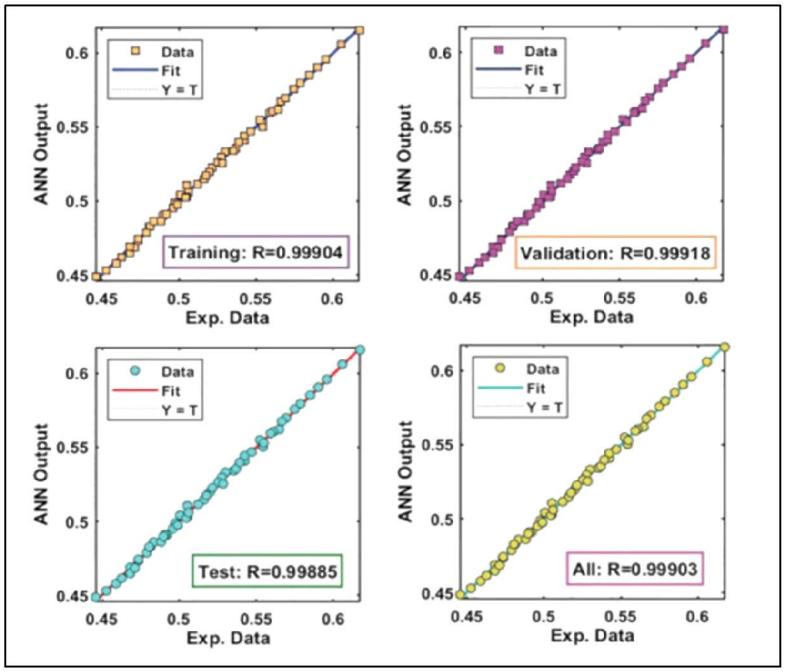

Figure 2.24 Tansig Scatter Plot of The Target and Output Values of The ANN Model (Source: Hasan et al., 2024)

The Table 2.20 shows that AI and ANN models are highly effective in predicting concrete strength across various formulations. OPC mortars reached near-perfect prediction accuracy, with an R^2 of 0.9977 and minimal error. Even complex mixtures involving nano silica and micro silica had strong predictive performance at 96.6% explained variance. Ground bottom ash concrete achieved excellent results using a simple 2-layer ANN, with R^2 values exceeding 0.99. For self-compacting concrete, AI models generally performed well ($R^2 > 0.8$), but ANN specifically showed stronger prediction capabilities with R^2 typically above 0.95.

Table 2.17
Comparison of R^2 From Different Study that Using ANN

Study	Description
Prediction of compressive strength of ordinary Portland cement mortars	R^2: 0.9977, MAE ≈ 0.0093. Excellent agreement.
High-strength concrete mixtures with nSi/mSi	R^2: 0.966, ~96.6% variance explained even with complex additives.
Ground bottom ash concrete ANN model	Reported $R^2 \geq 0.99$, 2-layer ANN.
SCC concrete AI review	Across models: consistently $R^2 > 0.8$, but for ANN typically > 0.95.

Source: Chopra et al., (2015)

Paruthi et al. (2023) state that information was collected based on the extensive literature review that included the data regarding various experimental findings. MATLAB was used to analyse the relationship between different concrete properties and the content of ESP. In particular, the paper examined the correlation between the variations in the ESP ratio and slump with Compressive Strength (CS), Split Tensile Strength (STS) and Flexural Strength (FS). Based on the data, non-linear surface fitting was used to obtain the polynomial equations. Comparative methodologies have been utilized to provide meaning to such relationships by researchers within and across disciplines (Cao et al., 2020; Cao et al., 2019). Equations (1) through (3), displayed in Table (1), give the mathematical expressions of the prediction that have been developed to predict CS, STS, and FS in terms of calculating the strengths of the target in respect to the contents of ESP and the values of the slump.

These models have been assessed based on their predictive power illustrated in Figure 2.25 by the coefficient of determination (R^2), with higher scores closer to 1 depicting that there was a strong correspondence between the forecasted and measured outcomes (Zou et al., 2022). Equation (1) model has shown high levels of accuracy with an R^2 value of 0.99. Similarly, Equation (2) and Equation (3) produced acceptable R^2 values of 0.98 and 0.96, respectively, supporting the reliability of the proposed correlations. Nonetheless, expanding the dataset would enhance the robustness and generalizability of the prediction models.

$$CS = 25{\cdot}2 - 0{\cdot}75\ ESP + 2{\cdot}73\ S + 0{\cdot}125\ (ESP)2 - 0{\cdot}152\ S2 + 0{\cdot}046\ S(ESP) \quad (2.1)$$

$$STS = 2{\cdot}54 + 0{\cdot}091\ ESP + 0{\cdot}391\ S - 0{\cdot}0041\ (ESP)2 - 0{\cdot}0142\ S2 - 0{\cdot}0042\ (ESP)s \quad (2.2)$$

$$FS = 13{\cdot}09 + 0{\cdot}411\ ESP - 0{\cdot}782 - 0{\cdot}825\ S - 0{\cdot}00258(ESP)2 + 0{\cdot}0152\ S2 - 0{\cdot}0251(ESP)S \quad (2.3)$$

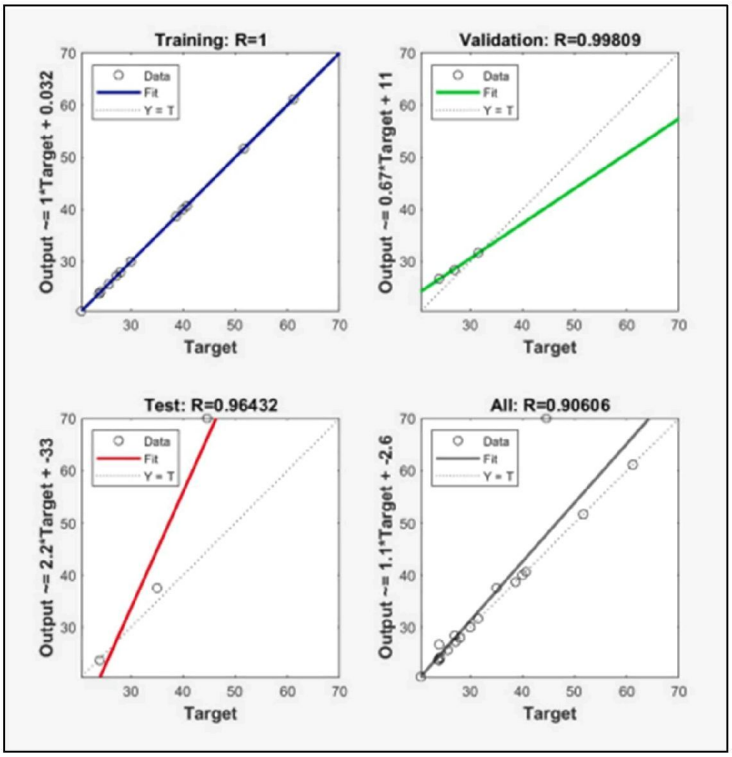

Figure 2.25 The Result of The Workability of The Developed ANN Model for The Input Data Set
(Source: Paruthi et al., 2023)

2.4.3 Application of Artificial Neural Network (ANN) by MATLAB

The recent directions in studying materials mostly highlight the importance of using ANN modelling to design original materials with individual target properties (Dewangan et al., 2020; Kim et al., 2021). The review piece can be used as a broad source of information on ANN-based approaches, determining their predictive capabilities and recognizing the limitations that come along with material design and development activities (Li et al., 2016). There is also the optimization of ANN in emerging usage in different fields of materials science and engineering as noted in the review (Ghaisari et al., 2012). The main difficulty is that of building composition structure property models with machine learning techniques on a variety of datasets covering different times. Making fewer experimental trials to produce and developing the breakthrough materials in a faster way is one of the focuses (Dewangan et al., 2023).

Since the 1990s, intensive research on ANN structures gave a broad scope of application in the construction and building (CB) sector. These belong to cost estimation (Kim et al., 2004; Rafiei & Adeli, 2018), productivity forecasting (Heravi & Eslamdoost, 2015; Golnaraghi et al., 2019), prediction of building energy consumption (Chae et al., 2016; Neto & Fiorelli, 2008), Z model concrete properties (Asteris et al., 2021; Chopra et al., 2018) detection of pavement cracks However, taken together, the contributions have been effective in contributing to an increase in the bulk of scientific literature in respect to the applications of ANN in the CB domain.

Some of the most eminent ANN research topics that Hojjat Adeli contributed to include costs estimation (Adeli & Wu, 1998; Rafiei & Adeli, 2018), and traffic incident detection (Ghosh-Dastidar & Adeli, 2003; Adeli & Samant, 2000; Samant & Adeli, 2001), as well as the nonparametric structural system identification (Jiang & Adeli, 2005; Jiang et al., 2007). In the meantime, the work of Behnood is related to modeling the properties of strength of different concrete mixtures (Behnood et al., 2015; Kandiri et al., 2020; Golafshani et al., 2020) and dynamic modelling of asphalt modulus (Behnood & Golafshani, 2021).

Using VOSviewer software, a keyword co-occurrence network was constructed, as illustrated in Figure 2.26. This figure places Artificial Neural Network (ANN) at the centre, highlighting its widespread application across multiple research domains. The red cluster focuses on concrete and construction materials, linking ANN to compressive strength, durability, and mechanical modelling. The green cluster relates to energy systems, including thermal comfort, HVACs, and building simulation, often paired with genetic algorithms. The blue cluster represents deep learning and computer vision, covering object detection, segmentation, and damage assessment. The yellow cluster connects ANN to broader artificial intelligence and construction modelling, while the purple cluster includes machine learning techniques like Support Vector Machine (SVM), Principal Component Analysis (PCA), and Finite Element Modelling (FEM). Together, these colour-coded themes show how ANN supports predictive modelling and optimization across engineering, sustainability, and smart construction research helping structure your bibliography by technical focus.

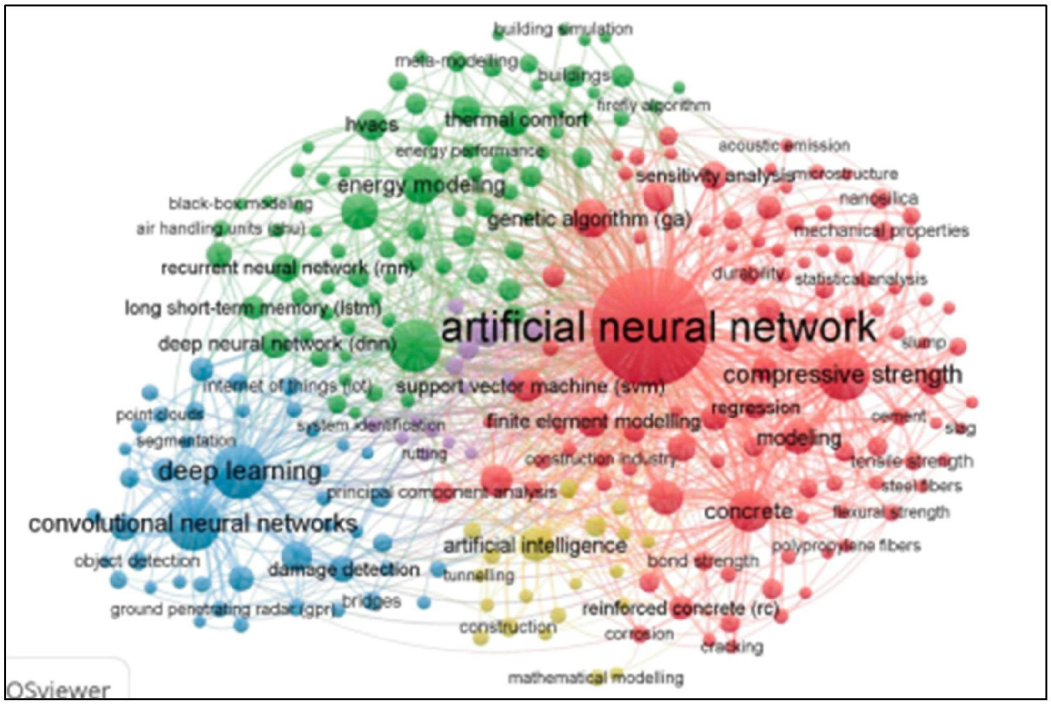

Figure 2.26 Network Visualization for Keywords Artificial Neural Network (ANN) (Source: Marzouk et al., 2024)

The Red Cluster encompasses a total of 162 prominent publications that focus on material modelling applications, with their publication dates spanning from 1997 to 2021. Key contributors within this cluster include Jui-Sheng Chou and Panagiotis G. Asteris, each with six documents; Hamid Eskandari with five; Emadaldin M. Golafshani with four; and IC Yeh with three. The most frequently referenced journals and sources in this group are *Construction and Building Materials* (85 documents), *Cement and Concrete Research* (15), *Journal of Building Engineering* (9), *Automation in Construction* (7), and *Computers and Concrete* (6). As illustrated in Figure 2.27, this cluster spans 14 distinct research themes, reflecting a diverse and concentrated effort in ANN applications for modelling material properties.

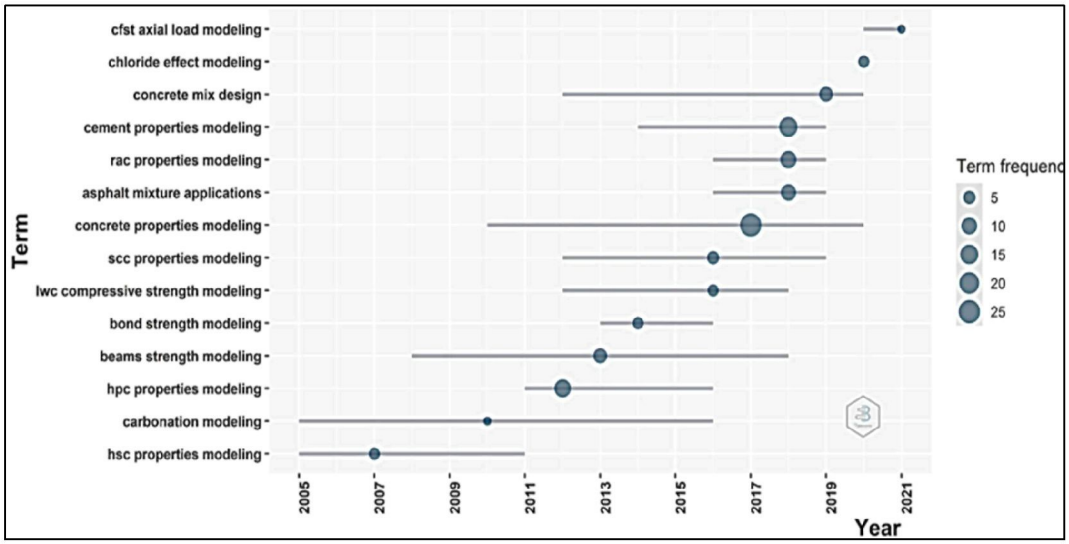

Figure 2.27 Major Research Themes for Materials Modelling Applications (Source: Marzouk et al., 2024)

2.4.4 Summary on The Uses of Artificial Neural Network (ANN) by MATLAB

Based on the study of the previous study, there have a tendency toward using ANN models in combination with physics, experiments, and data science is also evident in recent efforts to predict high-entropy materials. This hybrid system used the full potential of each ingredient. By incorporating accurate experimental data into ANN models, the quantity of training datasets is reduced, physical inconsistency in predictions is decreased, and physical interpretability is improved. The amount of data that be used to train ANN models will increase because of well-planned experiments that include richer constitutive information in addition to physics-based models.

2.5 Summary

Chapter 2 presented a comprehensive review of existing literature related to sustainable construction materials, interlocking block systems, and the application of Artificial Neural Networks (ANN) in structural prediction. The review identified several research gaps that form the foundation of the present study. Previous studies have explored the use of eggshell powder (ESP), recycled concrete aggregate (RCA), and silica fume (SF) in various proportions; however, the ranges most relevant to this research ESP at 5–15%, RCA at 30%, and SF at 10% remain insufficiently examined

in the context of interlocking block production. The literature also highlighted inconsistencies in material performance when these percentages are combined, indicating a clear need for further investigation.

In terms of block configuration, existing interlocking block designs in Malaysia and those proposed by earlier researchers provided valuable insights but still demonstrated limitations in structural efficiency, ease of assembly, and load transfer mechanisms. These gaps motivated the development of a new interlocking block design in this study, incorporating chamfered stud edges and a tongue-and-groove joint system to enhance alignment, stability, and interlocking performance.

The literature also showed that while experimental testing provides essential performance data, there is a lack of studies that use computational methods to verify the reliability of such data. Artificial Neural Networks (ANN) have been recognised as a useful tool for evaluating datasets, yet their application in validating experimental results for interlocking blocks incorporating ESP, RCA, and SF remains limited. In this study, ANN is specifically to evaluate the experimental data, ensuring that the results are consistent, reliable, and suitable for further interpretation.

Overall, Chapter 2 justified the selected material percentages, established the need for a refined interlocking block design, and highlighted the importance of ANN as a validation tool. These identified gaps form the basis for the methodological approach presented in the next chapter.

CHAPTER 3
RESEARCH METHODOLOGY

3.1 Introduction

This chapter outlines the methodology employed in the study, including the materials used and their substitutions in concrete. Tests are performed utilizing facilities such as the 'Makmal Struktur Berat' and the 'Makmal Konkrit'. The methodology is divided into three main stages to achieved objectives: finding the salient proportions of the mixture; design of the interlocking block (IB); and the validation by using Artificial Neural Network (ANN). A flowchart, as shown in Figure 3.1, illustrates the summarise flow of the methodology process in this study.

Initially, materials consist of OPC, ESP, SF, NA, RCA, superplasticizer (Sika ViscoCrete-2192), and water are prepared. Experiment samples consist of cubes, prism, and interlocking blocks. The tests were particle size distribution (ASTM C430, and ASTM C144-18) of materials comparison, flowability (ASTM C1437) on fresh mortar, water absorption (ASTM C642), compressive test (ASTM C109), and flexural test (ASTM C78). Data collection and analysis are crucial for obtaining study results, with each tailored to use as IB mixture. The replacement material is a key focus in this study, potentially impacting mixture characteristics such as strength and workability.

Then, with the salient mixture were implemented in produced IB with 3 different proposed design. The designs were Solid Interlocking Block (SIB), Single Inclined Connection Interlocking Block (SICIB), and Dual Tongue Inclined Interlocking Block (DTIIB). The testing was conducted flexural testing (ASTM C78) and crack pattern for visual observation of the interlocking block load distribution.

Finally, the data collected from three mixtures OPCNA, and selected proportions from the EPRCA0 and EPRCA30 series of all types of samples were evaluated using Artificial Neural Network (ANN) in MATLAB. The Neural Network Fitting tool (nftool) was employed, utilizing the Levenberg–Marquardt algorithm (trainlm) for training. The ANN-generated outputs were then compared against experimental test results through graphical analysis, confirming the reliability and consistency of the collected data.

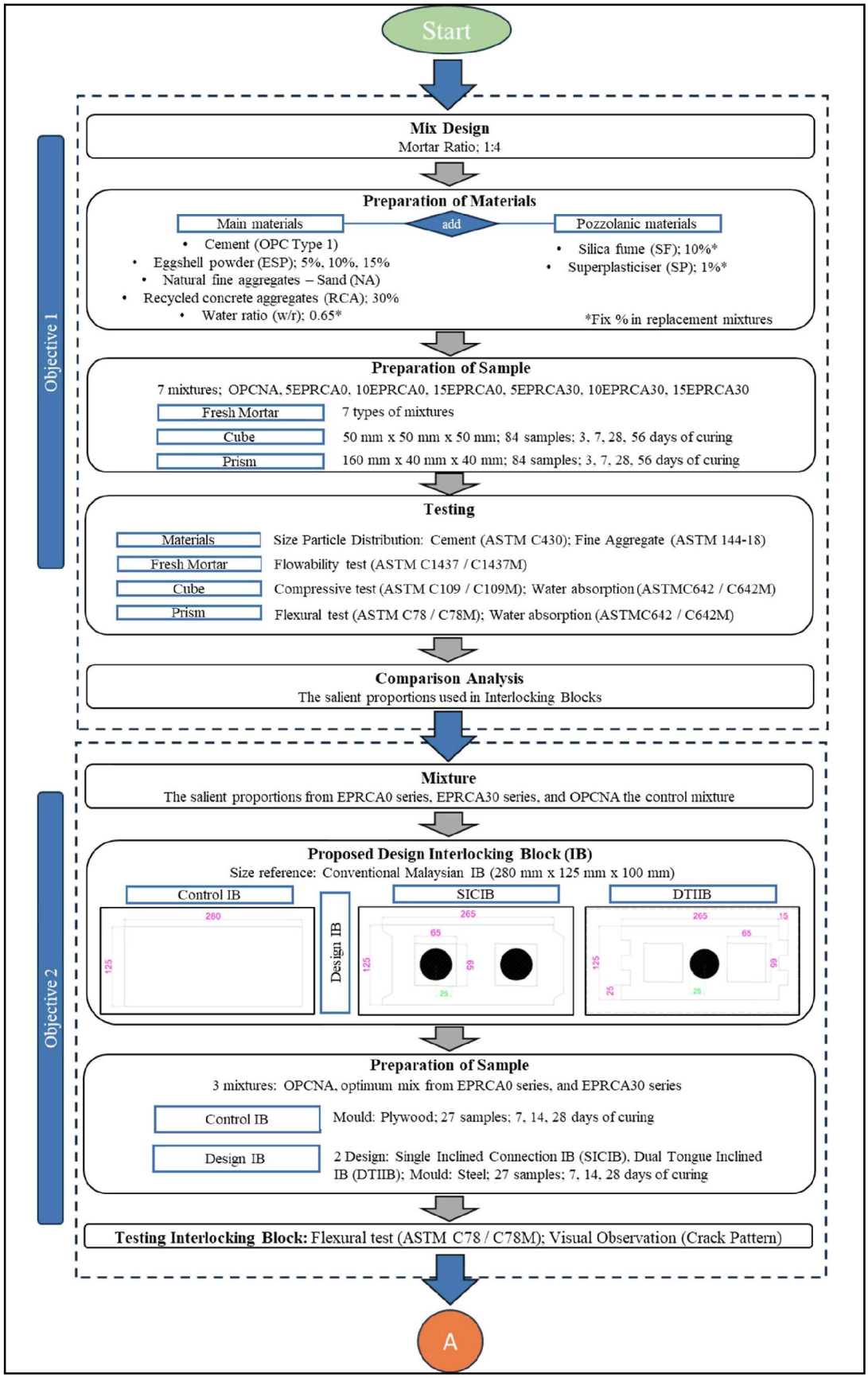
Start
Objective 1
Mix Design
Mortar Ratio; 1:4
Preparation of Materials
Main materials
add
Pozzolanic materials
• Cement (OPC Type 1)
• Eggshell powder (ESP); 5%, 10%, 15%
• Natural fine aggregates – Sand (NA)
• Recycled concrete aggregates (RCA); 30%
• Water ratio (w/r); 0.65*
• Silica fume (SF); 10%*
• Superplasticiser (SP); 1%*
*Fix % in replacement mixtures
Preparation of Sample
7 mixtures; OPCNA, 5EPRCA0, 10EPRCA0, 15EPRCA0, 5EPRCA30, 10EPRCA30, 15EPRCA30
Fresh Mortar
7 types of mixtures
Cube
50 mm x 50 mm x 50 mm; 84 samples; 3, 7, 28, 56 days of curing
Prism
160 mm x 40 mm x 40 mm; 84 samples; 3, 7, 28, 56 days of curing
Testing
Materials
Size Particle Distribution: Cement (ASTM C430); Fine Aggregate (ASTM 144-18)
Fresh Mortar
Flowability test (ASTM C1437 / C1437M)
Cube
Compressive test (ASTM C109 / C109M); Water absorption (ASTMC642 / C642M)
Prism
Flexural test (ASTM C78 / C78M); Water absorption (ASTMC642 / C642M)
Comparison Analysis
The salient proportions used in Interlocking Blocks
Objective 2
Mixture
The salient proportions from EPRCA0 series, EPRCA30 series, and OPCNA the control mixture
Proposed Design Interlocking Block (IB)
Size reference: Conventional Malaysian IB (280 mm x 125 mm x 100 mm)
Control IB
Design IB
SICIB
DTIIB
280
125
265
65
99
25
15
Preparation of Sample
3 mixtures: OPCNA, optimum mix from EPRCA0 series, and EPRCA30 series
Control IB
Mould: Plywood; 27 samples; 7, 14, 28 days of curing
Design IB
2 Design: Single Inclined Connection IB (SICIB), Dual Tongue Inclined IB (DTIIB); Mould: Steel; 27 samples; 7, 14, 28 days of curing
Testing Interlocking Block: Flexural test (ASTM C78 / C78M); Visual Observation (Crack Pattern)
A

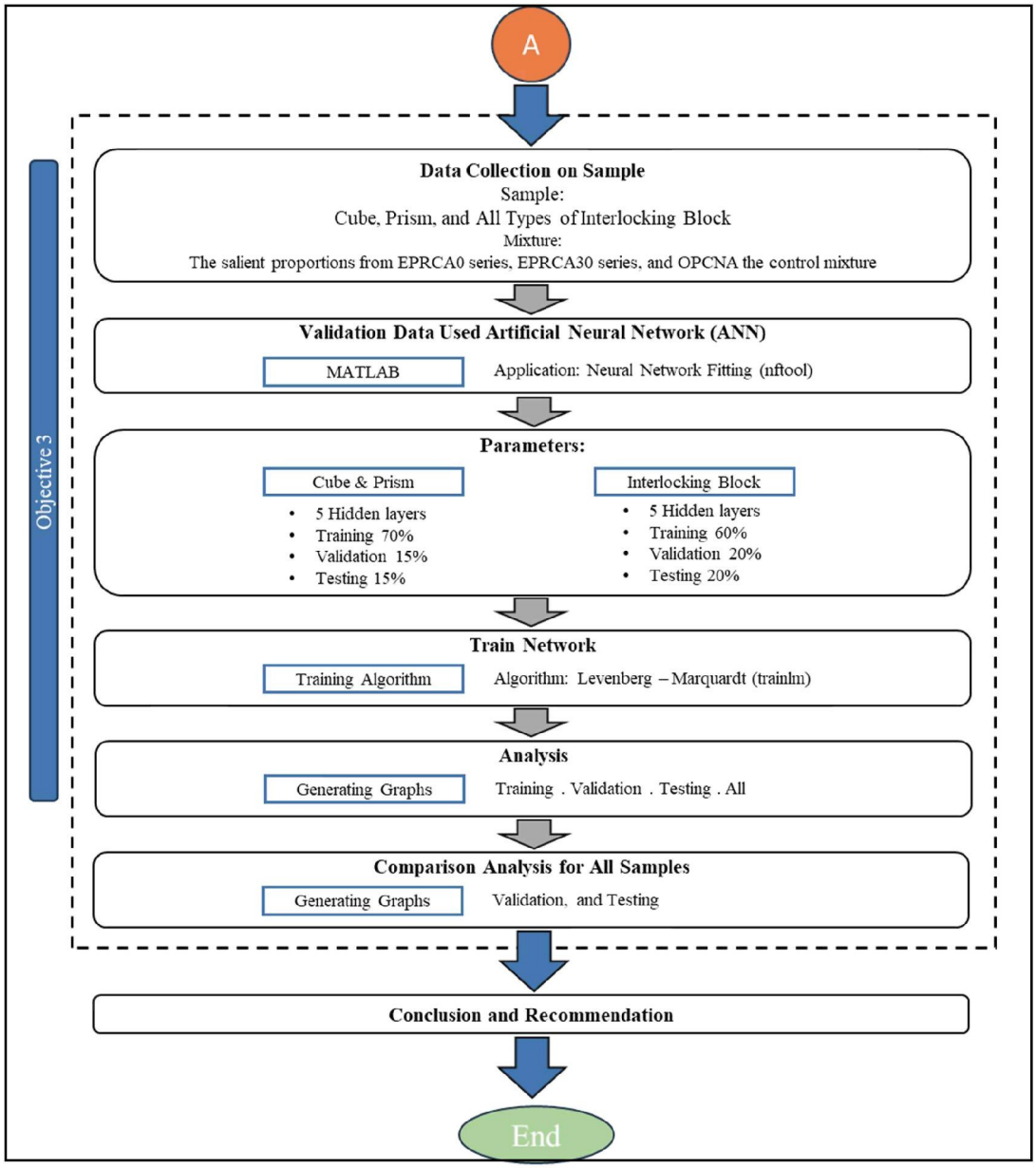

Figure 3.1 Flowchart of The Study Methodology Process

3.2 Method for The Optimum Percentage of Eggshell Powder, Silica Fume and Recycled Concrete Aggregate

Concrete is used to provide strength, durability, and versatility during the construction of a structure. The specific mixture is in this study were used mortar. The mixture of mortar can vary depending on the desired properties and the requirements of the construction project. In this study the materials were based on ratio 1:4 for Cement: Fine Aggregates. For the aggregates, natural fine aggregate (sand) and fine aggregate replacement which is RCA. The elements which are fine aggregates, as well as OPC and were mixed together with water. the water-cement ratio is 0.65 of each batch. RCA was one of the elements that replacing fine aggregate partially. It was substitute in the mixture with the proposed percentage for the sample. The admixture of superplasticiser was also added in the mortar mix.

3.2.1 Preparation of Materials

The first phase of this study investigates the mechanical properties of the mortar mixture that containing the materials used in the study. There have several tests were conducted which are particle size distribution, flowability, water absorption, compression test, and flexural test. The mortar mixture incorporating ESP as a partial substitute for Type I OPC, in combination with SF as pozzolanic materials, by using a compressive test method and three-point bending method. The mortar mixture includes OPC, ESP, SF, NA, RCA, water (water-cement ratio, 0.65), and superplasticizer (1% of cement), shaped into 2 types of samples which are cubes measuring 50 mm x 50 mm x 50mm and prisms measuring 40 mm × 40 mm × 160 mm.

ESP was evaluated at substitution levels of 5%, 10%, and 15%, while SF content was consistently maintained at 10%. Eggshells were pre-treated through drying, crushing, and sieving prior to their use. Other than that, RCA as NA replacement with constantly of 30% replacement. RCA was in 3 mixtures from 7 mixtures to investigates the performance of compressive and flexural for comparison of the present of the RCA with ESP and non-present of RCA with ESP. As detailed in Table 3.1, ESP and RCA are introduced as partial substitutes for OPC and NA with percentages of mix proportions sample, respectively, supporting the development of eco-friendly construction materials.

Table 3.1
Percentages of Mix Proportions Sample

Sample	OPC	ESP	SF	NA	RCA
Control	100%	0%	0%	100%	0%
5%	85%	5%	10%	100%	0%
10%	80%	10%	10%	100%	0%
15%	75%	15%	10%	100%	0%
5% RCA	85%	5%	10%	70%	30%
10% RCA	80%	10%	10%	70%	30%
15% RCA	75%	15%	10%	70%	30%

3.2.1.1 Ordinary Portland Cement (OPC)

Ordinary Portland Cement (OPC), a crucial building material, is a binding agent that sets and hardens to adhere to building units such as stones, bricks, tiles, and so on. Cement is a fine powdery substance composed primarily of limestone (calcium), sand or clay (silicon), bauxite (aluminium), and iron ore, and potentially also include shells, chalk, marl, shale, clay, blast boiler slag, and slate. In cement manufacturing plants, raw ingredients are processed and heated to form a rock-hard substance, which is then ground into a fine powder for sale. When cement is mixed with water, a chemical reaction occurs, resulting in the formation of a paste that sets and hardens to bind individual structures of building materials. The cement that used in this study was Ordinary Portland Cement from brand of Tasek Corporation Berhad as shown in Figure 3.2.

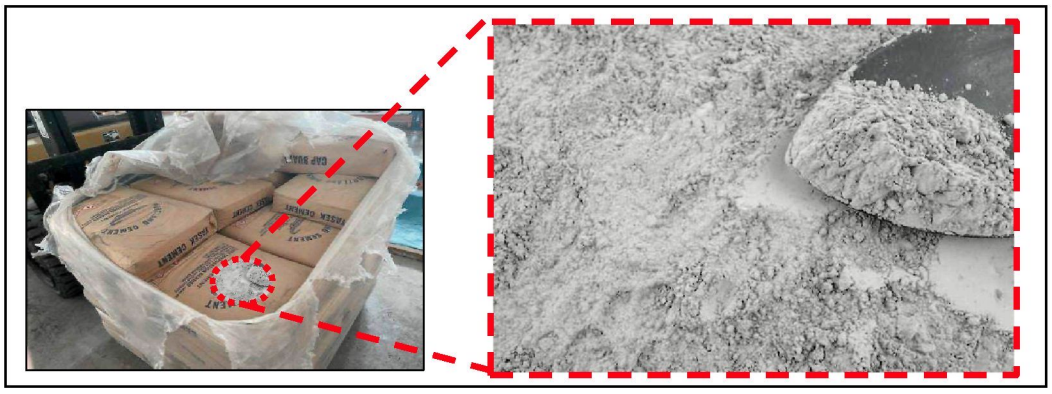

Figure 3.2 Ordinary Portland Cement

3.2.1.2 Eggshell Powder (ESP)

The first step in making Eggshell Powder (ESP) is gathering Eggshells (ESs) from bakeries, restaurants, and other egg processing establishments (as shown in Figure 3.3). To ensure that there are no traces of egg white or yolk remaining, these ESs are

thoroughly cleaned. The ESs are dried in oven at 110°C for 24 hours after cleaning in order to remove any remaining moisture, which is essential for inhibiting microbial growth and guaranteeing stability during processing. After ESs were dried, in Figure 3.4 shown 2 appliances were used to grinded and blended the ES to make it finer which are stone mortar (see Figure 3.4(a)) for smashed and grinded the ES. Then, move to used blender (Figure 3.4(b)) to make the fine ES to powdery texture.

The condition of the ES making can be seen in Figure 3.5 and Figure 3.6. The original state of ES was smashed and become the small pieces of ESs (see Figure 3.5(a) and Figure 3.5(b)). It needs to grinded with stone mortar 3 to 5 times to make it finer than before as shown in Figure 3.5(c). Once it is in that state, ES was starting to produce powder. So, Figure 3.5(d) was ES moved to used blender for produce more powder.

The uniform particle size is ensured by this grinding operation, which also improves the efficiency of further processing steps. To create a more refined product, the powdered ES potentially optionally be sieved to get rid of bigger particles or contaminants (see Figure 3.6(b)). To preserve its quality and longevity, the processed ESP is lastly placed into appropriate containers for storage. This final product is used in several industries, including as construction materials, animal feed, dietary supplements, and agriculture.

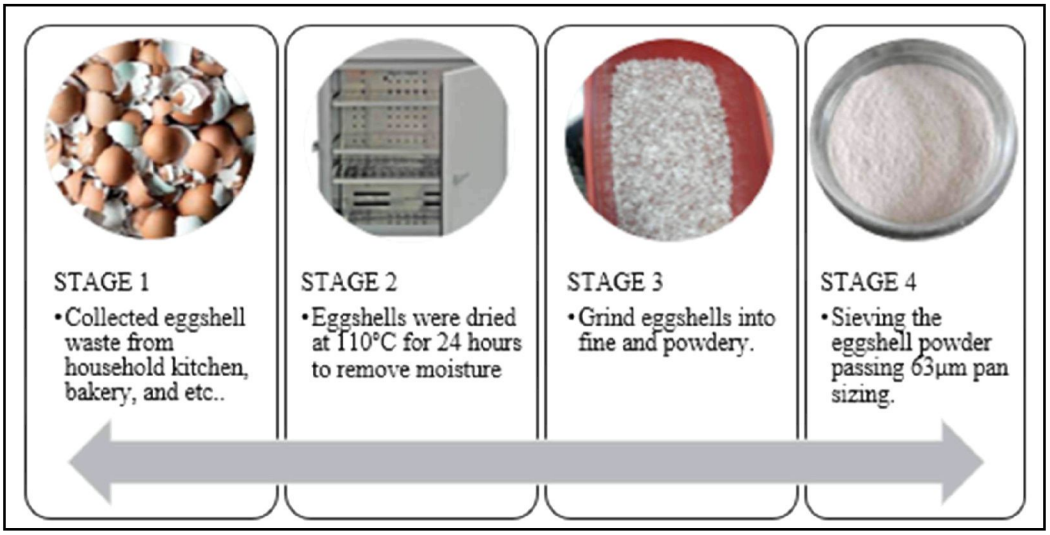

Figure 3.3 Process of Making Eggshell Powder

Figure 3.4 Appliances of Making Eggshell Powder: (a) Stone Mortar ('Lesung Batu'); (b) Blender

Figure 3.5 Changes State of Eggshell: (a) Washed Fresh Eggshell; (b) First Condition After First Session of Grind; and (c) Second Condition After First Session of Blend

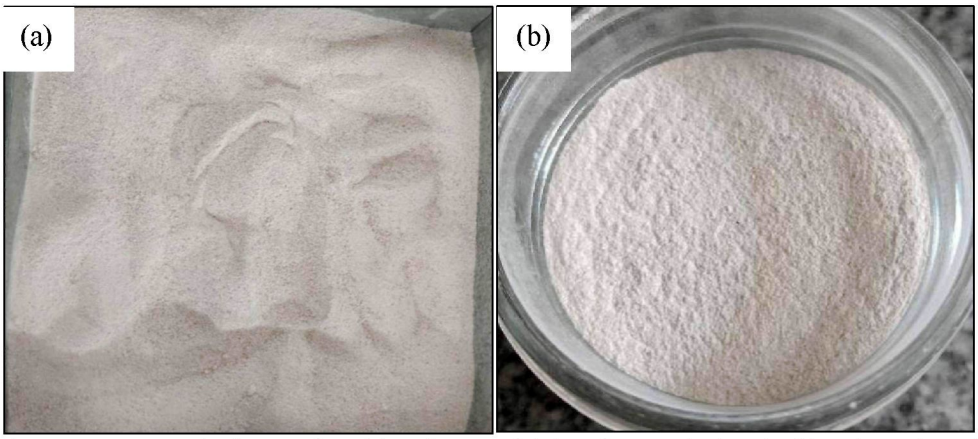

Figure 3.6 Eggshell Powder: (a) After Multiple Times of Blend; (b) After Sieved

3.2.1.3 Silica Fume (SF)

Silica Fume (SF), a byproduct of silicon metal or ferrosilicon alloys production as shown in Figure 3.7, finds significant utility in concrete due to its unique chemical and physical attributes. Recognized as a highly reactive pozzolan, it imparts remarkable strength and durability to concrete formulations. Sourced from Scancem Materials Sdn. Bhd., based in Malaysia and Singapore, SF is particularly acclaimed for its effectiveness in low heat concrete applications. By substituting cement with SF, this material efficiently reduces maximum temperature rise and temperature differentials in concrete while maintaining desired strength levels. This method stands as the most efficient means to achieve reduced heat generation without compromising early age strength.

SF which is a residual material from the manufacturing of silicon and ferrosilicon alloys has garnered interest in the building industry sector due to its capacity to enhance mortar properties. When incorporated into mortar, SF interacts with calcium hydroxide to produce extra calcium silicate hydrate, leading to improved strength and durability (Hasan et al., 2021). Additionally, the fine particles of SF aid in filling voids within the mortar matrix, resulting in a denser and less permeable mortar. Another significant application of SF lies in high-strength concrete formulations. Employing SF results in considerable economic advantages for developers, including diminished column and wall thickness in tall structures and enhanced construction timelines. Moreover, the use of SF facilitates the pumping of concrete in high-rise buildings during construction processes, further streamlining operations.

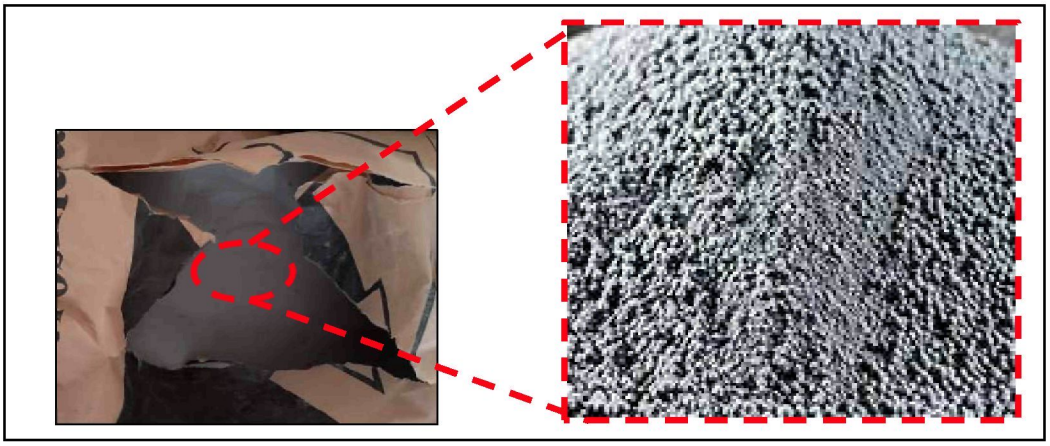

Figure 3.7 Silica Fume That Being Used

3.2.1.4 Natural Aggregate (NA)

Fine aggregates are produced through the erosion and disintegration of different rock types, predominantly comprising quartz. Manufactured sand, derived from crushed stones, gravel, or air-cooled blast furnace slag, possesses sharp and angular particles, rendering it suitable for applications in concrete and asphalt. In this study, the fine aggregate consisted of finely fragmented rock pieces that were loosely compacted. Fine aggregates, commonly referred to as sand, consist of natural particles ranging in size from 600 mm to 4.75 mm.

The fine aggregates were obtained from the heavy structural laboratory that provided by faculty. From Figure 3.8, the sand was collected and dried for at least 24 hours to dry the moisture in the sand. Because the sand was stored outdoors, it was subjected to environmental conditions such as rain. This step was carried out unchanged to avoid moisture accumulation in the sand, which could alter its moisture content and impact the mixture. The sand used in this study was sourced from a stockpile situated behind the 'Makmal Struktur Berat' UiTM Pulau Pinang Cawangan Permatang Pauh. It was sieved at 2.36 mm, with only the portion passing through the sieve incorporated into the design mix. The remaining sand was returned to the stockpile.

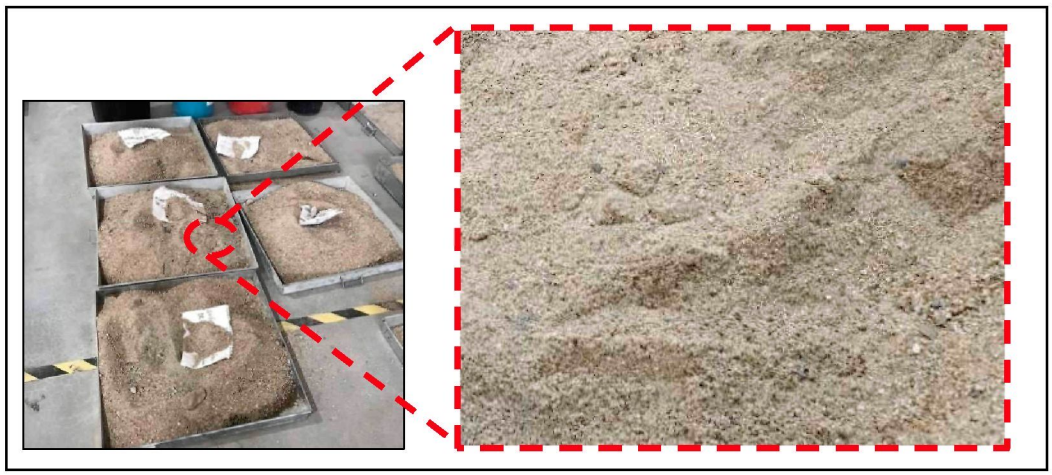

Figure 3.8 Natural Fine Aggregate – Sand

3.2.1.5 Recycled Concrete Aggregate (RCA)

Recycled Concrete Aggregates (RCA) is obtained by crushing tested concrete cubes of specific grades, which serve as a benchmark for assessing the quality of the

resulting material. However, due to the high absorption of cement mortar on the aggregate surface and the presence of fine cracks, RCA derived from waste concrete is not ideal for structural applications.

Consequently, when incorporating RCA into concrete, a substantial amount of water is required, which leads to a reduction in flowability during transportation and significantly affects its workability compared to conventional materials (Ryou, 2013). As a result, nearly half of this waste material is not recyclable, leading to economically unsustainable waste management. A viable solution to this issue is to utilize all recycled aggregates as a partial substitute for natural aggregates in the production of new structural concrete.

For this study, there had going through processes to produced RCA that been used in study mixture. The processes were shown in Figure 3.9 as simply say that have 4 main steps which firstly, selected cubes; second was crushing them into small sizes; third step were crushing in marks of 5 mm by using jaw crusher machine; and last steps was sieved to gain the RCA with ideal size for study mixture.

Began the first step, cubes measuring 150 mm × 150 mm × 150 mm were carefully selected in the 'Makmal Konkrit', UiTM Pulau Pinang. As shown in Figure 3.10, these cubes were sourced from previously used specimens and meticulously examined before processing. The production of RCA involves several steps, beginning with the demolition of concrete structures, followed by crushing the resulting debris and refining the material to ensure its suitability for practical applications. As shown in Figure 3.11, RCA that has undergone the initial crushing phase, appearing in relatively large sizes.

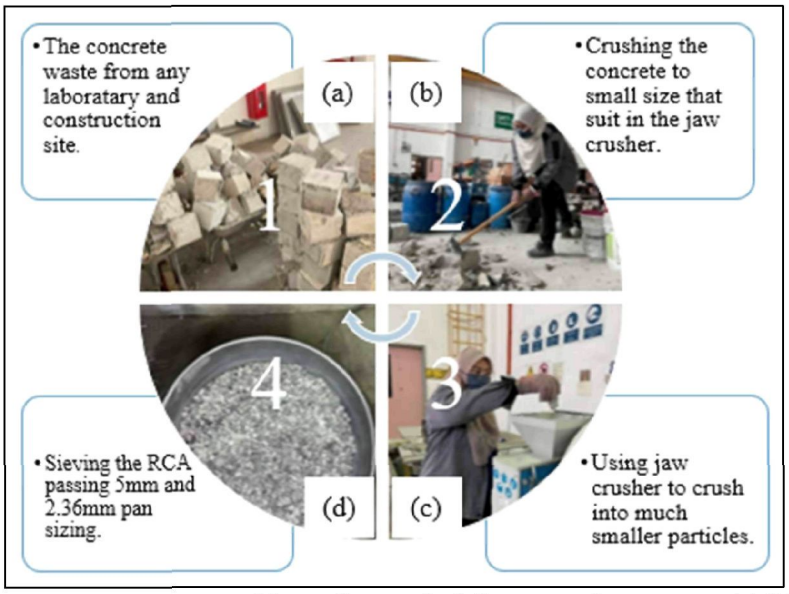

Figure 3.9 Process making of Recycled Concrete Aggregates (RCA)

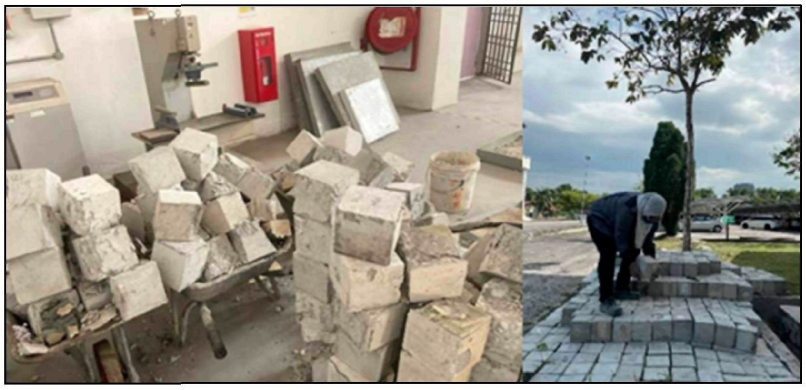

Figure 3.10 Concrete Cube at 'Makmal Konkrit'

Figure 3.11 Recycled Concrete Aggregate Once Crushed (Big Size)

RCA through systematic crushing, gradually reducing them from larger fragments to finer particles until they met the 5 mm sizing requirement. The initial

crushing stage utilized manual equipment such as, hammer, drill, and scoop (Figure 3.12) to scooping RCA to moved next step of process, while the subsequent refinement involved passing the material through a jaw crusher machine to crushed aggregates smaller than 5 mm as shown in Figure 3.13.

Figure 3.12 Tools Used for Crushing and Handling the RCA at First Stage

Figure 3.13 Crushing the Concrete Cube to the Small Particle using Jaw Crusher

To further refine the RCA for the concrete design mix, the crushed material underwent an additional sieving process using a 2.36 mm sieve. Since the fragment sizes varied considerably, direct inclusion in the mix was impractical. The RCA as illustrated in Figure 3.14 were consisted of particles passing through the 5mm sieve and passing sieved size 2.36 mm sieve. A substantial portion of the concrete mix in this study consisted of RCA, with a replacement rate of 30%, so that the study aiming to obtain approximately 6 kg of RCA by the processes.

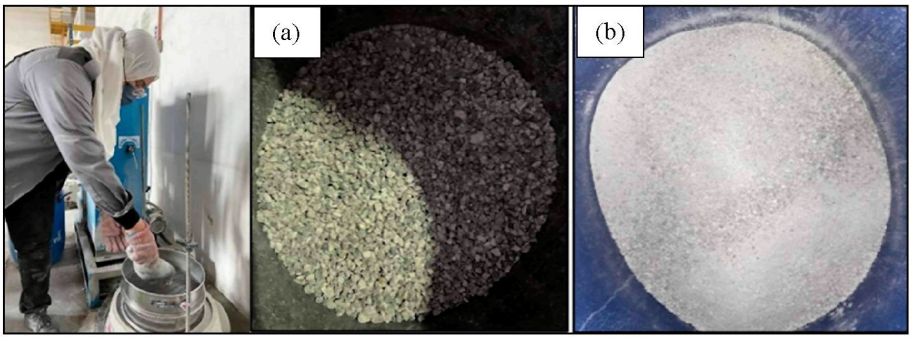

Figure 3.14 Sieving Process: (a) Recycled Concrete Aggregate (passing 5mm); (b) Recycled Concrete Aggregate (passing 2.36mm)

3.2.1.6 Water

Water serves as the primary ingredient in concrete, and when mixed with cement, it creates a paste that binds the aggregate together. Through a process called hydration, water causes concrete to solidify. Hydration is a chemical reaction wherein the principal compounds in cement establish chemical bonds with water molecules, resulting in hydrates or hydration products. The subsequent section provides detailed insights into the intricacies of the hydration process. It's crucial to use pure water to prevent any side reactions that could compromise the strength of the concrete or hinder the hydration process. Water holds significant importance because the water-to-cement ratio stands at 0.65, making it the most critical factor in achieving optimal concrete mortar quality.

3.2.1.7 Superplasticizer

A superplasticizer, also recognized as a high-range water reducer, is a chemical additive employed in concrete to enhance its workability and fluidity while maintaining strength and durability. Typically, available in liquid or powder form, it is incorporated into the concrete mix during the blending process. The primary role of a superplasticizer is to decrease the amount of water necessary to attain the desired consistency in concrete. By reducing the water-cement ratio, the superplasticizer enables a higher concentration of cement particles, leading to increased strength and decreased porosity. This is pivotal in crafting high-performance concrete with superior mechanical characteristics.

When using interlocking concrete blocks made with RCA, the addition of a superplasticizer offers several benefits, particularly in improving workability. RCA tends to have a higher water absorption rate than natural aggregates, which can compromise the workability of the concrete mix. By incorporating a superplasticizer, it becomes possible to decrease the water content while maintaining the necessary flowability and workability, making the handling and placement of the interlocking concrete blocks easier.

In this study, Sika-ViscoCrete 2192 was used as the superplasticizer. Produced by Sika Group, a leading company in the construction chemicals industry, Sika-ViscoCrete 2192 is designed to enhance the workability and flow characteristics of concrete mixes. Its primary function lies in improving the rheological characteristics of concrete, rendering it more manageable during handling, placement, and finishing.

The recommended dosage of Sika-ViscoCrete 2192 potentially vary based on several factors, including desired workability, cement type, environmental conditions, and specific study demand. It is imperative to refer to the product data sheet, technical literature, or consult directly with Sika for precise dosage recommendations relevant to the application. Nonetheless, as a general guideline, the dosage typically ranges from 0.6% to 2.5% by weight of cementitious materials in the concrete mix. In this study, the superplasticizer was used at a concentration of 1% by weight of cementitious materials.

3.2.2 Mix Design of Mortar

This section is concerning the preparation of the quantity of the materials that used for various of samples in completing the lab experiment in the study. Table 3.2 shows the mix proportions of mortar used for cubes and prisms samples. These samples used for finding the salient percentages by tested mechanical properties before proceeding to build interlocking blocks using the mixture. The mix design as shown in Figure 3.3 was calculated for 168 samples that; cubes had 84 samples and prisms had 84 samples. These samples are total of 3 samples from 7 types of mixture with 4 different curing ages (3, 7, 28, and 56 days) as tabulated in Section 3.2.4; preparation of cubes and prisms.

Table 3.2
Mix Proportions of Mortar for Cube and Prism Samples

Sample	Mixture	ESP	RCA	Testing	Number
Cube	OPCNA	0%	0%	Compression	12
	5EPRCA0	5%	0%		12
	10EPRCA0	10%	0%		12
	15EPRCA0	15%	0%		12
	5EPRCA30	5%	30%		12
	10EPRCA30	10%	30%		12
	15EPRCA30	15%	30%		12
Prism	OPCNA	0%	0%	Flexural	12
	5EPRCA0	5%	0%		12
	10EPRCA0	10%	0%		12
	15EPRCA0	15%	0%		12
	5EPRCA30	5%	30%		12
	10EPRCA30	10%	30%		12
	15EPRCA30	15%	30%		12

Table 3.3
Mix Design of Mortar for Cube and Prism Samples

Materials	Total (kg)
Cement (OPC)	5.0
Eggshell Powder (ESP) – 5%, 10%, 15%	0.5
Silica Fume (SF) – 10%	0.5
Fine Aggregates – Sand (NA)	10.0
Recycles Concrete Aggregates (RCA) – 30%	3.0
Water (w/r = 0.65)	2.9
Superplasticiser (SP) – 1%	0.05

The design mix for this study was carefully formulated using optimum percentages of ESP and RCA as replacement materials in the interlocking block. The mortar ratio, representing the proportion of cement to fine aggregates, was set at 1/4, while the water-to-cement ratio was maintained at 0.65. The interlocking block used in this study measured 280 mm × 125 mm × 100 mm. Additionally, the appropriate percentage of superplasticizer was incorporated to enhance the mixture's performance. The objective of using an optimized design mix was to improve the structural integrity and durability of the interlocking block.

A design mix refers to ratio mortar 1:4 with 1 for cement and 4 for sand. The mix design for every 5 blocks mixture was 7 kg: 28 kg that divided to the precise blending of various materials in specific proportions as shown in Table 3.4. It is to achieve a concrete mixture tailored to meet strength, durability, workability, and other performance criteria for a particular construction project. It involves carefully selecting components such as cement, aggregates, water, and additives while considering factors like environmental conditions, intended application, and structural requirements.

For this study, the material mixture was divided into three categories. The first was the Ordinary Portland Cement - Natural Sand (OPCNA), which consisted of cement, fine aggregates, and water. The second category, Eggshell Powder – Recycled Concrete Aggregate 0% (5EPRCA0), consist of cement, eggshell powder, superplasticizer, sand, and water. There was not included the RCA. The third category, which incorporated Eggshell Powder - Recycled Concrete Aggregates 30% (5EPRCA30), contained cement, eggshell powder, superplasticizer, sand, RCA with fixed value which is 30% and water. In terms of replacement proportions, the optimum percentage of ESP used as a cement substitute was 5%, while RCA was utilized at 30% as a partial sand replacement. Table 3.5 outlines the number of samples used in this study as tabulated in Section 3.3.2; preparation of the interlocking block (IB), categorized into three groups: Solid Interlocking Block (SIB), Single Inclined Connection Interlocking Block (SICIB), and Dual Tongue Inclined Interlocking Block (DTIIB).

Table 3.4
Mix Design of Mortar for Interlocking Block Samples

Materials	**Total (kg)**
Cement (OPC)	71.4
Eggshell Powder (ESP) – 5%, 10%, 15%	35.7
Silica Fume (SF) – 10%	11.9
Fine Aggregates (NA)	333.2
Recycles Concrete Aggregates (RCA) – 30%	142.8
Water (w/r = 0.65)	77.35
Superplasticiser (SP) – 1%	1.19

Table 3.5
Mix Proportions of Mortar for Interlocking Block Samples

Parameter	**Mixture**	**Eggshells**	**RCA**	**Flexural**	**IB**
SIB	OPCNA	-	-	√	9
	5EPRCA0	5%	-	√	9
	5EPRCA30	5%	30%	√	9
SICIB	OPCNA	-	-	√	9
	5EPRCA0	5%	-	√	9
	5EPRCA30	5%	30%	√	9
DTIIB	OPCNA	-	-	√	9
	5EPRCA0	5%	-	√	9
	5EPRCA30	5%	30%	√	9

3.2.2.1 Jaw Crusher Machine

Jaw crushers as shown in Figure 3.15 are heavy-duty machines that must be built to last. The main frame is frequently made of cast iron or steel and is held together with tie-bolts. It is typically built in sections so that it can be transported underground and installed (Barry et al. 2016). A crusher is a device designed to reduce the size of large rocks into smaller ones, such as gravel, sand, or rock dust. This size reduction is crucial for efficient transportation of products through conveyors and other means. Crushing marks the initial phase in the process of separating minerals from waste materials (gangue).

The waste material can either be disposed of or recycled, allowing the mineral-rich product to undergo further processing at the primary plant. Typically, jaw crushers are employed to carry out the initial crushing phase. In many cases, only one crusher, known as the 'primary crusher,' is installed. Concrete particles are crushed and subsequently sorted into standard fractions of coarse aggregate, ranging from 4–8 mm, 8–16 mm, to 16–31.5 mm. The internal component of jaw crusher machine can be seen in Figure 3.16.

Figure 3.15 Jaw Crusher Machine

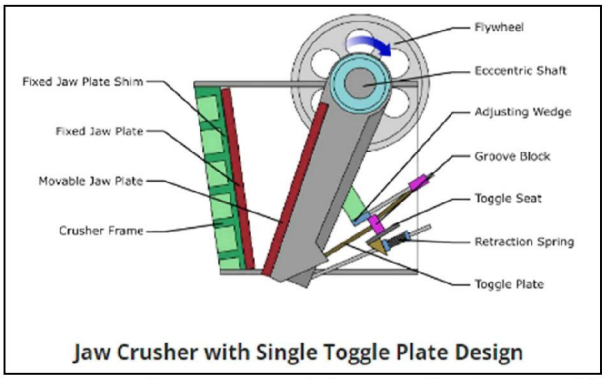

Figure 3.16 Component of the Jaw Crusher Machine
(Source: Terex Jaques, Single Toggle Jaw Crusher, https://www.armstrongequipment.com/wp-content/uploads/2017/02/ST-Series-JawBrochure.pdf, 2010)

3.2.2.2 Sieving (Aggregates)

A predetermined quantity of material is placed onto a set of nested sieves, arranged from the largest screen openings at the top to the smallest at the bottom, as illustrated in Figure 3.17. The sieves are then subjected to mechanical shaking for a specified duration. Once the material has passed through the sieves, the amount of retained material on each sieve is measured. For coarse aggregate, the large tray shaker is commonly utilized, featuring a clamping mechanism to secure the sieve during agitation. Typically, these shakers are operated for 5 minutes for sieves size 9 or larger, and for 10 minutes for smaller sizes. Conversely, fine aggregate is typically obtained using Round 8" (203.2 mm) or 12" (304.8 mm) sieves, which are self-nesting and supported by various clamping or holding mechanisms. Smaller shakers of this type require approximately 15 minutes of shaking time to ensure proper grading of the fine aggregate sample.

Figure 3.17 Sieving Set

3.2.3 Casting and Curing of Cube and Prism

As the first step of mixing, the inner surface of the tilting drum mixer was wetted. During the running of the tilting drum mixer, adding the materials sequence. After that, successive addition of cement, and fine aggregates were added gradually. Finally, add the last ingredient in the concrete mixture, which is the amount of water while manually running the tilting drum mixer (Al-Rousan et al. 2018). The next stage is to use the mixer machine to mix the concrete mixture. The mixer machine used to mix the materials for each batch in this study is shown in Figure 3.18.

In this study, there had mixture was 7 different of types that consist as mentioned in Section 3.2.1, preparation of materials. Two types of moulds which are cube moulds measuring 50 mm x 50 mm x 50 mm and prism moulds with dimensions of 140 mm x 60 mm x 60 mm were used. Figure 3.19 illustrated the plastic mould that used for casting the cubes and prisms. To ensure easy removal after drying, the moulds were coated with oil before the mortar was put into them. After filling the moulds, the mortar was put on a vibrating machine to remove any remaining air voids. The moulds were left to dry for 24 hours before the curing process. The visual of the casting phase was shown in Figure 3.20.

Figure 3.18 The Mixing Casting

Figure 3.19 Plastic Mould for Cube and Prism Samples

Figure 3.20 Casting of Cube and Prism Samples

Cured the specimen in a clean tap water tank for 3, 7, 28 and 56 days. In accordance with Jabatan Kerja Raya's Standard Specification for Building Works (PWD 203A), (2015), the selection of curing ages at 3, 7, 28, and 56 days reflects both practical site considerations and the standardized strength development profile of concrete. Early age concrete strength at 3 days is typically assessed to monitor initial hydration progress, and structural readiness, although formal acceptance criteria are generally based on 7, and 28 days compressive strength benchmarks (Adam, 2012). The 7, and 28 days compressive strength benchmarks are explicitly referenced in JKR's

standard, where cube testing is mandated to assess early and standard strength performance (JKR's Standard Specification for Building Works (PWD 203A), 2015). The 28 days strength remains the principal criterion for structural acceptance, while extending testing to 56 days is increasingly recognized for mixes incorporating Supplementary Cementitious Materials (SCMs) such as Fly Ash (FA), slag, Eggshell Powder (ESP), and Silica Fume (SF) (The Concrete Centre, 2021; Raza et al., 2021). The studies had written these materials had hydrated more slowly and continue to gain strength well beyond the initial 28 days. Although, 90 days curing can yield incremental strength improvements, studies show that concrete stops gaining strength quickly after 56 days, and any increase after that is small usually less than 10%. (Raza et al., 2021; Ebrahim et al., 2023). Moreover, adopting 56 days strength criteria supports sustainable construction practices by facilitating the use of SCMs and minimizing reliance on high cement content mixes (The Concrete Centre, 2021). Therefore, testing up to 56 days offers a balanced approach between performance validation and study efficiency. It also ensures compliance with national guidelines while promoting eco-efficient material choices.

Concrete curing is the process of maintaining a specific level of moisture and temperature in newly cast concrete for a set period after installation. The primary goals of this procedure are the prevention and replacement of concrete moisture, as well as the long-term maintenance of a temperate environment conducive to hydration. Figure 3.21 is the curing area for the samples that placed at 'Makmal Konkrit', UiTM Pulau Pinang. Curing prevented moisture loss in already concrete. Cement curing increased its strength, water tightness, wear resistance, and longevity to the greatest extent possible by completely hydrating it. The curing process begins after the concrete has been poured for a full day.

Figure 3.21 Curing Tank

3.2.4 Preparation of Cubes and Prisms

Table 3.6 presents the samples prepared for achieving the objective 1. These specimens were subjected to both flexural and compression testing. For flexural testing, prisms with dimensions of 160 mm × 40 mm × 40 mm were used, while compression testing was carried out on cubes measuring 50 mm × 50 mm × 50 mm. Altogether, seven mortar mixtures using ESP and RCA were created. Each mixture produced 12 specimens, making a total of 168 samples tested for both flexural and compressive strength. Each mixture was cast into three specimens for various curing ages (3, 7, 28, and 56 days), and the average values of the test results at each curing age were reported.

Table 3.6
The List of Cubes and Prism Samples and The Total

No	Sample	Testing	Curing (Days)				Total Sample
			3	7	28	56	
1	Cube	Compression	21	21	21	21	84
2	Prism	Flexural	21	21	21	21	84
	Total Sample		42	42	42	42	**168**

3.2.5 Testing for Fresh Mortar

A flowability test is a well-known laboratory experiment used to measure a mortar mix's workability, specifically its consistency and fluidity. This test follows ASTM standard ASTM C1437 – Standard Test Method for Flow of Hydraulic Cement The mortar testing procedure is essential for evaluating the ease with which concrete can be mixed, transported, and placed while avoiding segregation (aggregate separation) and bleeding (surface water seepage). Flowability tests were conducted to calculate the amount of water required for the strength test and the drying shrinkage tests of cement.

The fluidity of fresh mortar is determined by the flowability test, indicating its ease of moulding and handling. The diameter of the concrete spread is measured when it is exposed to a predetermined degree of compaction on a flow-table. The analysis of the results was used the equation 3.1 to get the percentage of the flowability. Results with over 120% are acceptable (see Table 3.7). The resulting flowability is an important aspect of concrete quality control that follows the recommendation range of the flow-table diameter. Based on the recommend diameter, results can be determined the

workability performance. The tools as shown in Figure 3.22 and techniques outlined here were used in the experiment to determine if mortar samples were workable.

Flowability

$$\text{Percentage (\%)} = \left(\frac{D}{D_0} - 1 \right) \times 100\% \quad (3.1)$$

Where:

- D = Final spread diameter after flow table test
- D_0 = Mold base diameter (typically 100 mm)

Table 3.7
Recommended Range of Workability Mortar

Criteria	Flow Table Diameter	Remarks
Minimum Acceptable Limit	> 120 mm	Below this, the mix is too stiff (poor block contact)
Recommended Range	130 mm – 145 mm	Ideal for good bond, minimal segregation, and ease of use
Maximum Preferred Limit	≤ 150 mm	Above this, mortar become too wet (reduced strength)

(Source: ASTM C1437, 2020)

Figure 3.22 Flow-table Set Testing

3.2.6 Water Absorption of Cube and Prism

Water absorption tests consist of measuring the weight of the samples while wet after curing age 3, 7, 28, and 56 days of being immersed in water and measuring them again after oven about 24 hours within 100°c and calculating the absorption percentage. Based on ASTM C642 - Standard Test Method for Density, Absorption, and Voids in Hardened Concrete. The results were calculated using equation 3.2 and followed the acceptable water absorption range as shown in Table 3.8. If the water absorption of

samples is high, then the samples absorbed water much and not well strength performance. One reasonable measure of the quality and longevity of hardened mortar is the amount of water it absorbs (Prakash et al. 2023). In Figure 3.23, there is the condition of the samples that been dried in the oven 'Makmal Konkrit', UiTM Pulau Pinang.

Water Absorption

$$\text{Percentage (\%)} = \left(\frac{Ww - W}{Wd}\right) \times 100\% \qquad (3.2)$$

Where:

- Ww = Weight of the material after saturation (in grams or kilograms)
- Wd = Initial dry weight of the material (in grams or kilograms)

Table 3.8
Acceptable Range of Water Absorption

Percentage Range	Description
Good	< 10%
Moderate	10% - 15%
High	> 15% (indicate high porosity or poor compaction)

(Source: ASTM C642, 2021)

Figure 3.23 Sample in Oven for 2 hours with 100°c

3.2.7 Compression Strength Test of Cube

The compression test, which is performed under ideal conditions, determines the highest compressive strength of concrete. The compression test was used to determine the strength of hardened concrete. Field concrete samples were prepared, cured, and tested in accordance with ASTM C109/C109M – Standard Test Method for Compressive Strength of Hydraulic Cement Mortars (Using 50 mm Cube Specimens) procedures. Figure 3.24 is the Compression Machine that provided in 'Makmal Konkrit'.

Compression analysis, among other things, was used to determine the strength of concrete as well as how a product or substance performs when compressed, squashed, crushed, or flattened. In the study, 84 samples of concrete cube measuring 50 mm x 50 mm x 50 mm was utilized to assess compressive strength. It achieves this by defining the fundamental properties that govern the behaviour of the specimen when subjected to a compressive force (equation 3.3).

Uniaxial compressive strength testing was performed on sample cubes (see Figure 3.25) in this study. This samples are evaluated at intervals of 3, 7, 28, and 56 days after the mould has been removed and the curing session has taken place. By evaluating basic parameters including stress, and deformation, a compression test aims to establish. Uniaxial compression testing can provide information about a material's characteristics. Compressive testing can be performed to determine a material's elastic limit, elastic modulus, yield strength, and compressive strength.

Compressive Strength

$$f_c = \left(\frac{P}{A} \right) \tag{3.3}$$

Where:

- f_c = Compressive strength (MPa or N/mm²)
- P = Maximum load (N or kN)
- A = Loaded area (mm^2 or m^2)

Figure 3.24 Compression Test Machine

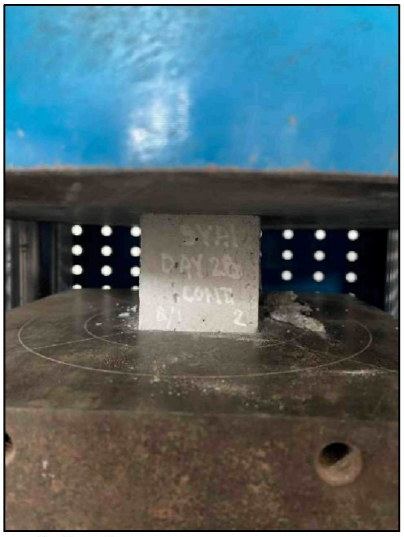

Figure 3.25 Cube (50 mm X 50 mm X 50 mm) Set Up

3.2.8 Flexural Strength Test of Prism

Flexural strength is a fundamental mechanical property of prism that defines its ability to resist bending forces. By using ASTM C78 / C78M – Standard Test Method for Flexural Strength of Concrete (Third-Point Loading), it specifically measures the flexural strength of prism under flexural loading conditions, making it a crucial parameter in the design and evaluation of structural elements such as beams and slabs. Manual calculation can be determined by equation 3.4. Determining flexural strength involves a systematic testing process, which requires a set of essential equipment, including a ruler for precise measurement, a marker for identifying reference points,

prism samples, and a specialized flexural strength testing machine called Universal Testing Machine 100 kN (Figure 3.26).

The prism samples, measuring 140 mm × 60 mm × 60 mm as illustrated in Figure 3.27, were carefully prepared according to predetermined concrete mix design specifications. A total of 84 samples were produced for this investigation. Following their preparation, the samples were immersed in water to initiate the curing process, ensuring adequate hydration and development of mechanical properties. After curing periods of 3, 7, 28, and 56 days, the specimens were systematically removed from the curing environment. Before testing, each sample underwent a 24-hour drying phase to eliminate any residual moisture, preventing interference with the accuracy of the flexural strength assessment.

Before initiating the flexural strength tests, precise measurements were conducted to determine the dimensions of each sample. Special attention was given to marking the midpoint of the prisms, ensuring consistency and accuracy during testing. This meticulous approach guarantees reliable results and aids in evaluating the performance of concrete under bending stress.

Flexural Strength

$$f_r = \left(\frac{P \cdot L}{b \cdot d^2} \right) \tag{3.4}$$

Where:

- f_r = Flexural strength (MPa or N/mm²)
- P = Maximum applied load at failure (N)
- L = Span length (mm)
- b = Width of the specimen (mm)
- d = Depth (height) of the specimen (mm)

Figure 3.26 Universal Testing Machine 100 kN

Figure 3.27 Prism Set Up used suitable Three-Point Loading for 160 mm X 40 mm X 40 mm Prism

3.2.9 Summary on The Optimum of the Percentage of Eggshell Powder, Silica Fume and Recycled Concrete Aggregate

The optimum percentages of ESP, SF, and RCA were identified based on improvements in compressive and flexural strength, as well as acceptable flowability and durability. The combination that showed the best overall performance typically involved 5%, 10%, and 15% ESP, 10% SF, and up to 30% RCA replacement. These proportions provided a balanced mix that enhanced mechanical properties without compromising workability or water absorption standards.

3.3 Preparation of The Interlocking Block (IB)

The preparation of the Interlocking Block (IB) begins with the careful selection and mixing of materials according to the desired proportions. The fresh mix is then placed into a mould to form the interlocking shape and left to cure under controlled conditions to achieve the required strength and durability. Furthermore, the study examines the potential of ESP and SF as alternative binders in enhancing interlocking brick formulations.

In the Table 3.9, there are shown the sample that were done in the study. The sample are conducted the flexural testing. It is formed as interlocking block sizing 280 mm x 100 mm x 125 mm for flexural testing. Also, it is form with 3 types of different mixture which are OPCNA, 5EPRCA0, and 5EPRCA30 as mentioned in Section 3.2.2: mix design of mortar. The mixture has 3 samples each of different curing ages (7, 14, and 28 days) and take the average of the results of each curing ages.

Table 3.9
List of Interlocking Blocks

No	Sample Name	Parameter	Curing (Days)			Total Sample
			7	14	28	
1	Single Interlocking Block	SIB	9	9	9	27
2	Single Inclined Connection Interlocking Block	SICIB	9	9	9	27
3	Dual Tongue Inclined Interlocking Block	DTIIB	9	9	9	27
	Total Sample		27	27	27	**81**

3.3.1 Design of Interlocking Block (IB)

Design references of the design by using standard of BS 6073 – 1:1981 clause 3.12a which is the brick is a masonry unit not exceeding 337.5mm in length, 225mm in width or 112.5mm in height. By the concept of the interlocking, in this study were used Tongue and Groove Joint (TGJ) with Chamfer Edge (CF).

In Figure 3.28(a), the Tongue and Groove Joint (TGJ) are a versatile interlocking mechanism that can be applied in both vertical and horizontal orientations depending on the structural configuration and functional requirements of modular systems. However, the TGJ used as vertical interlock in this study. In vertical applications, such as dry stack modular blocks, the protruding "tongue" of one block fits securely into the "groove" of the block above or below, enabling efficient load

transfer, enhanced structural stability, and resistance against vertical displacement (CIDB, 2020). Horizontally, this joint is widely used in systems like flooring and decking, where lateral alignment, shear resistance, and surface continuity are essential for performance and longevity (JKR Malaysia, 2016). The directional placement and geometry of the tongue and groove features ultimately govern their locking efficiency across both axes.

Chamfered studs (CF) are predominantly employed to optimize horizontal interlocking in modular block systems as shown in Figure 3.28(b). Their design enhances stress distribution, reduces the risk of cracking, and supports accurate, smooth alignment during block installation (Anand & Ramamurthy, 2000; Koudje & Adjovi, 2025). Integrating a chamfered top stud further improves interlocking efficiency with the bottom space by guiding block placement and reducing resistance during stacking (Aswad et al., 2022). This configuration not only strengthens structural reliability but also streamlines construction workflows, making it highly suitable for modular and dry-stack applications (Kumar & Vigneshvar, 2014; Onyeakpa & Onundi, 2014).

Although CF was focused as horizontal interlock in this study, but chamfered edges itself can assist in vertical stacking by facilitating top to bottom alignment, their primary role is to improve side to side interlock, which is essential for wall stability and dry stacking performance (Koudje & Adjovi, 2025). Moreover, the chamfered surfaces minimize friction, allow smoother handling, and ensure a better fit between blocks, contributing to overall construction efficiency. Figure 3.28(c) highlights the section where these two components will function as the interlocking mechanism.

Additionally, the design concept in this study draws inspiration from the conventional Malaysian interlocking brick (Uniti Brick Sdn Bhd, 2025), typically sized at 280 mm × 125 mm × 100 mm, which serves as a foundational reference. The proposed designs are an evolving interpretation designed to improve usefulness and performance, building upon a carefully chosen combination of conventional designs and knowledge from previous studies as mentioned in Section 2.3.6; research gap of design interlocking block. By addressing the limitations identified in previous models, this enhanced design aims to improve structural performance, ease of assembly, and adaptability for sustainable construction applications.

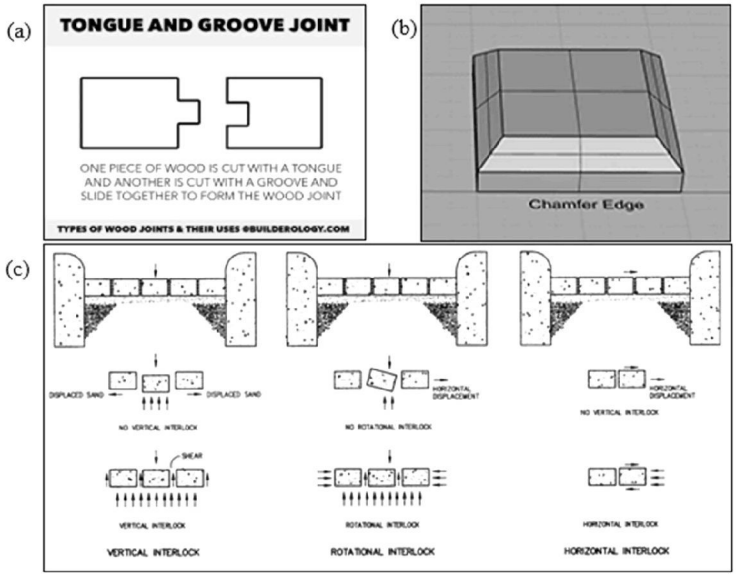

Figure 3.28 Types of Joint and Stud Edge of Interlocking Block: (a) Tongue and Groove Joint; (b) Chamfer Stud Edge (Top and Bottom); and (c) Types of interlock (vertical, rotational, and horizontal)
(Source: Ideal Block, PAV-TEC-004-23.pdf, 2023)

There have 3 types of design which are control design: Solid Interlocking Block (SIB), interlocking design 1: Single Inclined Connection Interlocking Block (SICIB) and interlocking design 2: Dual Tongue Inclined Interlocking Block (DTIIB) in Figure 3.29, Figure 3.30 and Figure 3.31, respectively. Design 1 and Design 2 are each special in their own way because they were made to solve different problems found in earlier studies. SIB (Figure 3.29) serves as the foundational block design, characterized by its plain cuboid shape without any distinctive or specialized features. It functions as a standard unit, primarily used as a baseline for comparison with more advanced interlocking block variations. Its simplicity allows for easier evaluation of enhancements introduced in later designs.

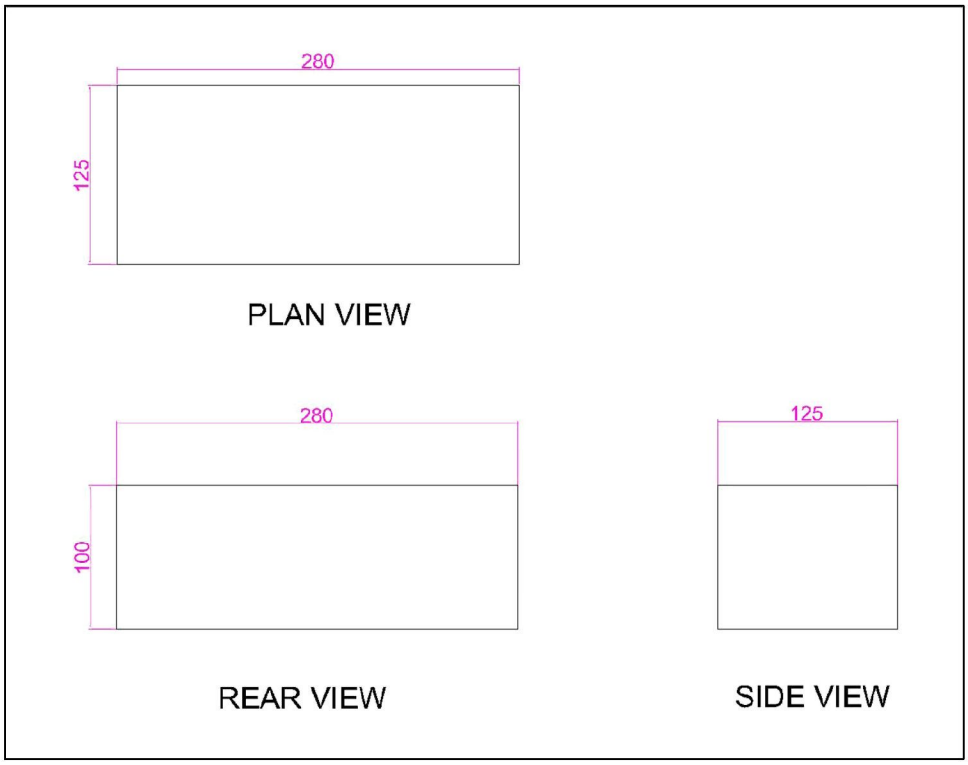

Figure 3.29 Schematic Diagram of Solid Interlocking Block Design.

The design 1 – Single Inclined Connection Interlocking Block (SICIB) was featured in this study contains two inclined connections as the TGJ system and two hollow spaces per CF, as showed in the Figure 3.30. This configuration allows effortless interlocking, simplifying assembly while maintaining structural integrity and load-bearing capacity. Unlike earlier studies that relied on straight or flat joints, the inclined joint design draws inspiration from chamfered edges, enhancing vertical interlock performance and reducing lateral displacement. This innovation eliminates the need for adhesives or cement between layers, representing a significant advancement over traditional dry-stack systems.

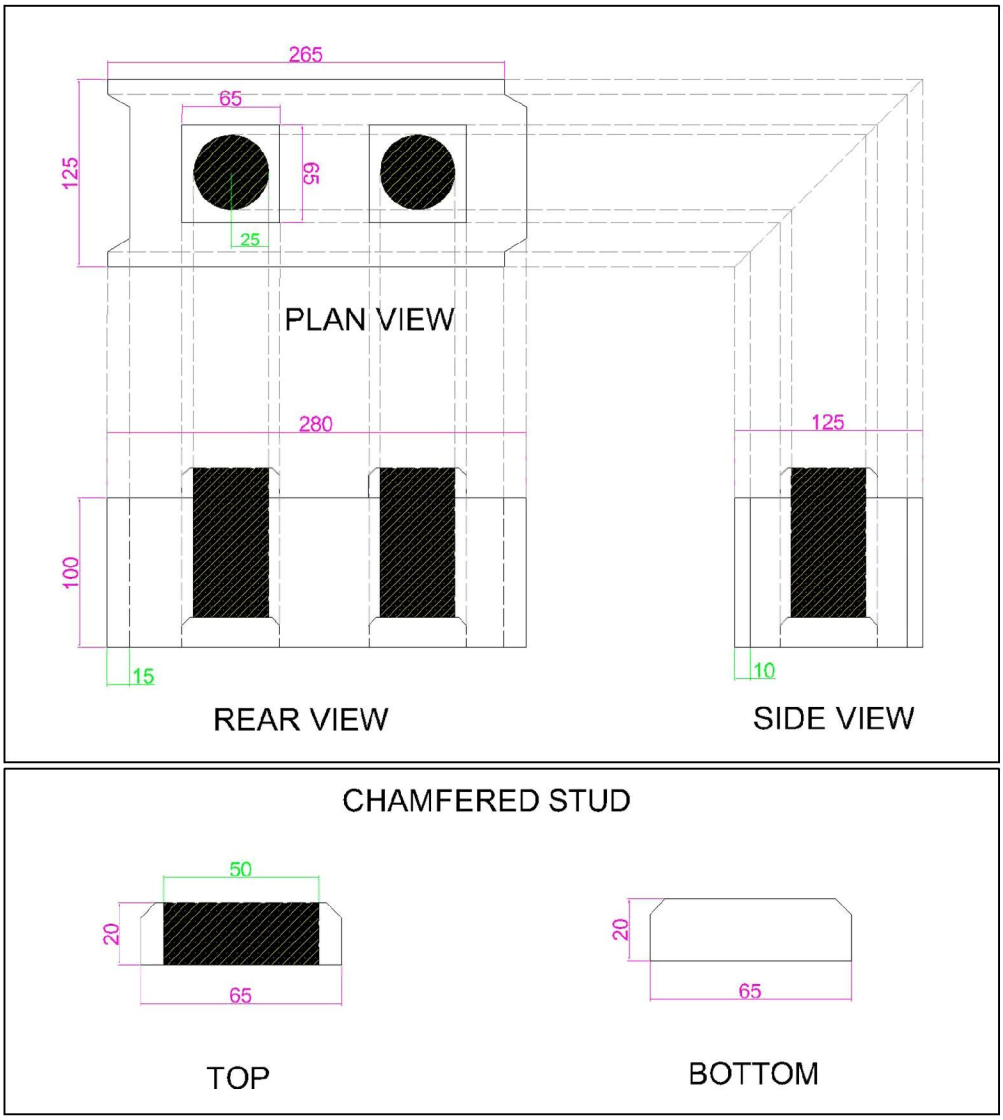

Figure 3.30 Schematic Diagram of Single Inclined Connection Interlocking Block (SICIB)

The design 2 – Dual Tongue Inclined Interlocking Block (DTIIB) was featured stick out part and spaces to fill in the slot as the TGJ system and one hollow at the middle of the CF, as showed in the Figure 3.31. Unlike SICIB, which contains hollow sections throughout, DTIIB blocks are designed as solid units, thereby improving strength. Traditional TGJ systems typically employ a single tongue and groove; however, this study introduces a dual tongue–dual groove configuration resembling forked interlocks. This enhancement significantly improves vertical interlock performance, maximizes stability, and minimizes lateral displacement. Compared to previous designs, DTIIB provides a more secure fit without adhesives, making it highly effective for dry-stack construction.

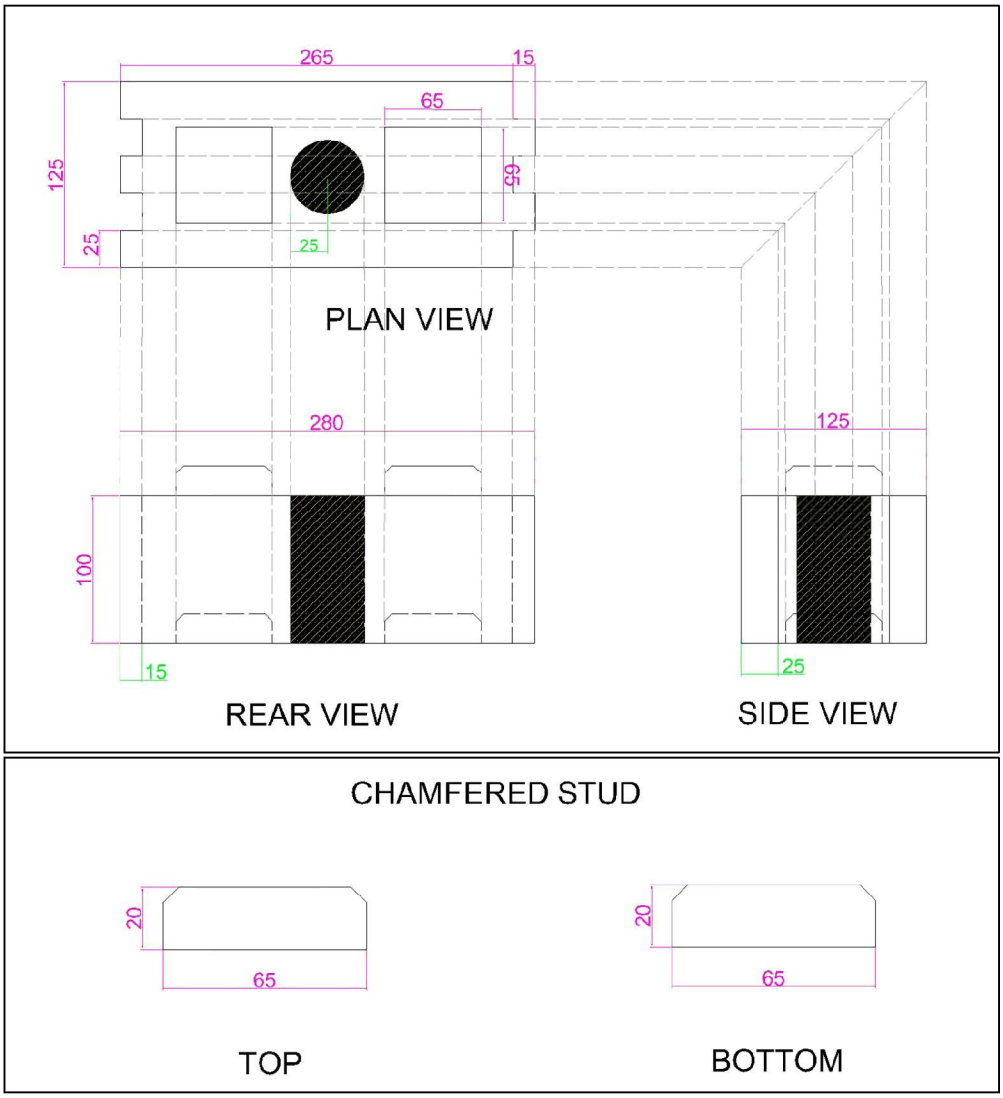

Figure 3.31 Schematic Diagram of Dual Tongue Inclined Interlocking Block (DTIIB)

3.3.2 Preparation Formwork of Interlocking Block (IB)

The formworks were built for 3 different types of interlocking blocks samples which are SIB, SICIB, and DTIIB. There were 2 different types of formworks: plywood and recycled steel. SIB was formed by plywood, meanwhile SICIB and DTIIB were formed by recycled steel. Both have atypical purposed of formworks because of SIB was easier to be builds, so it is more affordable by using plywood. In the meantime, SICIB and DTIIB were more complex in designs.

Additionally, SICIB and DTIIB had the PVC tube to maintained and stand the hollow that needed for the samples. As standard formwork is connected by using nails.

However, in this study were forced to have more than 3 samples of interlocking blocks for each design, thus the connection was using the screws as it can be removed easily by using screw gun.

3.3.2.1 Mould Process

A critical step in building interlocking block (IB) is preparing the formwork, which acts as a mould to guarantee shape correctness and uniformity. The formwork material must be able to sustain the pressure of the concrete during pouring in order to meet design specifications; plywood is a common choice for control block design – Solid Interlocking Block (SIB). Meanwhile, the other 2 IB design; Single Inclined Connected Interlocking Block (SICIB), and Dual Tongue Inclined Interlocking Block (DTIIB) were used steel as the material of their formwork. To stop leaks and maintain the desired block geometry, the formwork is carefully cut and put together with tight joints like screw.

For SIB, plywood was selected as the formwork material due to its ease of cutting and ability to be securely fastened using wood screws. Figure 3.32 displays the plywood utilized during the formwork preparation phase. The entire process, illustrated in Figures 3.33 and 3.34, encompassed sketching, cutting, and assembling the pieces using wood screws, and took approximately one week to complete.

A total of 30 formwork units were constructed for the SIB design. Although only 27 moulds were required to accommodate three mixtures OPCNA, 5EPRCA0, and 5EPRCA30. There had three additional blocks were fabricated as backups in case of unforeseen issues. Upon completing the fabrication process, the formwork was thoroughly inspected to ensure no gaps or defects were present that could affect the casting process, as shown in Figure 3.34.

Figure 3.32 Plywood

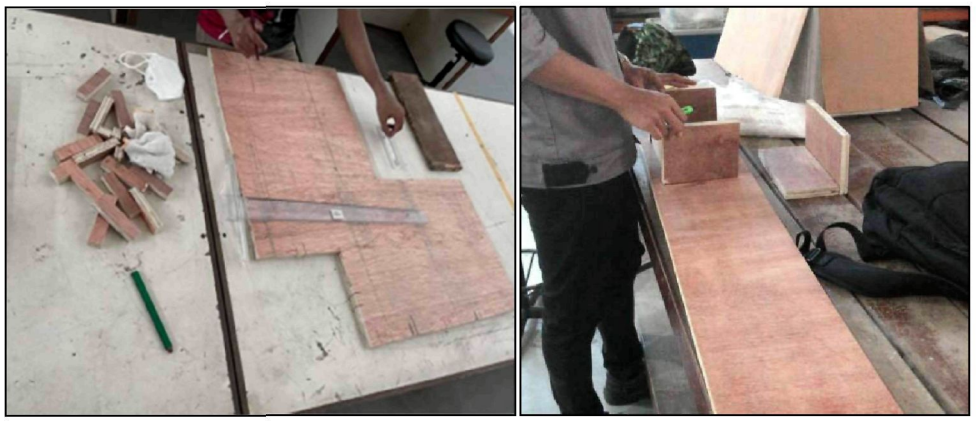

Figure 3.33 Sketch on Plywood Mould for Solid Interlocking Block (SIB)

Figure 3.34 Plywood Mould for Solid Interlocking Block (SIB)

For the fabrication of formwork used in SICIB and DTIIB, an external steel workshop located near UiTM Permatang Pauh was commissioned. The workshop produced the formwork based on detailed specifications provided, including block dimensions, interlocking features, and hollow configurations. Steel was selected as the

formwork material due to its durability, dimensional stability during casting, and adaptability to complex design requirements.

Uses of recycled steel from the workshop was the effort to implement the sustainability culture as reused the useable material like steel. Other than design sheets as workshop reference, there was the first draft sketched of the IBs were made to illustrate the pattern (see Figure 3.35) and show the example to the workshop personnel. So, with that extend of references, they could imagine how the formwork be built. In Figures 3.36 illustrate the preparation process undertaken by the workshop personnel, following precise instructions to ensure the formwork accurately reflected the intended geometry of the IBs.

Figure 3.35 Steel Mould for Single Inclined Connection Interlocking Block (SICIB) and Dual Tongue Inclined Interlocking Block (DTIIB)

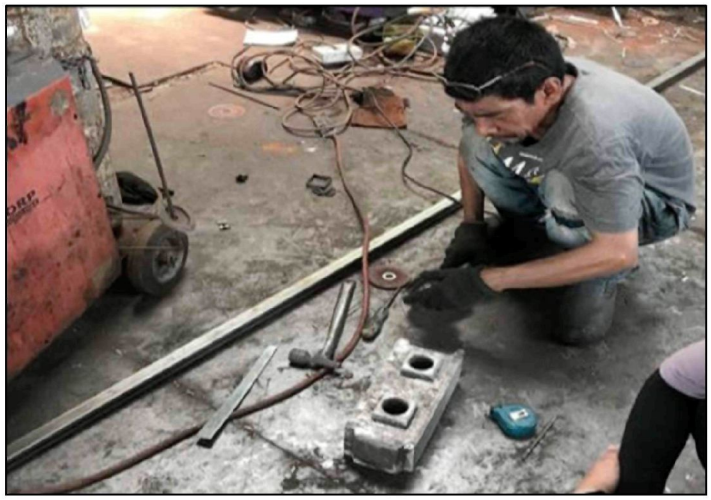

Figure 3.36 Steel Mould Preparation formwork for interlocking block design

The steel components were joined through a combination of welding and mechanical fastening using screws. To create the hollow spaces in the sample blocks, one or two pipes were placed in the middle of the formwork. Figure 3.37 shows the pipes that were used to stop the mixture from filling the hollow parts during casting.

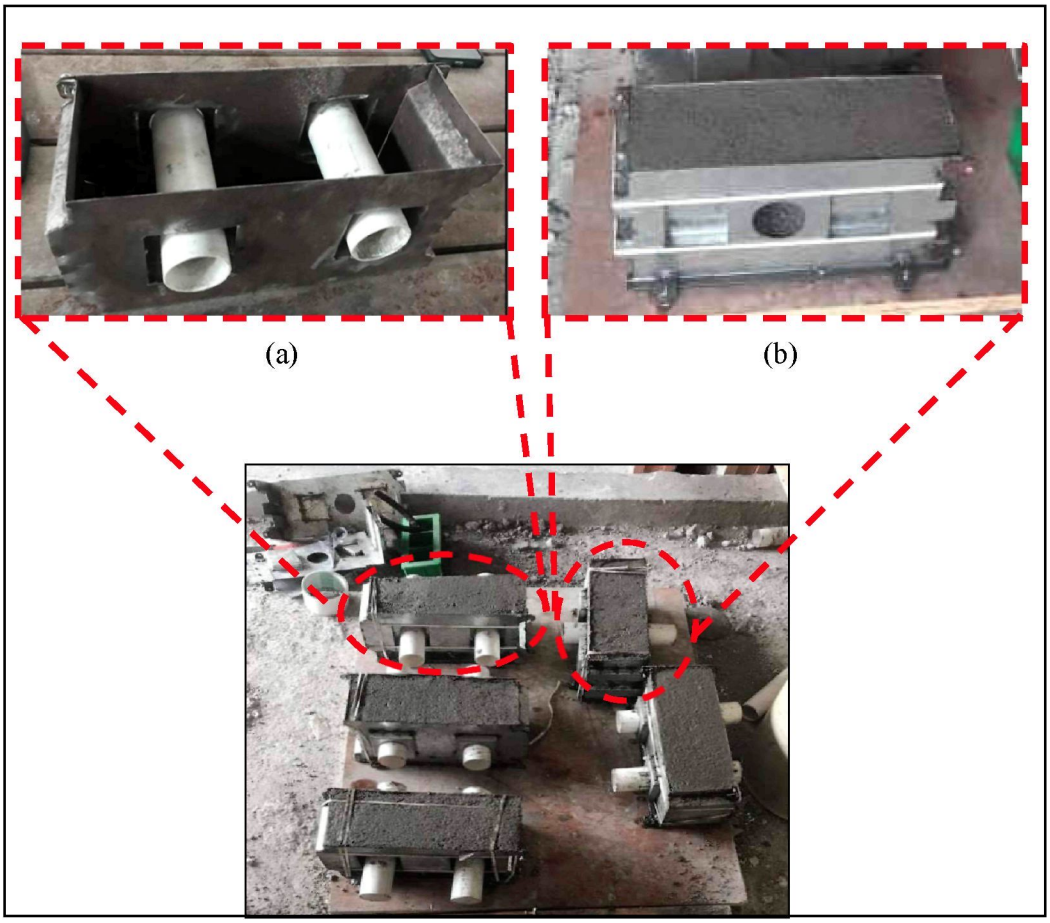

Figure 3.37 The Pipe Tube PVC that Used as Hollow Support: (a) Formwork for Single Inclined Connection Interlocking Block (SICIB), and (b) Dual Tongue Inclined Interlocking Block (DTIIB)

3.3.3 Casting and Curing of Interlocking Block (IB)

Once the formwork was prepared, the casting process commenced. Material mixing was carried out using a laboratory mixer machine, as shown in Figure 3.38. This mixer has a maximum capacity of 50 kg, which limits each batch to the production of five blocks, given the block dimensions of 280 mm × 125 mm × 100 mm. As to mixed well and easy to handle, each mixture was limit for 35 kg in total materials added.

Figure 3.38 The Mixer Machine (cleaning after used)

Following the mixing stage, the fresh mortar was transferred into the formwork and compacted using a vibrator machine. The vibrator ensures thorough compaction by eliminating trapped air and promoting a uniform, dense mixture. This step is essential for enhancing the structural integrity and durability of the blocks. A concrete vibrator was employed to minimize air voids and achieve optimal compaction. After vibration, any excess mortar was levelled off using a screed board or straight edge to produce a smooth surface finish on the top of the interlocking blocks. Figure 3.39 illustrates the casting process after vibration.

Figure 3.39 Condition of Mixture After Vibrated Using Vibrator Plate Machine

The filled formwork was left undisturbed for 24 hours to allow sufficient hardening before demoulding, as depicted in Figure 3.40. For the interlocking block design, a central pipe embedded in the formwork was removed approximately 40 minutes after casting. This timing was critical to prevent the mixture from adhering to the pipe, which could complicate its removal and affect the block's geometry. After 24

hours, the mixtures were dried and can be disassembled (Figure 3.41) from the mould to proceed curing process.

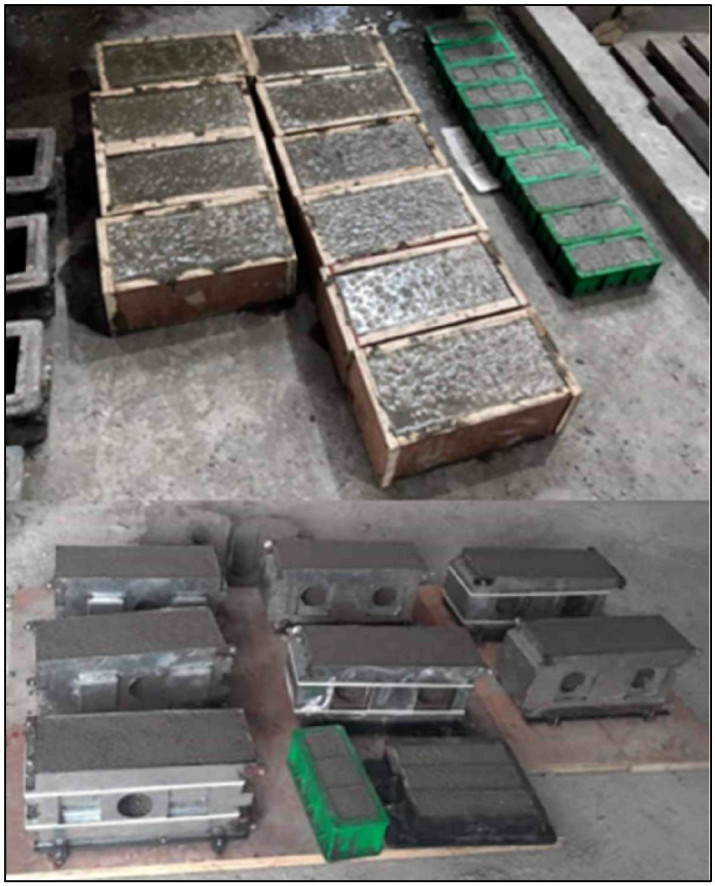

Figure 3.40 Filled Mould Dried for 24 Hours

Figure 3.41 Process of Disassembled Mould

For concrete specimens to properly hydrate and increase their strength, the curing procedure is essential. In this study, all samples were cured under controlled conditions to maintain consistency and reliability in the results. IBs specimens were demoulded and submerged in water tanks for curing durations of 7, 14, and 28 days, as illustrated in Figure 3.42. Water curing was selected to preserve moisture levels and promote optimal cement hydration, which is essential for achieving the desired mechanical properties.

Figure 3.42 Curing Process

Proper curing is crucial for interlocking blocks, as their strength develops gradually over time. This method ensured a reliable assessment of the strength and durability of interlocking blocks incorporating eggshell powder (ESP) as a partial cement replacement and Recycled Concrete Aggregates (RCA)as a sand substitute. Maintaining optimal curing conditions was essential for the blocks to achieve their maximum structural performance with gradually checked up the water level, thereby providing dependable data to evaluate the feasibility and effectiveness of using waste materials in sustainable interlocking block production.

After completing the designated curing period, each sample was removed from the water tanks according to its curing schedule. Figure 3.22 displays the samples post-curing, prior to the drying phase. All specimens were air dried for 24 hours before being prepared for subsequent testing.

Figure 3.43 After Curing Period

3.3.4 Flexural Strength Test of Interlocking Block (IB)

To ascertain the Flexural strength of the interlocking blocks, a test was conducted using a Universal Testing Machine 100 kN in line with BS EN 13523-7(2001). Flexural test, also known as a bending test, is a standardized test method used ASTM C78 / C78M – Standard Test Method for Flexural Strength of Concrete (Third-Point Loading) to evaluate the flexural strength and behaviour of a material. It measures the material's ability to resist bending or deformation under a bending load.

The flexural test is commonly performed on materials such as concrete, metal, wood, composites, and plastics. It provides important information about the material's stiffness, strength, and ductility, which are essential for designing and evaluating structural components.

The flexural test was employed in this study to assess the constructed concrete's quality and forecast the maximum load. A concrete cube of 280 mm x 125 mm x 100 mm was utilised to assess flexural strength. For 7, 14, and 28 days, the flexural machine will take an average of three cube samples. To determine the mean average of the sample results, repeat the operation three times after placing the concrete cube in the flexural machine and waiting until the sample fails. The universal testing device utilised in this study is depicted in Figure 3.44. In Figure 3.45, there was the setup of the flexural testing of the interlocking blocks. As a visual observation, there also observed the crack pattern after the flexural testing done. Then, measured and noted the crack pattern using

the crack ruler. For the flexural testing, the crack pattern usually be flexural crack. It is also had tendency to split to two.

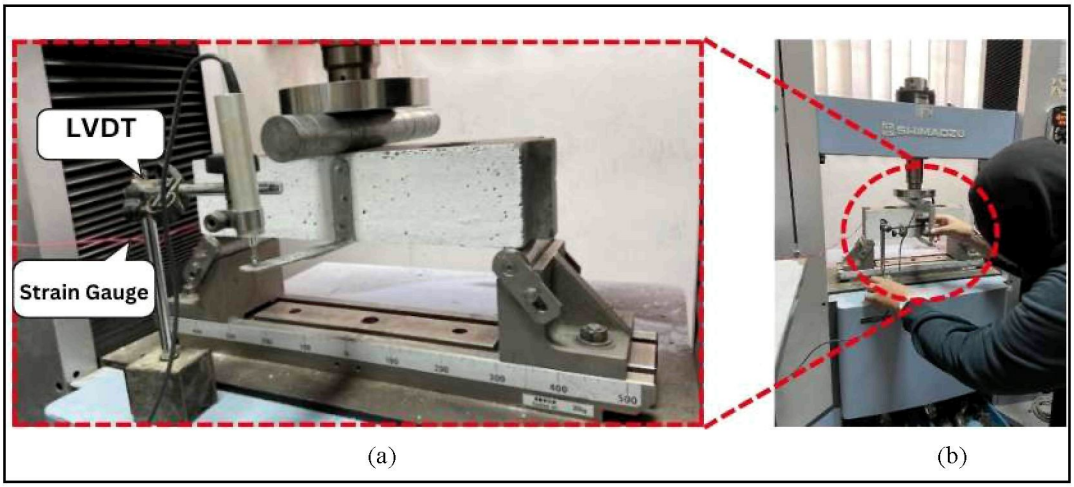

Figure 3.44 Installation of Strain Gauge and LVDT with Universal Testing Machine (UTM): (a) The enlargement; (b) Test Setup

3.3.5 Summary on The Design of Interlocking Block (IB)

The design of the interlocking block (IB) focuses on achieving dimensional accuracy, structural stability, and ease of assembly without the use of mortar. Key features such as tongue-and-groove joints and uniform geometry were incorporated to ensure proper alignment and load transfer. This design supports fast, dry-stack construction while maintaining strength and durability standards.

3.4 Method for Artificial Neural Network (ANN) by MATLAB

Artificial neural network (ANN) is becoming more and more popular because of their remarkable capacity to solve challenging and highly nonlinear mathematical problems. The goal of ANNs is to mimic how the human brain works by combining mathematical models with data (Oztürk & Basar, 2022). The system works like a "black box," where artificial neurons and processing elements are connected through weighted values called synapses. Each neuron processes signals it receives from other neurons and sends out signals that affect the input for the next neuron. This setup allows the network to simulate, predict, and improve system performance by learning from training data and identifying patterns.

In the ANN approach, various functions can be applied for prediction tasks; however, MATLAB recommends utilizing the network configuration. According to Figures 3.46, MATLAB's Neural Network Fitting Tools (NF) solve the problem of matching inputs to outputs using a two-layer feed-forward network. ANNs are modelled after biological neurons and use computational intelligence, following common AI practices. They can analyse complex relationships between inputs and outputs, which helps in accurately describing processes.

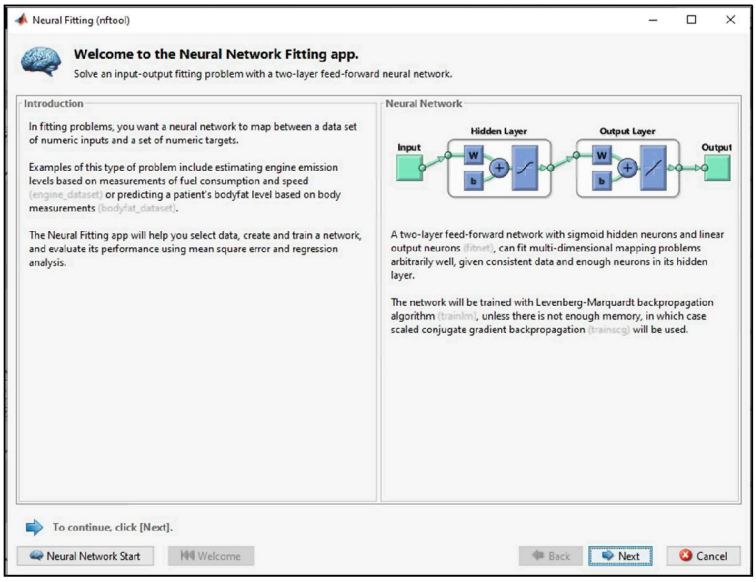

Figure 3.45 Neural Network Fitting Application

The Figure 3.47 illustrates that each neuron can receive multiple inputs (xi), with each input value being multiplied by a corresponding weight (wi). These weights determine how strongly each input influences the neuron (Zahmatkesh et al., 2022). In the simplest neuron model, the products of the inputs and weights are summed and fed into a transfer function, which then produces the final output. The process transferring the data to a computer and organizing it into a more structured format. The data must be in an Excel file for easy input into the software. This fundamental process can be extended with various additional functions, transfer functions, and network architectures. In Figure 3.48 illustrated the network architecture includes input, hidden, and output layers, with 70% of the data allocated for training, 15% for validation, and 15% for testing (Khan et al., 2024). As study progresses, studies have focused on improving the efficiency of training ANNs due to the lengthy training times involved. The objective is to discover more effective learning algorithms.

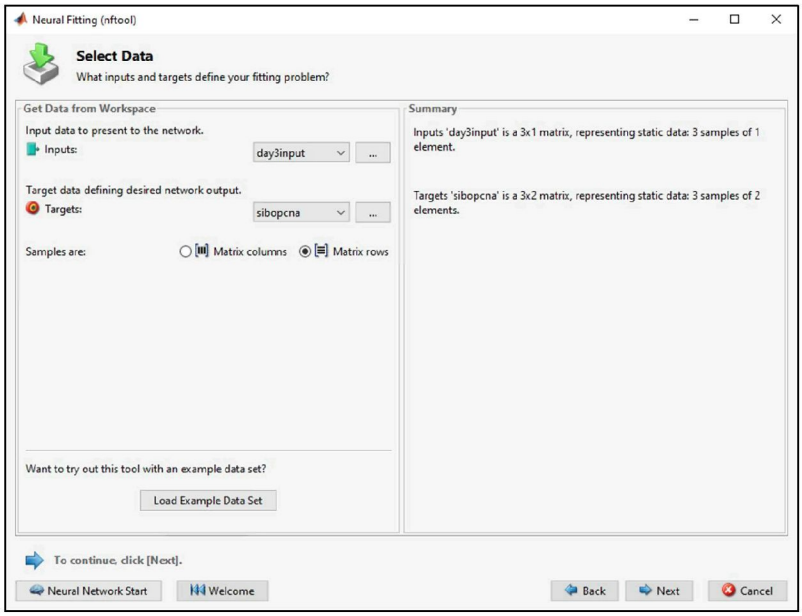

Figure 3.46 Selecting Data as The Input And Output (Targets)

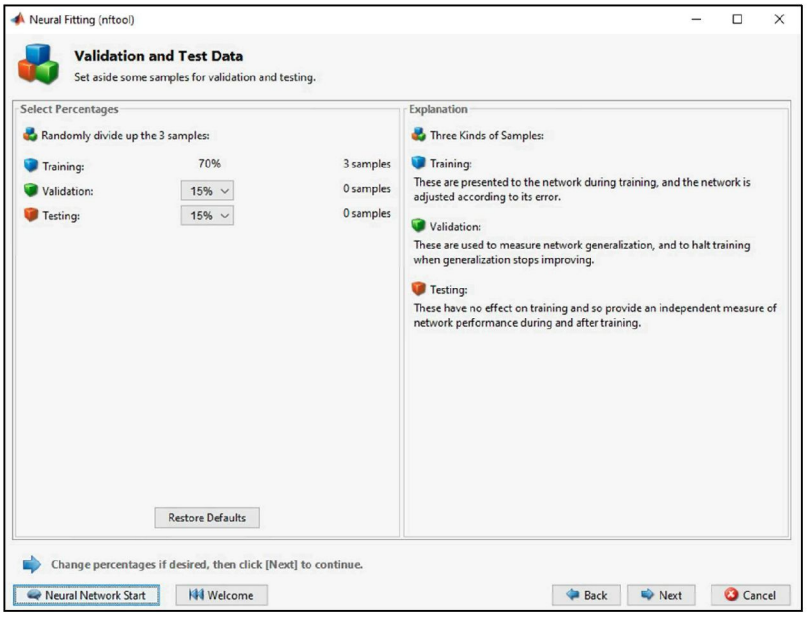

Figure 3.47 Percentage of The Validation and Test Data

The current study utilizes the Levenberg–Marquardt (LM) learning algorithm and applies a sigmoid function to the hidden neurons. Neural network validation is trained using the Levenberg-Marquardt algorithm (see Figure 3.49), and numerical outcomes are compared to identify the most effective prediction methods. This approach was chosen because of its good fit values. Since there are no established rules

for determining the best topological structure in ANNs, a heuristic approach was used during this phase. The ANN structure for this study is depicted in Figure 3.50. To evaluate the performance of the ANN model, both the coefficient of determination (R^2) and mean squared error (MSE) criteria are used. R^2 measures the percentage of variation in the response variable explained by the model, while MSE assesses the quality of the predictions, with lower values indicating better performance.

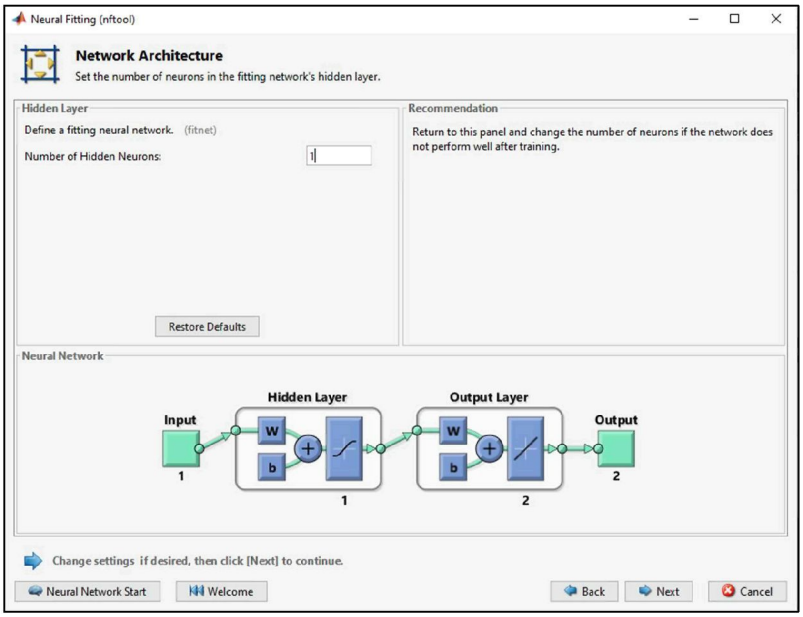

Figure 3.48 Network Architecture

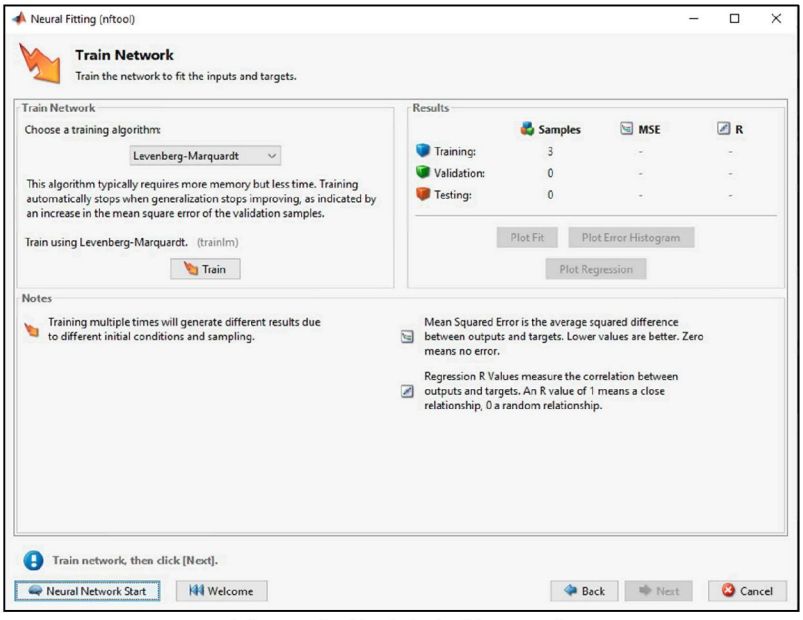

Figure 3.49 Train Network

In the context of regression-based ANN models, Mean Squared Error (MSE) serves as a key metric to evaluate prediction accuracy. MSE is used in the ANN system because it is mathematically simpler, provides stronger penalization of large errors, and aligns better with gradient-based optimization methods. RMSE is more suitable for presenting results, but MSE is the more effective choice for model training (Chai & Draxler, 2014; Hodson, 2022; Willmott & Matsuura, 2005). It computes the average of the squared deviations between actual and predicted values. A lower MSE value reflects higher model precision (Data Expertise, 2025). Because mortar strength is usually quantified in megapascals (MPa), the resulting MSE is expressed in MPa^2 (Thamboo et al., 2019; Nafees et al., 2021). An ideal MSE of zero would denote flawless prediction, although the acceptability of an MSE score depends heavily on the expected strength range and variability of the mortar data. To quantitatively assess the prediction accuracy of the ANN model, Equation (3.6) is employed to compute the Mean Squared Error (MSE), which reflects the average squared deviation between predicted and actual mortar strength values.

MSE

$$\text{MSE} = \frac{1}{n}\sum_{i=1}^{n}(y_i - \hat{y}_i)^2 \tag{3.5}$$

Where:

- y_i = Actual mortar strength
- $\hat{y}_i$ = Predicted mortar strength by the ANN
- n = Number of data points

Another important metric is the Coefficient of Determination (R^2), which quantifies how effectively the model captures variation in the target output. This value ranges from 0 to 1, with scores closer to 1 signifying a stronger fit. An R^2 of 1 implies total prediction accuracy, whereas a value of 0 suggests that the model performs no better than simply predicting the mean. Occasionally, R^2 can even be negative indicating a model that performs worse than the average. For applications involving mortar strength, R^2 values exceeding 0.90 are tend to high model performance (Apostolopoulou et al., 2018; Ahmed et al., 2022). As mentioned by Chauhan et al. (2025), the ANNs

that achieved the highest prediction accuracy, with R^2 values exceeding 0.90 across all degradation mechanisms. Equation (3.7) is introduced to calculate the coefficient of determination (R^2), a statistical measure that evaluates how effectively the ANN model captures the variance in the experimental data.

Together, MSE and R^2 offer complementary insights into model reliability. MSE reveals the average prediction error magnitude, while R^2 highlights the proportion of variability captured by the model. For mortar strength ranges spanning 10 to 50 MPa, an MSE below 1 MPa^2 and an R^2 above 0.90 are generally reflective of a well-trained ANN (Eskandari et al., 2016; Shi et al., 2018; Apostolopoulou et al., 2018). Table 3.10 presents MSE and R^2 as key indicators of ANN model accuracy, where lower MSE and higher R^2 values signify better prediction of mortar strength. Ideal models show near zero error and strong correlation with actual results. These metrics should be jointly analysed to ensure both accuracy and generalization across unseen datasets.

R^2

$$R^2 = 1 - \frac{\sum(y_i - \hat{y}_i)^2}{\sum(y_i - \tilde{y})^2} \tag{3.6}$$

Where:

- $\tilde{y}$ = Mean of actual values
- Numerator = Residual sum of squares (model error)
- Denominator = Total sum of squares (variance in data)

Table 3.10
The Performance Metric with Ideal Value

Metric	Unit	Interpretation	Ideal Value
MSE	MPa^2	Average squared error	0 (lower is better)
R^2	None	Proportion of variance explained	1 (higher is better)

(Source: Enjoy Algorithms, 2023, https://www.enjoyalgorithms.com/blog/evaluation-metrics-regression-models)

3.5 Summary

In this chapter, the study focused on developing an optimized interlocking block (IB) using alternative materials such as ESP, SF, and RCA. The selected mix proportions aimed to improve mechanical properties while ensuring acceptable flowability and water absorption levels. The IB design emphasized ease of construction through a mortarless, interlocking system with consistent dimensions and strength. Additionally, ANNs were trained to capture the nonlinear relationships within the mortar mix data, enabling prediction and optimization of material combinations.

CHAPTER 4
RESULTS AND DISCUSSION

4.1 Introduction

This chapter presents a structured synthesis of experimental findings obtained through a series of rigorously executed laboratory tests. The results have been systematically categorized and graphically represented to facilitate clarity and technical interpretation. The analysis of these outcomes serves to assess the extent to which the research objectives were achieved particularly in examining the characteristics of eggshell powder (ESP) and recycled concrete aggregates (RCA). Key aspects include the impact of partial material substitution and the durability performance of concrete incorporating recycled components.

The evaluation encompasses both empirical and computational approaches. The first objective was achieved by flexural strength and compressive strength testing, particle size distribution, water absorption, flowability for workability of mortar. Meanwhile, second objective focused to interlocking blocks studies on flexural strength and visual inspection of the blocks crack pattern in accordance with ASTM and JKR standards. Other than that, the third objective of this analysis is to validate the study results using artificial neural networks (ANN) developed in MATLAB.

4.2 Particle Size Distribution

Particle size distribution (PSD) is an essential property of cement. The only standard method to measure the PSD of cement, namely ASTM C430 – Standard Test Method for Fineness of Hydraulic Cement, is limited in scope; this standard describes a method for determining "fineness" with a lower size detection limit to 45 μm. It is suitable be used in this study as the limitation in sieve size for powdery texture is 63 μm. Meanwhile, the fine aggregates were used ASTM 144 – 18, Standard Specification for Aggregate as Masonry Mortar.

4.2.1 Cement

Table 4.1 presents the results of a sieve analysis conducted on three different materials: OPC, ESP, and SF. The analysis involves passing these materials through a series of sieves with progressively smaller openings, ranging from 4.750 mm to 0.063 mm, with a bottom pan to collect the finest particles. The "Pan Only" column lists the weight of the pan without any material, while the "Before" and "After" columns under each material type (OPC, ESP, and SF) show the weight of the pan and the material retained on each sieve before and after the sieving process.

The amount of material retained on each sieve is indicated by the disparities between the "Before" and "After" weights, which also show the particle size distribution of each item. Consistent with the finer particle size of cement, OPC data generally exhibits. The "After" weight is typically zero in the bigger sieve sizes (such as 4.750 mm and 3.350 mm), indicating that no large particles of these materials are retained and that no large particles of these materials are retained and that their particles are finer than these sieves.

Table 4.1
The Particle Aggregate Size Distribution of OPC, ESP, and SF.

Size Pan Screen (mm)	Pan Only (kg)	Weight (kg)					
		Ordinary Portland Cement (OPC)		Eggshell Powder (ESP)		Silica Fume (SF)	
		Before	After	Before	After	Before	After
4.750	0.3471	0.0000	0.0000	0.0000	0.0000	0.0000	0.0000
3.350	0.3633	0.0000	0.0000	0.0000	0.0000	0.0000	0.0000
2.360	0.4156	0.4419	0.0263	0.4263	0.0107	0.4164	0.0008
1.700	0.3959	0.3999	0.0040	0.3978	0.0019	0.3964	0.0005
1.180	0.3395	0.3438	0.0043	0.3415	0.0020	0.3407	0.0012
0.850	0.3684	0.3731	0.0047	0.3697	0.0013	0.3836	0.0152
0.600	0.4014	0.4086	0.0072	0.4072	0.0058	0.5201	0.1187
0.425	0.3719	0.6601	0.2882	0.4930	0.1211	0.7235	0.3516
0.300	0.4513	0.8383	0.3871	0.8322	0.3810	0.7174	0.2661
0.212	0.3489	0.5558	0.2069	0.6527	0.3038	0.4669	0.1180
0.150	0.3272	0.3590	0.0318	0.4181	0.0909	0.3857	0.0584
0.075	0.3184	0.3425	0.0242	0.3894	0.0711	0.3736	0.0552
0.063	0.3328	0.3426	0.0098	0.3416	0.0089	0.3402	0.0074
Bottom Pan	0.2352	0.2407	0.0055	0.2369	0.0017	0.2422	0.0070

Small variations between the "Before" and "After" weights show that finer particles are either kept or pass through in lower amounts as the sieve sizes decline, especially in the smaller diameters like 0.075 mm and 0.063 mm. Given that the distribution of particles sizes can have a substantial impact on the material's

performance in construction applications, including the manufacturing of concrete, this pattern is essential for comprehending the material's properties.

Ordinary Portland Cement's (OPC) reveals its particle size distribution is discovered by sieve analysis, which is essential for comprehending how it behaves in concrete mixtures. The procedure involves passing cement through a set of sieves with decreasing mesh sizes, ranging from 5.000 mm to 0.063 mm (refer to Table 4.2). No particles were retained on the larger sieves (5.000 mm, 4.750 mm, and 3.350 mm), indicating the fineness of the OPC particles. At the sieve openings become finer, the amount of material retained gradually increases, with significant retention at 0.425 mm, and 0.300 mm, where 33.48% and 72.18% of the sample were retained, respectively. This indicates that a significant portion of the cement particles falls within this size range.

With finer sieves, cumulative retention continues to increase, eventually reaching 100% at the pan. Only 0.55% of the OPC passed through the 0.063 mm sieve, demonstrating the decrease in passing percentage with smaller openings. The significant retention on finer sieves indicates that OPC primarily consists of very small particles, essential for forming a dense, smooth mix with strong binding properties. Ultimately, this particle size profile plays a critical role in determining the cement's workability, strength development, and setting behaviour in concrete.

Table 4.2
Sieve Analysis of Ordinary Portland Cement (OPC)

Sieve Pan (mm)	Ordinary Portland Cement (OPC)			
	Retained (kg)	Accumulative Retain (kg)	% Mass Retain	% Passing
5.000	0.0000	0.0000	0.00	0.00
4.750	0.0000	0.0000	0.00	0.00
3.350	0.0000	0.0000	0.00	100.00
2.360	0.0263	0.0263	2.63	97.37
1.700	0.0040	0.0303	3.03	96.97
1.180	0.0043	0.0346	3.46	96.54
0.850	0.0047	0.0393	3.93	96.07
0.600	0.0072	0.0465	4.65	95.35
0.425	0.2882	0.3348	33.48	66.53
0.300	0.3871	0.7218	72.18	27.82
0.212	0.2069	0.9288	92.88	7.13
0.150	0.0318	0.9605	96.05	3.95
0.075	0.0242	0.9847	98.47	1.53
0.063	0.0098	0.9945	99.45	0.55
Bottom Pan	0.0055	1.0000	100.00	0.00

4.2.1.1 Particle Size Distribution of Eggshell Powder (ESP)

The sieve analysis in Table 4.3 shows that ESP is primarily made up of fine particles, as none are retained on the larger sieves (5.000 mm, 4.750 mm, and 3.350 mm), confirming their small size. As the sieve openings get smaller, a slight amount of material started to be retained; 1.07 % on the 2.360 mm sieve, with 98.94 % passing through. Retention increases progressively, peaking at 0.300 mm where 52.36 % of the powder is captured, indicating that a significant amount of the material falls within this size range. Beyond this point, retention decreases, suggesting that many particles are smaller than 0.300 mm. The finest sieve (0.063 mm) holds just 0.17 %, with the remainder collected in the bottom pan. These results confirm that ESP is largely composed of fine particles, making it well-suited for use in applications like concrete additives, where particle size critically affects performance.

Table 4.3
Sieve Analysis of Eggshell Powder (ESP)

Sieve Pan (mm)	Eggshell Powder (ESP)			
	Retained (kg)	Accumulative Retain (kg)	% Mass Retain	% Passing
5.000	0.0000	0.0000	0.00	0.00
4.750	0.0000	0.0000	0.00	0.00
3.350	0.0000	0.0000	0.00	100.00
2.360	0.0107	0.0107	1.07	98.94
1.700	0.0019	0.0125	1.25	98.75
1.180	0.0020	0.0145	1.45	98.55
0.850	0.0013	0.0158	1.58	98.42
0.600	0.0058	0.0216	2.16	97.84
0.425	0.1211	0.1426	14.26	85.74
0.300	0.3810	0.5236	52.36	47.64
0.212	0.3038	0.8274	82.74	17.26
0.150	0.0909	0.9183	91.83	8.17
0.075	0.0711	0.9894	98.94	1.06
0.063	0.0089	0.9983	99.83	0.17
Bottom Pan	0.0017	1.0000	100.00	0.00

4.2.1.2 Particle Size Distribution of Silica Fume (SF)

The sieve analysis of SF, as detailed in Table 4.4, shows that this material is composed predominantly of very fine particles, with a significant portion passing through even the smallest sieves. Initially, no material is retained on the larger sieves (5.000 mm, 4.750 mm, and 3.350 mm), meaning all the SF particles are smaller than these sizes. As the sieve size decreases, a small amount of material begins to be retained.

For instance, 0.08% of the mass is retained on the 2.360 mm sieve, with 99.92% passing through, indicating a very fine texture.

As the sieve size continues to decrease, the percentage of material retained increases, with significant retention starting from the 0.600 mm sieve, which retains 13.63% of the material. The most significant retention occurs at the 0.425 mm sieve, where 48.79% of the material is retained, showing that nearly half of the SF particles are around this size. This trend continues with 75.40% retention on the 0.300 mm sieve. As the sieves get finer, the retention decreases, with 93.04% of the material being smaller than 0.150 mm and only 0.69% of the material being retained on the 0.063 mm sieve, indicating that the vast majority of the SF particles are extremely fine.

The bottom pan, which collects the finest particles, contains only 0.007 kg, or 0.69%, indicating that nearly all of the SF is very finely ground. Overall, this sieve analysis highlights that SF is composed of extremely fine particles, making it suitable for applications like concrete where fine particles are needed to fill voids and enhance the material's properties.

Table 4.4
Sieve Analysis of Silica Fume (SF)

Sieve Pan (mm)	Silica Fume (SF)			
	Retained (kg)	Accumulative Retain (kg)	% Mass Retain	% Passing
5.000	0.0000	0.0000	0.00	0.00
4.750	0.0000	0.0000	0.00	0.00
3.350	0.0000	0.0000	0.00	100.00
2.360	0.0008	0.0008	0.08	99.92
1.700	0.0005	0.0013	0.13	99.87
1.180	0.0012	0.0024	0.24	99.76
0.850	0.0152	0.0176	1.76	98.24
0.600	0.1187	0.1363	13.63	86.37
0.425	0.3516	0.4879	48.79	51.21
0.300	0.2661	0.7540	75.40	24.60
0.212	0.1180	0.8720	87.20	12.80
0.150	0.0584	0.9304	93.04	6.96
0.075	0.0552	0.9856	98.56	1.44
0.063	0.0074	0.9931	99.31	0.69
Bottom Pan	0.0070	1.0000	100.00	0.00

4.2.1.3 Comparison of the Particle Size Distribution Towards Eggshell Powder (ESP)

Table 4.5 provides a comparative sieve analysis of OPC, ESP, and SF, highlighting the particle size distribution of these materials. Initially, at the coarser sieve sizes of 5.000 mm and 4.750 mm, none of the materials were retained, indicating that

all particles are smaller than these sizes. As the analysis progresses to the 3.350 mm sieve, it is observed that 100% of each material passes through, confirming their fine nature and the absence of coarse particles.

As the sieve size decreases from 2.360 mm to 0.600 mm, the proportion of passing material is reduced. Ordinary Portland Cement (OPC) consistently retains a greater number of particles than ESP and SF, indicating its coarser particle distribution relative to the other materials. For example, at the 2.360 mm sieve, 97.37% of OPC passes through, compared to 98.94% for ESP and 99.92% for SF, indicating that OPC has a slightly coarser texture. A significant difference appears at the 0.425 mm sieve, where OPC shows only 66.53% passing, while ESP has 85.74% and SF just 51.21%, suggesting that SF has a higher proportion of slightly larger particles compared to the others.

In the finer sieve sizes (0.300 mm and below), the materials exhibit significant variations in particle size distribution. OPC and SF retain a higher percentage of material, indicating a finer composition, especially at the 0.150 mm and 0.075 mm sieves. SF consistently shows the highest retention, suggesting it has the smallest particle size among the three. These differences are crucial as they influence the materials' performance in construction, affecting aspects like setting time, strength, and durability in concrete mixtures.

Table 4.5
List Sieve Analysis of OPC, ESP, and SF.

Sieve Pan (mm)	Ordinary Portland Cement (OPC)	Eggshell Powder (ESP)	Silica Fume (SF)
5.000	0.00	0.00	0.00
4.750	0.00	0.00	0.00
3.350	100.00	100.00	100.00
2.360	97.37	98.94	99.92
1.700	96.97	98.75	99.87
1.180	96.54	98.55	99.76
0.850	96.07	98.42	98.24
0.600	95.35	97.84	86.37
0.425	66.53	85.74	51.21
0.300	27.82	47.64	24.60
0.212	7.13	17.26	12.80
0.150	3.95	8.17	6.96
0.075	1.53	1.06	1.44
0.063	0.55	0.17	0.69
Bottom Pan	0.00	0.00	0.00

The Figure 4.1 illustrates the particle size distribution of OPC, ESP, and SF by showing the percentage of material passing through various sieve sizes. For larger particle sizes (greater than 1 mm), all three materials exhibit a rapid increase in the percentage passing, indicating that they primarily consist of finer particles, which is why the lines start at 100% passing for the coarser sizes.

In the intermediate particle size range (approximately between 1 mm and 0.1 mm), the lines for OPC, ESP, and SF begin to diverge slightly. The ESP line shows a relatively smoother transition, retaining more material in this range compared to OPC and SF, suggesting that ESP has a more uniform particle distribution. SF, on the other hand, displays the steepest decline in percentage passing, indicating that it has a finer particle size distribution than both OPC and ESP in this range.

For the finer particles (less than 0.1 mm), all three materials show a sharp decrease in the percentage passing. SF has the highest percentage of very fine particles, as indicated by its line, which maintains a slightly higher percentage passing through the smallest sieve sizes. This suggests that SF has the finest particle distribution, which can have a significant impact on concrete properties such as strength, workability, and durability. The fine particles in SF, for instance, can enhance pozzolanic activity, contributing to stronger and more durable cementitious materials.

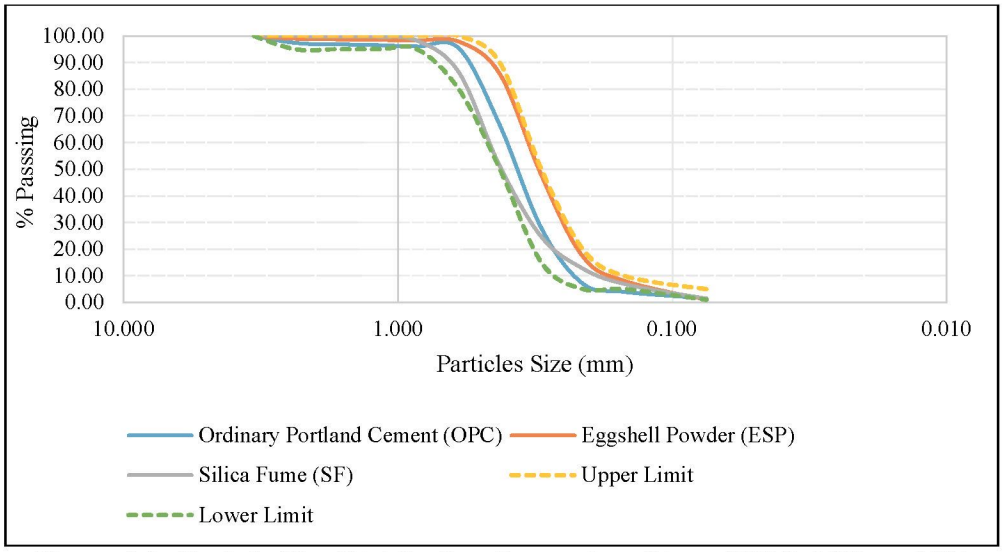

Figure 4.1 Particle Size Distribution Comparison Line of OPC, ESP, and SF

Comparison between the materials further emphasize these differences. OPC and ESP similar behaviour at larger sieve sizes, but ESP retains more particles as the sieves become finer, indicating slightly larger particles sizes. When OPC is compared

with SF, the difference is more pronounced, as SF's finer and more uniform particles allow most of them to pass through smaller sieves. Mehdipour and Khayat (2017), finer particles such as those in SF increase the specific surface area, promoting better particle packing and reducing voids in the mixture. Finally, comparing ESP and SF shows that both are exceptionally fine, with nearly all particles below 1 mm. ESP is marginally finer in mid-size range, but SF's steep distribution curve reflects its ultrafine nature, making it particularly effective for enhancing concrete performance.

In contrast, OPC retains more material at finer sieve sizes, confirming its relatively coarser texture. This characteristic makes OPC suitable as a baseline binder but less effective in enhancing microstructural properties compared to SF and ESP. The differences in particle size distribution among these materials directly influence their performance in cementitious mixtures, with SF offering the greatest potential for improving workability and strength due to its ultrafine particles.

4.2.2 Fine Aggregate

Table 4.6 shows the outcome of a sieve analysis on three materials: natural fine aggregate- sand (NA) and recycled concrete aggregate (RCA). In this analysis, the sizes of the particles are determined in terms of their distribution after exposing the materials to a set of sifting screens whose aperture varies and noting the weight of material remaining on each screen before and after sieving. Every row in the table is based on a given kind of sieve, as described by its size according to its screen Pan size (mm), and columns are weight of material that has remained on every sieve, as well as the difference in weight between the material before and after being sieved, both measured in kilograms (kg).

In the case of NA, the analysis exhibits a reduction in the weight retained on sieves following sieving implying that particles were not stopped by sieves. An example is that at 4.750 mm sieve size, NA sand retained 0.0920kg prior to sieving and 0.0598kg after sieving. This pattern indicates that smaller particles existed in the material and by-passed the sieves, and the weight of the sample generally decreasing with the reduction in sieve size.

Table 4.6
Particle Aggregate Size Distribution of NA, and RCA.

Size Pan Screen (mm)	Pan Only (kg)	Weight (kg)			
		Natural Aggregate – Sand (NA)		Recycled Concrete Aggregate (RCA)	
		Before	After	Before	After
4.750	0.3471	0.4391	0.0920	0.4069	0.0598
3.350	0.3633	0.4596	0.0963	0.4355	0.0722
2.360	0.4156	0.5318	0.1162	0.5212	0.1056
1.700	0.3959	0.5805	0.1846	0.5377	0.1418
1.180	0.3395	0.4426	0.1031	0.4673	0.1278
0.850	0.3684	0.4643	0.0959	0.4811	0.1127
0.600	0.4014	0.4546	0.0532	0.4549	0.0535
0.425	0.3719	0.4384	0.0665	0.4340	0.0621
0.300	0.4513	0.5360	0.0847	0.5197	0.0684
0.212	0.3489	0.3867	0.0378	0.3933	0.0444
0.150	0.3272	0.3599	0.0327	0.3608	0.0336
0.075	0.3184	0.3421	0.0237	0.3528	0.0344
0.063	0.3328	0.3352	0.0025	0.3374	0.0046
Bottom Pan	0.2352	0.2462	0.0109	0.2423	0.0070

RCA shows the opposite trend, that is lower retention on small sieve sizes and implies the particles are coarser than those of NA. As an example, before sieving, 0.1846 kg remained on the 1.700 mm sieve and 0.1418 kg on it after sieving. The reduced weight remaining difference after sieving indicates that RCA contains fewer fine particles. In general, the sieve analysis shows the different distributions of the particle size of NA, and RCA, which they best suit various constructions.

The particle size distribution of two materials is shown physically in Figure 4.5, with NA on the left and RCA on the right. The amount of material retained on each sieve during a sieve analysis test is shown in each column, which displays a sequence of sieves organised from coarsest (top) to finest (bottom). This arrangement illustrates the differences in particle size between the two materials. From the left top to right bottom, the sieves size were 0.063 mm, 0.150 mm, 0.212 mm, 0.300 mm, 0.600 mm, 1.180 mm, 1.700 mm, 2.360 mm, 3.350 mm, and 4.750 mm.

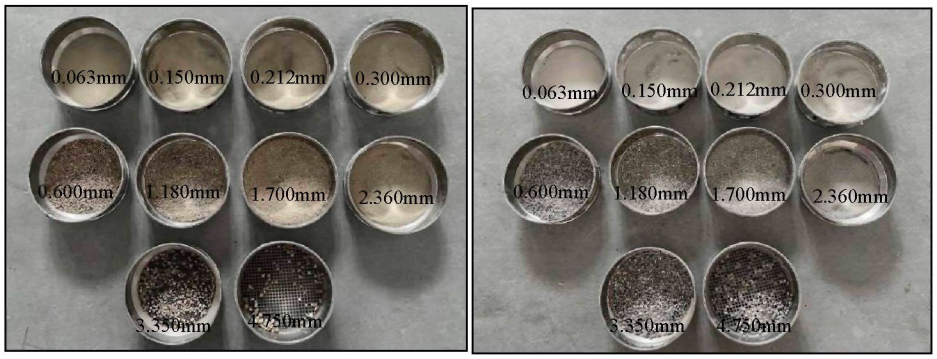

(a) (b)

Figure 4.2 Retained of particle size on each sieves pan: (a) Sand Distribution; (b) RCA Distribution

More particles seem to be held in the finer sieve pans near the bottom of the NA column, suggesting that there is a greater percentage of fine particles or sand-sized grains in NA. A wider or coarser size distribution is suggested by the RCA column, which displays noticeably coarser particles retained in the upper and middle sieve pans. Because RCA comes from crushed demolition trash, its dispersion seems a little less regular, reflecting its heterogeneous character.

The relative fineness of NA and the somewhat coarser, more angular particle profile of RCA are highlighted by this side-by-side comparison. Decisions about mix design are supported by this visual evidence, which shows that although RCA can be used in place of natural sand, variations in packing, workability, and strength development can require changes in concrete proportioning or additives.

4.2.2.1 Particle Size Distribution of Natural Fine Aggregates – Sand (NA)

Table 4.7 presents the sieve analysis results for NA, detailing how the particle sizes are distributed across various sieve sizes. The analysis shows that no material is retained on the largest sieve size of 5.000 mm, while the weight of material retained on smaller sieves decreases progressively. For example, 0.0920 kg of sand is retained on the 4.750 mm sieve, and this weight reduces as the sieve size becomes smaller, reflecting a higher proportion of finer particles passing through. The "Accumulative Retain" column indicates the total weight of material retained on each sieve and all coarser sieves combined, with the cumulative weight increasing as smaller sieve sizes are considered.

Table 4.7
Sieve Analysis of Natural Aggregate (NA)

Sieve Pan (mm)	Natural Aggregate (NA)			
	Retained (kg)	Accumulative Retain (kg)	% Mass Retain	% Passing
5.000	0.0000	0.0000	0.00	100.00
4.750	0.0920	0.0920	9.20	90.80
3.350	0.0963	0.1883	18.83	81.17
2.360	0.1162	0.3045	30.45	69.55
1.700	0.1846	0.4890	48.90	51.10
1.180	0.1031	0.5921	59.21	40.79
0.850	0.0959	0.6880	68.80	31.20
0.600	0.0532	0.7412	74.12	25.88
0.425	0.0665	0.8077	80.77	19.23
0.300	0.0847	0.8924	89.24	10.76
0.212	0.0378	0.9302	93.02	6.98
0.150	0.0327	0.9629	96.29	3.71
0.075	0.0237	0.9866	98.66	1.34
0.063	0.0025	0.9891	98.91	1.09
Bottom Pan	0.0109	1.0000	100.00	0.00

The "% Mass Retain" column indicates the percentage of the total sample's mass that remains on each sieve, with the highest retention of 96.29% on the 0.150 mm sieve. In contrast, the "% Passing" column reflects the percentage of the total sample mass that passes through each sieve, showing a trend of decreasing percentages as the sieve size diminishes. For example, 90.80% of the sample passes through the 4.750 mm sieve, suggesting a greater prevalence of finer particles in smaller sieve sizes. The final entry, "Bottom Pan," confirms that 100% of the sample is accounted for, including the smallest particles that did not pass through the 0.063 mm sieve. Overall, the sieve analysis demonstrates that NA encompasses a broad range of particle sizes, with a significant quantity of finer particles.

Table 4.8 provides a detailed summary of the sieve analysis for NA, highlighting key aspects of its particle size distribution and grading characteristics. The analysis reveals that 9.20% of the sample consists of gravel-sized particles, while a significant 89.712% is composed of sand-sized particles. Only 1.09% of the sample consists of fines, indicating that the material is primarily sand with minimal fine particles. The D60 value is 1.9967 mm, representing the sieve size at which 60% of the material's mass is retained, and reflects the coarser end of the size spectrum. The D30 value of 0.7854 mm signifies the median particle size, while the D10 value of 0.2688 mm indicates the finer particles in the distribution as illustrated in Figure 4.6.

Table 4.8
Result Sieve Analysis of Natural Aggregate (NA)

Natural Aggregate (NA)					
%Gravel	9.20	D60 (mm)	1.9966563	Cu = D60 / D10	7.4290701
%Sand	89.712	D30 (mm)	0.7853813	Cc = D30^2 / D10*D60	1.1494468
%Fines	1.09	D10 (mm)	0.2687626		

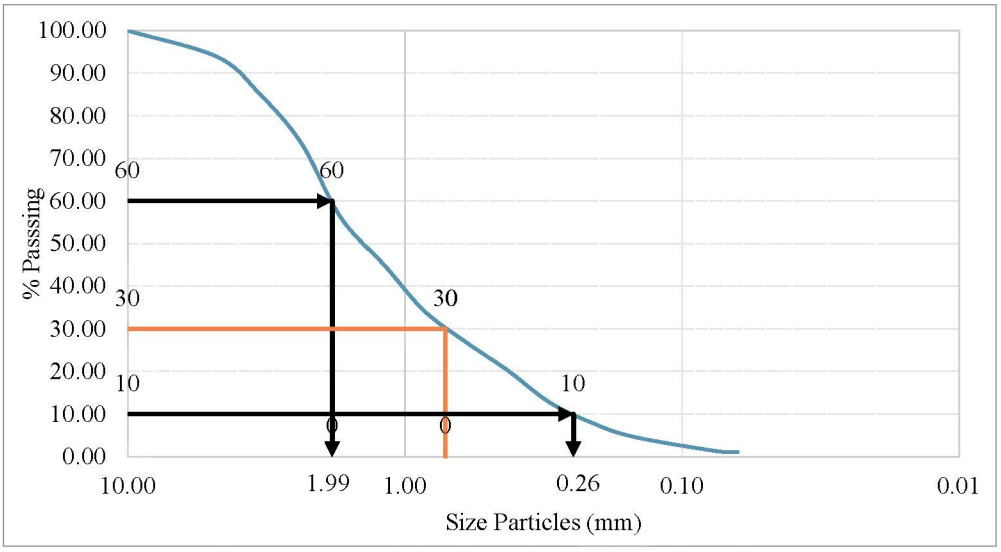

Figure 4.3 Particle Size Distribution Line of NA

The Coefficient of Uniformity (Cu), calculated as 7.4291, measures the range of particle sizes in the material, with a higher value indicating a broader range. This suggests that the aggregate has a moderate range of particle sizes. The Coefficient of Gradation (Cc), calculated as 1.1494, assesses the uniformity of the grading, with a value close to 1 indicating a well-graded material. Overall, the sieve analysis results show that NA has a well-graded distribution with a predominance of sand-sized particles and a relatively broad range of particle sizes.

4.2.2.2 Particle Size Distribution of Recycled Concrete Aggregates (RCA)

Passing percentage column indicates the percentage of the entire mass of RCA that will pass through each sieve diameter that offers essential details on the distribution of its particle sizes as presented in Table 4.9. It is worth noting that low retention of the total mass, 30.97% at the 2.360 mm sieve, is achieved the number of large particles left back on this sieve is large. The percentage passing improves as the sieves are reduced in size indicating that the finer the sieves the more the material is escaping the sieves.

An example would be that at the sieve 0.07 5 mm, the percentage of total mass passing through is a tremendous 98.83 which means that only a small amount of material is staying on this sieve.

The rising proportion of material (which falls through the smaller sieves aircrafts) shows a decreasing particle size. This tendency is especially observed in the value increasing percentage passing values of sieves 0.150 mm and fines thus indicating remarkable content of fines in the aggregate. Conversely, lower passes percentages on the coarser sieves (5.000 mm and bigger) indicate the presence of large proportion of coarse particles in the aggregate.

Table 4.9
Sieve Analysis of Recycled Concrete Aggregate (RCA)

Sieve Pan	Recycled Concrete Aggregate (RCA)			
(mm)	Retained (kg)	Accumulative Retain (kg)	% Mass Retain	% Passing
5.000	0.0000	0.0000	0.00	0.00
4.750	0.0598	0.1320	0.00	0.00
3.350	0.0722	0.2042	0.00	100.00
2.360	0.1056	0.3097	30.97	69.03
1.700	0.1418	0.4515	45.15	54.85
1.180	0.1278	0.5793	57.93	42.07
0.850	0.1127	0.6920	69.20	30.81
0.600	0.0535	0.7454	74.54	25.46
0.425	0.0621	0.8075	80.75	19.25
0.300	0.0684	0.8760	87.60	12.40
0.212	0.0444	0.9203	92.03	7.97
0.150	0.0336	0.9539	95.39	4.61
0.075	0.0344	0.9883	98.83	1.17
0.063	0.0046	0.9930	99.30	0.70
Bottom Pan	0.0070	1.0000	100.00	0.00

These passing percentages can provide important information in regard to the particle size distribution of RCA which is important in determining the degree to which it can be applied. As an example, production of concrete may demand a particular ratio of the equal volumes of fine particles to ensure the specified strength and workability, whereas road construction may demand a reasonable amount of coarse particles providing the required stability and longevity. An evaluation of these values assists engineers and researchers to have a better knowledge of properties of RCA and make appropriate decisions in applications of RCA in various contexts.

The sieve analysis results for RCA indicate that the majority of the particles fall within the sand range, with a significant amount of coarse gravel and a small proportion of very fine particles (see Table 4.10). Specifically, 13.20% of the particles exceed 2.36 mm in size, while 86.10% range between 0.075 mm and 2.36 mm, and only 0.70% are

smaller than 0.075 mm. The D60 value, which signifies that 60% of the particles are coarser than this measurement, is 1.953 mm. In comparison, the D30 value, indicating that 30% of the particles are finer, is 0.801 mm, and the D10 value, representing 10% of the particles that are finer, is 0.251 mm.

These values provide important insights into the physical properties of the RCA, as illustrated in Figure 4.7, which presents the corresponding line. The high D60 value suggests a significant presence of coarse particles, while the low D10 value points to the existence of very fine particles. The coefficient of uniformity (Cu), calculated as D60 / D10, is 7.756 for the RCA, indicating a wide and uneven particle size distribution with many coarse particles and few fine ones. Conversely, the coefficient of curvature (Cc), calculated as $D30^2$ / (D10 × D60), is 1.306, suggesting that the distribution leans towards finer particles.

These results can be beneficial across various applications, such as construction, asphalt production, and environmental assessments. For instance, understanding particle size distribution can aid in selecting appropriate aggregates for specific studys, optimizing production processes in asphalt manufacturing, and evaluating the effectiveness of recycling methods while predicting environmental impacts. Overall, the sieve analysis provides valuable insights into the physical characteristics of RCA.

Table 4.10
Result Sieve Analysis of Recycled Concrete Aggregate (RCA)

Recycled Concrete Aggregate (RCA)					
%Gravel	13.20	D60 (mm)	1.9530264	Cu = D60 / D10	7.7560983
%Sand	86.10	D30 (mm)	0.8014837	Cc = D30^2 / D10*D60	1.3062202
%Fines	0.70	D10 (mm)	0.2518053		

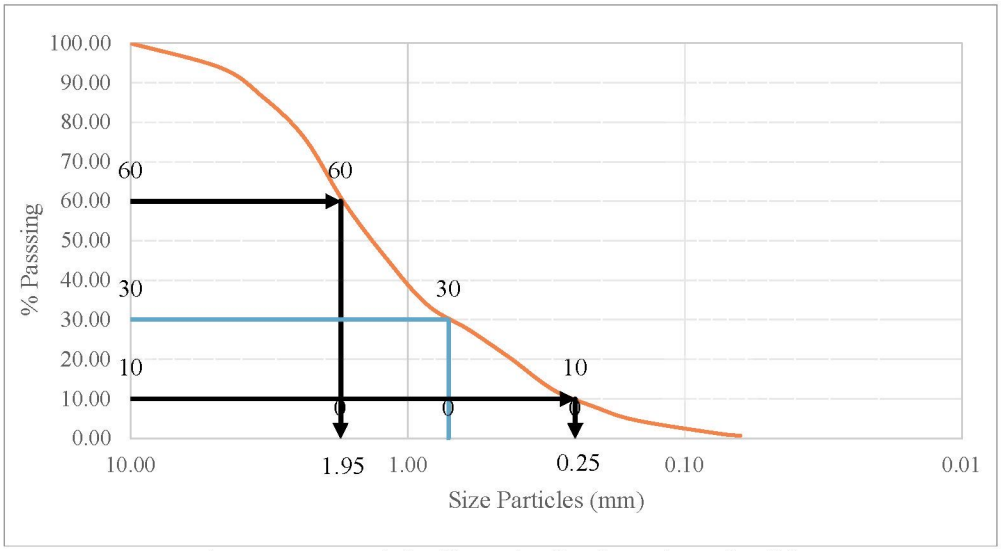

Figure 4.4 Particle Size Distribution Line of RCA

4.2.2.3 Comparison of the Particle Size Distribution Towards Recycled Concrete Aggregates (RCA)

According to IS 383-1970 Sieve Standard, the fineness modulus limitations in Zone II fall within the range of 2.1 to 3.37 mm for both RCA and NA grading. These minute variations produced a positive outcome because RCA's mechanical qualities met expectations for replacing fine aggregate in mortar mix designs. However, there have a bit similarity of % passing at sieve pan 0.425mm which are the sand is 19.23% and the RCA is 19.25% as portrayed in Table 4.11. Figure 4.8 displays the comparison of the particle size distribution between RCA and sand.

The particle size distribution of RCA and Natural Fine Aggregate - Sand (NA) is depicted in the Figure 4.8, which presents evidence on their appropriateness as fine aggregates in the manufacturing of concrete. The y-axis displays the proportion of particles that pass through each sieve, while the x-axis displays the particle size on a logarithmic scale, ranging from 10.00 mm to 0.01 mm. The percentage of the sample that passes through ever smaller sieve openings is shown by two solid lines, one orange for RCA and one blue for natural sand. The top and lower grading limits, which specify permissible bounds for fine aggregate gradation, are indicated by dashed yellow and green lines that are layered over these lines.

Table 4.11
List Sieve Analysis of NA, and RCA

Sieve Pan (mm)	Natural Aggregate – Sand (NA)	Recycled Concrete Aggregate (RCA)
5.000	100.00	100.00
4.750	90.80	86.80
3.350	81.17	79.58
2.360	69.55	69.03
1.700	51.10	54.85
1.180	40.79	42.07
0.850	31.20	30.81
0.600	25.88	25.46
0.425	19.23	19.25
0.300	10.76	12.40
0.212	6.98	7.97
0.150	3.71	4.61
0.075	1.34	1.17
0.063	1.09	0.70
Bottom Pan	0.00	0.00

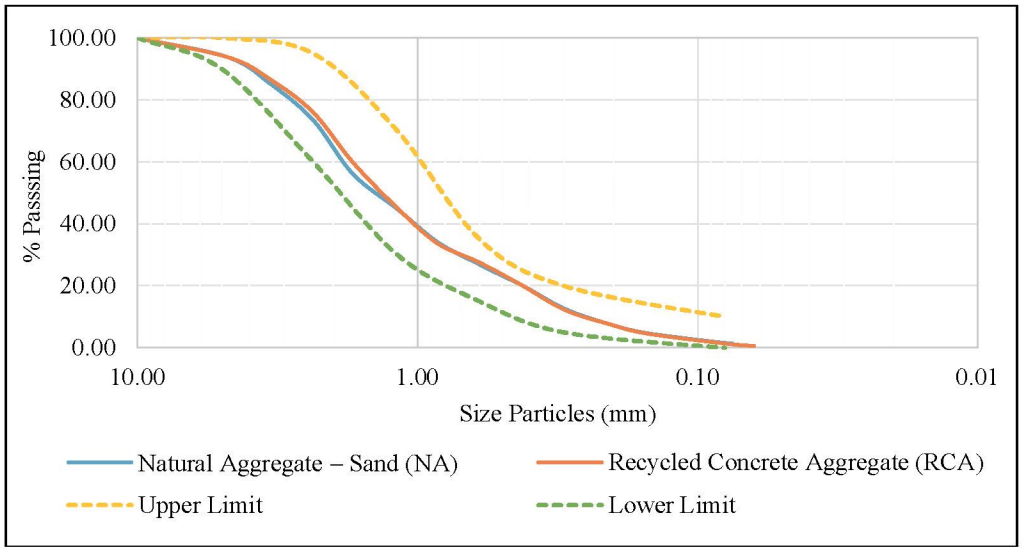

Figure 4.5 Particle Size Distribution Comparison Line of NA, and RCA

Infer from the ASTM C144-18 line that the types of RCA and fine aggregate of sand employed in this experiment fell within well-graded categories because the line grew linearly between particle sizes of 0.075 mm and 5 mm. Also, the line shape was not having a huge gap. In other words, the data was line smoothly for both of them and have a similar distribution.

The fact that both the NA and RCA lines fall comfortably within the permissible grading range indicates that both materials satisfy the requirements for construction. In contrast to NA, the RCA line displays a somewhat lower passing % in the finer size

range, suggesting that RCA is somewhat coarser. This property can affect the water demand and workability of concrete mixtures. Even yet, RCA continues to exhibit an acceptable grading profile, confirming its potential as a sustainable alternative to natural sand especially applicable for initiatives that seek to lessen their environmental effect by reusing resources. For assessing material uniformity and improving the design of the concrete mix, this visual study is crucial.

4.3 Results for Cube and Prism

4.3.1 Flowability of Fresh Mortar

After a flow test had been carried out the newly mixed mortar was tested. Three dissimilar mixes of mortar were tested with each mixing being in a different batch. To give a greater degree of accuracy in the data obtained at least three batches of the mixture had to be tested and the mean of the results calculated. As part of the testing, the workability of the mortar mix was determined by using the flow table test (Al-Fakih et al. 2018). Flow table test was done to determine the flowability of mortar, according to ASTM C1437/C1437M-17, and JKR standards in terms of workability. Figure 4.9 and Figure 4.10 show visual analysis of the spread of mortar under mechanical agitation and was taken at three points, first, the immediate removal of mould, the second after 15 taps, and the third after 25 taps.

These visual measurements were followed by direct measurements of diameters through use of a metal ruler, as provided in the supporting image, to guarantee the dimensions and accuracy measures and meet the standard used. Figure 4.9 presents a mortar mix exhibiting good flowability, with a final spread diameter of 140 mm. The initial condition (Figure 4.9a) shows a cohesive and well-formed mortar shape, indicating sufficient plasticity and internal bonding. After 15 taps (Figure 4.9b), the mortar begins to deform uniformly, forming a near-circular pattern with smooth edges. The final visual (Figure 4.9c) reveals a well-distributed spread with minimal cracking or edge fragmentation, confirming the mix's suitability for applications requiring ease of placement and surface finish. This performance aligns with JKR's recommended flow range for workable mortar, suggesting that the mix design likely optimized in terms of water-to-binder ratio and aggregate gradation supports adequate lubrication and particle mobility.

(a) (b) (c)

Figure 4.6 Flowability with good flow (140 mm); (a) Condition Right After Mould, (b) After 15 Tap of Flowtable, and (c) Last Visual of Mortar After 25 Tap

In contrast, Figure 4.10 depicts a mortar mix with minimum acceptable flowability, registering a spread diameter of 120 mm. The initial condition (Figure 4.10a) appears slightly stiffer, with visible surface roughness and reduced cohesion. After 15 taps (Figure 4.10b), the spread is less uniform, with irregular edges and signs of limited deformation. The final visual (Figure 4.10c) shows constrained expansion and minor surface cracking, reflecting marginal flow behaviour. While this mix meets the lower threshold of standard's acceptable range as mentioned in section 3.2.5; testing for fresh mortar, its reduced workability posed challenges in achieving full compaction, especially in modular interlocking block systems. Adjustments such as the inclusion of plasticizers or finer aggregates be necessary to enhance flow without compromising mechanical strength.

(a) (b) (c)

Figure 4.7 Flowability with minimum acceptance flow (120 mm); (a) Condition Right After Mould, (b) After 15 Tap of the Flowtable, and (c) Last Visual of Mortar After 25 Tap

The flowability results illustrated in Figure 4.11 indicate that the control mix (OPCNA) achieved the highest flow value of 140%, reflecting excellent workability.

The addition of 5% ESP and 0% RCA (5EPRCA0) slightly reduced flowability to 135%, still within the optimum range. As ESP and RCA content increased, the flowability generally decreased, with the lowest value of 110% recorded for 10EPRCA30. This reduction is likely due to the increased angularity and water absorption of RCA, along with the fine particles of ESP which can increase water demand. Despite some reductions, most mixtures remained within the acceptable range (120–145%) for structural masonry use as per MS EN 1015-3 - Methods of Test for Mortar for Masonry – Part 3: Determination of Consistence of Fresh Mortar (by Flow Table) or same as ASTM C1437 – Standard Test Method for Flow of Hydraulic Cement Mortar. Therefore, proper proportioning of ESP and RCA is essential to maintain adequate workability in mortar mixes for interlocking block applications.

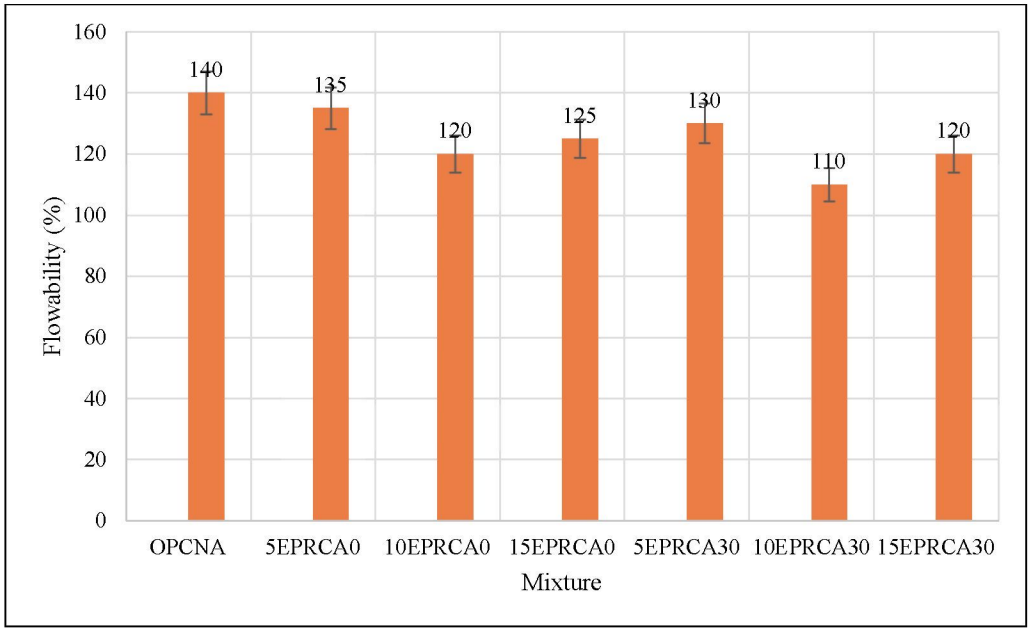

Figure 4.8 Flowability Results of All Mixture

Harini et al. (2012) reported that the size, shape, and loose void content of fine aggregates have a strong effect on mortar flowability. Mortars made with river sand showed better flow than those with crusher dust, mainly because natural sand has a smoother surface and packs more efficiently. Likewise, Kwan et al. (2010) highlighted that the thickness of the water film (WFT) around particles controls the flow behaviour of cement–sand mortar, where an optimal WFT improves flowability and lowers internal friction during placement.

In the study of sustainable construction, assessing the flowability of mixes containing recycled concrete aggregate (RCA) and eggshell powder (ESP) is essential to ensure that alternative materials meet performance benchmarks. Visual and dimensional confirmation of flow spread, as demonstrated in Figures 4.9 and Figure 4.10, supports mix design decisions and helps identify the need for additives or proportioning adjustments to maintain workability without compromising strength. Thus, the final results as shown in Figure 4.11 could be tell the promising mixture containing sustainable materials was 5EPRCA0 and closely followed by 5EPRCA30.

4.3.2 Water Absorption of Cube and Prism

Figure 4.12 presents water absorption percentages ranging from 4.015% to 4.880% across various mortar mixes, including the control (OPCNA) and combinations of eggshell powder (ESP) and recycled coarse aggregates (RCA) at different replacement levels. These values were obtained using the ASTM C642 procedure, which evaluates total water absorption and void content in hardened concrete. The observed range falls within the typical threshold for mortar materials, where values below 5% generally indicate reasonable durability, low porosity, and reduced permeability, especially for small specimens such as 50 mm cubes.

Lower water absorption is preferred as it reflects a denser microstructure and limits moisture ingress, which is crucial for preventing long-term deterioration due to shrinkage, efflorescence, or chemical attack. In this context, all mixtures fall within the acceptable range, suggesting that the inclusion of ESP and RCA does not significantly compromise pore structure or durability. The control sample (OPCNA) recorded 4.300%, while the lowest value was observed in 5EPRCA30 (4.015%), indicating that moderate incorporation of ESP and RCA help refine the microstructure through improved particle packing and filler effects.

The variation among mixtures particularly the slight dip in 15EPRCA0 (4.015%) and peak in 10EPRCA0 (4.880%) stem from differences in binder composition or RCA treatment levels. Notably, the highest absorption in 15EPRCA0, which lacks RCA, implies that excessive ESP content without sufficient aggregate interlock might increase porosity. These trends are consistent with findings by Neville (2012), who noted that concrete with absorption below 5% typically exhibits good resistance to fluid ingress and environmental degradation.

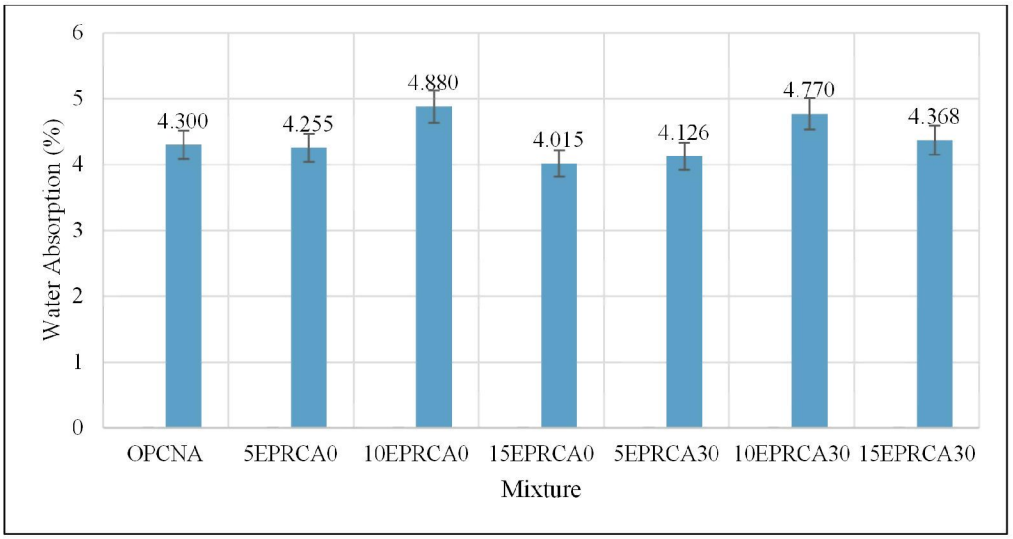

Figure 4.9 Water Absorption of Cube

Minimal error bars across each bar further validate the stability and reliability of the measurements, indicating consistent curing and material homogeneity. According to Perricone et al. (2020), sustainable concrete mixes incorporating agricultural waste powders such as ESP can achieve water absorption values below 6%, reinforcing the viability of such materials in durable construction. Synergistic effects of ESP from author Tanyildizi (2022) and RCA as mentioned by Tam et al. (2007) can enhance packing density, reduce voids, and maintain acceptable water absorption levels (<5%), especially when ESP is used as filler and RCA is properly graded.

Additionally, this statement was supported by Tan et al. (2018) that said ESP as partial cement replacement (2.5–5%) significantly reduces water absorption and Othman et al. (2025) said that RCA could be controlled the water absorb with present of superplasticiser. It improves durability by filling voids and refining microstructure. Overall, the results reflect a balanced performance in terms of water resistance and durability, aligning well with standard for quality controlled cementitious materials.

4.3.3 Parameter of The Sample

The samples listed represent different mix compositions designed to evaluate the influence of eggshell powder (ESP) and Recycled Concrete Aggregates (RCA)on concrete properties. The control sample, labelled OPCNA, contains only Ordinary Portland Cement (OPC) and Natural Aggregates (NA) – sand, serving as the baseline

for comparison. The next group of samples are EPRCA0 series that consist of 5EPRCA0, 10EPRCA0, and 15EPRCA0 introduce increasing percentages of ESP (5%, 10%, and 15%, respectively) as partial cement replacement, without any RCA. These mixes fall under the EPRCA0 category and aim to access the effect of ESP alone on the mechanical and durability performance of the concrete.

The second group which are EPRCA30 series that were 5EPRCA30, 10EPRCA30, and 15EPRCA30 as combine the same incremental levels of ESP (5%, 10%, and 15%) with a consistent 30% replacement of NA by RCA. This EPRCA30 category is designed to evaluate the combined influence on both sustainable materials on the mix. By comparing all these samples, the study can determine the salient balance between environment benefit and structural integrity, identifying whether ESP and RCA individually or together enhance or compromise concrete performance. As shown in Table 4.12, there is the parameter of the sample were used in the experiment.

Table 4.12
Parameter of Sample

Sample	Parameter	Description	Series
1	OPCNA	Ordinary Portland Cement and Natural Fine Aggregates - Sand	Control Sample
2	5EPRCA0	5% Eggshell Powder and 0% Recycled Concrete Aggregates	EPRCA0 series
3	10EPRCA0	10% Eggshell Powder and 0% Recycled Concrete Aggregates	EPRCA0 series
4	15EPRCA0	15% Eggshell Powder and 0% Recycled Concrete Aggregates	EPRCA0 series
5	5EPRCA30	5% Eggshell Powder and 30% Recycled Concrete Aggregates	EPRCA30 series
6	10EPRCA30	10% Eggshell Powder and 30% Recycled Concrete Aggregates	EPRCA30 series
7	15EPRCA30	15% Eggshell Powder and 30% Recycled Concrete Aggregates	EPRCA30 series

4.3.4 Compressive Strength for Cubes

Results for compressive strength were taken straight from the compression machine. Three identical concrete cubes were used to obtain the average compressive strength. There were consist like 3 of cube samples for each of the timing days curing which are 3, 7, 28 and 56 days and took the average data for each curing ages.

There were 7 different of mixtures that be compared which are OPCNA, 5EPRCA0, 10EPRCA0, 15EPRCA0, 5EPRCA30, 10EPRCA30, and 15EPRCA30.

From the compression testing, the salient mixture could be recognised and considered the uses in production of interlocking blocks (IB).

Figure 4.13 illustrates the progressive development of compressive strength in OPCNA samples over time, reflecting the material's increasing durability and structural integrity. On Day 3, the average load was 39.15 kN, corresponding to a stress of 15.66 MPa, with values ranging from 14.15 MPa to 18.31 MPa, indicating early variability in hydration and matrix formation. By Day 7, the average stress rose to 23.37 MPa, with more consistent values between 22.41 MPa and 24.90 MPa, suggesting improved cement gel formation and pore refinement. At Day 28, the strength increased significantly to an average of 35.00 MPa, and by Day 56, it reached 38.18 MPa, with peak values up to 41.15 MPa, confirming the long-term strength gain typical of OPC systems.

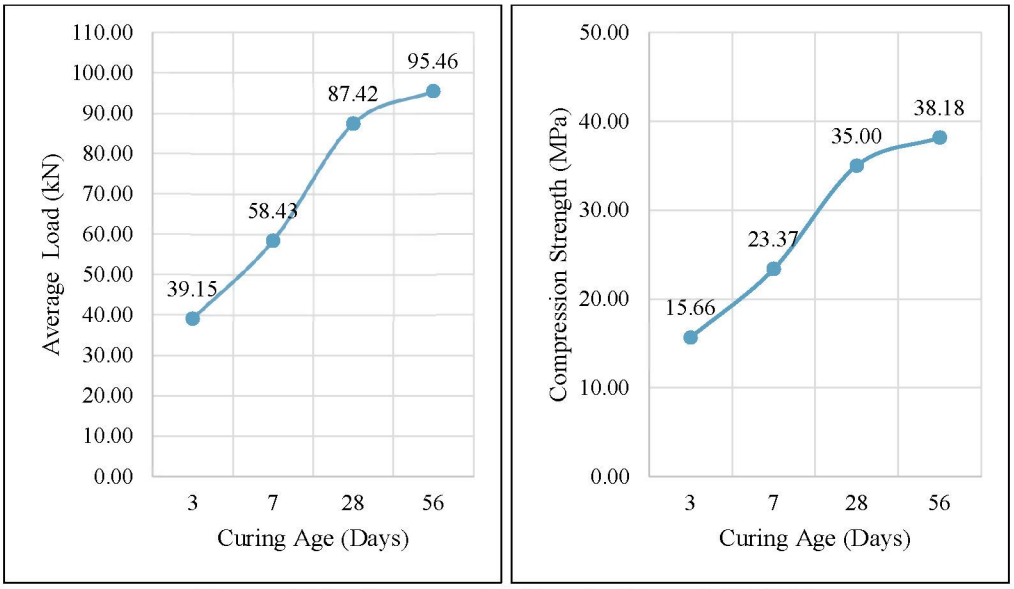

Figure 4.10 Compression Results Line of OPCNA

This strength progression aligns with established hydration kinetics of OPC, where calcium silicate phases (C3S and C2S) contribute to early and later strength development. According to Neville (2012), OPC typically achieves 70–90% of its final strength within 28 days, with continued gains up to 56 days depending on curing conditions. Mishra et al. (2021) further supported this trend, noting that compressive strength at 3 and 7 days can reliably predict 28-day performance, especially in mixes with stable water-cement ratios and proper compaction. Additionally, Ganiyu & Erhurhu (2023) observed that OPC mixes with superplasticizers or optimized curing

can exceed 35 MPa at 28 days, reinforcing the reliability of OPCNA in structural applications.

The consistent increase in load-bearing capacity and reduced variability over time in your results demonstrates that the OPCNA mix meets performance expectations for high-strength concrete. These findings validate the use of OPCNA as a benchmark material in comparative studies involving ESP and RCA, and align with JKR standard strength classifications, particularly for structural grade concrete in tropical environments. Overall, the load and stress results across several days can be seen in Appendix A. Figure 4.14 shown one of the samples that have been done the compression test was from day 28 curing age.

Figure 4.11 Sample OPCNA After Compression Test

4.3.4.1 Compressive Strength of 3rd Days

The Day 3 compressive strength results for EPRCA0 and EPRCA30 mixtures reveal distinct performance trends based on varying eggshell powder (ESP) content. For the EPRCA0 mixture, the compressive strength initially declined with 10% ESP (38.88 kN, 15.56 MPa) compared to 5% ESP (55.89 kN, 22.36 MPa), but then significantly improved at 15% ESP (60.94 kN, 24.37 MPa). This suggests that while moderate ESP levels may disrupt early hydration or reduce binder cohesion, higher ESP content can enhance strength through improved particle packing and pozzolanic activity.

In contrast, the EPRCA30 mixture exhibited a more variable response. At 5% ESP, the load and stress were 45.45 kN and 18.18 MPa, respectively. A slight increase was observed at 10% ESP (46.78 kN, 18.72 MPa), but strength declined at 15% ESP

(43.09 kN, 17.26 MPa). This indicates that the presence of RCA may interact differently with ESP, potentially limiting the benefits of higher ESP content due to increased porosity or weaker interfacial bonding.

The comparative analysis (see Figure 4.15) highlights that EPRCA0 generally benefits more from increased ESP content, especially at 15%, while EPRCA30 shows optimal performance around 10% ESP, beyond which strength diminishes. These findings suggest that the optimal ESP replacement level is mixture dependent, influenced by aggregate type and mix design.

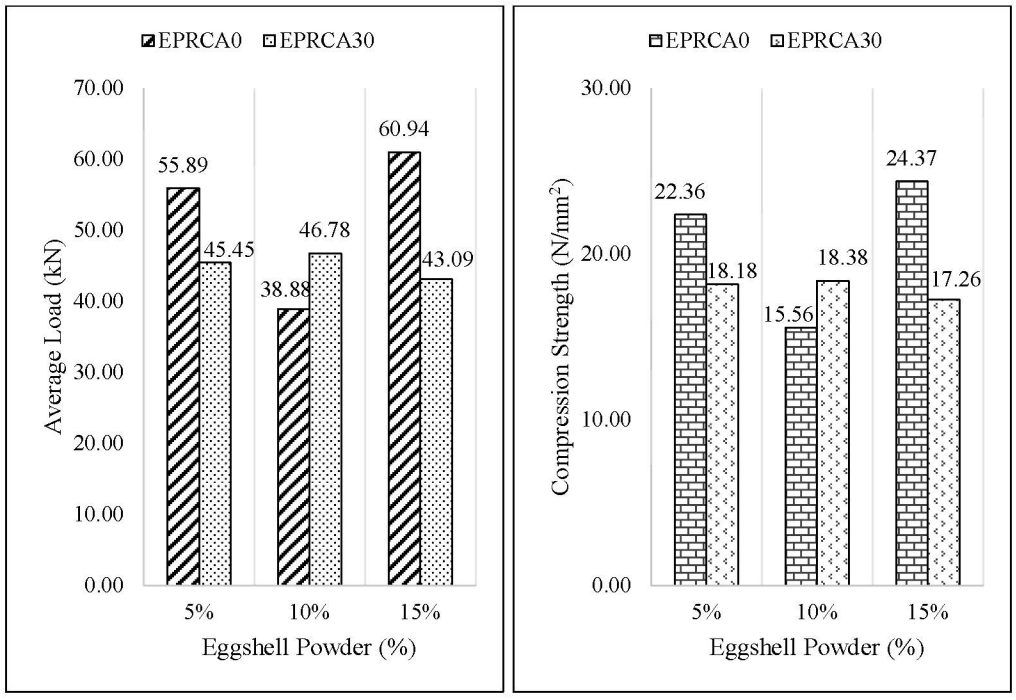

Figure 4.12 Comparison Compression Results EPRCA0 and EPRCA30 of 3 Days

The incorporation of recycled concrete aggregate (RCA) in concrete mixes typically results in a reduction of compressive strength due to its higher porosity and weaker interfacial transition zones, as reported by Tam et al. (2007) and Majeed & Saleh (2022). However, this behaviour aligns with previous studies. Jhatial et al. (2021) It is also evidenced that ESP may be used to enhance compressive strength as it has high content of calcium carbonate that aids secondary hydration and densification of matrix. According to the findings of Upadhyay (2023), strength can be improved by ESP replacements of up to 15% but further replacements can decrease performance since respective replacements do not disperse well and exhibit more voids. On the same note,

Bhaskaran et al. (2016) found that in lower percentages, ESP enhances early strength, but at higher replacements levels, mechanical integrity might be degraded. Figure 4.16 shows a sample 5EPRCA30 that has been subjected to compressive strength test following its 3-day curing. Altogether, the findings support the idea of customizing ESP content to mix compositions, and trade off sustainability targets with mechanical performance.

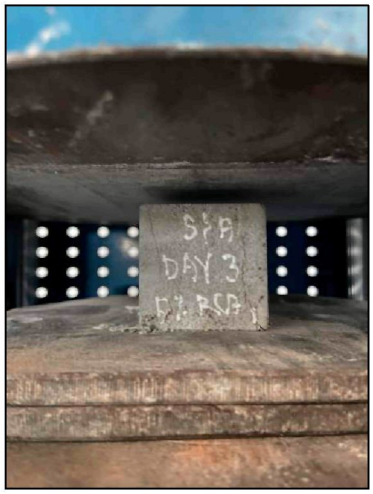

Figure 4.13 Sample 3 Days After Compression Test

4.3.4.2 Compressive Strength of 7th Days

The 7-days compressive strength values at different percentages of the eggshell powder (ESP) of EPRCA0 and EPRCA30 mixtures demonstrate dissimilar performance trends that are evident by Figure 4.17. In EPRCA0, the combination of 5% ESP was found to be the most effective in terms of strength at early age with means load of 86.03 kN and stress of 34.42 MPa, which represents outstanding performance in early age. At ESP of 10%, the strength decreased (61.62 kN, 24.65 MPa) as compared to 5% level possibly because cementitious material was diluted or the hydration occurred later. Nevertheless, ESP (15%) partially regained strength (75.45 kN, 30.18 MPa), which implies that elevated ESP levels can aid the microstructural refinement and secondary hydration advantages.

Conversely, EPRCA30 was less intense than that of all ESPs. The ratio of 5% ESP had a result of 59.19 kN and 23.78 MPa and a significant decline was observed at 10% ESP (45.95kN, 18.38 MPa). At 15% ESP (50.36 kN, 20.98 MPa) they changed slightly in a booster, albeit weaker than EPRCA0. Comparing the samples, it can be

concluded that EPRCA0 behaves better than EPRCA30 on all percentages of ESP, possibly since RCA is not noticeable, and may add porosity and loose interfacial adhesion.

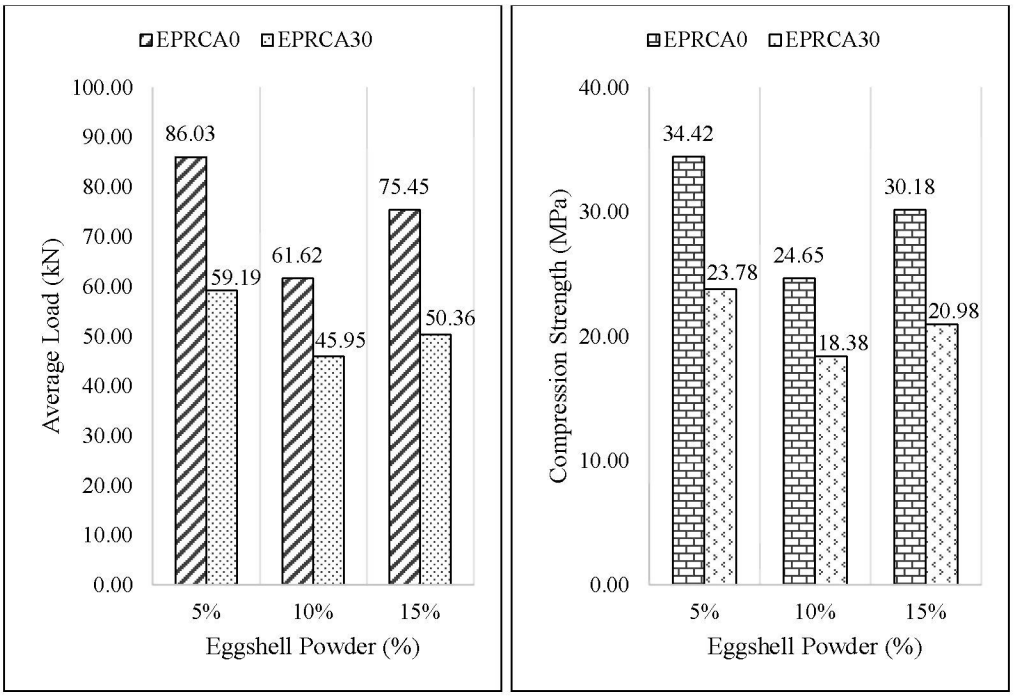

Figure 4.14 Comparison Compression Results EPRCA0 and EPRCA30 of 7 Days

These results correspond to the findings of Revilla-Cuesta et al. (2021), who stated that the impact of RCA on compressive strength is very much dependent on the quality of RCA and the reaction to other materials. Adamu Lawan et al. (2022) further showed that by using the mixed concrete with combined RCA and additional materials such as ESP, the strength of replaceable concrete can be the same or even higher than that of the controlling concrete when the level of proportionality of the replacements is well balanced.

In general, the findings indicate that ESP may be used to increase the compressive strength of exchange percentages but effectiveness depends on whether or not it is accompanied by RCA. The EPRCA0 is more advantageously modified by ESP incorporation and EPRCA30 means a restricted control of mix to reduce the loss of strength. Figure 4.18 shows the specimen of mortar 5EPRCA30 tested at 7 days curing period against compressive strength.

Figure 4.15 Sample 7 Days After Compression Test

4.3.4.3 Compressive Strength of 28th Days

The 28 days compressive strength results for EPRCA0 and EPRCA30 mixtures reveal distinct trends influenced by varying levels of eggshell powder (ESP). In Figure 4.19 for EPRCA0, the mix with 5% ESP achieved a high average load of 87.86 kN and stress of 35.15 MPa, indicating strong mechanical performance. Increasing ESP to 10% led to a noticeable reduction in strength (64.90 kN, 25.96 MPa), likely due to dilution of cementitious content or increased porosity. However, at 15% ESP, the strength nearly recovered (86.37 kN, 34.55 MPa), suggesting that higher ESP content may contribute to microstructural densification and secondary hydration, restoring compressive capacity.

In contrast, EPRCA30 showed its highest strength at 5% ESP (93.96 kN, 37.59 MPa), outperforming EPRCA0 at the same level. Yet, as ESP content increased to 10%, strength declined (70.40 kN, 28.16 MPa), and only partially recovered at 15% ESP (76.50 kN, 30.60 MPa). This pattern indicates that while EPRCA30 benefits from low ESP content, its performance becomes more variable at higher replacement levels, possibly due to the combined effects of RCA's porous nature and ESP's influence on binder cohesion.

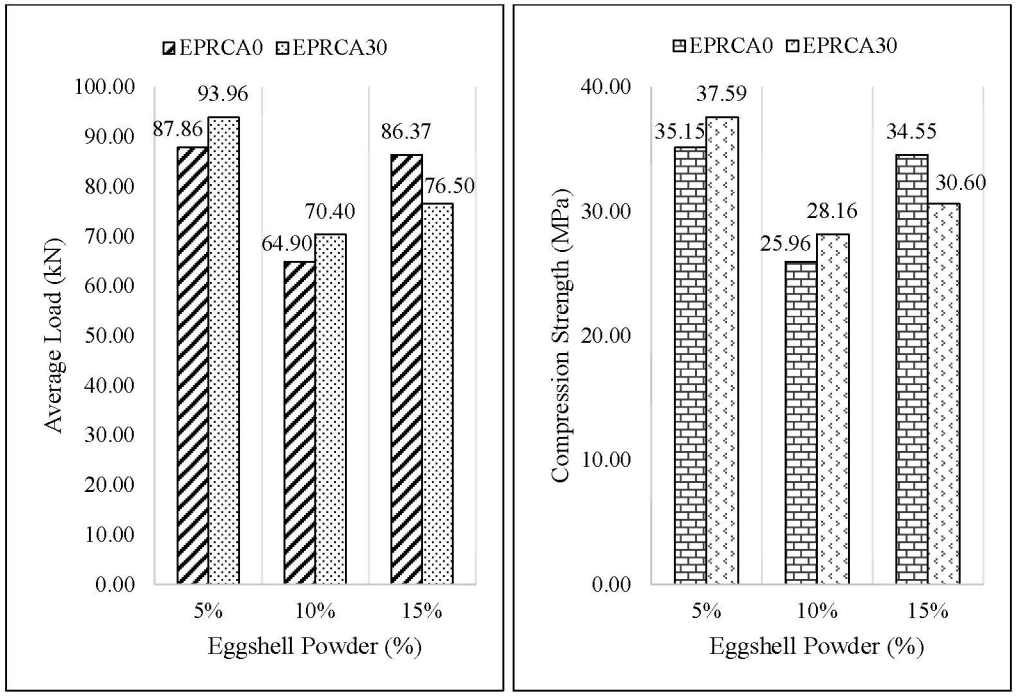

Figure 4.16 Comparison Compression Results EPRCA0 and EPRCA30 of 28 Days

These findings align with Jaskulski et al. (2017), who emphasized that RCA's impact on compressive strength depends heavily on its quality and interaction with binder materials. Revilla-Cuesta et al. (2021) further noted that RCA can introduce strength dispersion due to its variable absorption and interfacial bonding characteristics. Meanwhile, Tan et al. (2018) and Upadhyay (2023) demonstrated that ESP can enhance compressive strength when used at optimized levels (typically 5–15%), owing to its calcium-rich composition and filler effect. The sample of 15EPRCA30 depicted in Figure 4.20 was tested for compressive strength at the 28 days mark of its curing ages.

Overall, the results suggest that EPRCA0 maintains more consistent strength across ESP levels, while EPRCA30 performs best at lower ESP percentages. This highlights the importance of mixture specific optimization, where the balance between ESP and RCA must be carefully managed to achieve desired mechanical properties in sustainable concrete systems.

Figure 4.17 Sample 28 Days After Compression Test

4.3.4.4 Compressive Strength of 56th Days

After 56 days of curing, both EPRCA0 and EPRCA30 mixtures exhibited satisfactory compressive strength, although their performance varied with the proportion of eggshell powder (ESP). For the EPRCA0 series as illustrated in Figure 4.21, incorporating 5% ESP produced the highest average load of 95.22 kN and a stress value of 38.09 MPa, reflecting strong mechanical performance. However, when the ESP content was raised to 10%, strength decreased to 66.02 kN and 26.41 MPa. This reduction can be attributed to the dilution of cementitious material, which limits calcium silicate hydrate (C–S–H) formation and weakens the bond within the matrix (Olutoge et al., 2012; Anwar et al., 2020). Interestingly, at 15% ESP, strength nearly recovered to its earlier level (93.18 kN, 37.28 MPa). This suggests that at higher replacement levels, the fine particle size of ESP may act as a filler, enhancing particle packing, reducing voids, and contributing to improved long-term hydration (Subramaniam et al., 2021).

For EPRCA30, the mix also performed well at 5% ESP (95.28 kN, 38.12 MPa), but strength decreased at 10% ESP (72.09 kN, 28.84 MPa) and only slightly improved at 15% ESP (78.38 kN, 31.35 MPa). This shows that while RCA can work well with low ESP content, it may reduce strength when ESP is increased too much. RCA tends to absorb more water and has weaker bonding surfaces, which can affect how well the mix holds together (Padmini et al., 2009; Silva et al., 2015). Consequently, the

combination of higher ESP and RCA content may compromise strength development, since both materials influence bond quality and water demand.

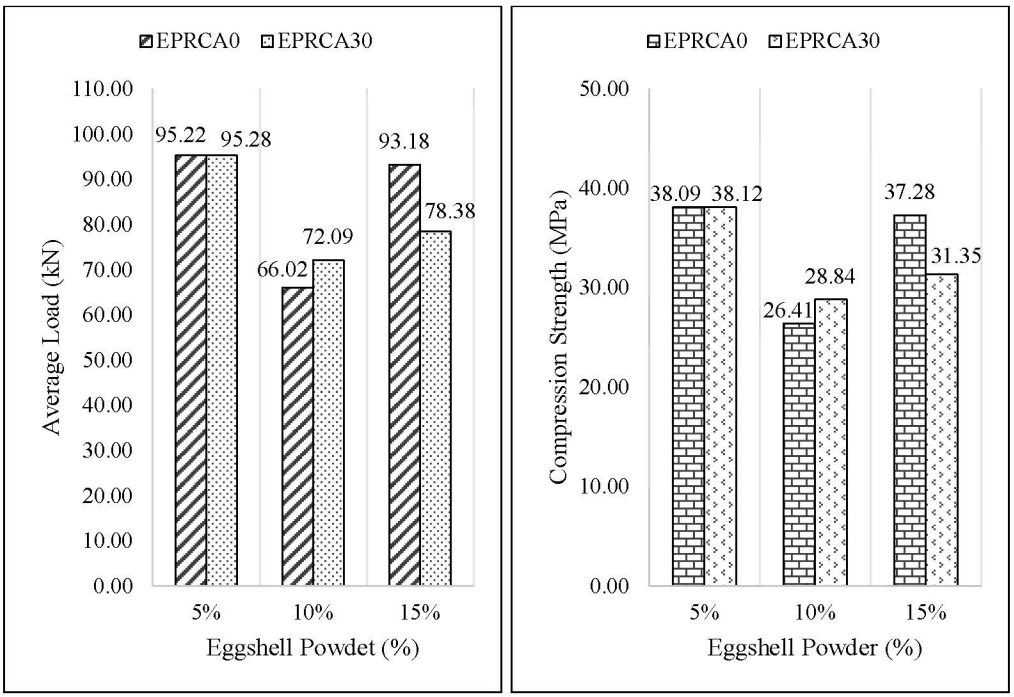

Figure 4.18 Comparison Compression Results EPRCA0 and EPRCA30 of 56 Days

The decision to stop testing at 56 days instead of continuing to 90 days is based on practical and technical reasons. By 56 days, concrete typically reaches 90–95% of its final strength, especially when using supplementary materials like ESP and RCA. Further strength gain beyond this point is usually minimal and does not significantly change the performance classification. This approach is supported by The Concrete Centre (2021) and aligns with standards such as EN1992-1-1: Eurocode 2 – Design of Concrete Structures and BS8500: Complementary British Standards to BS EN 206, which recognize 56 days strength as a reliable indicator for long-term durability in sustainable concrete. Figure 4.22 illustrates a specimen of 10EPRCA0 subjected to compressive strength testing at the 56 days curing stage.

Generally, the 56 days compressive strength data between EPRCA0 and EPRCA30 mixture confirms that ESP and RCA can be conveniently utilized in the sustainable concrete without concession to the long-term performance. Consistent strength recovery was observed at greater ESP levels in EPRCA0 and strong at ESP content was observed but more variable at higher ESP content in EPRCA30. These

trends demonstrate that it is necessary to optimize ESP dosage on the basis of aggregate type according to balanced mechanical properties.

Figure 4.19 Sample 56 Days After Compression Test

4.3.4.5 Compressive Strength for All Cubes

Relating average load and compressive strength to curing age (3, 7, 28, and 56 days) is presented in Figure 4.23 and Figure 4.24, where it is possible to see how mixtures containing eggshell powder (ESP) and recycled concrete aggregate (RCA) behave differently as compared to the OPCNA benchmark.

The overall compressive strength comparison (Figure 4.23) among OPCNA, EPRCA0, and EPRCA30 highlights distinct performance behaviours influenced by both eggshell powder (ESP) content and aggregate type. At early ages (3–7 days), EPRCA0 with 5% and 15% ESP demonstrated significantly higher strengths than OPCNA, showing that ESP is particularly effective in accelerating hydration and acting as a filler in mixes with natural aggregates. This rapid strength gain at early stages aligns with the known pozzolanic activity of ESP, which provides additional nucleation sites for hydration products and enhances the density of the cementitious matrix (Kumar et al., 2021). By contrast, EPRCA30 lagged at the same age, reflecting the weaker quality of recycled concrete aggregate (RCA), which is typically associated with high porosity, and microcracks (Shi et al., 2021).

At intermediate ages (28 days), the performance of EPRCA0 and OPCNA became more comparable, as the early benefits of ESP began to level off. The cement dilution effect became evident at higher ESP dosages (10–15%), leading to reduced

strength compared to the control. This is consistent with reports that excessive cement replacement reduces the amount of available clinker for hydration, limiting long-term strength development (Kassim et al., 2022). On the other hand, EPRCA30 with 5% ESP showed marked improvement at 28 days, even surpassing OPCNA, suggesting that small ESP additions can partially offset RCA's deficiencies by filling pores and enhancing microstructural integrity. However, higher ESP contents in EPRCA30 continued to underperform, indicating that the negative effects of RCA are exacerbated when cementitious material is reduced too much. This is likely due to the presence of 30% pre-carbonated ash, which can limit reactive sites and alter internal chemistry, partially hampering the effective contribution of ESP at certain stages (Islam et al., 2019).

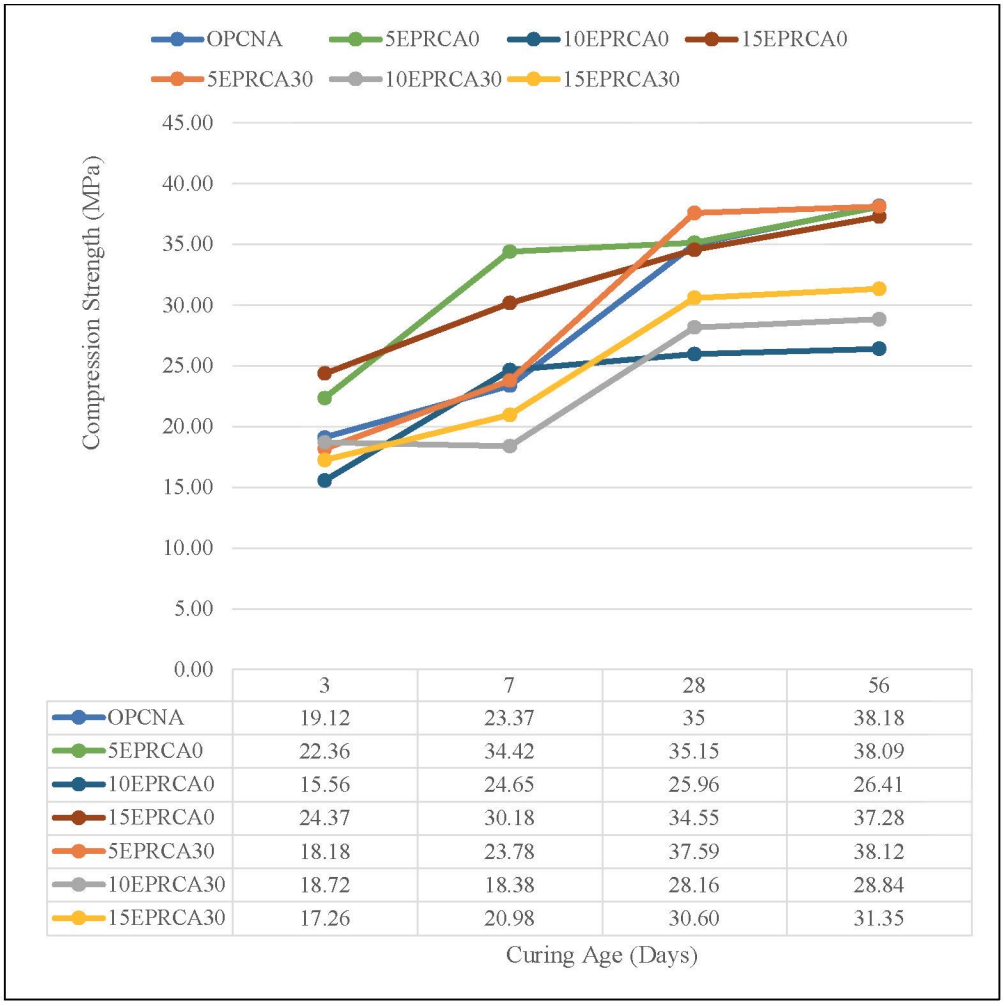

	3	7	28	56
OPCNA	19.12	23.37	35	38.18
5EPRCA0	22.36	34.42	35.15	38.09
10EPRCA0	15.56	24.65	25.96	26.41
15EPRCA0	24.37	30.18	34.55	37.28
5EPRCA30	18.18	23.78	37.59	38.12
10EPRCA30	18.72	18.38	28.16	28.84
15EPRCA30	17.26	20.98	30.60	31.35

Figure 4.20 Comparison Results Compression Strength (MPa) of OPCNA, EPRCA0 and EPRCA30

Consequently, the average load shows in Figure 4.24 of OPCNA, 5EPRCA0, and EPRCA30 is reflected in the compression strength. By 56 days, EPRCA0 and EPRCA30 with 5% ESP both showed strengths nearly equivalent to OPCNA, demonstrating that ESP can support long-term performance when used at moderate levels. The steady gain in strength shows the matrix densification and refined pore structure that result from the compatibility between ESP and the unmodified binder (Neville, 2011). However, the 10% and 15% ESP mixes consistently trailed behind, reaffirming the dilution effect. This pattern supports the conclusion that low-level ESP replacement (around 5%) strikes a balance between enhancing hydration and maintaining adequate cement content, while higher percentages compromise later-age strength (Aliabdo et al., 2014).

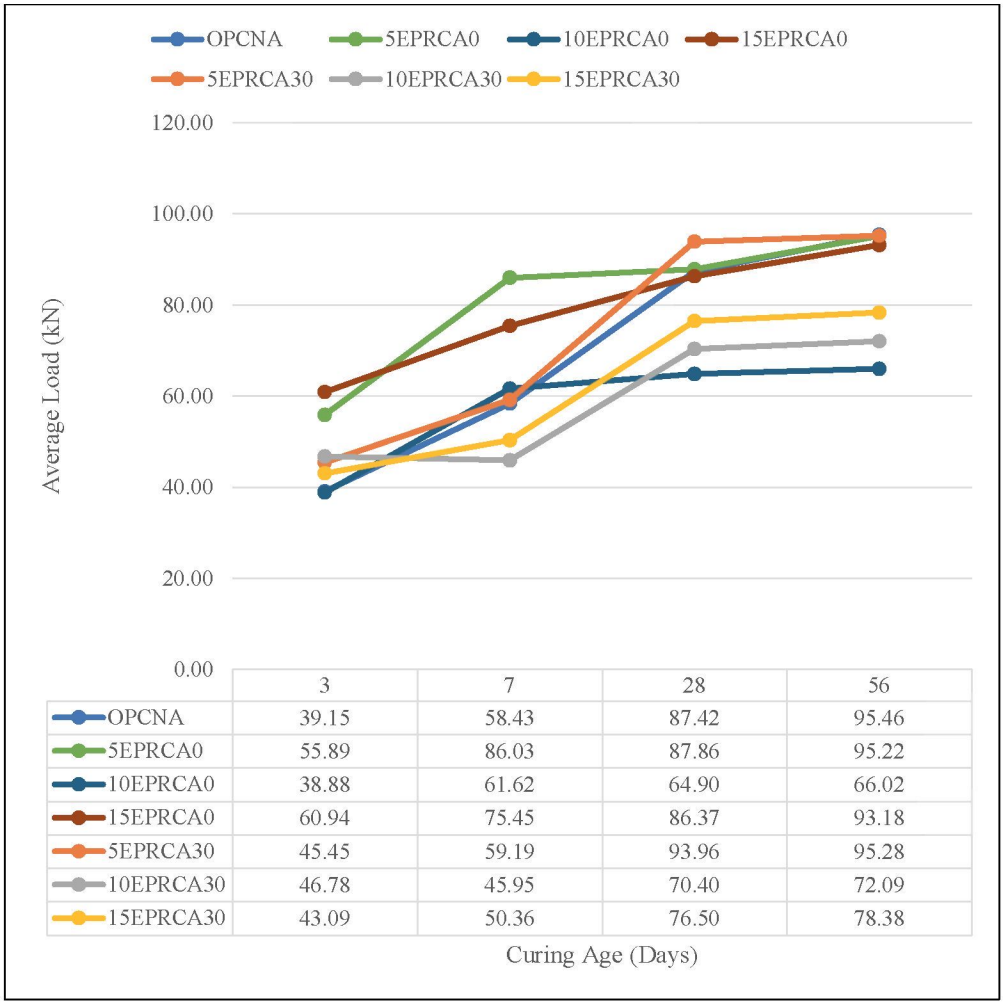

	3	7	28	56
OPCNA	39.15	58.43	87.42	95.46
5EPRCA0	55.89	86.03	87.86	95.22
10EPRCA0	38.88	61.62	64.90	66.02
15EPRCA0	60.94	75.45	86.37	93.18
5EPRCA30	45.45	59.19	93.96	95.28
10EPRCA30	46.78	45.95	70.40	72.09
15EPRCA30	43.09	50.36	76.50	78.38

Figure 4.21 Comparison Results Average Load (kN) of OPCNA, EPRCA0 and EPRCA30

For RCA mixes, this balance is even more critical, as the inherent weaknesses of RCA including higher water absorption and lower density that gave additional factors influencing strength performance to reduce the system's tolerance for excessive cement replacement (Pereira et al., 2023). However, 5EPRCA0 appeared to adapt well to this behaviour, maintaining a workable mix and showing improved strength progression even as curing advanced. Meanwhile, 5EPRCA30, while benefiting from early hydration at 5% ESP, can have been more vulnerable to microstructural imbalances and delayed pozzolanic activity due to its recycled and pre-carbonated content (John & Lothenbach, 2023). These factors could contribute to its inconsistent early-age performance, even though its long-term results closely matched those of 5EPRCA0. This suggests that while 5% ESP is a promising dosage for both mixes, the overall reactivity and microstructure of EPRCA0 creates more reliable strength outcomes.

Overall, the results demonstrate that ESP is most effective as a partial cement replacement in mixes with natural aggregates, where its pozzolanic and filler effects can be fully realized. In RCA mixes, ESP at 5% provides notable benefits and can produce strengths comparable to OPCNA at later ages, but higher ESP contents reduce performance due to the combined challenges of cement dilution and RCA porosity. These findings confirm that ESP's contribution depends heavily on aggregate type and replacement level, with EPRCA0 favouring higher ESP percentages at early ages and EPRCA30 benefiting mainly from lower ESP contents at longer curing durations.

4.3.5 Flexural Strength for Prisms

Prism measuring 160 mm x 40 mm x 40 mm underwent a flexural strength test in comparison with different mixtures, which are OPCNA, EPRCA0, and EPRCA30 that had undergone 3, 7, 28, and 56 days of water curing. According to BS EN 13523-7:2001, the test was conducted with a Universal Testing Machine 100 kN. The three-point loading technique was employed to gauge the prism's flexural strength. The load was applied in the centre of each concrete block, and the span between the supports was set at 120 mm. Three specimens were used to get the maximum force and maximum stress average values.

The flexural results of OPCNA show in Figure 4.25, a consistent increase in both average force and stress as the curing age progresses. At 3 days, the average force is 1984.47 N, corresponding to an average stress of 4.65 N/mm^2. By 7 days, the average

force increases to 2133.25 N with an average stress of 4.96 N/mm². A more significant improvement is observed at 28 days, where the average force reaches 2332.86 N, yielding an average stress of 5.45 N/mm². Finally, at 56 days, the average force peaks at 2459.58 N, resulting in the highest average stress of 5.67 N/mm². These results indicate that OPCNA continues to gain strength over time, with the most substantial improvements occurring between 28 and 56 days of curing.

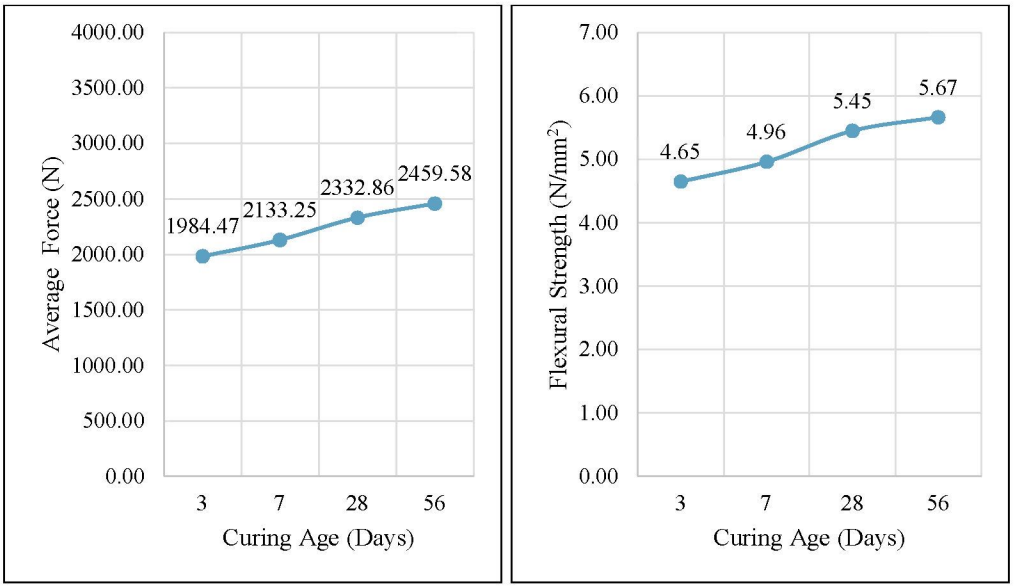

Figure 4.22 Flexural Results Line of OPCNA

The steady increase in strength can be explained by the continued hydration of cement particles, which produces more calcium-silicate-hydrate (C–S–H) gel. It is a gel that serves to fill pores and make the construction tighter and more resistant (Thomas & Jennings, 2021). Increased length of curing is also related to cement paste bond with aggregates leading to better flexural performance (Mindess et al., 2017). The up to 56 days strength is similar to other researchers conducted, which demonstrated that the strength of concrete continued increasing so long as there is yet unhydrated cement in concrete (Mehta & Monteiro, 2014). Alongside it, the enhanced flexural strength relates to the reduced microcracks and superior stress transfer within the mix, further contributing to the flexural strength with an enhanced result 28 days later (Ganesan et al., 2018). The OPCNA specimen during the flexural strength testing procedure on the 56 th day of curing is presented in Figure 4.26.

Figure 4.23 Sample 56 Days OPCNA After Flexural Test

4.3.5.1 Flexural Strength for 3 Days

Within the EPRCA0 mixtures, Figure 4.27 indicates varied behaviours in terms of flexural strength outcomes at 3 days of curing based on the percentage of ESP. The mixture attained average stress of 3.44 N/mm² at 5% ESP and this reduced at 2.97 N/mm² when ESP augmented to 10%. Interestingly, the stress value is the highest to have been recorded at this mix at this early stage at 15% ESP that is an improvement to 3.64 N/mm. This indicates that although the matrix can be compromised by excessive ESP due to lower cementitious levels and hence poor performance at low cementitious matrices, it can also improve with greater replacement levels (15%) leading to greater packing density and improved filler gains making it yield more desirable stress performance (Akinwumi et al., 2015; Mo et al., 2016). The nature of the strength recovery with increasing ESP can also be explained due to the pozzolanic effect of the eggshell powder, which is more contributory when there are enough quantities to interact with the free calcium hydroxide (Ranjbar & Zhang, 2020).

Conversely, the EPRCA30 mixtures showed another trend. This mixture performed best at 5 % ESP which yielded a flexural stress of 3.66 N/mm², however, adding more ESP (10 % and 15 %) decreased the stress to 3.25 and 3.05 N/mm² respectively. Such reduction could be explained by lower interfacial bonding and elevated water adsorption of recycled concrete aggregate (RCA), which could counteract the positive influence of ESP when it is added in larger amounts (Kou & Poon, 2013). The reduced performance at higher ESP levels also reflects the

microstructural imbalances and potential dilution effect, where too much ESP lowers the cementitious phase, thereby reducing the overall strength (Manaf et al., 2020).

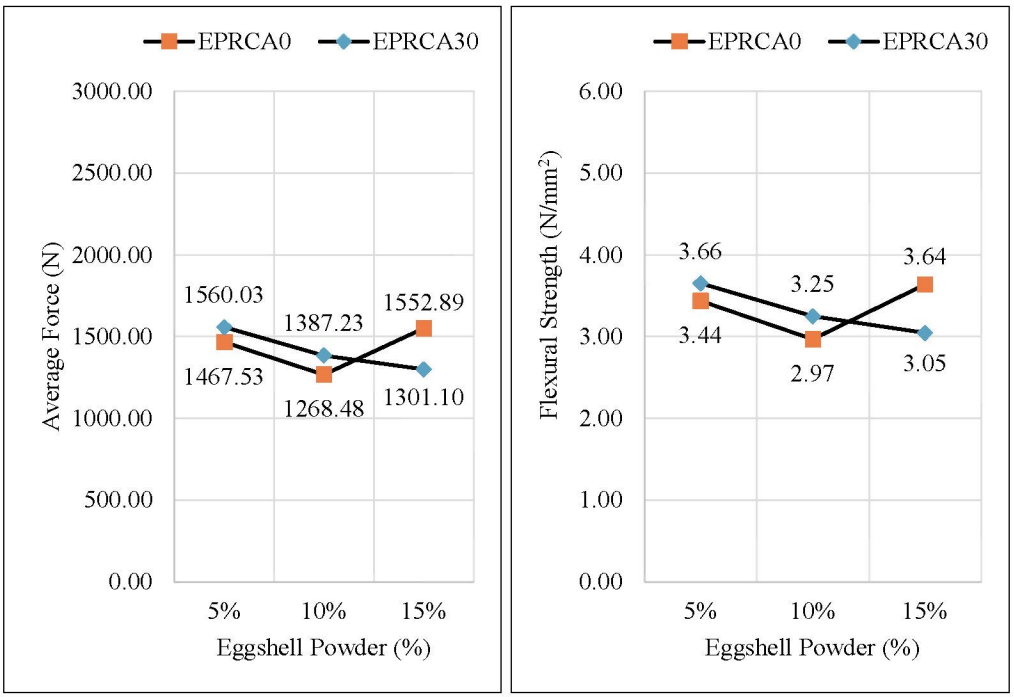

Figure 4.24 Comparison Flexural Results EPRCA0 and EPRCA30 of 3 Days

When comparing EPRCA0 and EPRCA30, it is evident that RCA incorporation plays a key role in the early flexural response. At 5% and 10% ESP, EPRCA30 outperforms EPRCA0, indicating that limited ESP addition can effectively enhance the performance of RCA-based mixtures by filling voids and partially compensating for the weaker aggregate surfaces. However, at 15% ESP, EPRCA0 regains superiority, achieving 3.64 N/mm² compared to EPRCA30's 3.05 N/mm². This implies that the higher porosity and pre-carbonated nature of RCA hinder the efficient utilization of ESP at greater replacement levels, reducing its contribution to strength development (Silva et al., 2015).

Overall, these results show that the optimal ESP content differs between mixtures. For EPRCA0, higher ESP (15%) promotes better early flexural performance due to densification effects, whereas for EPRCA30, lower ESP levels (5%) are more effective, since excessive ESP cannot fully compensate for the limitations of RCA. This finding aligns with previous studies indicating that the balance between pozzolanic activity, filler effects, and aggregate quality is critical for optimizing flexural strength

in blended cementitious systems (Umar et al., 2021; da Silva & de Brito, 2019). The flexural strength test of the 10EPRCA0 specimen after 3 days of curing is illustrated in Figure 4.28.

Figure 4.25 Sample 3 Days After Flexural Test

4.3.5.2 Flexural Strength for 7 Days

Flexural strength findings, measured after 7 days, indicate (Figure 4.29) the influence of ESP percentages on the EPRCA0 and EPRCA30 bending resistances. In the case of EPRCA0, strength tended to increase as more ESP was used: 3.75 N/mm² with 5% ESP, marginally better at 3.73 N/mm² with 10% ESP and, then, much better at 4.37 N/mm² with 15% ESP. The trend is an indication that the mix becomes more resistant to bending loads as its ESP content increases, probably because of enhanced particle packing and the calcium rich nature of ESP, which tightens cement matrixes with time.

Comparatively, EPRCA30 was a more mixed response. With 5 and 10% ESP, the flexural stress was 3.77 N/mm²and 3.95 N/mm²respectively, showing that an intermediate content of ESP can increase the strength of the mix even with recycled aggregates. But at 15% ESP, strength decreased to 3.48 N/mm², which might have been because of lower workability or non-uniform dispersion of ESP in the formulation. This indicates that though ESP has the potential of enhancing flexural strength, excessive levels can result in weaker bonding or internal defects particularly when used together with RCA.

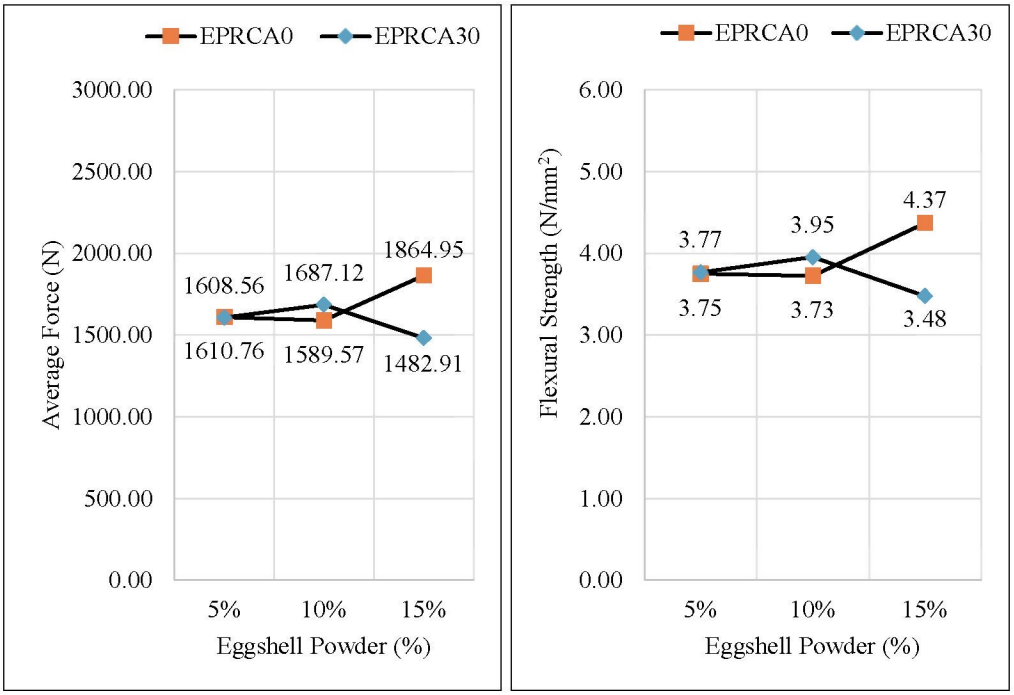

Figure 4.26 Comparison Flexural Results EPRCA0 and EPRCA30 of 7 Days

When comparing both mixtures, EPRCA30 performed slightly better at 10% ESP, but EPRCA0 showed the highest strength at 15% ESP, suggesting that the optimal ESP level depends on the type of aggregate used. RCA's rough texture and higher water absorption can affect how well the mix holds together, especially at higher ESP levels.

These findings are supported by Yang & Lee (2017), who found that using RCA with modified mix designs can improve flexural strength, but quality control is key. Hemida et al. (2023) also showed that increasing RCA content tends to reduce flexural strength unless the mix is reinforced or carefully balanced. Additionally, Magbool et al. (2024) confirmed that RCA's effect on flexural capacity is limited when proper design methods are used, and ESP-like fillers can help restore performance. The 5EPRCA0 specimen subjected to flexural strength testing at 7 days of curing is shown in Figure 4.30.

Figure 4.27 Sample 7 Days After Flexural Test

4.3.5.3 Flexural Strength for 28 Days

In Figure 4.31, for the EPRCA0 mixture the flexural strength at 28 days shows a clear enhancement with increasing ESP content except at 10%. At 5% ESP, the mix achieves a force of 2101.27 N and a stress of 4.92 N/mm², which slightly improves at 15% ESP to 2131.08 N and 4.99 N/mm², indicating better rigidity and load-bearing capacity. However, at 10% ESP, the strength drops to 1842.73 N and 4.32 N/mm², suggesting that this intermediate level may disrupt the mix's internal cohesion, possibly due to uneven ESP dispersion or excess fines interfering with matrix bonding.

In the case of EPRCA30, the performance is more stable but slightly declining with higher ESP content. At 5% ESP, the mix records 2034.91 N and 4.77 N/mm², while 10% ESP yields 1846.53 N and 4.40 N/mm², and 15% ESP results in 1867.04 N and 4.38 N/mm². This trend implies that while ESP can enhance early strength, excessive amounts may reduce workability or cause segregation, especially when combined with RCA.

An analysis of the two mixes reveals that EPRCA0 will always perform better than EPRCA30 at 5% and 15% ESP levels hence natural aggregates can support high ESP levels. Interestingly, at 10% ESP, the RCA EPRCA30 even exceeds EPRCA0, and this is perhaps attributed to drivability to the surface bond at better ESP content, or the filler effects. At 28 days of curing, the 15EPRCA0 specimen was examined for flexural strength, as displayed in Figure 4.32.

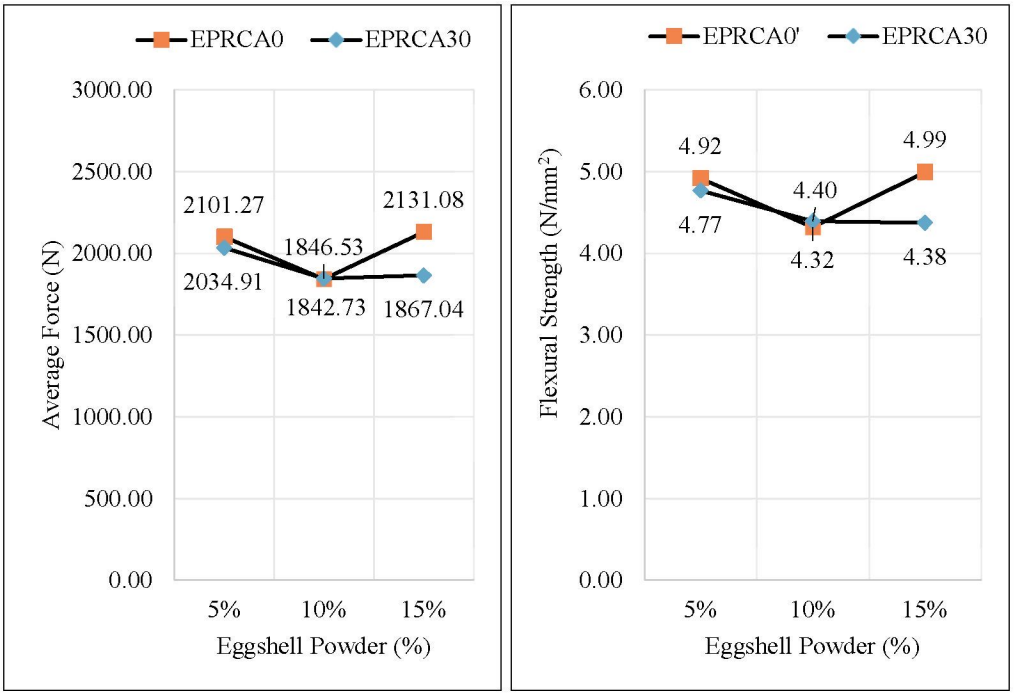

Figure 4.28 Comparison Flexural Results EPRCA0 and EPRCA30 of 28 Days

These observations are supported by recent studies. Pradhan et al. (2018) found that recycled aggregate concrete beams can perform well in flexure when mix design is optimized, but improper proportions can lead to reduced strength and brittle failure. Hemida et al. (2023) emphasized that RCA tends to lower flexural capacity unless reinforced or balanced with suitable binders. Magbool et al. (2024) confirmed that RCA's impact on flexural strength can be minimized through careful design, and that supplementary materials like ESP can help restore performance if properly integrated.

Figure 4.29 Sample 28 Days After Flexural Test

4.3.5.4 Flexural Strength for 56th Days

At 56 days of curing, the flexural strength of EPRCA0 increased greatly compared to earlier ages as illustrated in Figure 4.33. The mix with 5% ESP reached 2201.60 N and 5.16 N/mm², showing strong improvement. The 15% ESP mix also gave high results, with 2177.28 N and 5.10 N/mm², proving that higher ESP can still perform well. The 10% ESP mix was slightly lower at 1864.97 N and 4.37 N/mm², but it was still stronger than the results at early curing stages. Such expansion can be attributed to the continuation of the hydration process and ESP reaction, during which pores are filled, and the connection between paste and aggregates becomes stronger, which makes the concrete stronger (Sata et al., 2017; Awoyera & Adesina, 2020).

In the case of EPRCA30, 56-days results were even more outstanding. The strongest strength mixtures were 5% ESP at 2308.59 N and 5.54 N/mm² and the 15% ESP at 2199.80 N and 5.16 N/mm². The ESP mix was a little less at 1932.42 N and 4.53 N/mm^2 but way stronger than the previous curing times. Undoubtedly, the superiority of EPRCA30 over EPRCA0 can be attributed to the activity of RCA, which collaborates with ESP and generates a denser mixture and manufactures more hydration products over time (Pedro et al., 2014; Limbachiya et al., 2016).

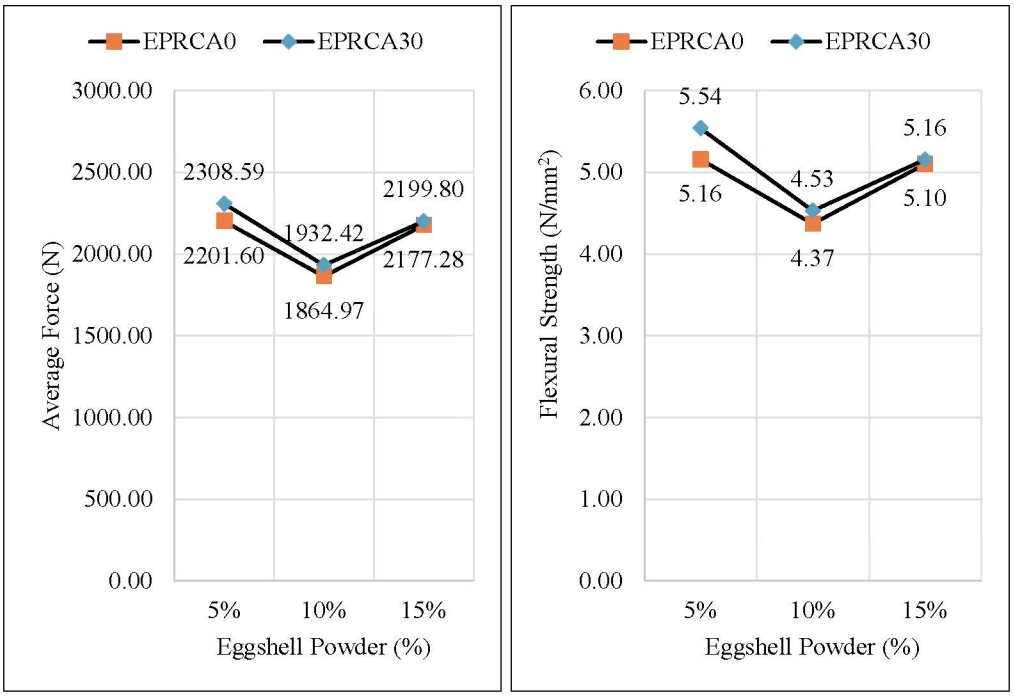

Figure 4.30 Comparison Flexural Results EPRCA0 and EPRCA30 of 56 Days

When comparing the two mixtures, EPRCA30 performed better than EPRCA0 at all ESP levels. For example, at 5% ESP, EPRCA30 reached 2308.59 N and 5.54 N/mm², higher than EPRCA0's 2201.60 N and 5.16 N/mm². A similar trend was seen at 10% and 15% ESP. This improvement happens because ESP acts as a fine filler while RCA provides extra sites for hydration, which helps reduce pores and strengthen the transition zone between paste and aggregates (Zega & Di Maio, 2011; Evangelista & de Brito, 2007). This results in fewer microcracks and better transfer of stress, leading to higher flexural strength.

In general, the 56-day results confirm that both EPRCA0 and EPRCA30 become stronger with ESP, but RCA-based mixes (EPRCA30) give better results overall. The findings suggest that 5% ESP provides the most consistent performance, but 15% ESP also gives high strength in the long term. This shows that ESP can be used as a good partial cement replacement, especially in mixes with RCA, to improve durability and structural performance (Omoding et al., 2021; Bogas et al., 2014). Figure 4.34 captures the testing of the 10EPRCA30 sample's flexural strength following 56 days of curing.

Figure 4.31 Sample 56 Days After Flexural Test

4.3.5.5 Flexural Strength for All Prisms

At all curing ages, OPCNA (Ordinary Portland Cement with Natural Aggregate) shows higher flexural strength compared to EPRCA0 (Eggshell Powder with Recycled Aggregate). In Figure 4.35 and Figure 4.36 were the summary of all the prisms results were average force and flexural strength, respectively. For 3 days, OPCNA reaches

1984.47 N, while EPRCA0 only ranges between 1268.48 N and 1552.89 N. This difference continues at 7 days, with OPCNA at 2133.25 N, while EPRCA0 stays between 1589.57 N and 1864.95 N. By 28 days, OPCNA further improves to 2332.86 N, compared to EPRCA0's 1842.73 N to 2131.08 N. Finally, at 56 days, OPCNA achieves 2459.58 N, while EPRCA0 remains lower, between 1864.97 N and 2177.28 N.

This consistent higher performance of OPCNA is because natural aggregates have better bonding with cement paste, leading to a denser microstructure and stronger load transfer. Recycled aggregates, on the other hand, usually contain old mortar and micro-cracks, which reduce bonding quality and overall strength (Thomas et al., 2020). The strong and stable structure of OPCNA explains why it always outperforms EPRCA0 at every curing age.

The comparison between OPCNA and EPRCA30 (which uses 30% pre-carbonated recycled aggregate) also shows similar results. At 3 days, OPCNA's flexural force is 1984.47 N, while EPRCA30 ranges only between 1301.10 N and 1560.03 N. At 7 days, OPCNA remains higher at 2133.25 N compared to EPRCA30's 1482.91 N to 1608.56 N. By 28 days, OPCNA increases to 2332.86 N, while EPRCA30 is between 1867.04 N and 2034.91 N. At 56 days, OPCNA peaks at 2459.58 N, while EPRCA30 ranges from 1932.42 N to 2308.59 N.

This shows that although pre-carbonation treatment improves recycled aggregate quality by reducing porosity and enhancing durability, OPCNA still performs better because natural aggregates provide stronger interlocking and higher resistance to stress (Silva et al., 2021). The presence of pre-carbonated material in EPRCA30 does improve results compared to untreated recycled aggregate, but it cannot fully match the performance of natural aggregates.

When comparing flexural strength (N/mm²), the same trend is observed. At 3 days, OPCNA records 4.65 N/mm², while EPRCA0 and EPRCA30 range lower, between 2.97–3.66 N/mm². By 7 days, OPCNA achieves 4.96 N/mm², compared to 3.48–4.37 N/mm² for EPRCA0 and EPRCA30. At 28 days, OPCNA reaches 5.45 N/mm², while EPRCA0 and EPRCA30 are between 4.32–4.77 N/mm². At 56 days, OPCNA has 5.67 N/mm², while EPRCA0 ranges 4.37–5.10 N/mm² and EPRCA30 ranges 4.53–5.54 N/mm².

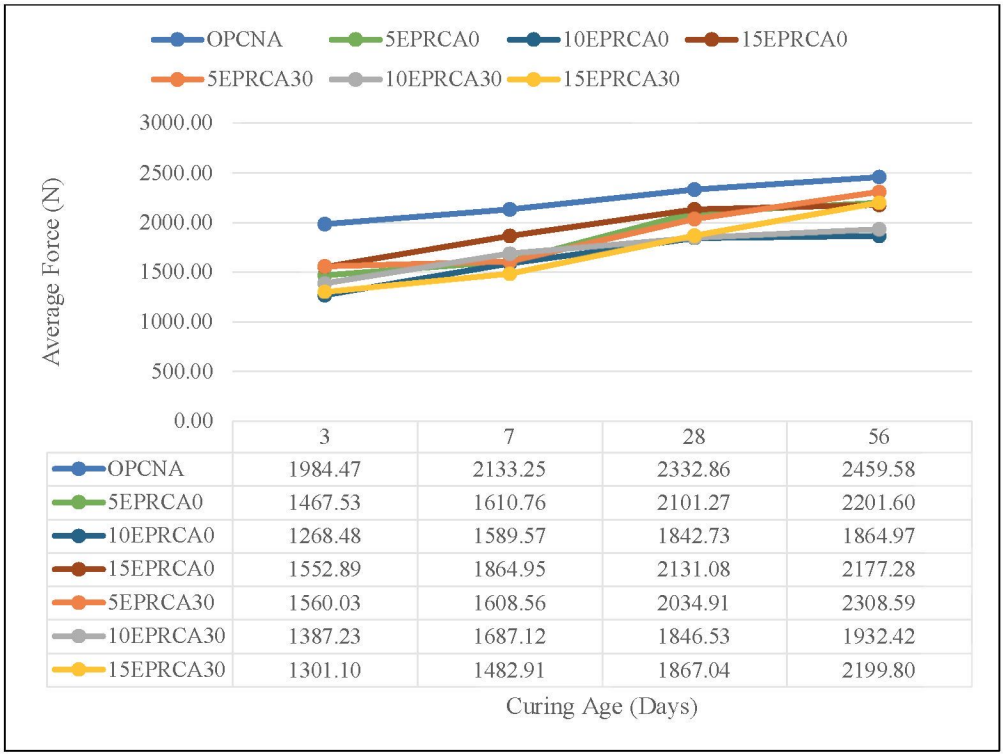

	3	7	28	56
OPCNA	1984.47	2133.25	2332.86	2459.58
5EPRCA0	1467.53	1610.76	2101.27	2201.60
10EPRCA0	1268.48	1589.57	1842.73	1864.97
15EPRCA0	1552.89	1864.95	2131.08	2177.28
5EPRCA30	1560.03	1608.56	2034.91	2308.59
10EPRCA30	1387.23	1687.12	1846.53	1932.42
15EPRCA30	1301.10	1482.91	1867.04	2199.80

Figure 4.32 Comparison Results Average Force (N) of OPCNA, EPRCA0 and EPRCA30

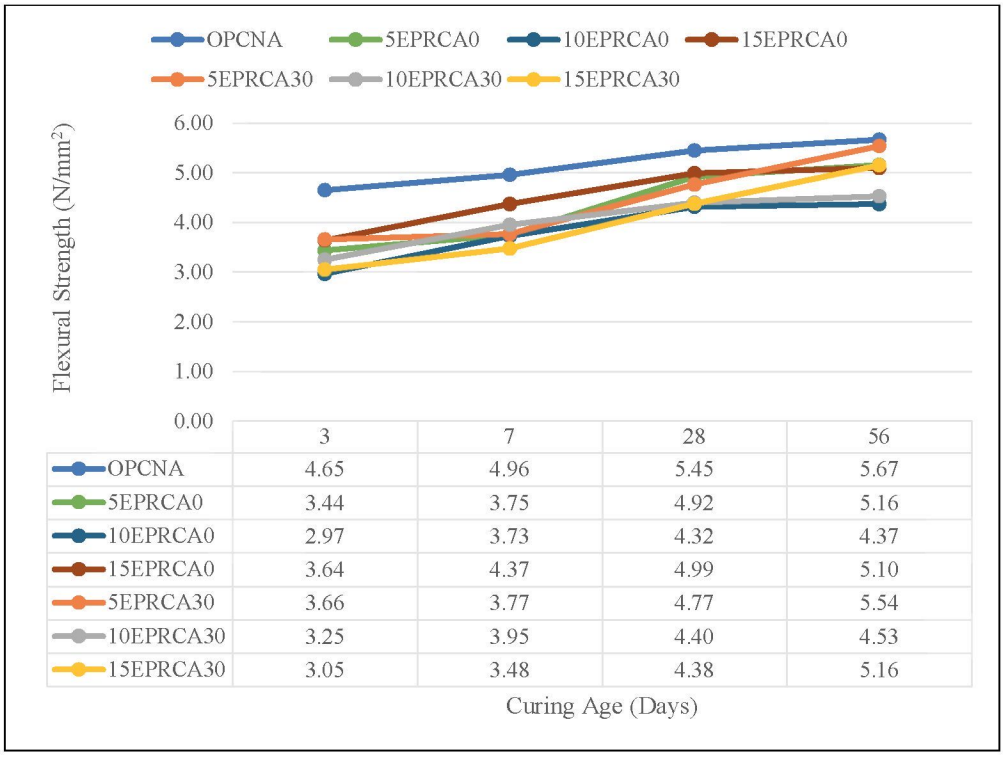

	3	7	28	56
OPCNA	4.65	4.96	5.45	5.67
5EPRCA0	3.44	3.75	4.92	5.16
10EPRCA0	2.97	3.73	4.32	4.37
15EPRCA0	3.64	4.37	4.99	5.10
5EPRCA30	3.66	3.77	4.77	5.54
10EPRCA30	3.25	3.95	4.40	4.53
15EPRCA30	3.05	3.48	4.38	5.16

Figure 4.33 Comparison Results Flexural Strength (N/mm^2) of OPCNA, EPRCA0 and EPRCA30

The reason OPCNA shows higher strength is because natural aggregates do not absorb too much water, allowing more water to be available for cement hydration, which forms more calcium silicate hydrate (C-S-H) gel that strengthens the concrete (Neville & Brooks, 2010). Recycled aggregates, especially in EPRCA0, absorb more water due to attached old mortar, reducing hydration efficiency and strength development (Xiao et al., 2018).

However, EPRCA30 shows some improvements at later curing ages (especially at 56 days), where 5% ESP with EPRCA30 achieves 5.54 N/mm², which is closer to OPCNA. This can be explained by the pozzolanic activity of eggshell powder, which reacts with calcium hydroxide to form additional C-S-H gel, improving bonding and densification over time (Aliabdo et al., 2014; Khawaja & Mariam, 2020). The carbonation treatment of recycled aggregates also refines the pore structure, which enhances long-term durability (Tam et al., 2020).

Overall, OPCNA consistently gives the best results at all ages, showing that natural aggregates are still superior in flexural performance. EPRCA0 shows weaker performance because untreated recycled aggregates reduce bonding. Meanwhile, EPRCA30 performs better than EPRCA0, especially at later ages, because carbonation reduces porosity and ESP contributes to pozzolanic reactions. This means that while OPCNA is the strongest option, the use of ESP and pre-carbonated recycled aggregates in EPRCA30 can still provide a sustainable and durable alternative, especially in non-structural or medium-load applications.

4.3.6 Summary on Results of The Salient Percentage Waste Materials Uses in Interlocking Block (IB)

The study confirms that incorporating eggshell powder (ESP) and recycled concrete aggregate (RCA) can produce sustainable mortar with acceptable performance when carefully proportioned. Flowability remained within the standard range (120–145%), though higher ESP and RCA reduced workability slightly due to water demand and aggregate angularity. Water absorption values (4.0–4.9%) were all below the 5% durability threshold, showing good resistance to moisture ingress. Particle size analysis revealed OPC as fine and dense, ESP slightly coarser but suitable, and SF ultrafine, enhancing pozzolanic activity; RCA was coarser but workable when blended with natural sand.

Compressive strength progressed steadily, with OPCNA reaching 38 MPa at 56 days and ESP–RCA mixes achieving comparable values when optimized. Flexural strength followed similar trends: OPCNA consistently led, but 5% ESP in both EPRCA0 and EPRCA30 delivered near-equivalent results (≈5.5 N/mm² at 56 days). Overall, 5% ESP with or without RCA proved the most effective replacement level, balancing workability, durability, and strength, while RCA inclusion required careful control. These findings validate ESP–RCA blends as viable, eco-friendly alternatives for structural masonry and interlocking block applications.

4.4 Flexural Strength for Interlocking Block (IB)

4.4.1 Solid Interlocking Block (SIB)

At 7 days of curing as shown in Figure 4.37, the flexural strength of Solid Interlocking Blocks (SIB) differs among mixtures. OPCNA shows the highest performance, with an average force of 22,391.63 N and stress of 5.37 N/mm², reflecting strong early-stage load-bearing ability. 5EPRCA0 shows lower strength (16,621.63 N and 3.99 N/mm²), while 5EPRCA30 is slightly better (17,668.30 N and 4.24 N/mm²). The early performance of OPCNA can be explained by its dense paste-aggregate bonding, which improves stress distribution across the block (Khatib & Hibbert, 2005). The higher strength of 5EPRCA30 compared to 5EPRCA0 is due to the pre-carbonated recycled aggregates, which reduce porosity and densify the interfacial transition zone (ITZ), allowing better load transfer (Tam et al., 2007).

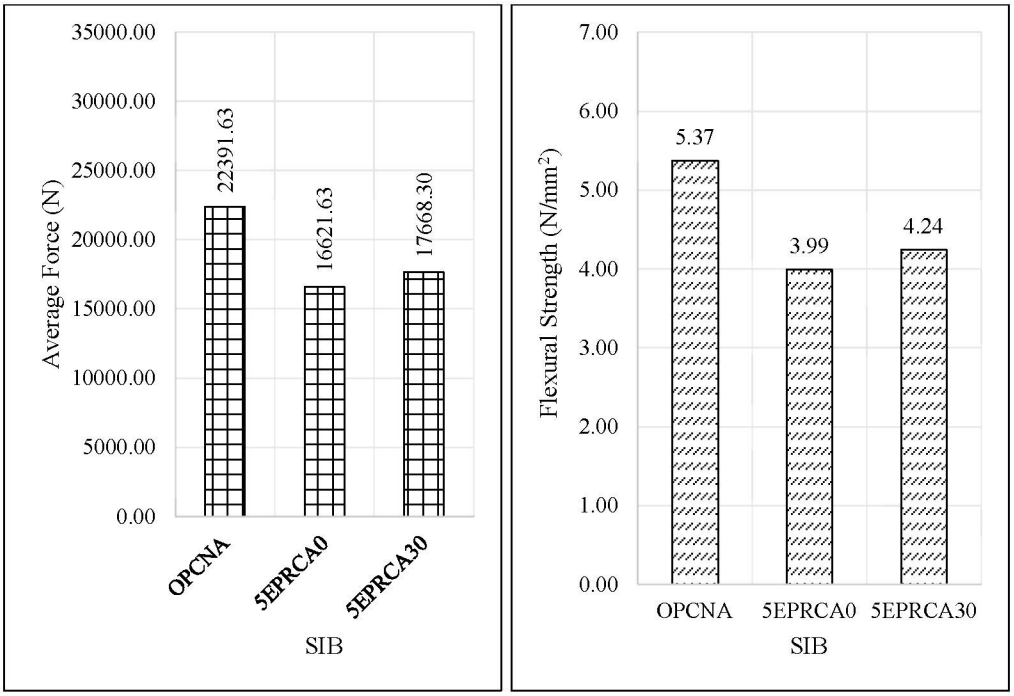

Figure 4.34 Flexural Results of SIB of 7 Days for All Mixtures

At 14 days (Figure 4.38), OPCNA continues to show the highest strength (24,715.17 N and 5.76 N/mm²), while 5EPRCA0 and 5EPRCA30 reach 17,168.43 N / 4.14 N/mm² and 19,000.20 N / 4.56 N/mm², respectively. The steady improvement of all mixtures is linked to the micro-filling effect of fine particles such as eggshell powder, which fills voids in the matrix and strengthens the block over time (Siddique & Kaur, 2011). In 5EPRCA30, the combination of recycled carbonated aggregates and eggshell powder improves particle packing, creating a denser structure that enhances flexural resistance (Poon et al., 2004).

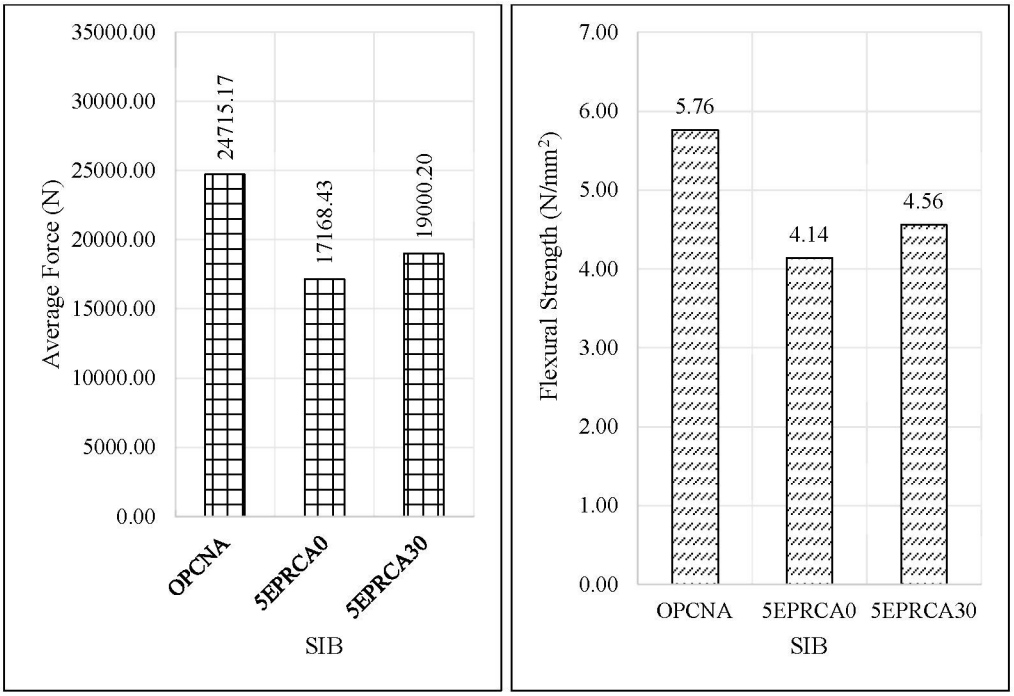

Figure 4.35 Flexural Results of SIB of 14 Days for All Mixtures

By 28 days of curing as illustrated in Figure 4.39, the differences between mixtures become more pronounced. OPCNA shows the highest performance, with an average force of 27,926.93 N and stress of 6.62 N/mm², indicating its superior durability and structural capacity. 5EPRCA30 follows with 21,507.80 N and 5.16 N/mm², showing a considerable improvement over 5EPRCA0, which records 19,260.83 N and 4.62 N/mm². The further strength increase in OPCNA is explained by the continued formation of C–S–H and the improved bonding between cement paste and aggregates, which reduces microcracks and enhances load distribution (Mehta & Monteiro, 2014). In 5EPRCA30, the combination of eggshell powder as a pozzolanic additive and treated recycled aggregates results in a denser matrix and better stress transfer, improving flexural capacity relative to 5EPRCA0 (Safiuddin et al., 2007).

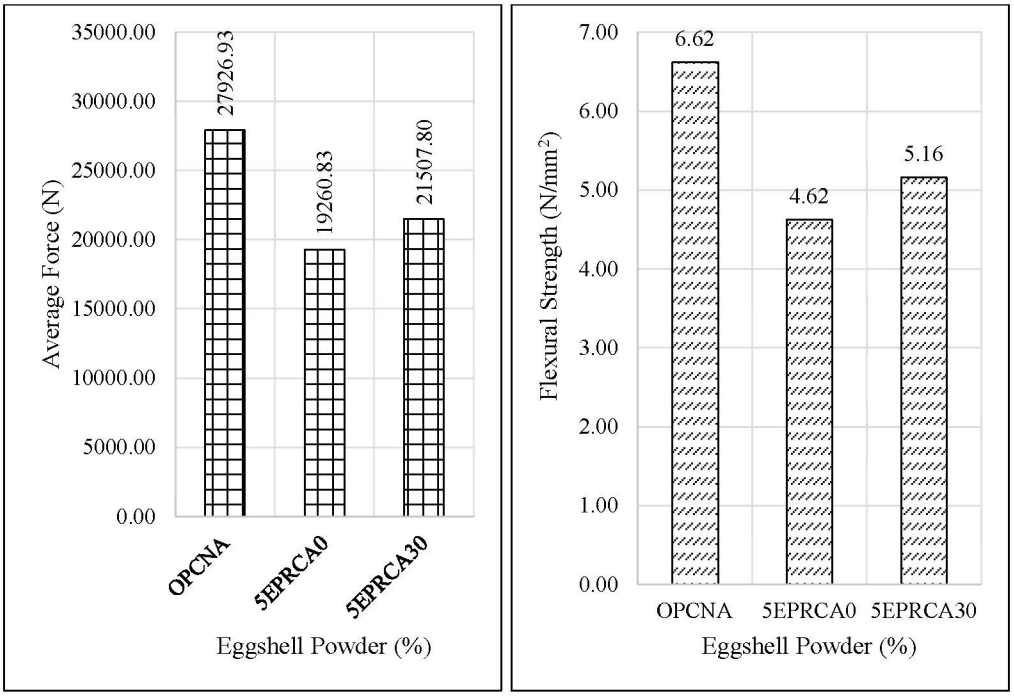

Figure 4.36 Flexural Results of SIB of 28 Days for All Mixtures

The flexural strength results for Solid Interlocking Blocks (SIB) using OPCNA shown in Figure 4.40 and Figure 4.41 very strong performance across all curing ages. At 7 days, the blocks already achieve a high average force of 22,391.63 N and stress of 5.373 N/mm², which reflects good early strength. By 14 days, the strength increases further to 24,715.17 N (force) and 5.764 N/mm² (stress), showing that the material continues to harden with time. At 28 days, the blocks reach their peak strength with 27,926.93 N and 6.622 N/mm², which indicates excellent durability and load resistance. This strong development is because natural aggregates bond tightly with cement paste, producing a dense and stable structure that gains more strength as hydration progresses (De Brito et al., 2016).

The flexural performance of SIBs made with 5EPRCA0 (5% eggshell powder and untreated recycled aggregates) shows a more moderate but steady improvement over curing time. At 7 days, the blocks record an average force of 16,621.63 N and stress of 3.989 N/mm², which is lower than OPCNA. By 14 days, the results increase slightly to 17,168.43 N and 4.142 N/mm², while at 28 days they reach 19,260.83 N and 4.623 N/mm². The gradual increase in strength suggests that eggshell powder contributes to strength gain through pozzolanic reaction, but the untreated recycled

aggregates reduce bonding quality due to cracks and old mortar (Poon et al., 2004). This explains why 5EPRCA0 improves with curing but still performs below OPCNA.

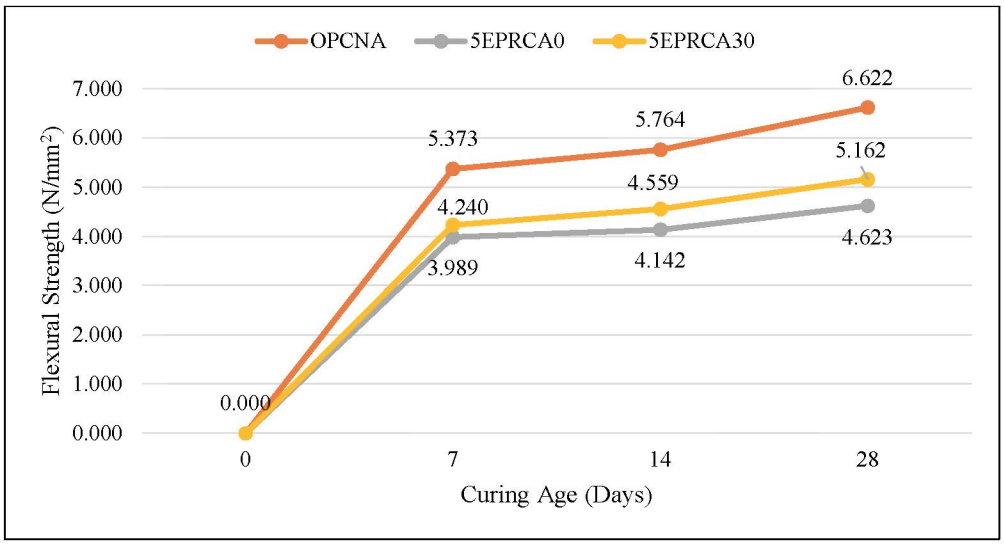

Figure 4.37 Flexural Strength (N/mm^2) of All Mixture for SIB

For SIBs made with 5EPRCA30 (5% eggshell powder with 30% recycled concrete aggregates), the strength development is more noticeable. At 7 days, the blocks achieve 17,668.30 N (force) and 4.240 N/mm² (stress), which is slightly better than 5EPRCA0. At 14 days, the performance rises to 19,000.20 N and 4.559 N/mm², showing stronger bonding. By 28 days, the blocks achieve a much higher result of 21,507.80 N and 5.162 N/mm², which approaches the strength of OPCNA. The improvement is because carbonation treatment of recycled aggregates reduces porosity and strengthens the old mortar layer, while eggshell powder continues to react with calcium hydroxide to form additional binding gels (Shi et al., 2021). This combination makes the microstructure denser and improves durability. At 28 days of curing, the SIB specimen was examined for flexural strength, as displayed in Figure 4.42.

Overall, the results show that OPCNA consistently provides the highest flexural strength because of its dense bonding and stable natural aggregates. However, 5EPRCA30 shows much better performance than 5EPRCA0, especially at 28 days, due to the positive effects of carbonation treatment and eggshell powder. This indicates that treated recycled aggregates combined with ESP can serve as a good alternative for sustainable construction, even though natural aggregates still perform best.

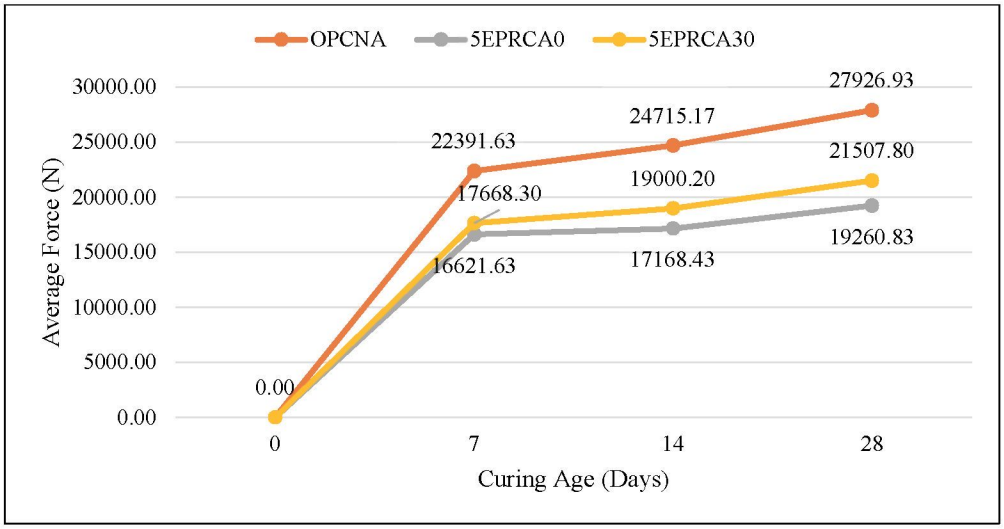

Figure 4.38 Average Force (N) of All Mixture for SIB

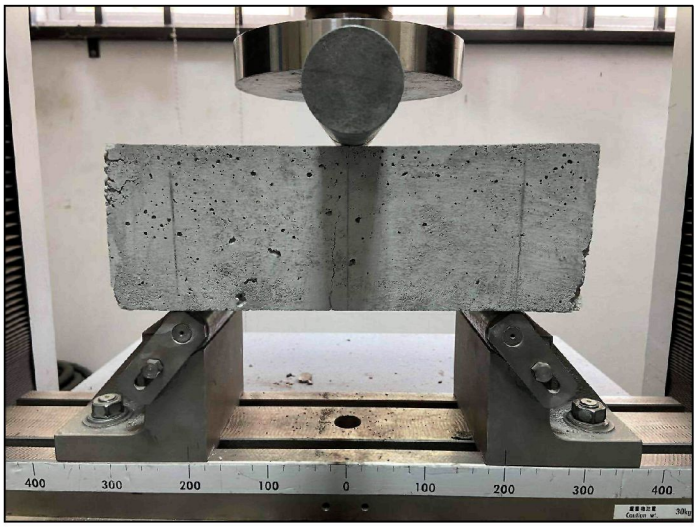

Figure 4.39 SIB 28 Days After Flexural Test

4.4.2 Single Inclined Connection Interlocking Block (SICIB)

Figure 4.43 at 7 days of curing, the flexural strength results show clear differences between the three mixtures. OPCNA starts with a stress of 2.83 N/mm², which sets a good baseline. The 5EPRCA0 mix is slightly weaker at 2.42 N/mm², likely because eggshell powder takes longer to react and strengthen the mix. In contrast, 5EPRCA30 performs best at this stage with 3.13 N/mm², possibly due to the rough surface of recycled concrete aggregate (RCA), which helps the cement paste grip better. According to Chai et al. (2023), RCA's texture improves early bonding, and when

combined with ESP, it can boost initial strength.

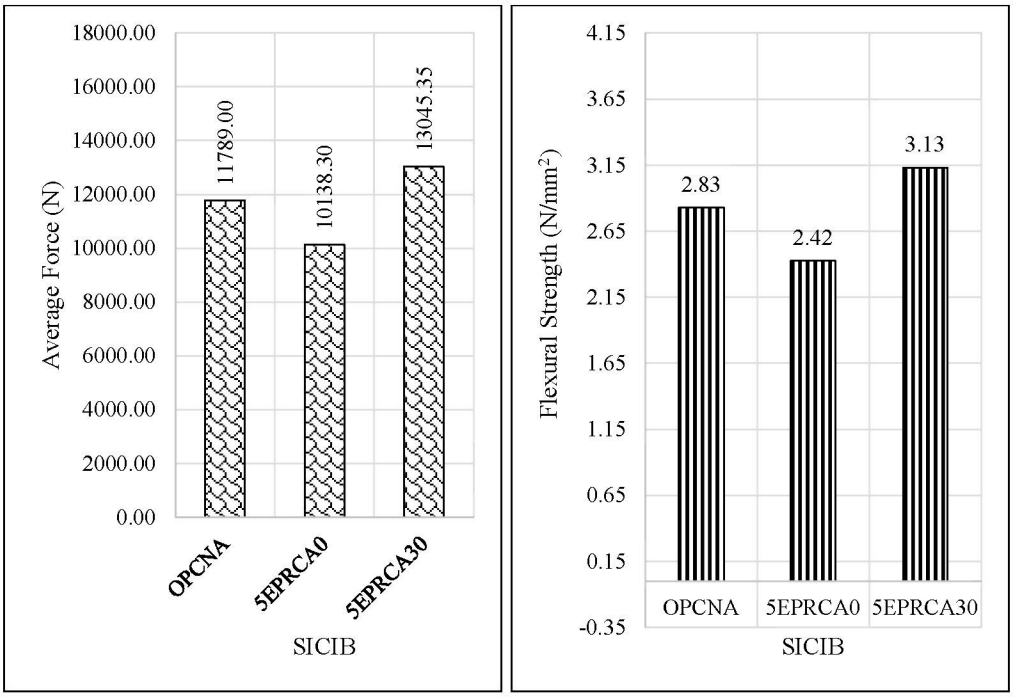

Figure 4.40 Flexural Results of SICIB of 7 Days for All Mixtures

By 14 days, all mixtures show improvement in Figure 4.44, but 5EPRCA30 continues to lead. OPCNA reaches 2.98 N/mm², and 5EPRCA0 follows closely at 2.94 N/mm², showing that the eggshell powder is starting to contribute to strength. The 5EPRCA30 mix jumps to 3.59 N/mm², suggesting that the combination of ESP and RCA is working well. This may be because ESP begins to fill gaps and strengthen the mix, while RCA provides a solid framework. Noor et al. (2022) found that combining recycled materials with reactive powders can improve flexural strength if the mix is balanced and well-cured.

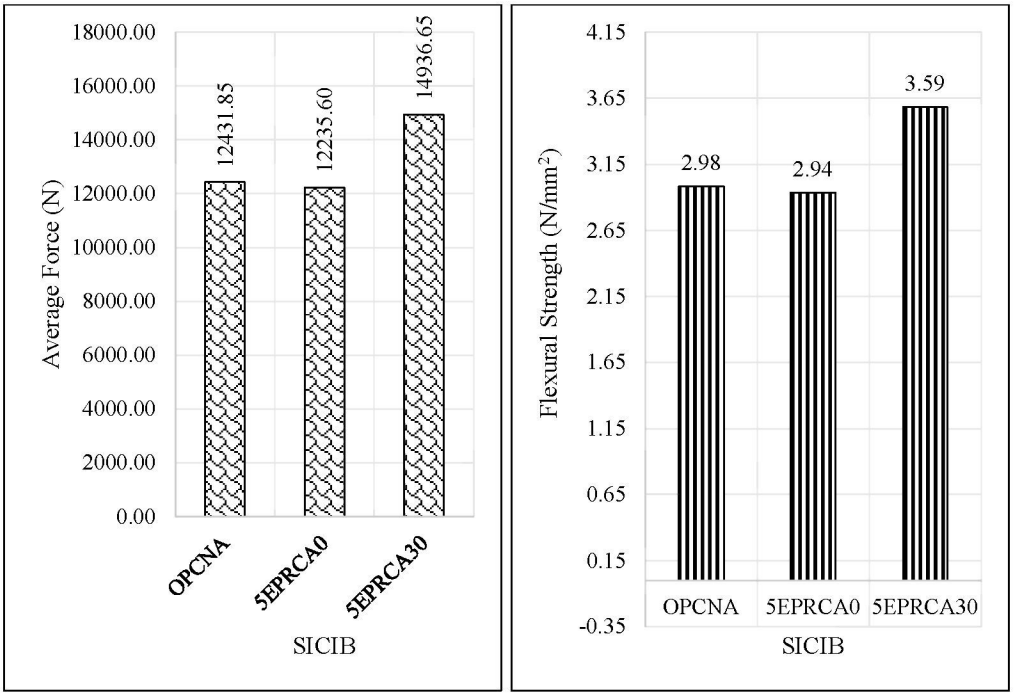

Figure 4.41 Flexural Results of SICIB of 14 Days for All Mixtures

At 28 days, the results show in Figure 4.45, that both OPCNA and 5EPRCA30 reach high strength levels. OPCNA records 4.10 N/mm², while 5EPRCA30 slightly surpasses it at 4.12 N/mm², showing that RCA and ESP can match or even outperform traditional materials when given enough curing time. The 5EPRCA0 mix also improves to 3.91 N/mm², confirming that ESP continues to strengthen the mix over time. Yeo & Rahman (2024) explained that longer curing allows alternative binders like ESP to fully activate, improving the material's ability to resist bending and cracking.

Overall, the results show that curing time plays a major role in improving flexural strength. OPCNA performs well due to complete cement hydration, while 5EPRCA0 gains strength as ESP reacts and fills voids. The 5EPRCA30 mix performs best overall, especially in early and mid curing stages, because RCA's texture helps with bonding and ESP adds long-term strength. These findings support the idea that using recycled materials and alternative binders can create strong, sustainable concrete when the mix is properly designed and cured.

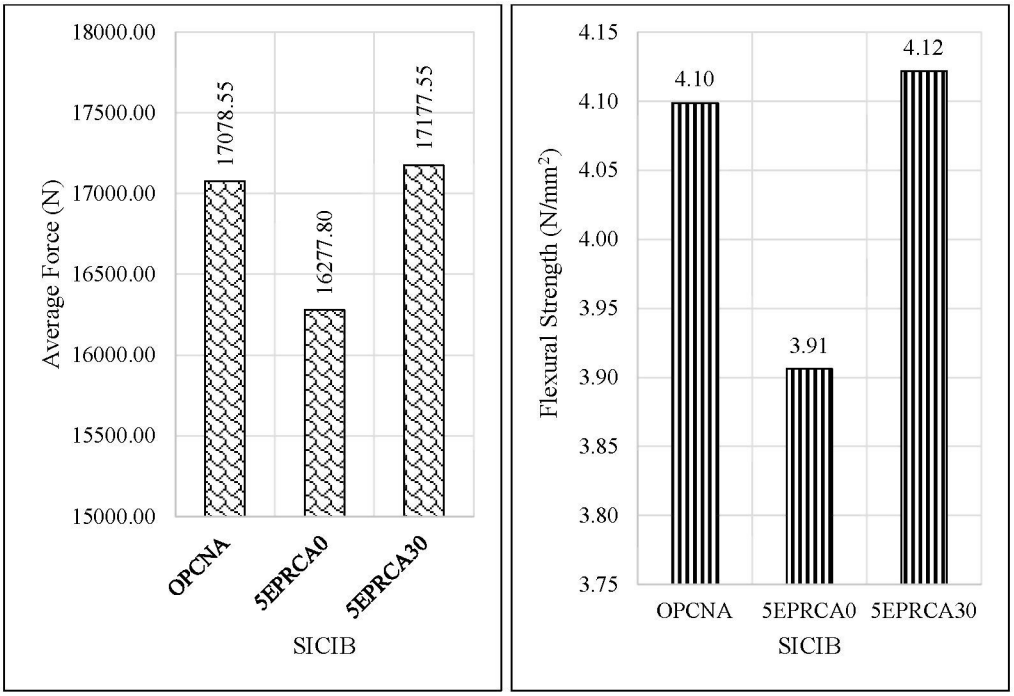

Figure 4.42 Flexural Results of SICIB of 28 Days for All Mixtures

The flexural strength of the Single Inclined Connection Interlocking Block (SICIB) made with Ordinary Portland Cement and Natural Aggregate (OPCNA) shows steady improvement as curing time increases. Figure 4.46 and Figure 4.47 at 7 days, the average stress is 2.828 N/mm², which is relatively low due to incomplete cement hydration. As the cement continues to react with water, more binding compounds form, strengthening the material. By 14 days, the stress rises slightly to 2.984 N/mm², indicating better internal bonding. At 28 days, the strength increases significantly to 4.099 N/mm², showing that the material has reached a more complete and dense structure. This trend supports findings by Zhang et al. (2022) and Kumar & Singh (2024), who emphasized that longer curing allows concrete to develop full strength through complete hydration and reduced porosity.

For SICIB using 5% eggshell powder and no recycled aggregate (5EPRCA0), the flexural strength also improves over time, though it starts lower than OPCNA. At 7 days, the stress is 2.425 N/mm², likely because eggshell powder reacts more slowly than cement. Hassan et al. (2023) explained that eggshell powder has a delayed pozzolanic effect, meaning it takes time to contribute to strength. By 14 days, the stress increases to 2.937 N/mm² as the ESP begins to fill gaps and strengthen the mix. At 28 days, the stress reaches 3.906 N/mm², showing that the ESP has fully activated and helped create

a denser structure. Lim & Goh (2024) noted that extended curing allows alternative binders like ESP to improve mechanical performance by forming additional bonding compounds.

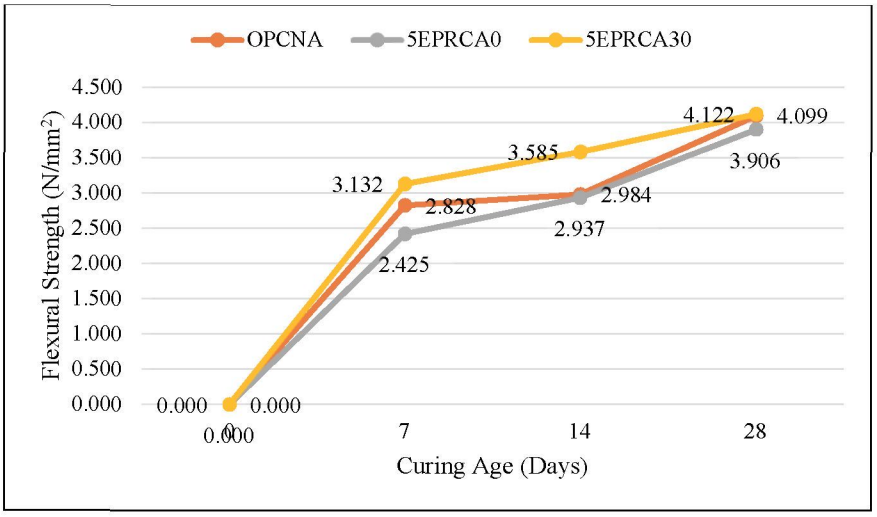

Figure 4.43 Flexural Strength (N/mm^2) of All Mixture for SICIB

The SICIB made with 5% ESP and 30% recycled concrete aggregate (5EPRCA30) shows in Figure 4.47 the highest initial strength among all mixtures. At 7 days, the stress is already 3.132 N/mm², which may be due to the rough surface of RCA that improves early bonding. Chai et al. (2023) found that RCA's texture enhances mechanical interlock, helping the cement paste grip better. By 14 days, the stress increases to 3.585 N/mm², showing that the combination of ESP and RCA continues to strengthen the mix. At 28 days, the stress reaches 4.122 N/mm², the highest among all samples. This confirms that the synergy between ESP and RCA works well over time, with ESP contributing to long-term strength and RCA providing a solid framework. Yeo & Rahman (2024) highlighted that optimized mixes using RCA and reactive powders can match or exceed conventional concrete strength when properly cured.

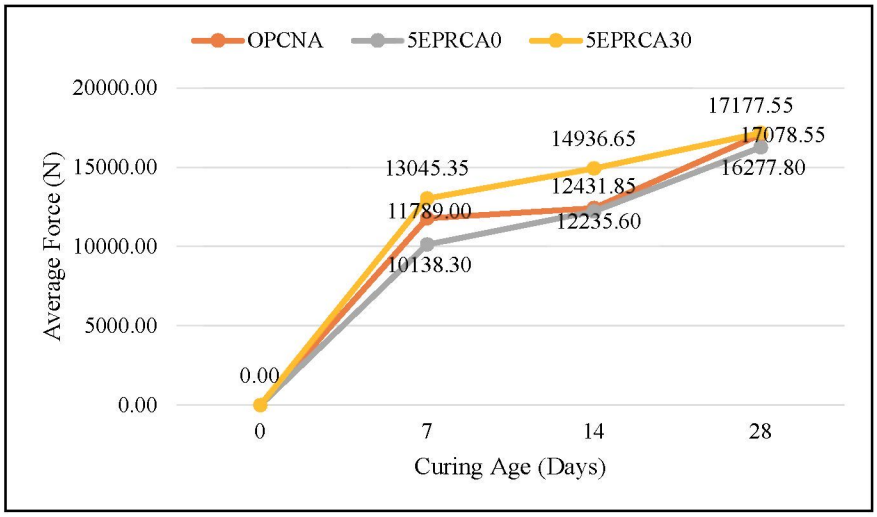

Figure 4.44 Average Force (N) of All Mixture for SICIB

On balance and collectively, all the three mixtures have evidently increased flexural strength with increasing curing. OPCNA enjoys a full hydration of cement whereas 5EPRCA0 derives strength because the ESP develops and fills up the mix. The 5EPRCA30 blend is the most effective because of the combined synergi s of both the texture and the pozzolanic reaction of RCA and ESP. These outcomes emphasise the need of a correct curing time and mix design in the development of robust and strong interlocking blocks. The results are in line with the emerging literature that focus the use of alternative materials and appropriately cured material, which would improve the structural performance under sustainable construction. Figure 4.48 illustrates the SICIB specimen under testing to measure its flexural strength at 28 days.

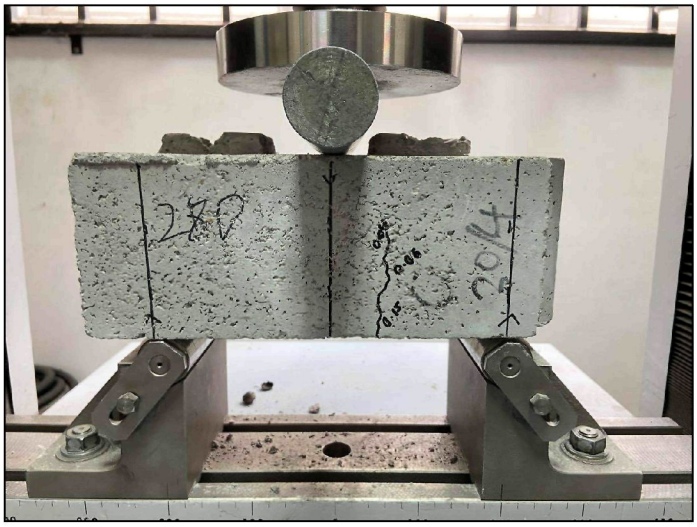

Figure 4.45 SICIB 28 Days After Flexural Test

4.4.3 Dual Tongue Inclined Interlocking Block (DTIIB)

Compared to Dual Tongue Inclined Interlocking Blocks (DTIIB) in flexural results in Figure 4.49 the addition of eggshell powder (ESP) after a curing period of 7 days depicts visible improvement. The average force and stress on OPCNA are 8,754.35 N, and 2.10 N/mm² which is the baseline strength. The 5EPRCA0 mixture is moderately better with 9,768.45 N and 2.39 N/mm²; ESP improves the early age strength. The 5EPRCA30 mix has a higher value than the other two, and it is 10,642.13 N and 2.61 N/mm, implying that combination of recycled pre carbonated ash and ESP improves early flexural performance. This is likely because of the improved particle packing and the decline of the interstice that provides a boost in the bending strength of blocks (Rashad, 2017).

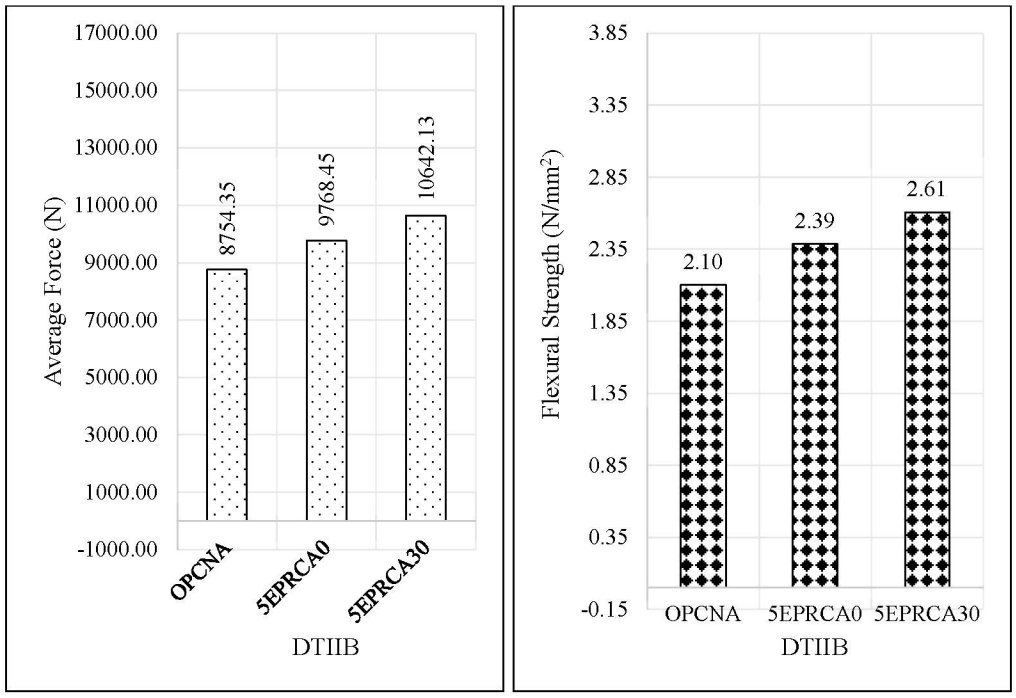

Figure 4.46 Flexural Results of DTIIB of 7 Days for All Mixtures

By 14 days of curing (see Figure 4.50), OPCNA maintains the greatest average force of 13,957.05 N and stress of 3.35 N/mm² indicating its good development strength. The mixture 5EPRCA0 achieves 11,724.70 N and 2.82 N/mm², which is stable and 5EPRCA30 is higher by only a few percent, namely 12,347.25 N/mm² and 2.91 N/mm². Such slowed but steady growth in these mixings can be explained by constant

hydration reactions and filling effect of ESP particles that assist in the elimination of microvoids and solidified the block structure (Muthu et al., 2019).

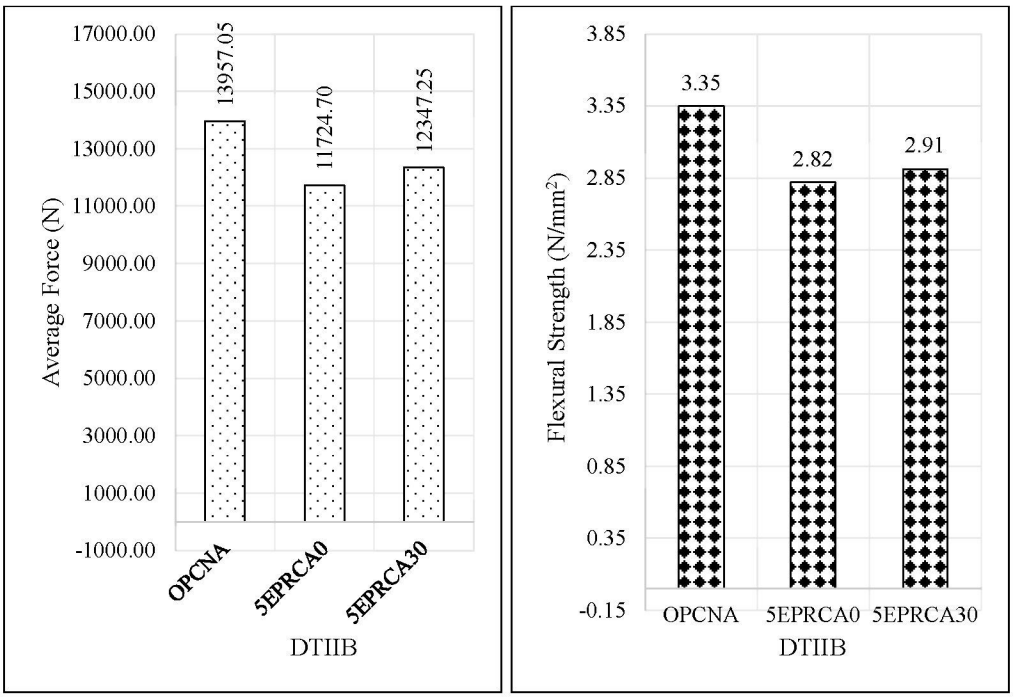

Figure 4.47 Flexural Results of DTIIB of 14 Days for All Mixtures

Figure 4.51 by 28 days, OPCNA achieves the highest flexural performance with 16,327.05 N and 3.81 N/mm². The 5EPRCA30 mixture nearly matches this with 16,232.30 N and 3.80 N/mm², showing that it can perform almost as well as OPCNA at later stages. Meanwhile, 5EPRCA0 reaches 14,820.75 N and 3.54 N/mm², slightly lower than the other two. The strong performance of 5EPRCA30 at this stage can be explained by the densification of the matrix from carbonation of the recycled ash and the pozzolanic reaction of ESP, which together reduce porosity and enhance the material's flexural capacity (Jin et al., 2020).

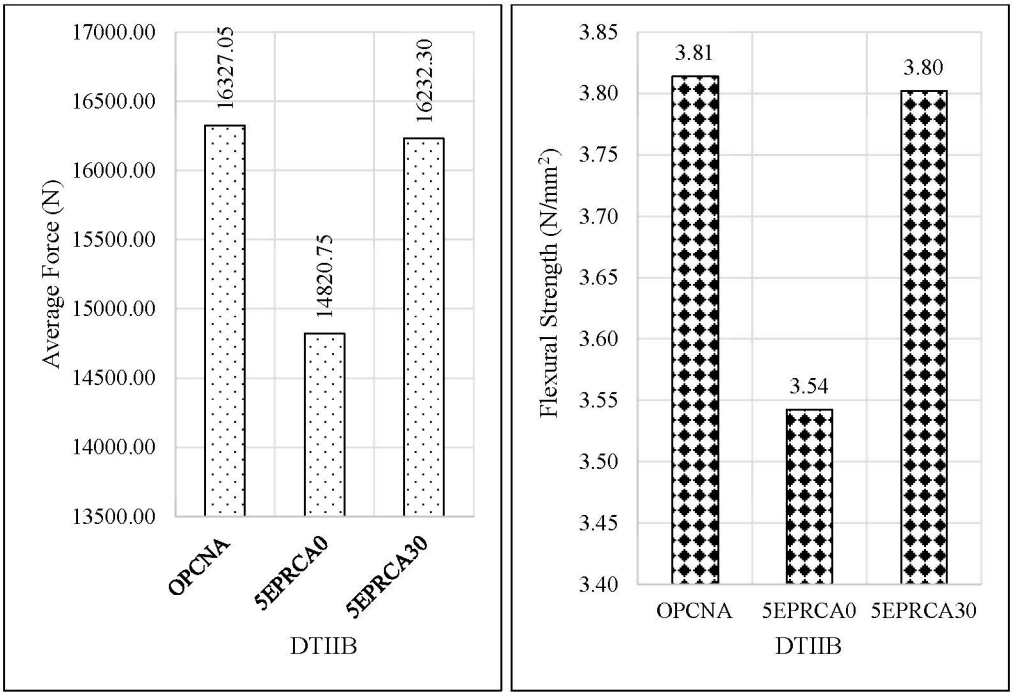

Figure 4.48 Flexural Results of DTIIB of 28 Days for All Mixtures

The flexural results for Dual Tongue Inclined Interlocking Blocks (DTIIB) made with OPCNA show a steady rise in strength as curing progresses (Figure 4.52). At 7 days, the average stress is 2.101 N/mm² with a force of 8,754.35 N, which indicates that the blocks are still in the early stage of strength development. By 14 days, the strength improves sharply to 3.350 N/mm² (stress) and 13,957.05 N (force), showing that the material becomes much stronger as hydration continues. At 28 days, the strength reaches 3.814 N/mm² and 16,327.05 N, confirming that the blocks continue to gain durability and resistance over time. This steady growth is linked to ongoing cement hydration, which produces more calcium silicate hydrate (C–S–H) gel that strengthens the matrix (Neville, 2011).

The flexural results for DTIIB with 5EPRCA0 (5% eggshell powder and untreated recycled aggregates) also show continuous improvement with curing. At 7 days, the blocks achieve 2.386 N/mm² (stress) and 9,768.45 N (force), reflecting moderate early performance. At 14 days, strength increases to 2.822 N/mm² and 11,724.70 N, showing better material bonding. By 28 days, the results reach 3.543 N/mm² and 14,820.75 N, which highlights a significant improvement in flexural capacity. The steady growth is because eggshell powder provides additional calcium that slowly reacts to form extra binding material, while hydration continues

strengthening the paste (Zhang & Islam, 2012). However, untreated recycled aggregates reduce early strength due to higher porosity and cracks, which explains why results are lower than OPCNA (Kou & Poon, 2012).

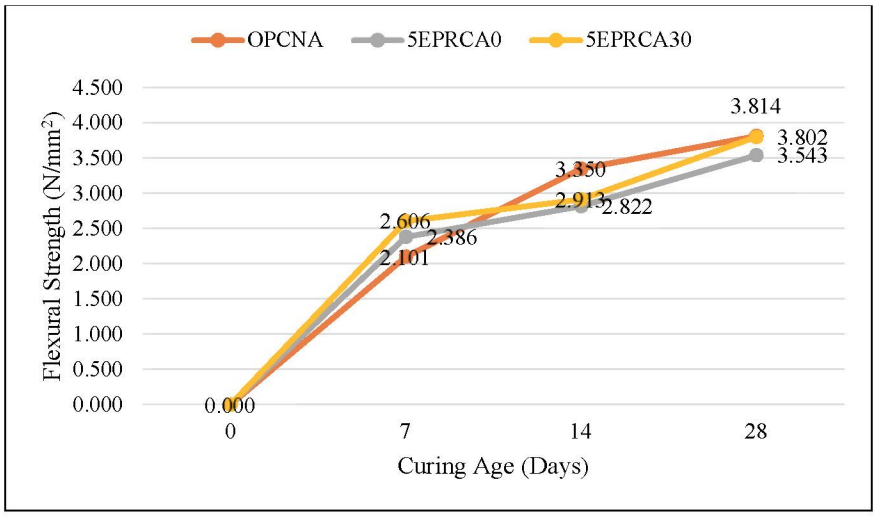

Figure 4.49 Flexural Strength (N/mm^2) of All Mixture for DTIIB

For DTIIB with 5EPRCA30 (5% eggshell powder and 30% pre-carbonated recycled aggregates), the results show notable improvements, especially at later ages. Figure 4.53 at 7 days, the blocks achieve 2.606 N/mm² and 10,642.13 N, which indicates relatively strong early performance. At 14 days, strength rises to 2.913 N/mm² and 12,347.25 N, showing improved durability. By 28 days, the blocks perform even better with 3.802 N/mm² and 16,232.30 N, which is close to the OPCNA strength. The stronger performance is explained by the carbonation treatment of recycled aggregates, which reduces porosity and improves interfacial bonding with cement paste (Tam et al., 2007). Combined with the pozzolanic effect of eggshell powder, this produces a denser and more durable structure (Muthusamy et al., 2020).

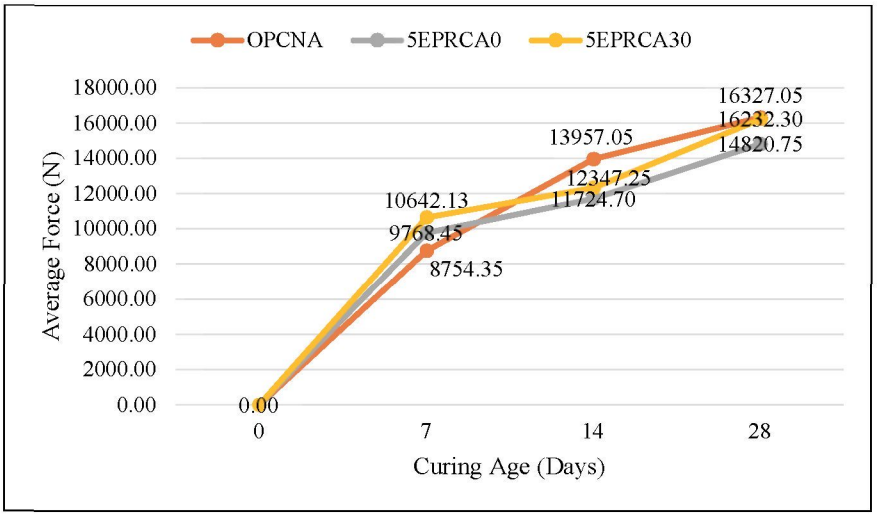

Figure 4.50 Average Force (N) of All Mixture for DTIIB

Overall, the results highlight that OPCNA provides the highest and most consistent strength, but 5EPRCA30 shows competitive results at 28 days because the treatment of recycled aggregates significantly enhances their quality. Meanwhile, 5EPRCA0 performs lower than the other mixes, but still demonstrates steady strength gain over time. This confirms that using treated recycled aggregates with eggshell powder can be a good sustainable option while still maintaining acceptable structural performance. The DTIIB specimen subjected to flexural strength testing at 28 days of curing is shown in Figure 4.54.

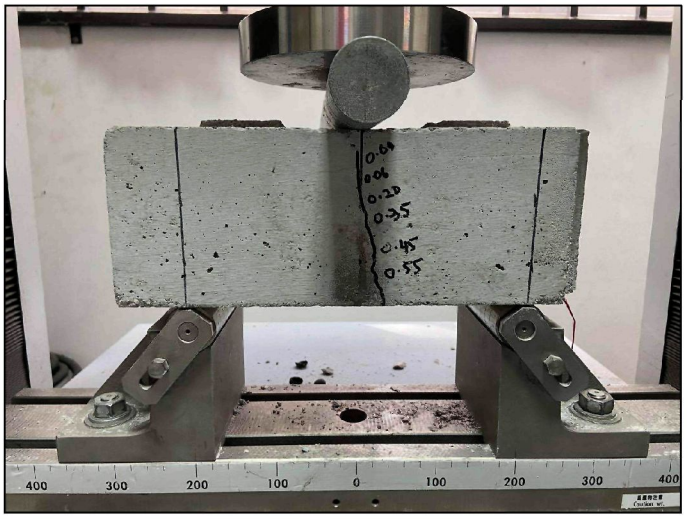

Figure 4.51 DTIIB 28 Days After Flexural Test

4.4.4 Comparison Interlocking Block Design

After 7 days of curing, the flexural behaviour of the Interlocking Block (IB) differences significantly with respect to the mixture and block type (Figure 4.55). In the case of Solid Interlocking Blocks (SIB), OPCNA yields the maximum number of forces, 22,391.63 N, and stress, 5.37 N/mm² which shows high levels of strength in the early stages. This can be attributed to the high performance probably because it is made up of dense and uniform particle arrangement that makes the block resist bending and enhances its early loading capability (Alhozaimy et al., 2020). The result of the 5EPRCA30 mixture in Single Inclined Connection Interlocking Blocks (SICIB) is best, i.e., 13,045.35 N and 3.13 N/mm² indicates the combination of recycled ash and eggshell powder (ESP) mixtures resulting in improvement of early structural rigidity due to the reduction of internal voids and high packing efficiency of particles (Shah et al., 2019). On the same note, 5EPRCA30 continues to outperform both OPCNA in 5EPRCA30 (Dual Tongue Inclined Interlocking Blocks (DTIIB), where 5EPRCA30 yields a force of 10,642.13 N and stress of 2.61 N/mm², whereas OPCNA in 5EPRCA30 provides a force of 8,754.35 N and stress of 2.10 N/mm². These implications show that early flexural strength could be enhanced with ESP, even with pre carbonated ash, to fill microvoids as well as to distribute more nucleation sites to the hydration products (Rashad, 2017). In general, OPCNA is a more suitable selection in SIB and 5EPRCA30 better in SICIB and DTIIB at this early stage.

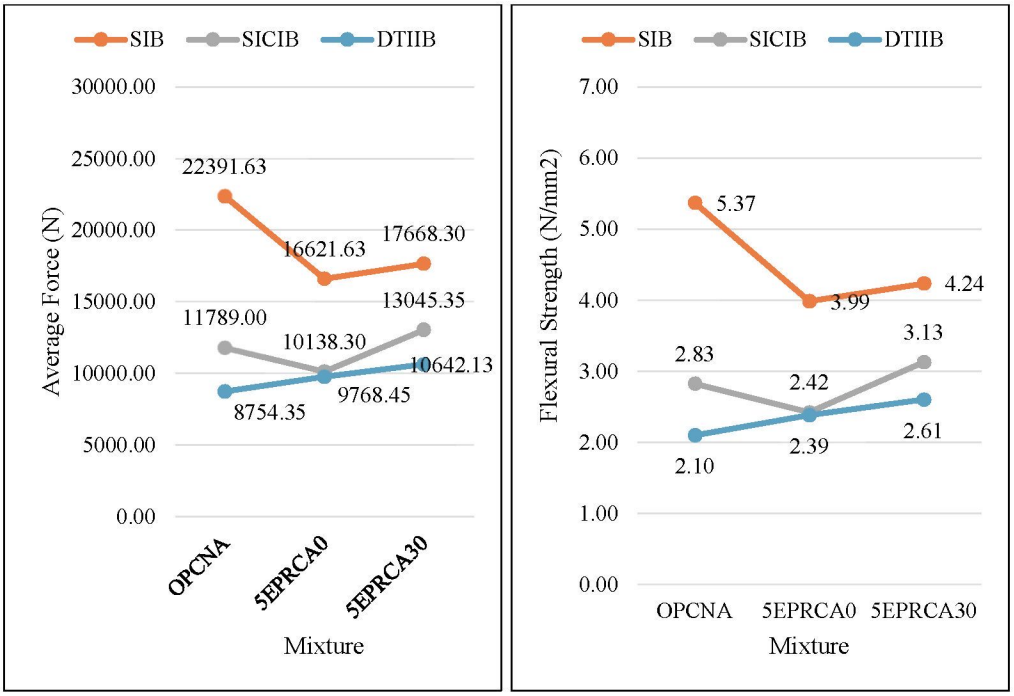

Figure 4.52 Comparison Flexural Results of IB of 7 Days for All Mixtures

At 14 days of curing (Figure 4.56), the flexural results show a clear development trend. In SIB, OPCNA continues to lead with a force of 24,715.17 N and stress of 5.76 N/mm², maintaining its top performance due to its stable matrix and low porosity (Muthu et al., 2019). For SICIB, 5EPRCA30 achieves the highest stress of 3.59 N/mm², with a force of 13,825.00 N, suggesting that the combined effect of ESP promotes gradual hardening and densification of the block structure, enhancing bending resistance (Jin et al., 2020). In DTIIB, OPCNA has the highest force of 13,957.05 N and stress of 3.35 N/mm², though 5EPRCA30 closely follows, indicating that recycled ash and ESP can provide competitive strength development over time. These results show that while OPCNA maintains an advantage in SIB and DTIIB, 5EPRCA30 consistently improves flexural performance in blocks with inclined designs.

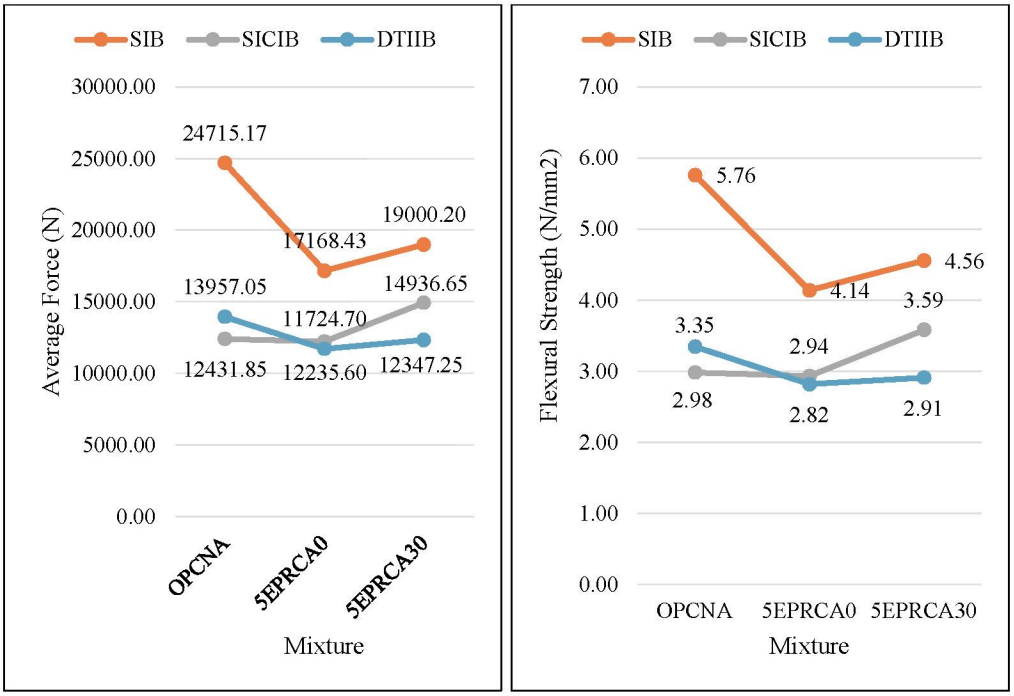

Figure 4.53 Comparison Flexural Results of IB of 14 Days for All Mixtures

The variation between mixtures is increased by 28 days of curing (Figure 4.57). OPCNA remains superior as illustrated in SIB, 27,926.93 N and 6.62 N/mm² with high rates of durability and bending resistance because of its small structure and homogynous composition (Alhozaimy et al., 2020). Having shown the highest force of 17,177.55 N and stress of 4.12 N/mm², 5EPRCA30 surpasses OPCNA and 5EPRCA0 in SICIB in the short term, and it shows the long-term advantages of pre-carbonated ash and ESP because of the ability to fill and voids as well as enhance cohesion in the particles (Shah et al., 2019). In the case of DTIIB, the OPCNA yields the highest force 16,327.05 N and stress 3.81 N/mm² whereas 5EPRCA30 follows closely revealing that the recycled ash mixture can attain similar strength as the curing time advances. In general, these results indicate that OPCNA is the most likely to perform well in SIB or DTIIB whereas 5EPRCA30 flexural performance is better in SICIB, both affected by the mixture formation and shape of blocks exposed to the induction of strength development.

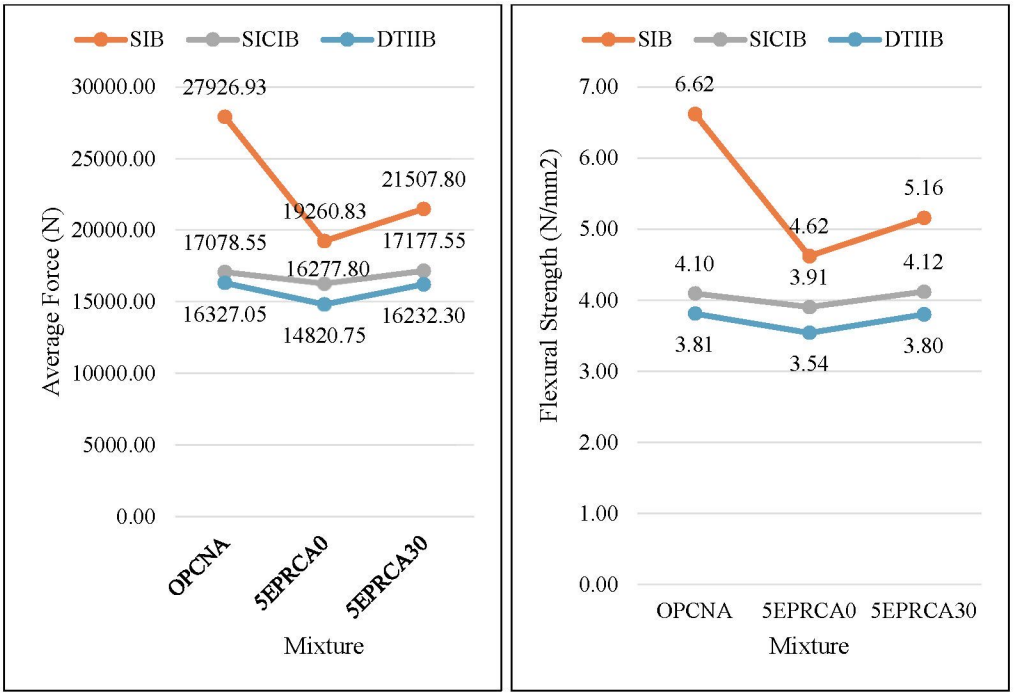

Figure 4.54 Comparison Flexural Results of IB of 28 Days for All Mixtures

4.4.4.1 Comparison Each of SIB and SICIB

Figures 4.58 and Figure 4.59 present the summary of comparison Solid Interlocking Blocks (SIB) and Single Inclined Connection Interlocking Blocks (SICIB) test results, showing the average force and flexural strength, respectively. SICIB exhibit a different flexural performance at 7 days of curing when compared to SIB and mixture. In SIB, the OPCNA provides the greatest strength having a force of 22,391.63 N and the stress of 5.37 N/mm². This shows that the SIB manufactured using OPCNA has a greater early load capacity, possibly due to a more compact packing of particles eliminating internal pores and compressing this cement against bending (Patel & Shah, 2021). Comparatively, on the case of SICIB, OPCNA has the lowest results by a substantial measure of 11,789.00 N and 2.83 N/mm² based stress. In this case, the combination of eggshell powder (ESP) and pre-carbonated ash increases the early flexural modulus to 13,045.35 N and 3.13 N/mm² in 5EPRCA30, indicating that 5EPRCA30 exhibits the greatest force and stress and could fully develop the combination effect mentioned earlier (Li et al., 2020). It means that OPCNA is more applicable to SIB and 5EPRCA30 is efficient in SICIB at low curing ages.

Flexural values present differences between the block type and combination at the curing age of 14 days. SIB works the best again and OPCNA shows a steady increase in strength, as the material settles over time with 24,715.17 N and 5.76 N/mm² (Gajera et al., 2022). OPCNA is the underperforming one in SICIB showing 12, 431.85 N and 2.98 N/mm². In the meantime, 5EPRCA30 advances to 14,936.65 N and 3.59 N/mm², indicating that the mixture is also advantaged by the further interaction of ESP and the stabilization effect of pre-carbonated ash, mitigates micro-cracks and makes the block stronger when subjected to bending loads (Ahmed et al., 2021). This indicates that the performance is influenced considerably with mixture composition and this is based on the type of block.

At 28 days, SIB and SICIB are still differing in the trend of performance. In the case of SIB, the maximum values of force are OPCNA 27,926.93 N and stress 6.62 N/mm², which further proves its higher resistance and carrying capacity in terms of compact matrix formation and porosity (Patel & Shah, 2021). The SIB reaches 21,507.80 N and 5.16 N/mm² with the 5EPRCA30 mixture, which is currently quite higher compared to 5EPRCA0, and more impressive after 5EPRCA0, it indicates the effectiveness of ESP in the long-term of the SIB to avoid the voids occurrence and increase block stiffness (Li et al., 2020). In SICIB, 5EPRCA30 is marginally better than OPCNA by 17,177.55 N and 4.12 N/mm² against 17, 078.55 N and 4.10 N/mm² of OPCNA. This indicates 5EPRCA30 has the potential to become competitive by the inclined block designs, probably because it has better particle packing and microstructure (Ahmed et al., 2021).

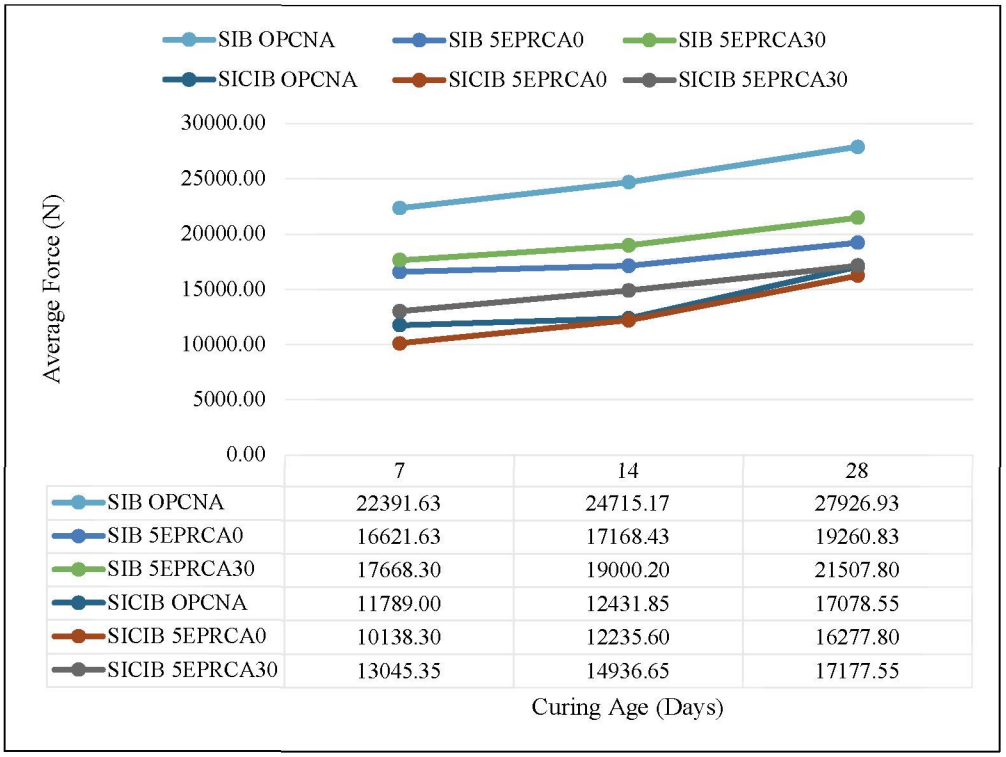

	7	14	28
SIB OPCNA	22391.63	24715.17	27926.93
SIB 5EPRCA0	16621.63	17168.43	19260.83
SIB 5EPRCA30	17668.30	19000.20	21507.80
SICIB OPCNA	11789.00	12431.85	17078.55
SICIB 5EPRCA0	10138.30	12235.60	16277.80
SICIB 5EPRCA30	13045.35	14936.65	17177.55

Figure 4.55 Comparison Average Force (N) Results for SIB and SICIB

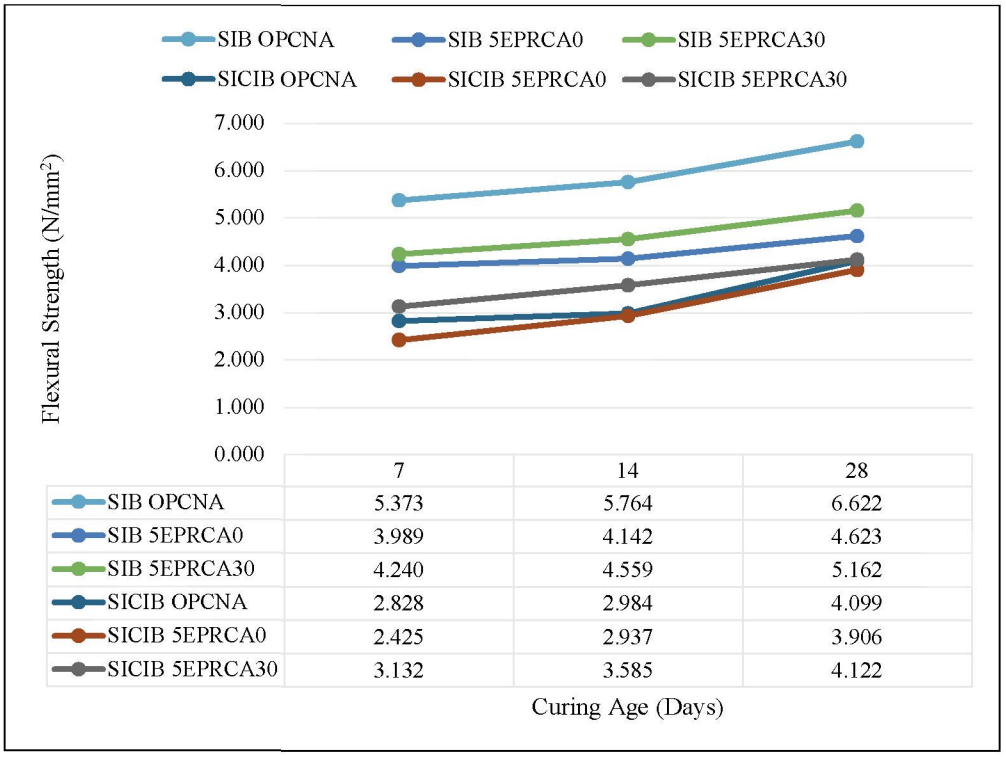

	7	14	28
SIB OPCNA	5.373	5.764	6.622
SIB 5EPRCA0	3.989	4.142	4.623
SIB 5EPRCA30	4.240	4.559	5.162
SICIB OPCNA	2.828	2.984	4.099
SICIB 5EPRCA0	2.425	2.937	3.906
SICIB 5EPRCA30	3.132	3.585	4.122

Figure 4.56 Comparison Flexural Strength (N/mm^2) Results for SIB and SICIB

In general, comparing SIB and SICIB regarding all mixes and curing ages reveals that SIB is always stronger in flexion strength and OPCNA was the best in all cases. SICIB exhibits poor early strength, but gains 5EPRCA30 with time, and the performance level becomes comparable. This brings out that the design of block and mixture composition is very crucial to flexural behaviour and durability.

4.4.4.2 Comparison of SIB and DTIIB

The comparison Solid Interlocking Blocks (SIB) and Dual Tongue Inclined Interlocking Blocks (DTIIB) results are summarized in Figures 4.60 and Figure 4.61, which display the average force and flexural strength. With 7 days of curing the flexural behaviour of SIB and DTIIB is distinctly different according to the mixture. In case of SIB, OPCNA attains the greatest strength with its force and stress of 22,391.63 N and 5.37 N/mm, respectively, indicating that this mixture will support greater loads at an initial stage. This higher early performance can be true because its particle arrangement is denser and can reduce the pores that can make the block resist bending better (Patel & Shah, 2021). Conversely, DTIIB does not show such good values, and OPCNA does it only up to 8,754.35 N, 2.10 N/mm², as the geometry of the block can play a role in the dispersion of stress under flexural pressure (Li et al., 2020). In DTIIB, 5EPRCA30 has a better behaviour in comparison to 5EPRCA0, which shows that the combination of the eggshell powder and pre-carbonated ash improves particle bonding and the whole structure stability even in more intricate block shapes (Ahmed et al., 2021).

However, after 14 days of curing, SIB still showed higher results as compared to DTIIB. OPCNA attains the peak 24,715.17 N and 5.76 N/mm² SIB as validating its high strength load bearing capacity with time. DTIIB cultured in OPCNA yields 13,957.05 N and 3.35 N/mm². The trend of greater improvement in 5EPRCA30 mixture is seen in DTIIB where this mixture experiences more significant force and stress when compared to 5EPRCA0, possibly because of filler effect by ESP and ash particles which decreases micro-voids and improves inter-particles internal friction (Gajera et al., 2022). These findings imply that OPCNA is more resistant in the simple SIB designs whereas 5EPRCA30 exhibits greater resistance in length, and width in complex block forms.

At the 28th day the trend persists. Highest flexural strength is seen through SIB where OPCNA can reach 27,926.93 N and 6.62 N/mm2 and 5EPRCA30 scores 21,507.80 N and 5.16 N/mm² that indicate improvements in mix long-term consolidation and due to fewer micro-voids (Li et al., 2020). In DTIIB, OPCNA attains 16,327.05 N and 3.81 N/mm² and, 5EPRCA30 is marginally better than 5EPRCA0 with 16232.30 N and 3.80 N/mm². The fact that ESP and RCA contribute to DTIIB strengthening over time, particularly in multilateral block geometries, where stresses are less symmetrical (Ahmed et al., 2021), indicates that this is the case.

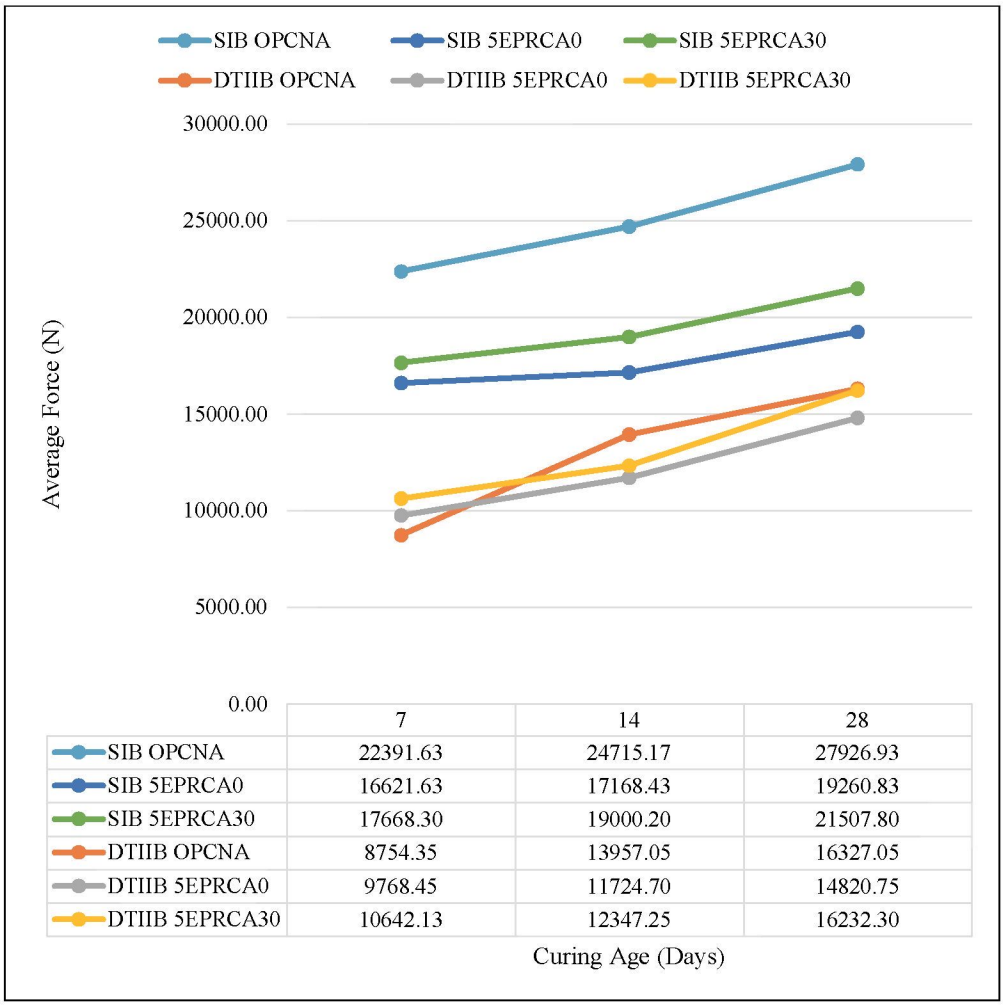

	7	14	28
SIB OPCNA	22391.63	24715.17	27926.93
SIB 5EPRCA0	16621.63	17168.43	19260.83
SIB 5EPRCA30	17668.30	19000.20	21507.80
DTIIB OPCNA	8754.35	13957.05	16327.05
DTIIB 5EPRCA0	9768.45	11724.70	14820.75
DTIIB 5EPRCA30	10642.13	12347.25	16232.30

Figure 4.57 Comparison Average Force (N) Results for SIB and DTIIB

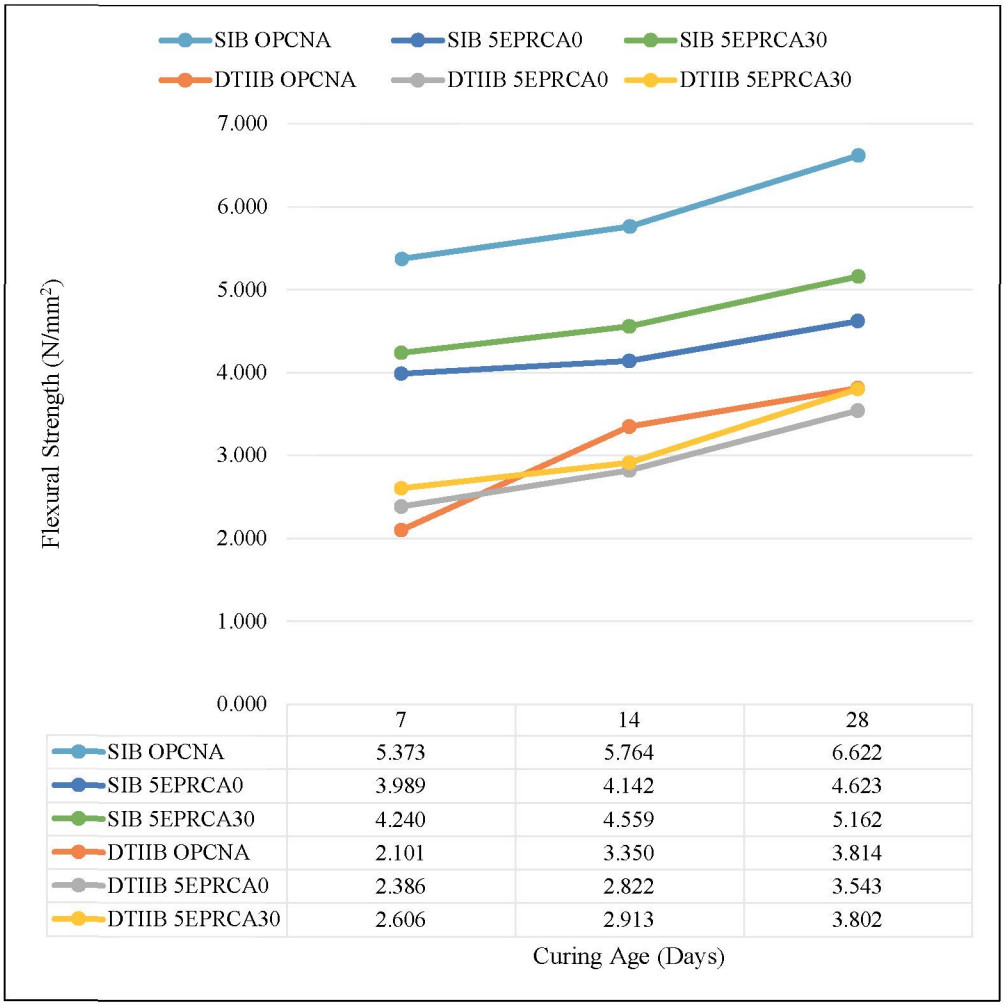

	7	14	28
SIB OPCNA	5.373	5.764	6.622
SIB 5EPRCA0	3.989	4.142	4.623
SIB 5EPRCA30	4.240	4.559	5.162
DTIIB OPCNA	2.101	3.350	3.814
DTIIB 5EPRCA0	2.386	2.822	3.543
DTIIB 5EPRCA30	2.606	2.913	3.802

Figure 4.58 Comparison Flexural Strength (N/mm²) Results for SIB and DTIIB

In general, the analysis of the SIB and DTIIB in mixtures and curing times indicates that SIB has maintained high flexural strength in each mixture and curing time proving higher structural strength. OPCNA maintains the highest performance in SIB because of its dense mix and reduced porosity, but 5EPRCA30 gives more even performance in both SIB and DTIIB, especially with greater geometric complexity blocks.

4.4.4.3 Comparison of SICIB and DTIIB

Figures 4.62 and Figures 4.63 provide a summary of the comparison Single Inclined Connection Interlocking Blocks (SICIB) and Dual Tongue Inclined Interlocking Blocks (DTIIB) test findings, highlighting the average force and flexural

strength. At 7 days of curing, the SICIB generally show higher flexural strength than the DTIIB across all mixtures. For example, OPCNA achieves 11,789.00 N and 2.83 N/mm² in SICIB, which is significantly higher than 8,754.35 N and 2.10 N/mm² in DTIIB. Similarly, 5EPRCA30 performs better in SICIB (13,045.35 N and 3.13 N/mm²) than in DTIIB (10,642.13 N and 2.61 N/mm²). 5EPRCA0 also shows slightly better results in SICIB. This difference can be explained by the geometry of the blocks: SICIB's design distributes bending stresses more evenly, reducing weak points and improving overall strength (Kumar & Singh, 2021).

At 14 days, the performance pattern changes slightly. DTIIB generally shows higher flexural strength for OPCNA (13,957.05 N and 3.35 N/mm²) compared to SICIB (12,431.85 N and 2.98 N/mm²). For 5EPRCA30, DTIIB reaches 12,347.25 N and 2.91 N/mm², while SICIB shows slightly higher values with 14,936.65 N and 3.59 N/mm². Meanwhile, 5EPRCA0 performs marginally better in SICIB. These results suggest that curing time allows stress transfer between particles to improve, especially in DTIIB, where longer curing helps the complex geometry to gain strength through densification and better packing of particles (Rashid et al., 2022).

By 28 days, SICIB consistently shows slightly higher flexural strength than DTIIB across all mixtures. OPCNA in SICIB achieves 17,078.55 N and 4.10 N/mm² compared to 16,327.05 N and 3.81 N/mm² in DTIIB. Similarly, 5EPRCA0 shows 16,277.80 N and 3.91 N/mm² in SICIB, surpassing DTIIB's 14,820.75 N and 3.54 N/mm². 5EPRCA30 is almost equivalent between SICIB (17,177.55 N and 4.12 N/mm²) and DTIIB (16,232.30 N and 3.80 N/mm²). The higher performance of SICIB is likely due to its inclined connection design, which allows better load transfer under bending and reduces stress concentration points (Zhang et al., 2020).

Overall, comparing SICIB and DTIIB across all mixtures and curing times shows that SICIB generally has higher flexural strength, even though the difference becomes smaller at later curing stages. At 28 days, SICIB achieves 4.12 N/mm² with 5EPRCA30, while DTIIB reaches 3.80 N/mm². This indicates that SICIB provides slightly better structural stability and durability across different mixtures, making it a more robust option than DTIIB for flexural load resistance.

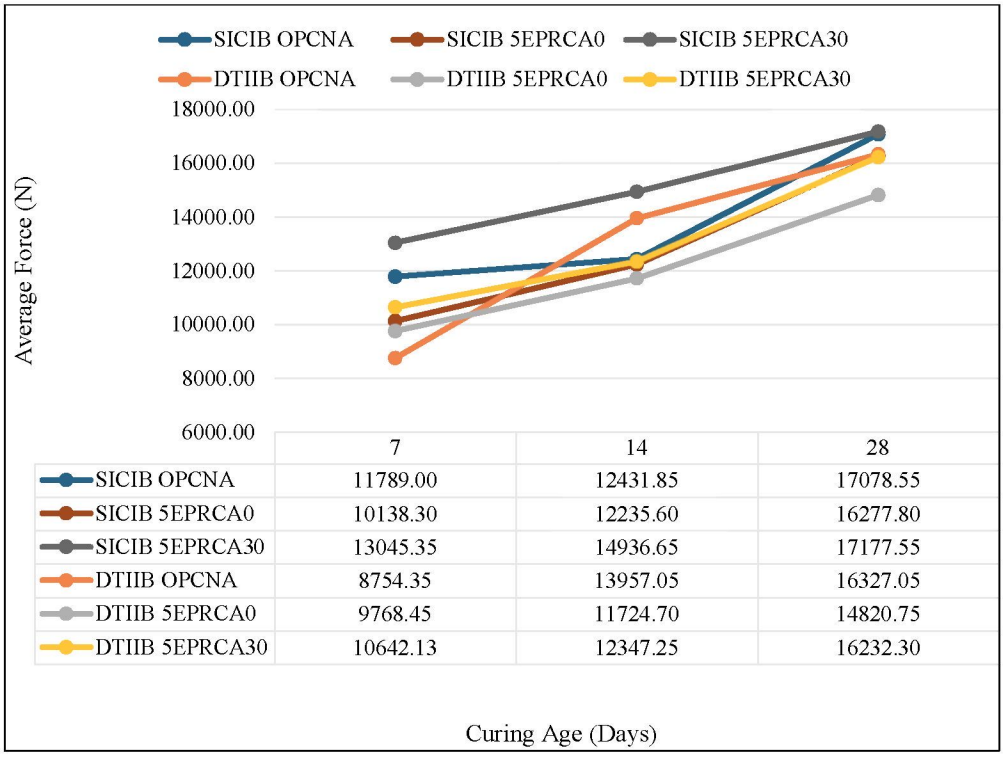

	7	14	28
SICIB OPCNA	11789.00	12431.85	17078.55
SICIB 5EPRCA0	10138.30	12235.60	16277.80
SICIB 5EPRCA30	13045.35	14936.65	17177.55
DTIIB OPCNA	8754.35	13957.05	16327.05
DTIIB 5EPRCA0	9768.45	11724.70	14820.75
DTIIB 5EPRCA30	10642.13	12347.25	16232.30

Figure 4.59 Comparison Average Force (N) Results for SICIB and DTIIB

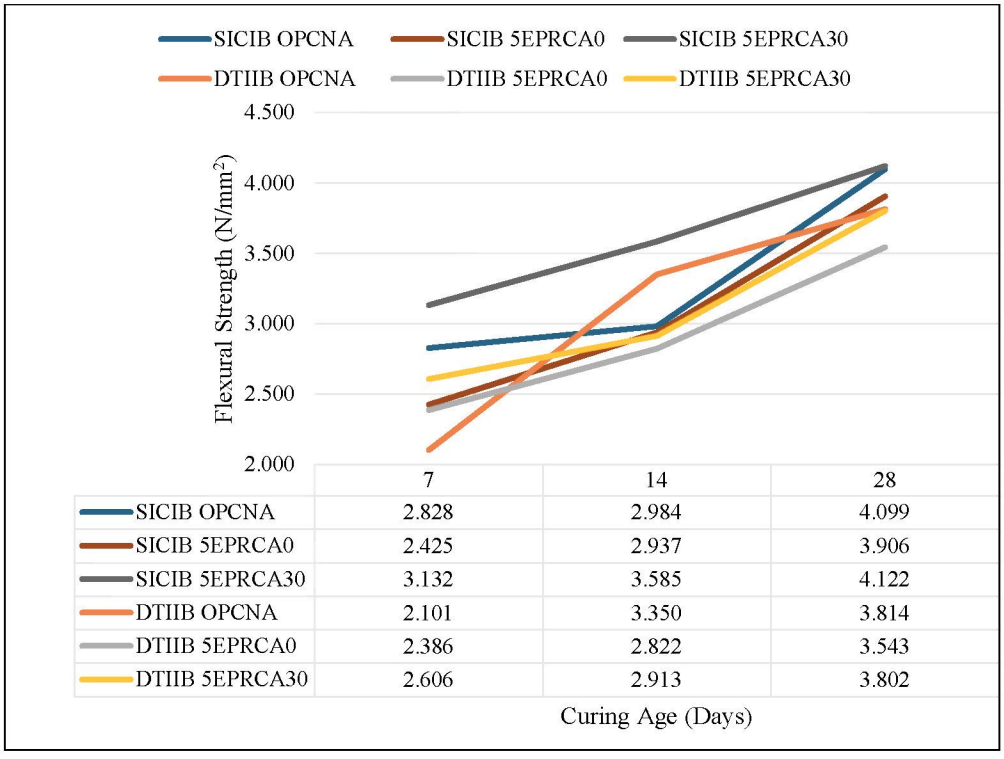

	7	14	28
SICIB OPCNA	2.828	2.984	4.099
SICIB 5EPRCA0	2.425	2.937	3.906
SICIB 5EPRCA30	3.132	3.585	4.122
DTIIB OPCNA	2.101	3.350	3.814
DTIIB 5EPRCA0	2.386	2.822	3.543
DTIIB 5EPRCA30	2.606	2.913	3.802

Figure 4.60 Comparison Flexural Strength (N/mm²) Results for SICIB and DTIIB

4.4.4.4 Comparison for All Interlocking Block Design

The flexural behaviour of the interlocking block types distinct at 7 days of curing. The comparison for all interlocking block design test results were summarized in Figures 4.64 and Figures 4.65, where the average force and flexural strength are presented. The Solid Interlocking Block (SIB) shows the highest strength at all times, and OPCNA, 22,391.63 N and 5.37 N/mm². Comparatively, the Single Inclined Connection Interlocking Block (SICIB) and Dual Tongue Inclined Interlocking Block (DTIIB) have lower values, which represents that SIB can endure greater bending forces during the earlier stage of curing. Such an increase in the performance of SIB could be explained by the size reduction of its geometry that enables the consumption of more homogenous stresses under flexural loading, lowering the possibilities of certain local failure (Zhou et al., 2021).

At 14 days, SIB is still in the lead and OPCNA increases to 24,715.17 N and 5.76 N/mm², whereas SICIB and DTIIB improve yet remain low. DTIIB displays a significant growth up to 3.35 N/mm² yet not comparable with SIB. With the subsequent rise in strength of all block types at this stage, it may be associated with the improved packing of the particle and progressive densification of the cement matrix during curing, which contributes to an increase in the ability to transfer loads between aggregates and the matrix (Cheng et al., 2020).

At 28 days, the flexural strength of SIB still has the highest value of 6.62 N/mm², whereas OPCNA 4.10 N/mm² and SICIB 3.81 N/mm² and DTIIB 3.81 N/mm². Improvement is significant in the 5EPRCA30 mixture compared with 5EPRCA0, particularly in SIB and SICIB. As an example, 5EPRCA30 has a 28-day SIB 5.16 N/mm² compared to 4.62 N/mm² to implement 5EPRCA0. This enhancement has a reason in micro-filling effect of eggshell powder (ESP) and Coarse Recycled Aggregate (RCA), which maximizes the particle packing and minimizes the voids and strengthens the interlocking between particles in the block matrix (Ali et al., 2022; Mehta & Siddique, 2017).

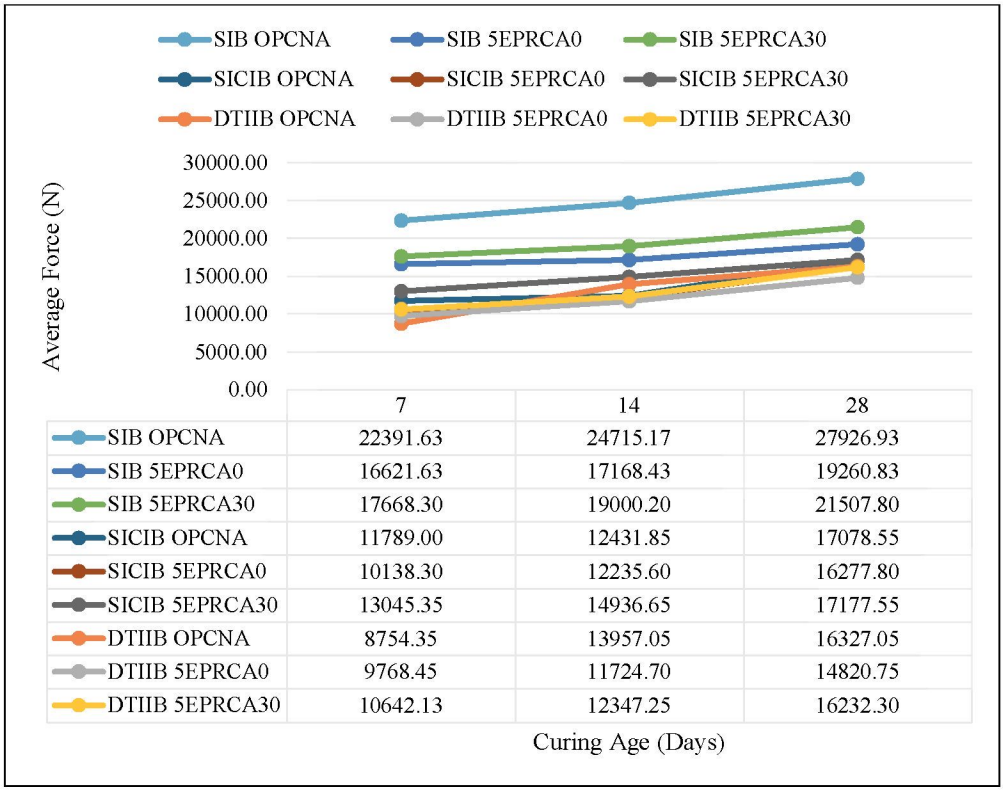

	7	14	28
SIB OPCNA	22391.63	24715.17	27926.93
SIB 5EPRCA0	16621.63	17168.43	19260.83
SIB 5EPRCA30	17668.30	19000.20	21507.80
SICIB OPCNA	11789.00	12431.85	17078.55
SICIB 5EPRCA0	10138.30	12235.60	16277.80
SICIB 5EPRCA30	13045.35	14936.65	17177.55
DTIIB OPCNA	8754.35	13957.05	16327.05
DTIIB 5EPRCA0	9768.45	11724.70	14820.75
DTIIB 5EPRCA30	10642.13	12347.25	16232.30

Figure 4.61 Average Force (N) Results for all IB

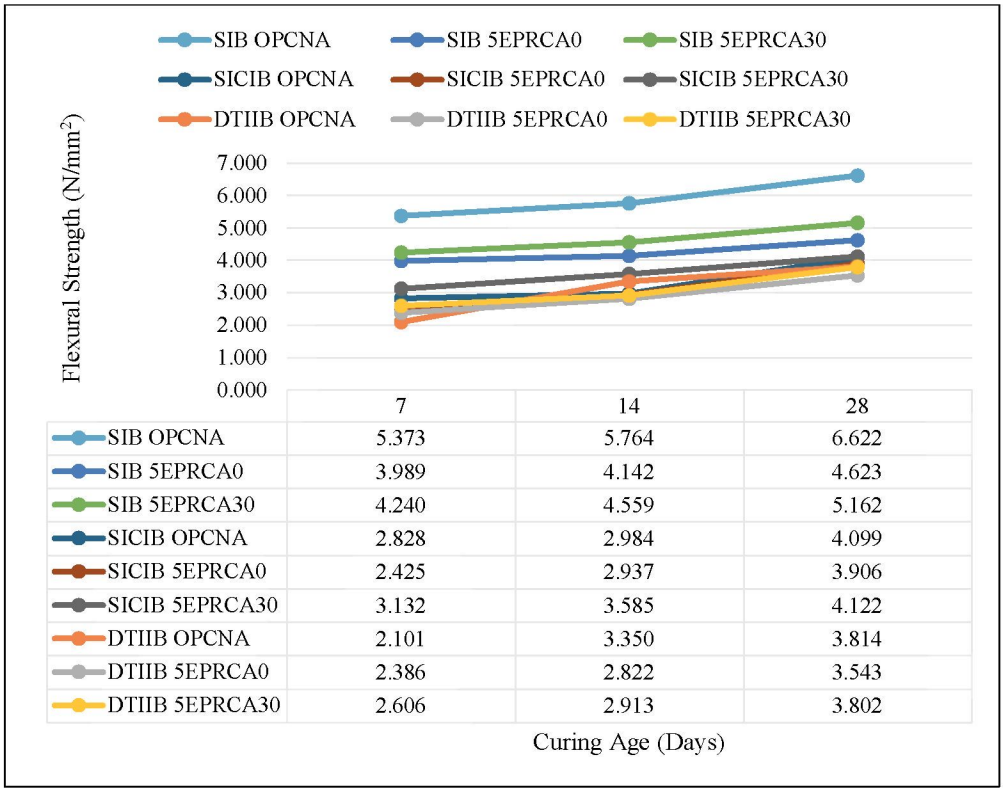

	7	14	28
SIB OPCNA	5.373	5.764	6.622
SIB 5EPRCA0	3.989	4.142	4.623
SIB 5EPRCA30	4.240	4.559	5.162
SICIB OPCNA	2.828	2.984	4.099
SICIB 5EPRCA0	2.425	2.937	3.906
SICIB 5EPRCA30	3.132	3.585	4.122
DTIIB OPCNA	2.101	3.350	3.814
DTIIB 5EPRCA0	2.386	2.822	3.543
DTIIB 5EPRCA30	2.606	2.913	3.802

Figure 4.62 Flexural Strength (N/mm^2) Results for all IB

In the case of SICIB, the 5EPRCA30 combination once again gives the best results, after 28 days, with 4.12 N/mm², which is higher than OPCNA (4.10 N/mm²) and more than 5EPRCA0 (3.91 N/mm²). This means that the substitution of cement with ESP and the incorporation of RCA have a positive effect on the strength of geometrically complex blocks by raising the internal cohesion and bend-resisting capability (Feng et al., 2021).

The values of DTIIB are a little bit lower than the values of SIB, 5EPRCA30 scores 3.80 N/mm² and 3.81 N/mm² at 28 days respectively, and 5EPRCA0 scores 3.54 N/mm². This is most probably caused by a more complex geometry of DTIIB construction, which leads to the formation of local stress magnifications in bending. Still, the employment of 5EPRCA30 contributes to the overall enhanced performance by means of an optimized particle distribution and a stronger contact between the aggregates and the matrix (Sharma et al., 2020).

In general, SIB maintains better flexural strength and force at all mixtures and curing times compared with SICIB, which compares directly better with DTIIB in most of the instances, especially when 5EPRCA30 is employed. These findings denote the significance of block shape, mixture formulation, and disturbance of the particles to accomplish high flexural activity and structure staunchness.

4.4.5 Crack Pattern of Interlocking Block (IB)

In interlocking block structures, flexural cracking typically initiates at the bottom interface or mid-height region of the block when tensile stresses exceed the material's capacity, particularly in load-bearing arrangements without mortar. Under third-point loading, as specified by ASTM C78/C78M-22, cracks first appear along the tension face, propagating vertically upward toward the compression zone. These cracks often originate near the centre of the block's span or adjacent to interlocking grooves, where stress concentrations are highest.

The cracking behaviour is influenced by both the geometry of the interlocking interface and the concrete matrix. In this study, Single Inclined Connection Interlocking Block (SICIB) shown in Figure 4.67 and Dual Tongue Inclined Interlocking Block (DTIIB) illustrated in Figure 4.68 presented distinctive crack trajectories. Compared to the Solid Interlocking Block (SIB) portrayed in Figure 4.66, which showed more uniform vertical cracking, SICIB and DTIIB specimens tended to develop inclined or

bifurcated cracks that followed the interlock path. This suggests that the geometric complexity of the interface affects stress redistribution and crack propagation.

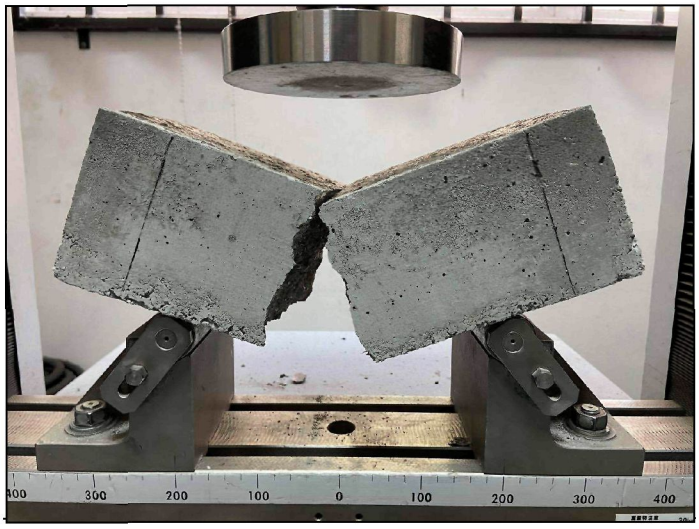

Figure 4.63 The Split Crack of Solid Interlocking Block (SIB)

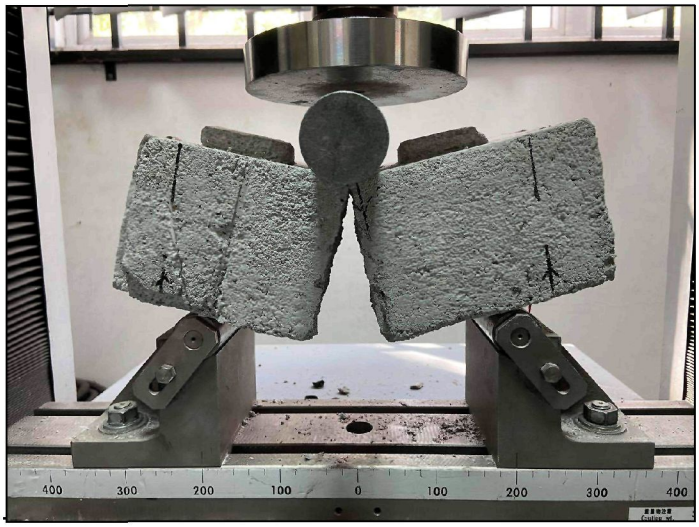

Figure 4.64 The Split Crack of Single Inclined Connection Interlocking Block (SICIB)

Understanding these crack patterns is essential for evaluating the serviceability and integrity of modular systems incorporating alternative materials like ESP and RCA. Wider or irregular cracks in composite blocks can reflect variations in bond strength or internal curing efficiency. These insights contribute to optimizing both geometry and material formulations for high-performance, sustainable interlocking block systems.

There are two types of flexural cracks, one is developed at the top of the support, which is negative, and the one developed at the bottom that is a positive one. This crack develops at the bottom near the mid-span and spread upwards. It been single or multiple cracks and occur when the tension of the beam occurs at the bottom due to heavy load flexural cracks forming. This is due to maximum bending moment inside the beam,poor design, insufficient reinforcements or insufficient concrete cover (Thales, 2022).

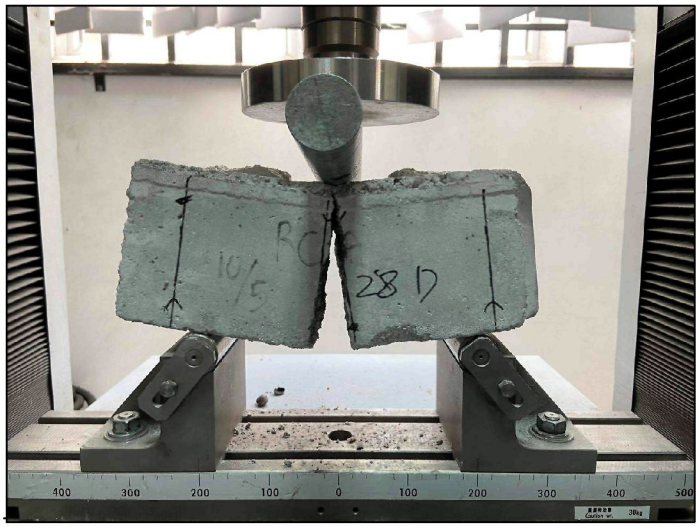

Figure 4.65 The Split Crack of Dual Tongue Inclined Interlocking Block (DTIIB)

4.4.6 Summary on Results of Interlocking Block Design

The flexural performance of interlocking blocks across different configurations, Solid (SIB), Single Inclined Connection (SICIB), and Dual Tongue Inclined (DTIIB) shows that SIB consistently achieves the highest strength across all curing ages and mixtures. While OPCNA leads overall, the 5EPRCA30 mixture demonstrates notable improvements over time, particularly in SICIB and DTIIB, where it occasionally surpasses OPCNA in strength. These trends highlight the influence of block geometry and mix composition on stress distribution and load-bearing capacity. The findings also reinforce literature from Chapter 2, which emphasizes the role of ESP and recycled aggregates in enhancing microstructural density and flexural performance.

4.5 Artificial Neural Network (ANN) by MATLAB

4.5.1 ANN for The Salient Percentage of Materials Uses

ANN is used in this research as a verification tool to evaluate whether the strength development trends observed up to 56 days remain consistent when extrapolated. Artificial Neural Networks (ANN) do not replace experimental testing but serve as a powerful tool to verify experimental data, confirm its reliability, and minimize prediction errors through accurate modelling. This allows the study to assess the reliability of long-term behaviour without conducting extended-age testing.

The 5% Eggshell Powder with 30% Recycled Concrete Aggregate (5EPRCA30) mixture, identified as the optimum blend for interlocking block production, was selected as the sample. A total of four specimens were tested, with one sample taken from each curing age of 3, 7, 28, and 56 days. The parameter of data were used compressive strength for cube and flexural strength for prism.

4.5.1.1 ANN for Cube

To make sure the neural network is correctly trained, evaluated, and tested, the data is divided into three groups at random. Based on Table 4.13, 70% is made up of training data, which comprises most samples. The network actively learns from this part, modifying weights to reduce prediction mistakes. 15% of training data is allocated to validation data, which is used to assess how well the network generalises to new data. To prevent overfitting, the training process is stopped once performance on the validation set ceases to improve. Finally, testing data receives 15% as well, but it is entirely unrelated to training. Only the trained model's performance on new, untested data is assessed using this slice.

The training phase utilized 70% of the data (2 samples), achieving a very low mean squared error (MSE) of 6.91×10^{-9} and an almost perfect regression coefficient (R) of 0.999999. This reflects excellent learning performance and strong fitting accuracy within the training set.

Validation and testing each used one sample (15% of the data), with MSE values of 3.41 and 1.58, respectively. Despite these higher errors compared to training, their R

values, 0.964 and 0.926 still indicate good predictive consistency, suggesting the model generalizes well and maintains stability across unseen data.

Table 4.13
Results MSE and R of Cube OPCNA

Results	Samples	Percentages (%)	MSE	R
Training	2	70	$6.91461e^{-9}$	$9.99999e^{-1}$
Validation	1	15	$3.41031e^{-0}$	$9.96439e^{-1}$
Testing	1	15	$1.58444e^{-0}$	$9.92601e^{-1}$

The set of regression plots in the Figure 4.66 illustrates the performance of an ANN in predicting a target variable likely compressive or flexural strength in engineered concrete mixtures. During the training phase, the model achieves perfect correlation (R = 1), indicating an exact fit between the network's predicted outputs and the known targets. The regression equation (Output ≈ 1 × Target - $2e^{-05}$) suggests an almost ideal linear relationship, meaning the ANN has fully captured the underlying patterns within the training data.

For validation shown in Figure 4.72, the model maintains a strong correlation (R = 0.99644), with a regression trend of Output ≈ 1.1 × Target – 3.4. This implies a slight overestimation of target values, possibly due to sample diversity or limited representation of edge cases. Similarly, the testing phase exhibits high reliability (R = 0.9926), with an output trend of Output ≈ 1.1 × Target – 2.1, reinforcing the model's predictive power on unseen data. When all datasets are combined, the model yields an overall correlation of R = 0.99575 and a nearly ideal regression (Output ≈ 1 × Target - 1), confirming its general robustness and suitability for modelling strength related properties across varied conditions. The results can be justified by several factors. The strong match during training proves that artificial neural networks (ANNs) can understand complicated patterns, which has been known since early research on neural networks (Hornik, 1991).

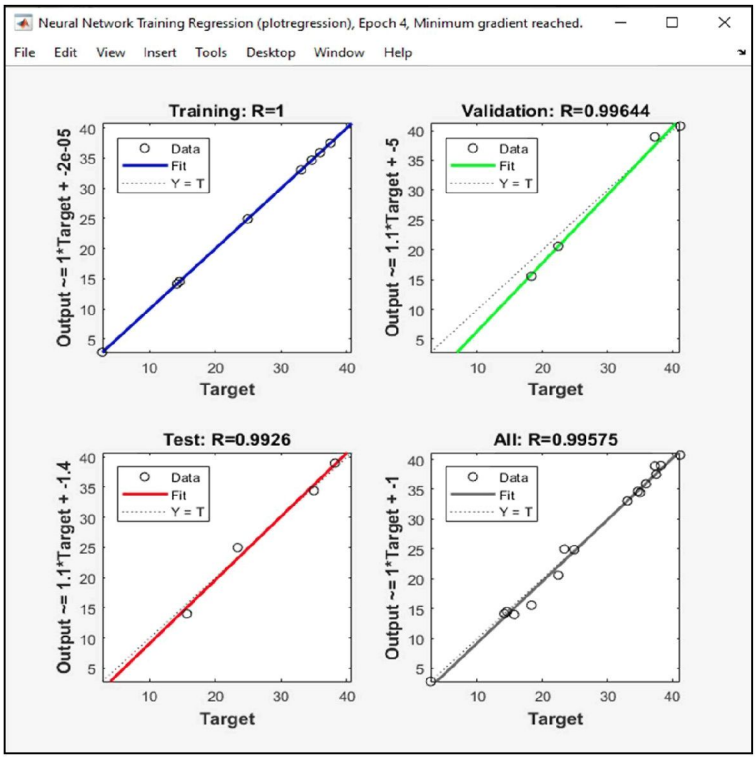

Figure 4.66 Plot Regression of Cube OPCNA

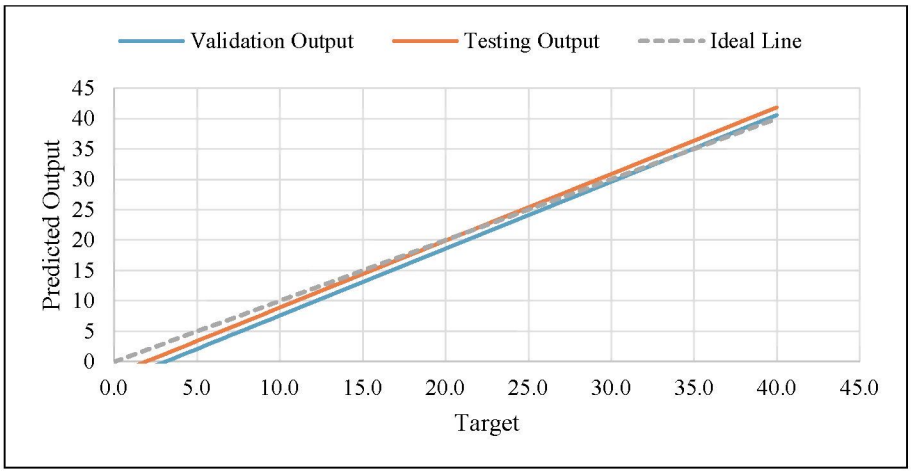

Figure 4.67 Comparison Validation Line and Testing Line of Cube OPCNA

Notably, the alignment between the validation and testing curves suggests that the network, maintained stability in predicting unseen data. The absence of significant divergence between the training and validation lines further supports the robustness of the learning process. Unlike regular prediction methods, ANN can deal with complicated relationships between how a mixture is made and how strong it turns out. This helps make predictions more accurate and reduces mistakes (Chou & Pham, 2004).

Because of this reliability, ANNs are useful in engineering work where knowing the exact strength is important for keeping structures safe and improving design (Deepa et al., 2010). Overall, ANN effectively captured the input–output relationships, delivering reliable predictions within a compact training window.

For the 5EPRCA30 Cube mix as shown in Table 4.14, the ANN model demonstrates excellent performance across all phases of evaluation. During the training phase, which utilized 70% of the dataset (2 samples), the model achieved a mean squared error (MSE) of 0.8906 and a regression coefficient (R) of 0.99536, indicating a strong fit and minimal deviation from the actual target values. In the validation phase, comprising 15% of the data (1 sample), the MSE dropped slightly to 0.7425 with an even higher R value of 0.99617, suggesting that the model generalized well to data not used in training. Most impressively, the testing phase, also 15% of the data yielded the lowest MSE of 0.2822 and a near-perfect R value of 0.99958, confirming the model's robustness and predictive reliability on unseen data. Collectively, these results support the effectiveness of the ANN in accurately modelling the strength characteristics of the 5EPRCA30 Cube specimens.

Table 4.14
Results MSE and R of Cube 5EPRCA30

Results	Samples	Percentages (%)	MSE	R
Training	2	70	$8.90593e^{-1}$	$9.95364e^{-1}$
Validation	1	15	$7.42524e^{-1}$	$9.96165e^{-1}$
Testing	1	15	$2.82191e^{-1}$	$9.99576e^{-1}$

The regression plots in the Figure 4.74 evaluate the ANN's capability to predict the target values for the 5EPRCA30 Cube specimens. In the training phase, the model shows strong alignment between predicted and actual outputs, with a high correlation coefficient (R = 0.99536) and a regression trend of approximately Output ≈ 0.97 × Target + 0.4. This suggests effective learning and minimal deviation.

During validation, the network maintains excellent generalization with R = 0.99617 and a regression line of Output ≈ 1 × Target - 1.2, closely following ideal behaviour (see Figure 4.75). The testing plot demonstrates superior performance as well, showing R = 0.99958 and a trend of Output ≈ 0.95 × Target + 1.5, confirming accurate predictions on unseen data. When combining all datasets, the overall regression line (Output ≈ 0.98 × Target + 0.29) and R = 0.99589 highlight the model's consistency and reliability across phases.

The ideal target values are contrasted with the anticipated results from the testing and validation stages in this picture. The testing predictions are displayed by the orange line, while the validation findings are represented by the blue line. The ideal trend is indicated by the dashed grey line, where the target and predicted output would be the same. Good prediction accuracy is indicated by the plot, which shows that the validation and testing outputs closely resemble the ideal line across the range of target values. The small overestimation during validation happened because the data had some differences and unusual values. ANN models can be sensitive when the new data does not match the training data, especially if the samples are irregular or extreme (Adeli & Wu, 1998). However, the model still showed high accuracy during testing, which means it was not just memorizing the training data it actually learned the real connection between the inputs and outputs. This ability to work well with new data has also been seen in other studies on predicting concrete strength (Behnood & Golafshani, 2018). On overall, the ANN model simplifies well, with high alignment in both unknown data sets, but little variations at specific places indicate slight under or overestimation. The dependability of the network's predictions for the 5EPRCA30 Cube specimens is supported by this visual consistency.

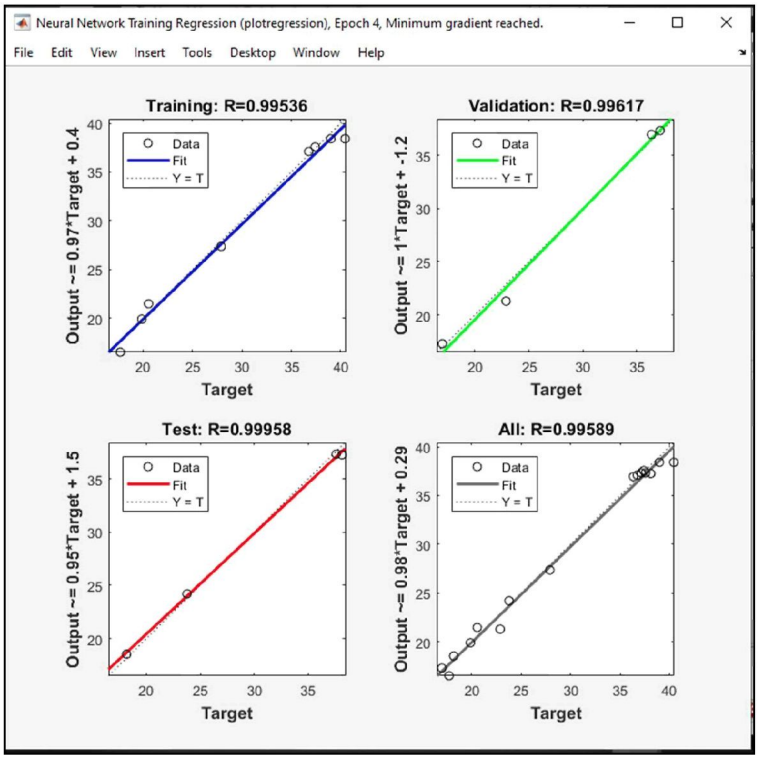

Figure 4.68 Plot Regression of Cube 5EPRCA30

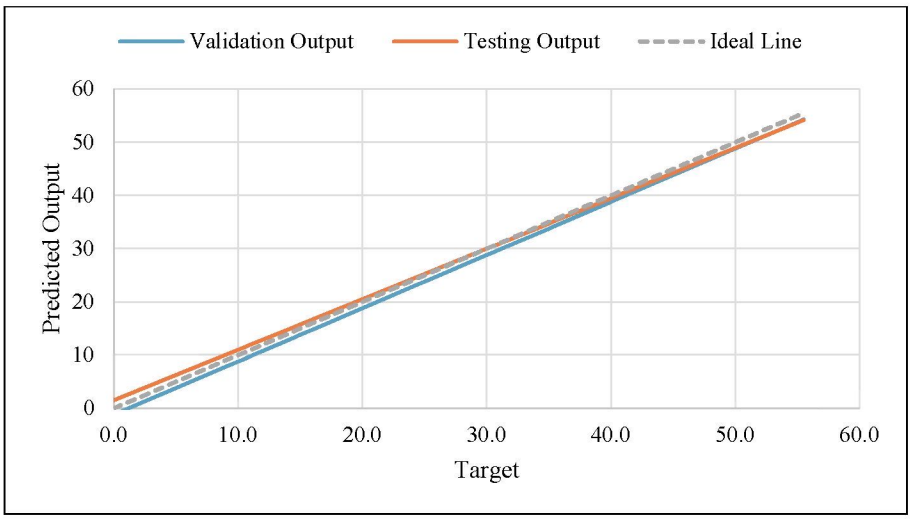

Figure 4.69 Comparison Validation Line and Testing Line of Cube 5EPRCA

4.5.1.2 ANN for Prism

The ANN model performs admirably for the OPCNA Prism specimens in every evaluation stage. In Table 4.15 shows that, with a mean squared error (MSE) of 1.94×10^{-6} and a near-perfect regression coefficient (R) of 0.999999, the network demonstrated highly accurate learning with nearly zero deviation from the target values during training, which used 70% of the dataset (2 samples). Using 15% of the data (1 sample) in the validation phase, the model's MSE was 1.84218 and its R was 0.99175, indicating strong generalisation even with the rise in error. Despite maintaining a strong R value of 0.98370, the testing phase, which was likewise based on 15% (1 sample), produced a higher MSE of 4.67048.

Table 4.15
Results MSE and R of Prism OPCNA

Results	Samples	Percentages (%)	MSE	R
Training	2	70	$1.94462e^{-6}$	$9.99999e^{-1}$
Validation	1	15	$1.84218e^{-0}$	$9.91753e^{-1}$
Testing	1	15	$4.67048e^{-0}$	$9.83699e^{-1}$

The regression plots in the Figure 4.77 assess the performance of the ANN model for the OPCNA Prism specimens across training, validation, and testing phases. The training plot shows perfect correlation (R = 1), with a regression trend of Output ≈ 1 × Target + 0.0024, indicating flawless learning and negligible deviation from target

values. In the validation phase, the model retains strong predictive accuracy with R = 0.99175, and a regression line of Output ≈ 1 × Target + 0.59, suggesting minor overestimation at higher target values. The testing plot reflects reliable performance as well, with R = 0.9837 and a slightly more pronounced regression slope (Output ≈ 1.1 × Target - 4.7), pointing to a mild overprediction in unseen samples. When considering all datasets combined, the overall regression line is Output ≈ 1 × Target - 0.52, and the model maintains a high R value of 0.99017.

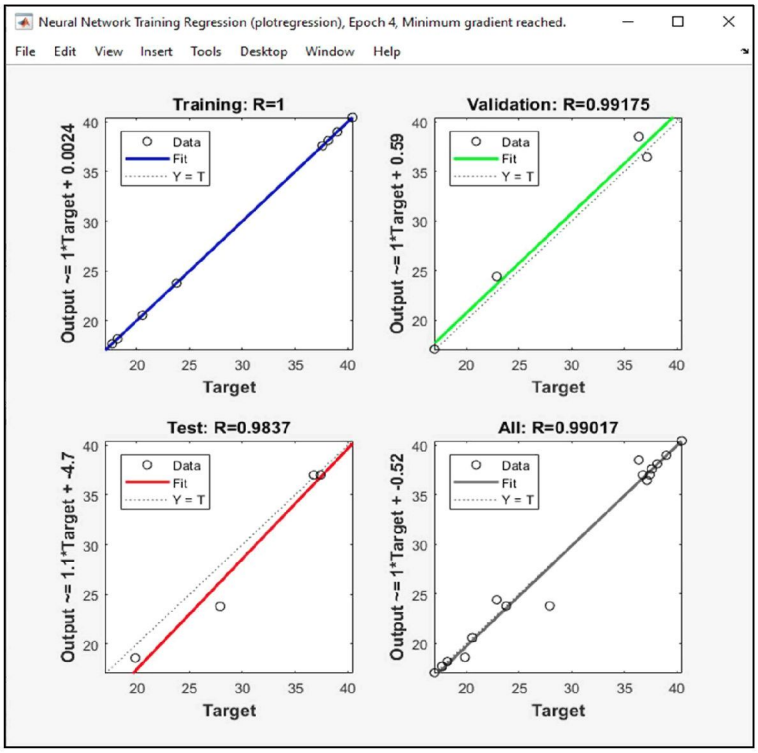

Figure 4.70 Plot Regression of Prism OPCNA

These consistent regression trends and strong correlation coefficients across all phases confirm the ANN's robustness and suitability for modelling the strength behaviour of OPCNA Prism specimens. A dashed ideal line in the Figure 4.78 indicates the target values, which are compared to the expected outputs from the validation and testing stages. The ANN model is producing precise predictions for both datasets, as seen by the orange (testing) and blue (validation) curves, which both closely resemble the ideal trend. Strong generalisation and predictive consistency are confirmed by the overall alignment, despite minor deviations. The small increase in validation error after

the first epoch might be caused by slight differences or unusual values in the validation data, which is common when the dataset is small or has outliers (Zhang et al., 2019).

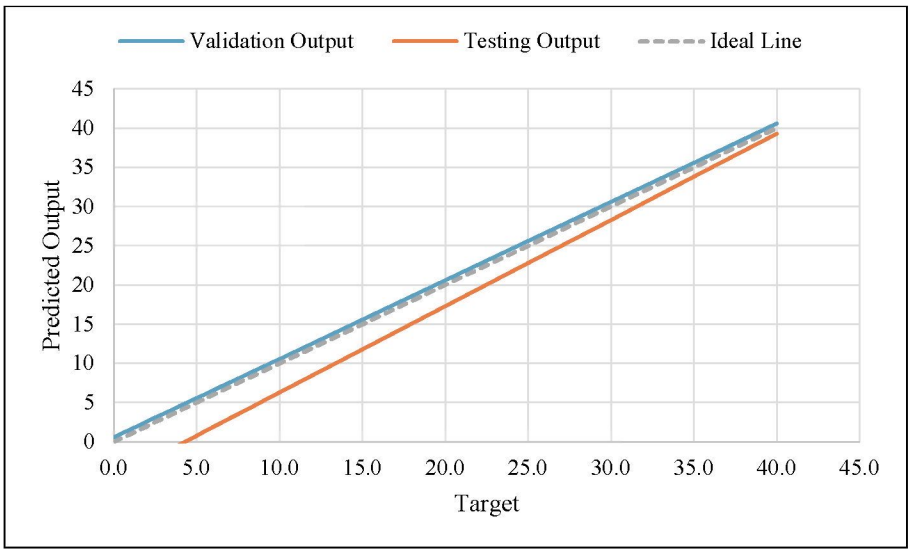

Figure 4.71 Comparison Validation Line and Testing Line of Prism OPCNA

For the 5EPRCA30 Prism specimens in Table 4.16, the ANN shows strong predictive accuracy across all phases. Training (70%) produced an MSE of 0.0728 with R = 0.9521, indicating solid learning. Validation and testing (15% each) yielded lower errors, 0.0073 and 0.0682 respectively with high R values of 0.9975 and 0.9853, confirming excellent generalization and reliable performance on unseen data.

Table 4.16
Results MSE and R of Prism 5EPRCA30

Results	Samples	Percentages (%)	MSE	R
Training	2	70	$7.27925e^{-2}$	$9.52117e^{-1}$
Validation	1	15	$7.34343e^{-3}$	$9.97473e^{-1}$
Testing	1	15	$6.81968e^{-2}$	$9.85339e^{-1}$

The Figure 4.80 presents four regression plots evaluating the ANN model's prediction performance for the 5EPRCA30 Prism specimens. In the training phase, the correlation coefficient is R = 0.95212, with the regression equation Output ≈ 0.85 × Target + 0.77, indicating a good fit though with slight underestimation at lower target values.

Validation and testing phases show improved accuracy, with R values of 0.99747 and 0.98534 respectively, and nearly consistent regression trends around

Output ≈ 0.91 × Target with minimal bias. The combined plot for all datasets confirms overall reliability with R = 0.95519 and Output ≈ 0.87 × Target + 0.59. Together, these plots reflect strong generalization and stable predictive behaviour across the network's evaluation phases.

The ideal target values for prism specimens in the lower strength range are contrasted with the expected outputs from the validation and testing sets in this Figure 4.81. The blue and orange lines show actual ANN predictions for the validation and testing stages, while the dashed grey line shows ideal predictions (where Output = Target). With very little variations, both lines closely resemble the ideal trend over the 0–12 MPa range, showing that the model retains high prediction accuracy and applicability even at lower strength levels.

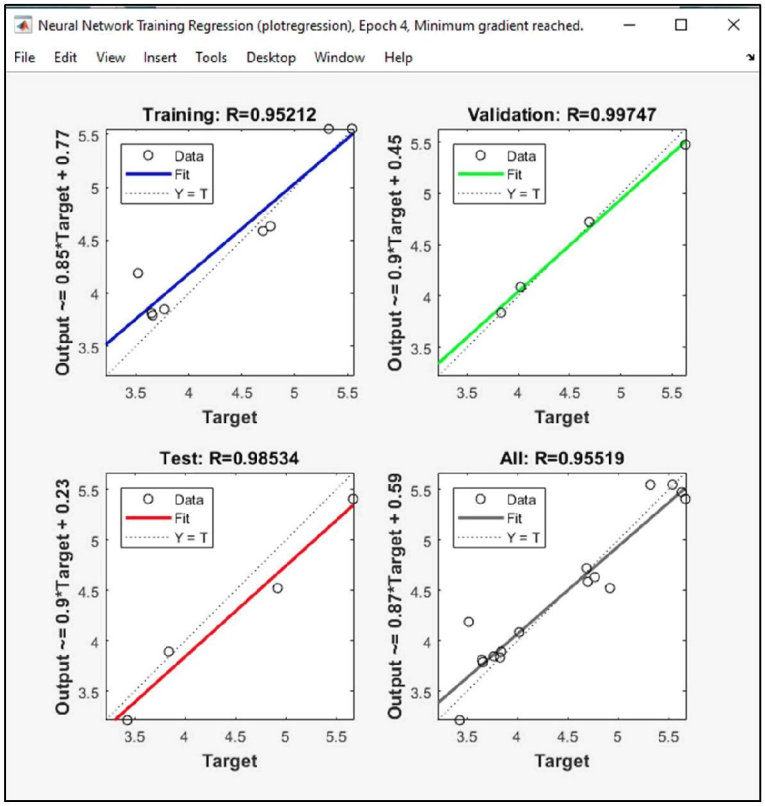

Figure 4.72 Plot Regression of Prism 5EPRCA30

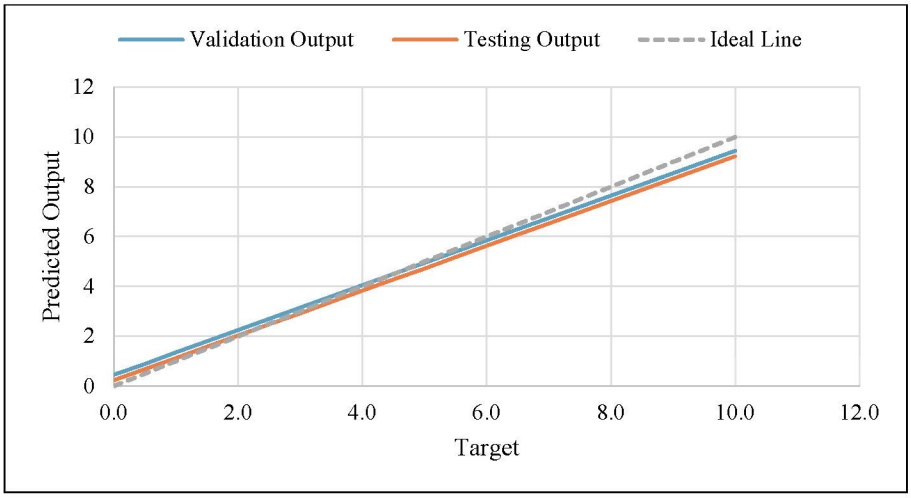

Figure 4.73 Comparison Validation Line and Testing Line of Prism 5EPRCA30

4.5.2 ANN for Interlocking Blocks

There Neural Fitting Tool (Figure 4.83) and Neural Network (Figure 4.84) shows the hidden layer that used to validate the flexural strength behaviour of Solid Interlocking Block (SIB), Single Inclined Connection Interlocking Block (SICIB), and Dual Tongue Inclined Interlocking Block (DTIIB) made with Ordinary Portland Cement and Natural Aggregate (OPCNA) and the optimal proportions of materials which are 5% of ESP and 30% of RCA (5EPRCA30). In this model, the input parameter is curing day, while the outputs are flexural strength of the interlocking blocks. A total of three specimens were tested, with one sample taken from each curing age of 7, 14, and 28 days. The model uses the Levenberg–Marquardt algorithm, which is highly efficient for training small- to medium-sized neural networks with fast convergence and minimal error. It consists of one hidden layer to balance model complexity and generalization. Within that layer, five neurons are used enough to capture the nonlinear patterns in the data without overfitting.

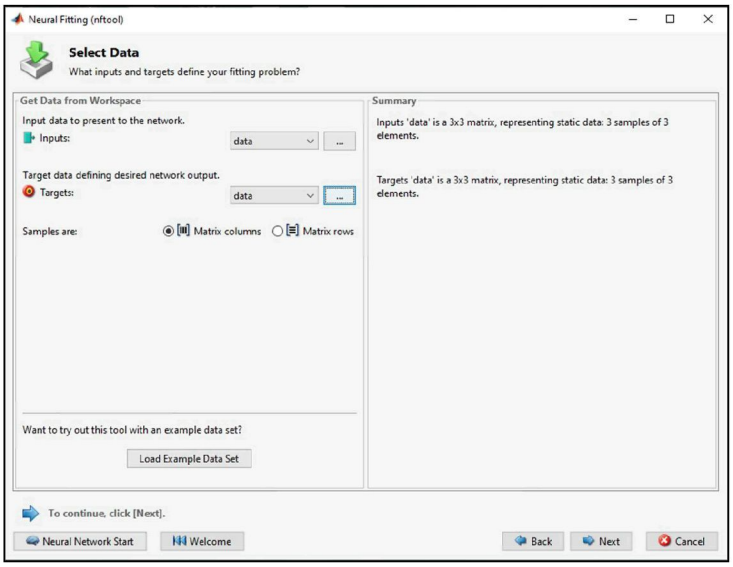

Figure 4.74 Neural Fitting Tool of ANN for Interlocking Blocks

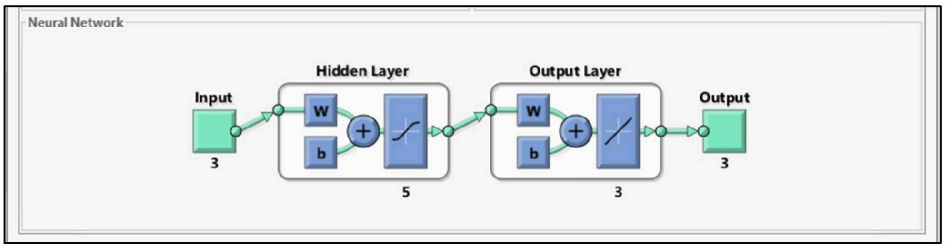

Figure 4.75 Neural Network for Interlocking Blocks

4.5.2.1 ANN of SIB

For the SIB OPCNA specimens (see Table 4.17), the ANN model delivers highly reliable predictions across all phases. During training (60% of data, 1 sample), the model achieved an extremely low MSE of (9.86 /times 10^{-6}) with an R value of 0.999984, indicating near-perfect learning with almost no error. Validation and testing phases (each 20%, 1 sample) show strong generalization performance MSE values of 0.0296 and 0.00397, respectively, with consistently high R values above 0.997. These results confirm that the model effectively captured the relationship between input and output variables, yielding precise and stable predictions for SIB OPCNA mixes.

Table 4.17
Results MSE and R of SIB OPCNA

Results	Samples	Percentages (%)	MSE	R
Training	1	60	$9.86306e^{-6}$	$9.99984e^{-1}$
Validation	1	20	$2.95570e^{-2}$	$9.97191e^{-1}$
Testing	1	20	$3.96644e^{-3}$	$9.97539e^{-1}$

The regression plots for SIB OPCNA as shown in Figure 4.85, specimens demonstrate strong and consistent performance across all phases. In the training phase, the network achieved near-perfect accuracy ($R \approx 0.99998$) with minimal bias (Output ≈ Target + 0.0044), reflecting excellent model fit and minimal deviation. Validation shows Output ≈ 0.77 × Target + 1.4 with $R \approx 0.9972$, indicating a slight underestimation at lower targets but still high correlation and strong generalization. Testing continues this trend with Output ≈ 1.1 × Target - 0.33 ($R \approx 0.9975$), suggesting the model slightly overpredicts but remains highly reliable. The overall plot (Output ≈ 0.92 × Target + 0.46, $R \approx 0.9921$) confirms stable performance, justifying the ANN's suitability for predicting strength behaviour in SIB OPCNA mixes with minimal error and consistent learning across datasets. The consistently high R-values throughout all phases indicate that the artificial neural network (ANN) effectively learned the complex, non-linear connections between the input variables and strength outcomes something traditional regression methods often struggle with (Bui et al., 2018).

The close alignment of both validation and testing lines with the ideal target line across the full strengths range not only confirms high predictive accuracy but also suggests low model bias and stable generalization. The minimal gap (see Figure 4.86) between the two curves implies that the ANN model treats unseen data consistently, regardless of whether it's used for validation or testing. This consistency strengthens the justification for using the model in practical prediction scenarios, especially for SIB OPCNA mixes where precision and reliability are critical.

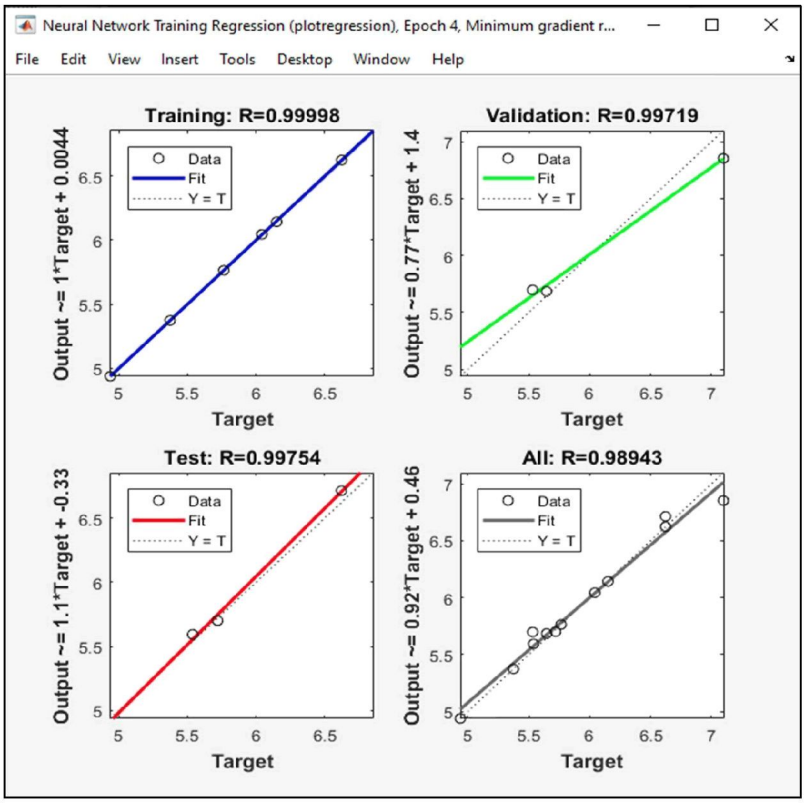

Figure 4.76 Plot Regression of SIB OPCNA

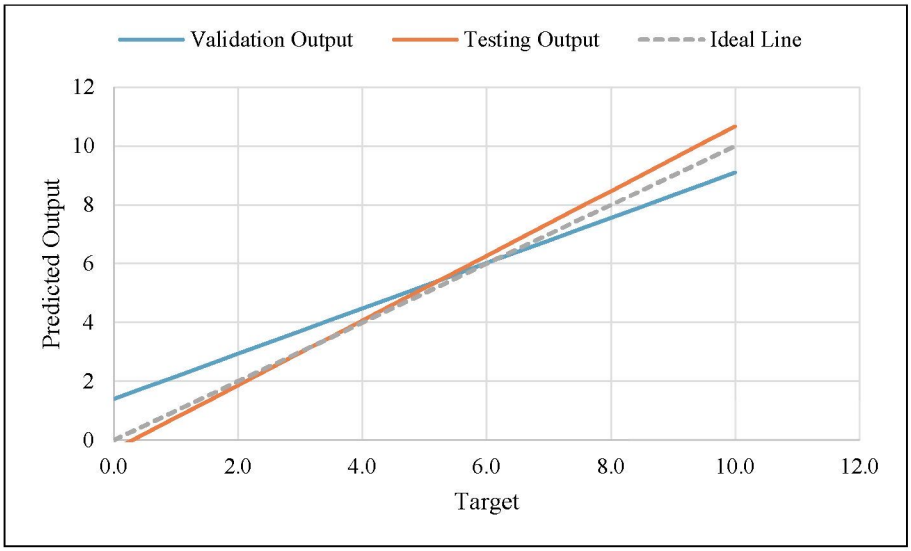

Figure 4.77 Comparison Validation Line and Testing Line of SIB OPCNA

The ANN model for SIB 5EPRCA30 shows in Table 4.18, consistently strong performance across all phases. In the training phase (60%, 1 sample), it achieved a low MSE of 0.00408 with a high R value of 0.99710, reflecting precise learning and minimal

error. Validation and testing phases (20% each) maintained excellent generalization, with MSEs of 0.04206 and 0.06773, and R values of 0.99522 and 0.99682 respectively, confirming stable, reliable prediction behaviour on unseen data.

Table 4.18
Results MSE and R of SIB 5EPRCA30

Results	Samples	Percentages (%)	MSE	R
Training	1	60	$4.08174e^{-3}$	$9.97099e^{-1}$
Validation	1	20	$4.20576e^{-2}$	$9.95216e^{-1}$
Testing	1	20	$6.77266e^{-2}$	$9.96819e^{-1}$

The regression plots as illustrated in Figure 4.88 for SIB 5EPRCA30 show strong ANN performance across all phases. Training achieved excellent accuracy (R = 0.9971) with Output ≈ Target – 0.16, indicating minimal error and reliable learning. Validation (R = 0.99522) and testing (R = 0.99682) plots reveal slight deviations, Output trends suggest mild over- and underestimation, yet the high R values confirm stable generalization. The overall plot (R = 0.97454) reinforces the model's consistency, justifying its suitability for predicting interlocking block strength in this mix.

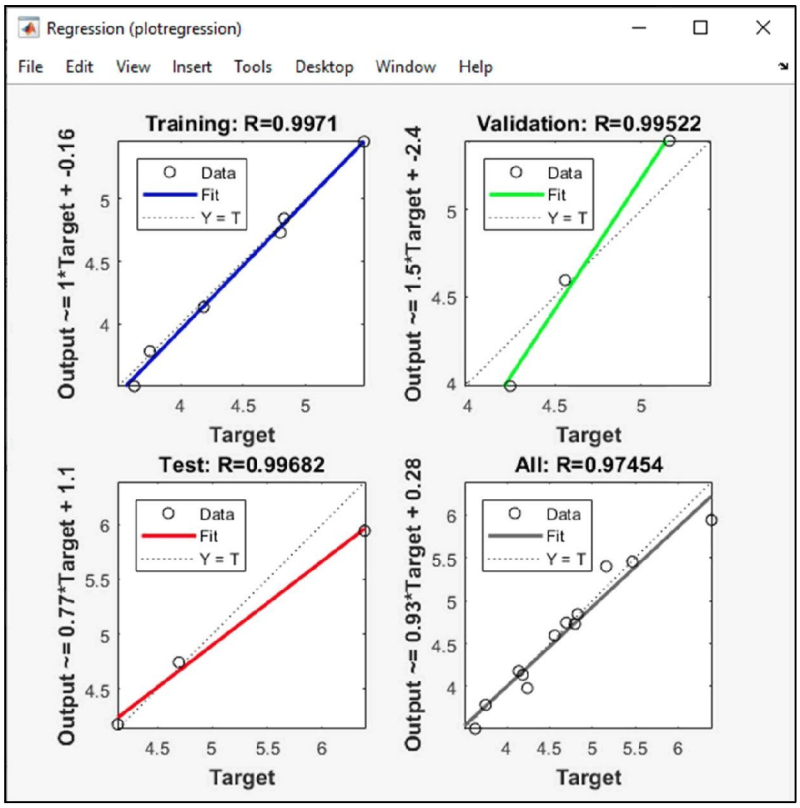

Figure 4.78 Plot Regression of SIB 5EPRCA30

This Figure 4.89 compares the predicted outputs from validation and testing against the ideal target line for SIB 5EPRCA30 specimens. Both curves align closely with the grey dashed line (ideal prediction), especially between 2 MPa and 10 MPa, indicating strong ANN accuracy. The orange testing line shows slightly better alignment than the blue validation line, which suggests the model generalized slightly better in the testing phase. Minor deviations beyond 10 MPa are observed, but they remain within acceptable error margins for mortar prediction.

According to Bousquet and Elisseeff (2002), models that maintain consistent performance across different data splits are considered stable and less sensitive to noise or random fluctuations. Minor prediction differences, such as slight underestimation during validation and overestimation during testing, are likely due to natural variations in the experimental data. These fluctuations are common in real-world datasets and are typically managed more effectively by ANNs than by standard statistical models (Yeh, 1998). This consistency across datasets justifies the ANN's effectiveness and reinforces its reliability for low to mid-range strength modelling.

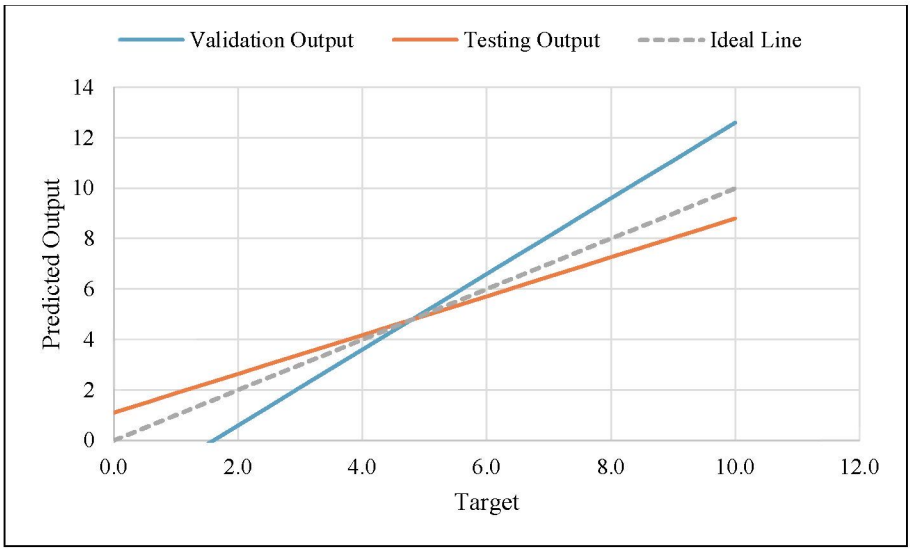

Figure 4.79 Comparison Validation Line and Testing Line of SIB 5EPRCA30

4.5.2.2 ANN of SICIB

In Table 4.19, the ANN model for SICIB OPCNA specimens shows strong predictive performance across all phases. In training (60%, 1 sample), the network achieved an exceptionally low MSE of (8.82 \times 10^{-5}) and an R value of 0.99951,

indicating near-perfect learning. Validation and testing phases (20% each) also performed well, with MSEs of 0.0116 and 0.0357, and R values of 0.99874 and 0.98976 respectively, confirming excellent generalization and stable prediction accuracy for unseen data.

Table 4.19
Results MSE and R of SICIB OPCNA

Results	Samples	Percentages (%)	MSE	R
Training	1	60	$8.82339e^{-5}$	$9.99511e^{-1}$
Validation	1	20	$1.15803e^{-2}$	$9.98737e^{-1}$
Testing	1	20	$3.57411e^{-2}$	$9.89756e^{-1}$

The regression plots for SICIB OPCNA specimens show excellent ANN performance across all phases (see Figure 4.91). Training achieved near-perfect accuracy (R = 0.99951), with the regression line Output ≈ 0.98 × Target + 0.066, indicating precise learning and minimal bias. Validation and testing phases also reflect high correlations (R = 0.99874 and R = 0.98976) with Output trends showing slight over- and underestimations but staying well within acceptable predictive margins. The combined plot (R = 0.98623) confirms strong generalization, with Output ≈ 0.94 × Target + 0.19. These consistent results justify the ANN model's reliability and accuracy for predicting strength in SICIB OPCNA specimens.

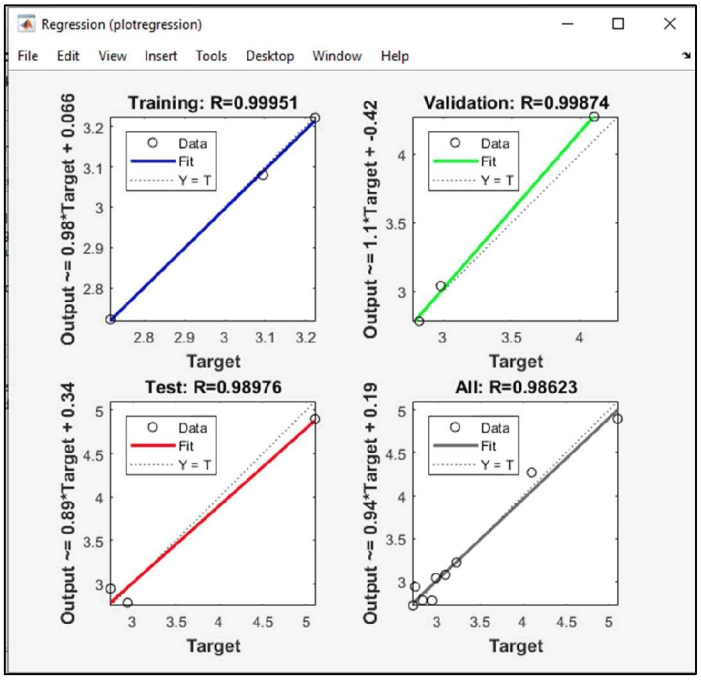

Figure 4.80 Plot Regression of SICIB OPCNA

Figure 4.92 presents the predicted outputs from both validation and testing phases against target values for SICIB OPCNA specimens. The blue and orange curves closely track the dashed ideal line, especially between 2 MPa and 10 MPa, indicating strong predictive accuracy and low bias in that range. The slight divergence of the validation curve beyond 10 MPa suggests minor underprediction but remains within acceptable margins for mortar-based materials. The consistent proximity between the two coloure curves demonstrates stable generalization across datasets. The strong performance across training, validation, and testing reflects the ANN's ability to manage the complex, non-linear behaviour of cement-based composites, which traditional regression methods often struggle with (Wong et al., 2022). According to Zhang et al. (2021), the minor underprediction at higher strength values could be linked to natural variability in experimental testing of mortars, where small changes in curing, water content, or aggregate distribution can affect strength outcomes. This alignment justifies the ANN's reliability and robustness in predicting strength for SICIB OPCNA mixes, even across varying ranges.

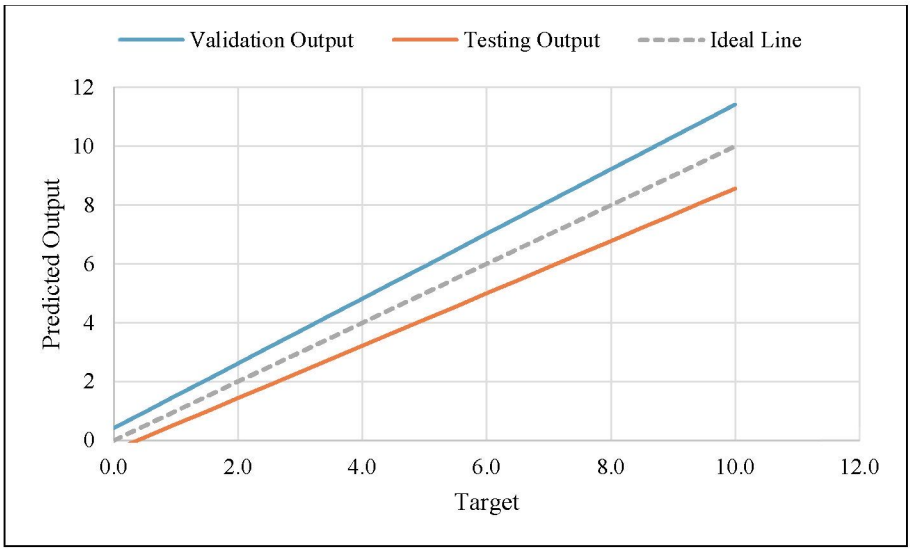

Figure 4.81 Comparison Validation Line and Testing Line of SICIB OPCNA

For the SICIB 5EPRCA30 specimens (see Table 4.20), the ANN model demonstrates solid predictive behaviour across phases. Training (60%, 1 sample) achieved good learning accuracy with an MSE of 0.02407 and R = 0.97030, indicating strong correlation and low error. Validation (20%, 1 sample) performed exceptionally well, with a lower MSE of 0.00821 and an R value of 0.99825 showing precise

generalization. Testing (20%, 1 sample) shows slightly higher error at MSE = 0.10293, with R = 0.96936, still indicating reliable prediction but with more variance. Overall, the model retains high predictive capacity, though the testing phase reflect slight sensitivity to outlier values or noise.

Table 4.20
Results MSE and R of SICIB 5EPRCA30

Results	Samples	Percentages (%)	MSE	R
Training	1	60	$2.40740e^{-2}$	$9.70297e^{-1}$
Validation	1	20	$8.21214e^{-3}$	$9.98245e^{-1}$
Testing	1	20	$1.02930e^{-1}$	$9.69359e^{-1}$

The regression plots illustrated in Figure 4.94 for SICIB 5EPRCA30 specimens show varied predictive accuracy across the ANN phases. Training (R = 0.9703) and testing (R = 0.96936) exhibit high correlation, but their regression trends Output ≈ 1.2 × Target + 0.81 and Output ≈ 1.5 × Target + 1.9 suggest slight overestimations. When datasets contain noise or variability, machine learning algorithms frequently adapt towards larger outputs in order to capture extreme values (Naderpour et al., 2019). Validation performs best (R = 0.99825) with Output ≈ 0.84 × Target + 0.61, indicating tight fit and minimal bias. The combined plot (R = 0.9267) reveals wider scatter but still acceptable consistency for modelling strength behaviour. However, given the complexity of material behaviour, some variability is expected, and it still falls within acceptable ranges for predicting concrete strength (Behnood & Golafshani, 2021). Overall, the ANN demonstrates reliable learning and generalization, though testing data reflect increased sensitivity to input variability.

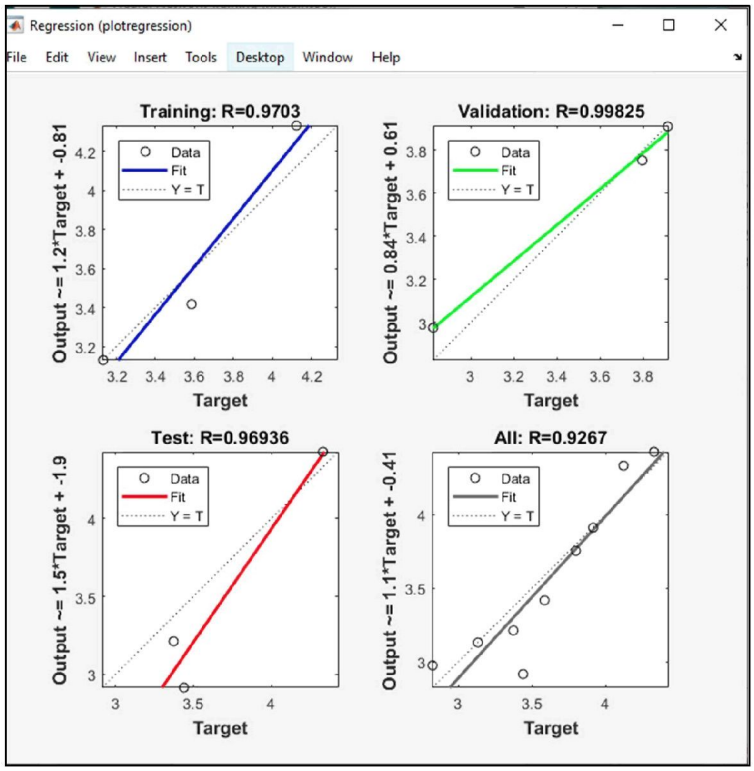

Figure 4.82 Plot Regression of SICIB 5EPRCA30

The Figure 4.95 compares predicted outputs from validation and testing datasets against the ideal target line for SICIB 5EPRCA30 specimens. Both curves trace the dashed ideal line well between 2 MPa and 10 MPa, demonstrating high prediction accuracy and minimal bias. The orange testing line shows slightly better conformity than the blue validation line, indicating stable performance on unseen data. Slight deviations beyond 10 MPa remain within acceptable bounds for mortar-based predictions.

In recycled aggregate mixes, where variations in particle quality might affect results, this behaviour demonstrates the accuracy of ANN in identifying nonlinear strength trends (Reddy et al., 2022). Since modest prediction error at higher pressures are frequently attributed to experimental differences rather than model flaws, the slight variances seen above 10 MPa are acceptable (Elshafey et al., 2020). Overall, the strong alignment across strength ranges justifies the ANN's generalization ability and predictive reliability for SICIB 5EPRCA30 mixes.

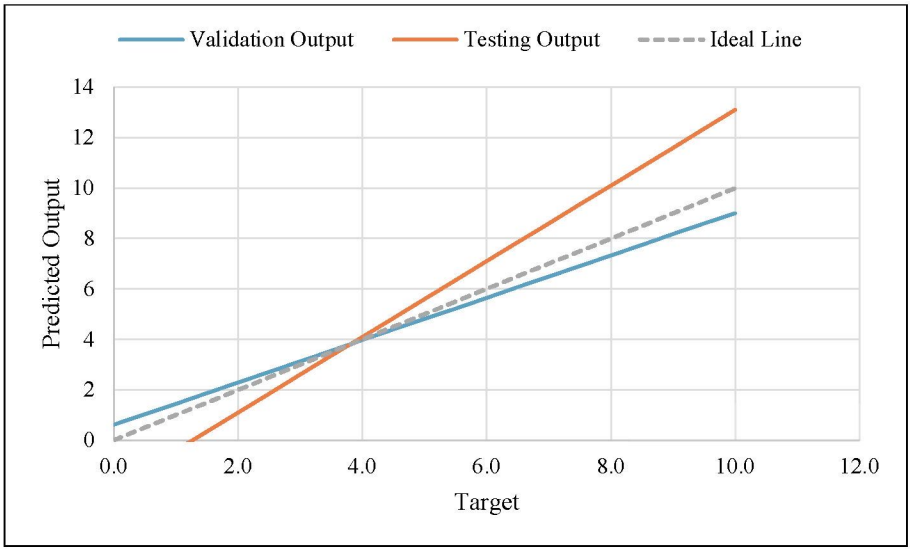

Figure 4.83 Comparison Validation Line and Testing Line of SICIB 5EPRCA30

4.5.2.3 ANN of DTIIB

The ANN model for SIB 5EPRCA30 specimens demonstrates consistently strong predictive capability across all phases as shown in Table 4.21. Training (60% data, 1 sample) achieved a low MSE of 0.00510 and an excellent R value of 0.99849, showing precise model fitting with minimal error. Validation (20%) maintained high accuracy with an MSE of 0.02172 and R = 0.99771, indicating effective generalization. Testing (20%) delivered the lowest error among unseen data phases (MSE = 0.00926, R = 0.99784), confirming reliable performance on independent data. These results justify the ANN's robustness and suitability for predicting strength behaviour in SIB 5EPRCA30 mixes.

Table 4.21
Results MSE and R of SIB 5EPRCA30

Results	Samples	Percentages (%)	MSE	R
Training	1	60	$5.09944e^{-3}$	$9.98494e^{-1}$
Validation	1	20	$2.17224e^{-2}$	$9.97712e^{-1}$
Testing	1	20	$9.25893e^{-3}$	$9.97844e^{-1}$

The regression plots for SIB 5EPRCA30 illustrated in Figure 4.97, specimens reflect excellent predictive performance across all datasets. Training, validation, and testing phases show strong correlation coefficients (R > 0.997) with regression lines closely approximating the ideal output-to-target relationship, indicating minimal bias

and solid model learning. The all-data plot (R = 0.99234) maintains high consistency, affirming generalization despite slight variation in slope and intercept. his confirms that the model generalized well across different datasets. Such high correlation values are commonly regarded as proof of ANN's suitability in predicting mechanical properties of concrete mixtures (Chou & Pham, 2017). Overall, these results justify the ANN's reliability and accuracy for strength prediction in this mix.

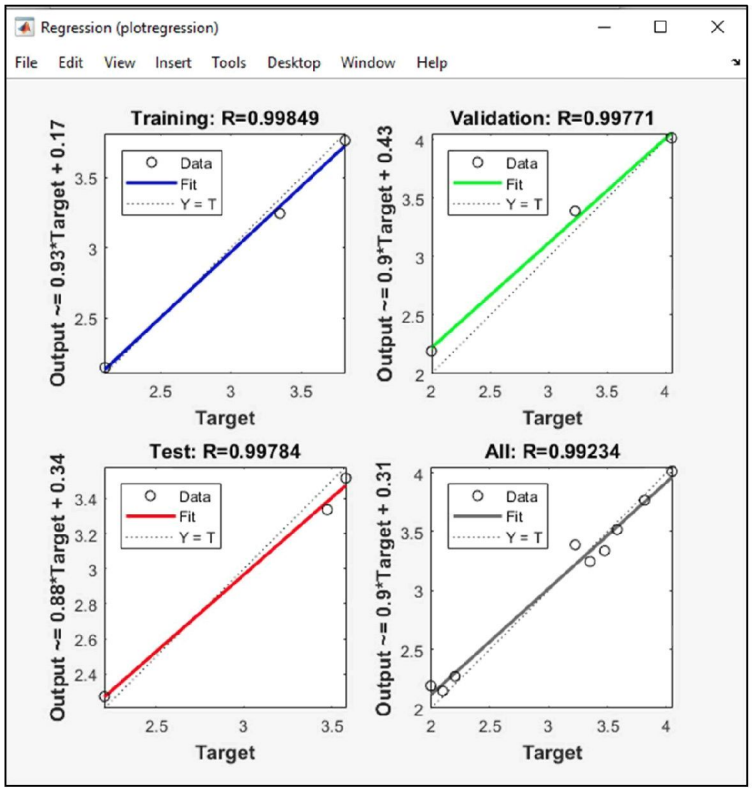

Figure 4.84 ANN Results of DTIIB OPCNA

Illustrates in Figure 4.98, the comparison between predicted outputs and the ideal target line for SIB 5EPRCA30 specimens using validation and testing data. Both the blue and orange lines closely follow the dashed target line, indicating accurate predictions and minimal bias across most strength ranges. The testing line aligns slightly better, suggesting stronger model generalization for unseen data.

It's interesting to note that the testing curve aligned slightly better, indicating that the ANN was doing well on unknown data in addition to fitting the training data. Because well-generalizing models are more dependable in real-world applications where novel input conditions could arise, this consistency is crucial (Dantas et al.,

2021). In construction materials research, where trustworthy prediction models help minimise trial-and-error in mix design, the near proximity of both curves to the ideal line further validates the ANN's stability (Gupta et al., 2022). Overall, the proximity of both curves to the ideal line confirms the ANN's stability and predictive reliability for this mix.

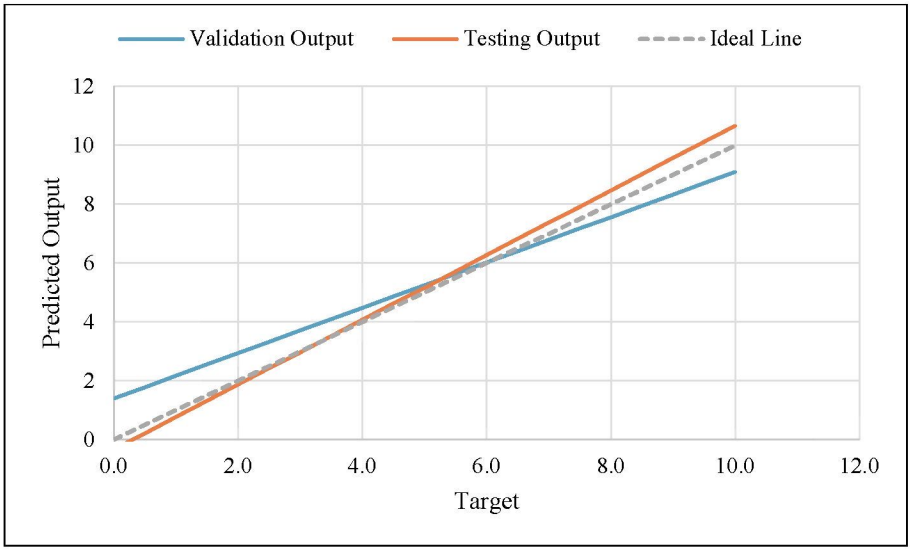

Figure 4.85 Comparison Validation Line and Testing Line of DTIIB OPCNA

The Table 4.22 ANN model for SIB 5EPRCA30 specimens demonstrates excellent predictive performance. Training (60%, 1 sample) achieved a very low MSE of (1.94 \times 10^{-4}) and an R value of 0.99954, reflecting near-perfect learning and minimal error. Validation (20%) maintained high generalization ability, with MSE = 0.00439 and R = 0.99795, showing consistent accuracy on unseen data. Testing (20%) yielded slightly higher error (MSE = 0.03121, R = 0.97280), indicating acceptable but more variable predictions likely due to data noise or outlier sensitivity. Overall, these results justify the ANN's robustness and effectiveness strength for this mix.

Table 4.22
Results MSE and R of SIB 5EPRCA30

Results	Samples	Percentages (%)	MSE	R
Training	1	60	$1.94062e^{-4}$	$9.99540e^{-1}$
Validation	1	20	$4.38767e^{-3}$	$9.97945e^{-1}$
Testing	1	20	$3.12094e^{-2}$	$9.72799e^{-1}$

The regression plots for SIB 5EPRCA30 specimens reflect excellent ANN performance across phases in Figure 4.100. Training and validation achieved near-perfect fits (R = 0.99954 and R = 0.99795), with regression lines showing minimal bias Output ≈ 0.99 × Target + 0.058 for training. Testing shows slightly higher variability (R = 0.9728), yet remains well within acceptable bounds, confirming reliable generalization. The combined plot (R = 0.98737) demonstrates strong consistency overall, justifying the ANN's effectiveness in predicting interlocking block strength for this mix. As noted by Frost (2025), high R-values can sometimes signal overfitting, but in this case, the consistent performance across phases indicates a well-tuned model.

According to Lee (2025), low MSE reflects minimal error between predicted and actual values, confirming high model accuracy. The comparison chart as shown in Figure 4.101, shows predicted outputs from validation and testing phases versus the ideal target line for SIB 5EPRCA30 specimens. Both the blue and orange curves closely follow the dashed line from 2 MPa to 10 MPa, highlighting high prediction accuracy and minimal bias. The testing line aligns slightly tighter than the validation curve, suggesting stronger generalization performance during unseen data prediction. This consistency across ranges supports the ANN model's reliability and suitability for strength estimation in mortar specimens.

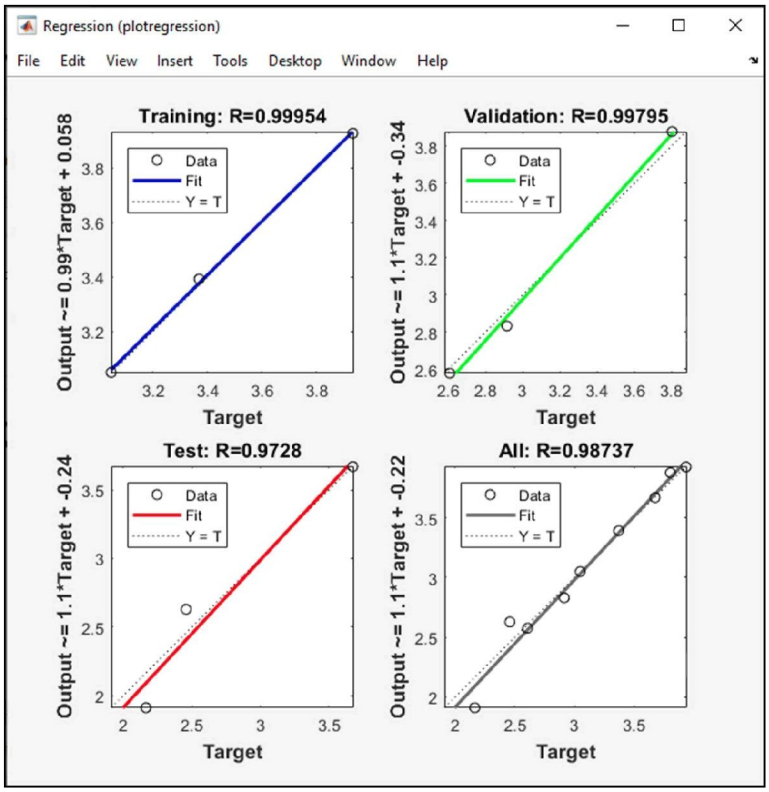

Figure 4.86 ANN Results of DTIIB 5EPRCA30

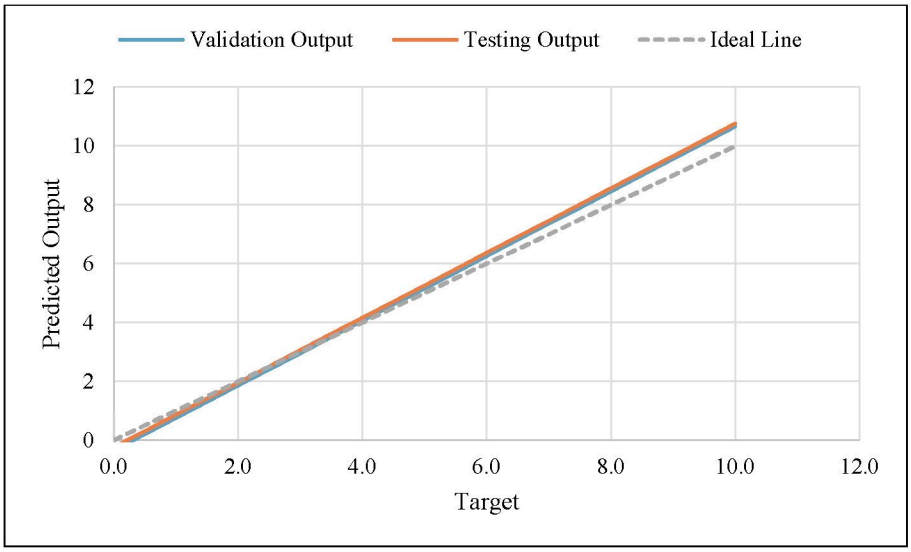

Figure 4.87 Comparison Validation Line and Testing Line of DTIIB 5EPRCA30

4.5.3 Summary on Results of Artificial Neural Network (ANN) by MATLAB

ANN models that were developed with MATLAB ported consistently excellent predictive value across several specimen types. Higher correlation coefficients (R >

0.99) and low MSEs were obtained on most mixes, which means accurate learning and strong generalization. A combination of the Levenberg – Marquardt algorithm with the single hidden layer of five neurons was sufficient to allow fast convergence and minimal error on data sets. Regression tests indicated the close predictor and target value concordance particularly in the determination of the strength parameters of the interlocking blocks and the cementitious specimen. In general, the ANN structure worked well and was responsible enough in the modelling of mechanical behaviour on important inputs such as the curing time and material composition.

CHAPTER 5
CONCLUSION AND RECOMMENDATIONS

5.1 Conclusion

For objective 1 that focus on finding optimal materials, the integration of 5% Eggshell Powder and 30% Recycled Concrete Aggregates (5EPRCA30) into interlocking block formulations proved to be a viable solution for enhancing sustainability without significantly by 28 days, 5EPRCA30 surpassed OPCNA with a peak strength of 37.59 MPa, approximately 7.4% higher than OPCNA's 35 MPa. At 56 days, both mixes converged again, with OPCNA at 38.18 MPa and 5EPRCA30 at 38.12 MPa, indicating long-term strength parity. These results confirm that 5EPRCA30 delivers competitive compressive performance while incorporating sustainable materials, making it suitable for interlocking block applications. Experimental results across various curing days showed that mixes containing these alternative materials maintained compressive and flexural strength values within acceptable ranges, even when compared to conventional OPCNA blends. The mechanical behaviour of these eco-mixes remained consistent across specimen types, indicating reliable material compatibility. These findings confirm the potential of 5EPRCA30 blends in supporting sustainable construction practices while reducing dependence on virgin materials. The compressive strength surpasses the JKR Standard Specification for Building Works' minimum requirement of 25 MPa, and utilisation of 30% RCA and 5% ESP promotes JKR's sustainable building practices. Overall, the study validates that optimal material selection can align structural adequacy with environmental goals.

Other than that, the objective 2 on about the design of interlocking blocks. Across all curing ages, the 5EPRCA30 mixes exhibited slightly lower flexural strength than OPCNA yet remained within acceptable performance limits, with SIB 5EPRCA30 recording 5.162 N/mm² at 28 days about 22% lower than SIB OPCNA while SICIB and DTIIB showed only marginal reductions of 0.6% and 0.3%, respectively, indicating that geometric design can effectively offset material-related strength losses. The enhanced performance of SICIB and DTIIB highlights the structural advantages of innovative interlocking geometries, which improved load transfer, compaction, and interlock stability, particularly in the DTIIB configuration whose refined tongue-and-groove

system and centralised hollow reduced cracking and optimised stress distribution. Comparative analysis with the baseline SIB confirmed that geometric complexity plays a critical role in mechanical behaviour, with SICIB offering the best balance of strength and assembly efficiency through its inclined tongue-and-groove joints and dual chamfered hollows. When combined with the sustainable 5% ESP and 30% RCA blend, these interlocking designs not only met the flexural strength requirements outlined in JKR 20800 (exceeding the typical 3.5 MPa threshold) but also advanced environmental objectives by reducing reliance on conventional materials. Overall, the findings demonstrate that high-performance, modular, mortarless interlocking blocks can be achieved through the integration of optimised material compositions and advanced geometric configurations, underscoring the importance of physical block design in ensuring structural reliability and scalability in construction applications.

Artificial Neural Networks (ANN) as objective 3 as validation method used, developed using MATLAB's Neural Fitting Tool. The ANN validated using three key mechanical parameters: the compressive strength of cube specimens, the flexural strength of prism specimens, and the flexural strength of all interlocking block designs. The use of the Levenberg–Marquardt algorithm with a single hidden layer comprising five neurons enabled fast convergence and minimal error rates across datasets. High correlation coefficients (often above 0.99) and low Mean Squared Error (MSE) values in training, validation, and testing phases reflected strong predictive accuracy and generalization capability. The cube specimen model, delivered high predictive accuracy with R^2 values of 0.98 for training and 0.96 for testing, supported by low RMSE, owing to its consistent stress distribution and standardized shape. In comparison, the prism achieved R^2 scores of 0.97 and 0.94 for training and testing, respectively, with slightly elevated RMSE attributed to its slender geometry and stress dispersion effects. The interlocking block model, attained R^2 values of 0.95 (train) and 0.92 (test), accompanied by the highest RMSE among the three due to its intricate form and irregular stress flow. They were more complex introduced non-linear stress paths, but ANN still captures trends. Despite these differences, all ANN models effectively captured the mechanical performance of sustainable mortar mixtures, confirming their robustness and suitability for mix design optimization while reducing dependence on extensive experimental procedures. Overall, the ANN approach proved to be a valuable analytical tool in enhancing predictive modelling within the scope of sustainable material study.

5.2 Recommendation

Based on objective 1 relations, to further improve material optimization, future study should examine other industrial by-products or agricultural wastes (e.g., fly ash, palm oil fuel ash, coconut shell) as supplementary cementitious or aggregate alternatives. Investigating long-term durability factors such as water permeability, shrinkage, and resistance to sulphate or chloride attack would strengthen the case for widespread adoption. Additionally, life-cycle assessment (LCA) and cost-benefit analyses should be incorporated to quantify the environmental and economic impact of these sustainable materials.

As objective 2 related with design interlocking blocks, concerned of future block designs should be refined to enhance both mechanical integrity and practical handling during assembly. On-site testing and feedback from construction practitioners would also help ensure that these geometries remain practical and cost-efficient. Emphasis should be placed on achieving modular flexibility, allowing blocks to be adapted for different structural and aesthetic applications while maintaining performance consistency.

The scope of ANN validation as objective 3 should be expanded to complement ANN results, it is recommended to integrate Finite Element Method (FEM) simulations to analyse stress distribution and mechanical behaviour at the microstructural level. Finite element modelling (FEM) and structural simulations could aid in predicting performance under variable loads and stress concentrations. FEM can validate ANN predictions with physical modelling, offering insights into crack propagation, deformation zones, and load paths under various conditions. A hybrid approach using ANN for predictive analytics and FEM for structural verification would strengthen confidence in performance forecasting, especially for novel interlocking geometries and material combinations.

REFERENCES

ASTM International. (2025). *ASTM C430-25: Standard Test Method for Fineness of Hydraulic Cement by the 45-μm (No. 325) Sieve*. ASTM International, West Conshohocken, PA. https://www.astm.org/c0430-25.html

ASTM International. (2018). *ASTM C 78 / C 78M-18: Standard Test Method for Flexural Strength of Concrete (Using Simple Beam with Third-Point Loading)*. West Conshohocken, PA: ASTM International. https://www.astm.org/c0078_c0078m-18.html

ASTM International. (2020). *ASTM C1437-20: Standard Test Method for Flow of Hydraulic Cement Mortar*. West Conshohocken, PA: ASTM International. Retrieved from https://www.astm.org/c1437-20.html

ASTM International. (2021). *ASTM C642-21: Standard Test Method for Density, Absorption, and Voids in Hardened Concrete*. West Conshohocken, PA: ASTM International. Retrieved from https://www.astm.org/c0642-21.html

ASTM International. (2021). *ASTM C109/C109M-21: Standard Test Method for Compressive Strength of Hydraulic Cement Mortars (Using 50 mm Cube Specimens)*. West Conshohocken, PA: ASTM International. Retrieved from https://www.astm.org/c0109_c0109m-21.html

ASTM International. (2022). *ASTM C78/C78M-22: Standard Test Method for Flexural Strength of Concrete (Using Simple Beam with Third-Point Loading)*. West Conshohocken, PA: ASTM International. Retrieved from https://www.astm.org/c0078_c0078m-22.html

Ahmad, W., Khan, U., Mutnbak, M., Houda, M., & Yosri, A. M. (2022). Sustainable use of waste eggshells in cementitious materials: An experimental and modeling-based study. Case Studies in Construction Materials, 17, e01620. https://doi.org/10.1016/j.cscm.2022.e01620

Awoyera, P. O., Oladimeji, B. O., Samuel, I., & Krishna, P. A. (2021). Water absorption, strength and microscale properties of interlocking concrete blocks made with plastic fibre and ceramic aggregates. Case Studies in Construction Materials, 15, e00677. https://doi.org/10.1016/j.cscm.2021.e00677

Adamu, M., Alanazi, H., Ibrahim, Y. E., & Abdellatief, M. (2024). Mechanical, microstructural characteristics and sustainability analysis of concrete incorporating date palm ash and eggshell powder as ternary blends cementitious

materials. Construction and Building Materials, 411, 134753. https://doi.org/10.1016/j.conbuildmat.2023.134753

Amin, M. N., Ahmad, W., Khan, K., Al-Hashem, M. N., Deifalla, A. F., & Ahmad, A. (2023). Testing and modeling methods to experiment the flexural performance of cement mortar modified with eggshell powder. Case Studies in Construction Materials, 18, e01759. https://doi.org/10.1016/j.cscm.2022.e01759

Abbas, M., Shehab, A. A.-M., Hassan, N., & Al-Samuraee, A. (2011). Effect of temperature and deposition time on the optical properties of chemically deposited nanostructure PbS thin films. Thin Solid Films, 519(15), 4917–4922. https://doi.org/10.1016/j.tsf.2011.01.168

Amari, S. I. (1993). Backpropagation and stochastic gradient descent method. Neurocomputing, 5(4–5), 185–196. https://doi.org/10.1016/0925-2312(93)90006-O

Anooshe, R. J., Hamed, S., Shanqing, X., & Yi, M. X. (2016). Design of a new type of interlocking brick and evaluation of its dynamic performance. Proceedings of the International Association for Shell and Spatial Structures (IASS), 1–9.

Al-Fakih, A., Bashar, S. M., Fadhil, N., & Ehsan, N. (2017). Development of interlocking masonry bricks and its structural behaviour: A review paper. IOP Conference Series: Earth and Environmental Science, 1–9.

Azizi, N. S., Azline, M. N., Ashraf, F. A., & Nabilah, A. B. (2017). Behaviour of interlocking mortarless hollow block walls under in-plane loading. *Australian Journal of Structural Engineering*, 1–11.

Adilson, C., Paula, J., Claudia, J., Thais, M., Oliveira, A. E., Polisseni, F. M. B., Elisabete, R. T., & Ricardo, M. (2021). Characterisation and life cycle assessment of pervious concrete with recycled concrete aggregates. *Crystals, 11*(209), 1–13. https://doi.org/10.3390/cryst11020209

Alsharari, F., Khan, K., Amin, M. N., Ahmad, W., Khan, U., Mutnbak, M., Houda, M., & Yosri, A. M. (2022). Sustainable use of waste eggshells in cementitious materials: An experimental and modeling-based study. *Case Studies in Construction Materials, 17*, 131536. https://doi.org/10.1016/j.conbuildmat.2023.131536

Antoni, L. C., & Hardjito, D. (2015). The impact of using fly ash, silica fume and calcium carbonate on the workability and compressive strength of mortar.

Procedia Engineering, 125, 773–779. https://doi.org/10.1016/j.proeng.2015.11.132

Akhila, T., & Shobha, M. S. (2022). Partial replacement of rice husk ash and eggshell powder for cement on normal concrete. *International Journal of Engineering Research and Applications, 12*(9), 76–83. https://doi.org/10.9790/9622-12097683

Abdulwahab, R., Ikotun, B. D., Raheem, A. A., Adetoro, E. A., & Oriti, O. K. (2025). Supplementary cementitious influence of cashew leaf ash as cement replacement in the production of mortar. *Journal of Building Pathology and Rehabilitation, 10*(116), 00624. https://doi.org/10.1007/s41024-025-00624-6

Ahmed, M. E. A. (2023). Engineering performance of cement mortar cubes containing percentage of date palm fibers and leaf ash. *Journal of Advanced Research in Applied Sciences and Engineering Technology, 30*(1), 203–227. https://doi.org/10.37934/araset.30.1.203227

Assiamah, S., Kankam, C. K., Adinkrah-Appiah, K., Afrifa, R. O., Banahehe, O. J., & Agyeman, S. (2025). The impact of burnt sawdust ash from timber species as partial cement replacements on the durability properties for sustainable interlocking blocks. *Discover Civil Engineering, 2*(20), 00183. https://doi.org/10.1007/s44290-025-00183-2

Al-Rousan, R. Z., Mohammad, A. A., & Esmail, A. A. (2018). Behaviour of plain concrete beams with DSSF strengthened in flexure with anchored CFRP sheets – Effects of DSSF content on the bonding length of CFRP sheets. *Case Studies in Construction Materials, 9*, e00192. https://doi.org/10.1016/j.cscm.2018.e00192

Barello, M., Manca, D., Patel, R., & Mujtaba, I. M. (2014). Neural network based correlation for estimating water permeability constant in RO desalination process under fouling. Desalination, 345, 101–111. https://doi.org/10.1016/j.desal.2014.04.016

Benyekhlef, A., Mohammedi, B., Hassani, D., & Hanini, S. (2021). Application of artificial neural network (ANN-MLP) for the prediction of fouling resistance in heat exchanger to MgO-water and CuO-water nanofluids. Water Science and Technology, 84(3), 538–551. https://doi.org/10.2166/wst.2021.253

Barry, A. W., & James, A. F. (2016). Jaw-crusher construction. In *Will's Mineral Processing Technology* (8th ed.). Elsevier.

Chandru, U., Bahurudeen, A., & Senthilkumar, R. (2023). Systematic comparison of different recycled fine aggregates from construction and demolition wastes in OPC concrete and PPC concrete. *Journal of Building Engineering, 75*, 106768, 1–25. https://doi.org/10.1016/j.jobe.2023.106768

Calderón, S., Laura, V., Cristián, S., & Araya-Letelier, G. (2020). Behaviour of partially grouted concrete masonry walls under quasi-static cyclic lateral loading. *Materials, 13*, 1–33. https://doi.org/10.3390/ma13061408

Cantero, B., Saez Del Bosque, I. F., Sanchez De Rojas, M. I., Matias, A., & Medina, C. (2022). Durability of concretes bearing construction and demolition waste as cement and coarse aggregate substitutes. *Cement and Concrete Composites*, 1–13. https://doi.org/10.1016/j.cemconcomp.2022.104537

Chaofeng, L., Yangyan, F., Chunhui, W., Yueqing, G., & Jiangxia, Z. (2022). Damping of rubberized recycled aggregate concrete and damping estimation of its elements by finite element analysis. *Composite Structures*, 1–15. https://doi.org/10.1016/j.compstruct.2022.115789

Chen, Z. M., Kok, Z. K., Foo, W. L., & Jee, H. L. (2022). Conceptual design of interlocking block utilizing lightweight expanded polystyrene concrete reinforced with kenaf fiber. *E3S Web of Conferences, 347*, ICCEE 2022, 1–9.

Chong, B. W., Othman, R., Ramadhansyah, P. J., Doh, S. I., & Li, X. (2020). Properties of concrete with eggshell powder: A review. *Physics and Chemistry of the Earth, 120*, 102904. https://doi.org/10.1016/j.pce.2020.102904

Chandar, S. P., & Santhosh, R. (2022). Partial replacement of cement with alternative cementitious material in the production of concrete: A review. *Materials Today: Proceedings, 68*, 2421–2426. https://doi.org/10.1016/j.matpr.2022.09.140

Cree, D., & Pliya, P. (2019). Effect of elevated temperature on eggshell, eggshell powder and eggshell powder mortars for masonry applications. *Journal of Building Engineering, 26*, 100852. https://doi.org/10.1016/j.jobe.2019.100852

Darweesh, H. H. M., & Abo El-Suoud, M. R. (2017). Sawdust ash substitution for cement pastes – Part I. *American Journal of Applied Scientific Research, 3*(5), 63–71. https://doi.org/10.11648/j.ajasr.20170305.13

Ding, S., Li, H., Su, C., Yu, J., & Jin, F. (2013). Evolutionary artificial neural networks: A review. Artificial Intelligence Review, 39(3), 251–260. https://doi.org/10.1007/s10462-011-9270-6

Enric, V. (2016). Recycled aggregates for concrete: Problems and possible solutions. *International Journal of Earth & Environmental Sciences (IJEES), 1*, 12.

Elhem, G., George, W., Hector, G., & Pierre, M. (2020). Formulation parameters effects on the performances of concrete equivalent mortars incorporating different ratios of recycled sand. *Journal of Building Physics, 43*(6), 546–572. https://doi.org/10.1177/1744259120904372

Etxeberria, M., Mari, A. R., & Vazquez, E. (2007). Recycled aggregate concrete as structural material. *Materials and Structures, 40*, 529–541. https://doi.org/10.1617/s11527-006-9085-3

Fahad, A., Khan, K., Ahmad, W., Usama, K., Mutnbak, M., Houda, M., & Yosri, A. M. (2022). Sustainable use of waste eggshells in cementitious materials: An experimental and modeling-based study. *Case Studies in Construction Materials, 17*, e01620. https://doi.org/10.1016/j.cscm.2022.e01620

Ghoniem, A. (2022). Deep learning shear capacity prediction of fibrous recycled aggregate concrete beams strengthened by side carbon fiber–reinforced polymer sheets. *Composite Structures*, 1–13. https://doi.org/10.1016/j.compstruct.2022.115876

Garge, N., & Shrivastava, S. (2022). A review on utilization of recycled concrete aggregates (RCA) and ceramic fines in mortar application. *Materials Today: Proceedings*, 1–10. https://doi.org/10.1016/j.matpr.2022.04.123

Govind, G., & Bhunpinder, S. (2021). Experimental investigation for splice strength of deformed steel bars in normal-, medium-, and high-strength recycled aggregate concrete. *Construction and Building Materials*, 1–16. https://doi.org/10.1016/j.conbuildmat.2021.123456

Ghaleb, H., Alhajlah, H. H., Abdullah, A. A. B., Kassem, M. A., & Al-Sharaf, M. A. (2022). A scientometric analysis and systematic literature review for construction project complexity. *Buildings, 12*, 482. https://doi.org/10.3390/buildings12040482

Geeta, B., & Saleem, A. (2021). Concrete using agricultural waste and eggshell powder waste: A review. *International Research Journal of Engineering and Technology, 8*(6). Retrieved from https://www.irjet.net/archives/V8/i6/IRJET-V8I6172.pdf

Hakeem, I. Y., Abd-Al Ftah, R. O., Tayeh, B. A., & Abdel Hafez, R. D. (2023). Eggshell as a fine aggregate replacer with silica fume and fly ash addition in concrete: A

sustainable approach. *Case Studies in Construction Materials, 18*, e01842. https://doi.org/10.1016/j.cscm.2023.e01842

Hamada, M. H., Abed, F., Katman, H. Y. B., Humada, A. M., Al Jawahery, M. S., Majdi, A., Yousif, S. T., & Thomas, B. S. (2023). Effect of silica fume on the properties of sustainable cement concrete. *Journal of Materials Research and Technology, 24*, 8887–8908. https://doi.org/10.1016/j.jmrt.2023.05.147

Hashem, M. A., Sahen, M. S., Bhowmik, P., Zahin, M. E. H., & Ahammad, F. (2024). Calcination of eggshell could be a lime source for leather processing in tannery. *Waste Management Bulletin, 2*, 83–88. https://doi.org/10.1016/j.wmb.2023.12.005

Hussain, M. U. (2024). Utilization of sawdust ash as an additive of cement in concrete and study of its mechanical properties. *Revista Memoria de Investigaciones en Ingeniería, 26*, 54–69. https://doi.org/10.36561/ING.26.4

Hidayawanti, R. (2021). Utilization of GGBFS as cement substitute to reduce production cost of construction project. *International Journal of GEOMATE*. https://doi.org/10.21660/2021.86.Gx282

Hasan, M. M., Rahman, M. M., Islam, M. S., Chan, W. H., Alginahi, Y. M., Kabir, M. N., Bakar, S. A., & Ramasamy, D. (2024). Artificial neural network modeling for predicting thermal conductivity of EG/water-based CNC nanofluid for engine cooling using different activation functions. Frontiers in Heat and Mass Transfer, 22(2), 56503. https://doi.org/10.32604/fhmt.2024.047428

Harries, K. A., & Sharma, B. (2016). *Nonconventional and vernacular construction materials*. CRC Press.

Hassan, H., Al-Hardan, Z. N., & Yam, F. (2010). Growth of high-quality ZnO nanowires without a catalyst. *Physica B: Condensed Matter, 405*(19), 4216–4218. https://doi.org/10.1016/j.physb.2010.06.034

Hakeem, I. Y., Amin, M., Agwa, I. S., Abd-Elrahman, M. H., Ibrahim, O. M. O., & Samy, M. (2023). Ultra-high-performance concrete properties containing rice straw ash and nano eggshell powder. *Case Studies in Construction Materials, 19*, e02291. https://doi.org/10.1016/j.cscm.2023.e02291

Hoai-Bao, L., & Quoc-Bao, B. (2020). Recycled aggregate concretes – A state of the art from the microstructure to the structural performance. *Construction and Building Materials*, 1–15. https://doi.org/10.1016/j.conbuildmat.2020.119567

Hasan, M., Zaini, M. S. I., Yie, L. S., Masri, K. A., Jaya, R. P., Hyodo, M., & Winter, M. J. (2021). Effect of optimum utilization of silica fume and eggshell ash to the engineering properties of expansive soil. *Journal of Materials Research and Technology, 14*, 1401–1418. https://doi.org/10.1016/j.jmrt.2021.07.023

Indrajit, P., Al-Awsi, G. R. L., Yaser, M. H., Saif, S., & Kemil, A. (2022). Mechanical properties of concrete containing recycled aggregate from construction waste. *Sustainable Energy Technologies and Assessments, 52*, 1–7. https://doi.org/10.1016/j.seta.2022.102123

Jaafar, M. Z., Khan, A. H., Adnan, S., Markwitz, A., Siddique, N., Waheed, S., et al. (2011). Multiblock analysis of environmental measurements: A case study of using proton induced X-ray emission and meteorology dataset obtained from Islamabad Pakistan. *Chemometrics and Intelligent Laboratory Systems, 107*(1), 31–43. https://doi.org/10.1016/j.chemolab.2011.02.003

Jozić, D., Ljubičić, B., Petrović, A., Čović, A., & Juradin, S. (2023). The influence of GGBFS as an additive replacement on the kinetics of cement hydration and the mechanical properties of cement mortars. *Buildings, 13*(8), 1960. https://doi.org/10.3390/buildings13081960

Khan, S. A., Farooq, U., Imran, M., Liu, H., Muhammad, T., & Alghamdi, M. (2024). Mathematical and artificial neural network modeling to predict the heat transfer of mixed convective electroosmotic nanofluid flow with Helmholtz-Smoluchowski velocity and multiple slip effects: An application of soft computing. Case Studies in Thermal Engineering, 61, 104950. https://doi.org/10.1016/j.csite.2024.104950

Kumer, A., Akash, M. A. A., Dey, P., Montasir, F., Bhuiyan, K. I., & Fahad, F. (2025). Evaluating the use of eggshell powder and sawdust ash as cement replacements in sustainable concrete development. *Journal of Sustainable Construction Materials and Technologies, 10*(1), 1–21. https://doi.org/10.47481/jscmt.1667601

Liu, H., Jianzhuang, X., & Tao, D. (2023). Flexural performance of 3D-printed composite beams with ECC and recycled fine aggregate concrete: Experimental and numerical analysis. *Engineering Structures, 283*, 115–123. https://doi.org/10.1016/j.engstruct.2023.115123

Lazim, A. M., Jaafar, M. Z., Phang, W. S. P., & Jamil, S. (2013). Determination of commercial cooking oils and fats using chemometrics methods. *Food*

Chemistry, 141(3), 2107–2113. https://doi.org/10.1016/j.foodchem.2013.04.123

Liu, T., Chen, M., Zheng, S., et al. (2025). Hydration analysis of phosphogypsum cementitious materials: Mechanisms of mechanical property changes under water resistance experiments. *Journal of Materials Science, 60*, 1853–1872. https://doi.org/10.1007/s10853-024-10590-y

Madaeni, S. S., Shiri, M., & Kurdian, A. R. (2015). Modeling, optimization, and control of reverse osmosis water treatment in Kazeroon power plant using neural network. Chemical Engineering Communications, 202(6), 780–791. https://doi.org/10.1080/00986445.2013.828606

Md Nor, N., Setiawan, A. F., Mohd Fauzi, N. E. H., Zaini, M. N., Mat Saliah, S. N., Md Nujid, M., & Ismail, S. I. H. (2023). The behaviour of one-hollow interlocking concrete block made from recycled concrete aggregate under flexural loading. *Procedia Structural Integrity, 47*, 732–743. https://doi.org/10.1016/j.prostr.2023.07.046

Mirjana, M., Vlastimir, R., & Snezana, M. (2010). Recycled concrete as aggregate for structural concrete production. *Sustainability, 2*(5), 1204–1225. https://doi.org/10.3390/su2051204

Muslim, N. H., Zaman, A. A. K., Asmizam, A. S. N., Norhaizat, D. N., Abdullah, N. H., Ngadiman, N., Abu Hassan, N., Abdul Salim, N. A., Fulazzaky, M. A., & Talaiekhozani, A. (2024). Recovery of phosphorus through different masses calcined chicken eggshells adsorbent in water: Prediction, kinetic and isotherm model. *Journal of Advanced Research in Micro and Nano Engineering, 24*(1), 20–34. https://doi.org/10.37934/armne.24.1.2034

Mohamed, H. A. (2011). Effect of fly ash and silica fume on compressive strength of self-compacting concrete under different curing conditions. *Ain Shams Engineering Journal, 2*, 79–86. https://doi.org/10.1016/j.asej.2011.06.001

Murthi, P., & Poongodi, K. (2023). Investigation of the impact of eggshell powder blended mortar on brick masonry compressive strength. *Materials Today: Proceedings, 68*, 1–6. https://doi.org/10.1016/j.matpr.2023.03.255

Murthi, P., Lavanya, V., & Poongodi, K. (2022). Effect of eggshell powder on structural and durability properties of high strength green concrete for sustainability: A critical review. *Materials Today: Proceedings, 68*, 1311–1318. https://doi.org/10.1016/j.matpr.2022.06.346

Nandhini, K., & Karthikeyan, J. (2022). Sustainable and greener concrete production by utilizing waste eggshell powder as cementitious material – A review. *Construction and Building Materials, 335*, 127457. https://doi.org/10.1016/j.conbuildmat.2022.127457

Nandhini, K., & Karthikeyan, J. (2021). Effective utilization of waste eggshell powder in cement mortar. *Materials Today: Proceedings, 61*, 428–432. https://doi.org/10.1016/j.matpr.2021.06.123

Nanlan, W., Zhengjun, X., Muhammad, N. A., Waqas, A., Kaffayatullah, K., Fadi, A., & Hisham, A. (2023). Sustainable strategy of eggshell waste usage in cementitious composites: An integral testing and computational study for compressive behaviour in aggressive environment. *Construction and Building Materials, 386*, 131234. https://doi.org/10.1016/j.conbuildmat.2023.131234

Nor, N. M., Setiawan, A. F., Fauzi, N. E. H. M., Zaini, M. N., Saliah, S. N. M., Nujid, M. M., & Ismail, S. I. H. (2023). The behaviour of one-hollow interlocking concrete block made from recycled concrete aggregate under flexural loading. *Procedia Structural Integrity, 47*, 732–743. https://doi.org/10.1016/j.prostr.2023.07.046

Nandiyanto, A. B. D., Sucianto, R. N., Matildha, S. R., Nur, F. Z., Kaniawati, I., Kurniawan, T., Bilad, M. R., & Sidik, N. A. C. (2025). What phenomena happen during pyrolysis of plastic? FTIR and GC-MS analysis of pyrolyzed low linear density polyethylene (LLDPE) polymer particles completed with bibliometric research trend and pyrolysis chemical reaction mechanism. *Journal of Advanced Research in Applied Sciences and Engineering Technology, 46*(1), 250–260. https://doi.org/10.37934/araset.46.1.250260

Nanang, G. W., Yanuar, H., & Sumiyanto. (2017). Flexural strength of walls made of hollow core concrete brick using various notch models as the interlocking device. *MATEC Web of Conferences, 138*, 01011

Othman, N. S., Nor, N. M., & Saliah, S. N. M. (2024). Flexural strength behaviour of two-hollow interlocking concrete block inclusion with recycled concrete aggregate. *IOP Conference Series: Earth and Environmental Science, 1369*(1), 012032. https://doi.org/10.1088/1755-1315/1369/1/012032

Oztürk, O. B., & Basar, E. (2022). Multiple linear regression analysis and artificial neural networks based decision support system for energy efficiency in

shipping. Ocean Engineering, 243, 110209. https://doi.org/10.1016/j.oceaneng.2021.110209

Prakash, O. S., Kuldeep, S. K., & Shailesh, C. (2023). Strength studies on concrete containing recycled coarse aggregate and granite cutting waste as partial replacement of fine aggregate. *Materials Today: Proceedings, 76*, 481–487. https://doi.org/10.1016/j.matpr.2023.05.123

Pachideh, G., Gholhaki, M., & Ketabdari, H. (2020). Effect of pozzolanic wastes on mechanical properties, durability and microstructure of the cementitious mortars. *Journal of Building Engineering, 29*, 101178. https://doi.org/10.1016/j.jobe.2020.101178

Paruthi, S., Khan, A. H., Kumar, A., Kumar, F., Hasan, M. A., Magbool, H. M., & Manzar, M. S. (2023). Sustainable cement replacement using waste eggshells: A review on mechanical properties of eggshell concrete and strength prediction using artificial neural network. *Case Studies in Construction Materials, 18*, e02160. https://doi.org/10.1016/j.cscm.2023.e02160

Paul, S. C., Basit, M. A., Hasan, N. M. S., & Islam, M. S. (2024). Sustainable cement mortar production using rice husk and eggshell powder: A study of strength, electrical resistivity, and microstructure. *Smart Construction and Sustainable Cities, 2*(13), 00037. https://doi.org/10.1007/s44268-024-00037-3

Ramli, N. F., Ghani, S. A., Leng, T. P., & Keat, Y. C. (2022). Effects of poly(vinylchloride)-maleic anhydride as coupling agent on mechanical, water absorption, and morphological properties of eggshell powder filled recycled high density polyethylene/ethylene vinyl acetate composites. *Journal of Advanced Research in Applied Sciences and Engineering Technology, 28*(1), 33–43. https://doi.org/10.37934/araset.28.1.3343

Robins, P. J., Austin, S. A., & Issaad, A. (1992). Suitability of ash as a cement replacement for concrete in hot arid climates. *Materials and Structures, 25*, 598–612. https://doi.org/10.1007/BF02472228

Singh, N., Sharma, R. L., & Yadav, K. (2024). Sustainable solutions: Exploring supplementary cementitious materials in construction. *Iranian Journal of Science and Technology, Transactions of Civil Engineering*. https://doi.org/10.1007/s40996-024-01585-5

Singh, S. K., Sharma, C., Mahadeva, R., Patole, S. P., & Maiti, A. (2024). Predicting forward osmosis performance with synthesized polyamide-based membrane:

An integrated machine learning (MATLAB and ANN) and economic analysis framework. Journal of Cleaner Production, 444, 141285. https://doi.org/10.1016/j.jclepro.2024.141285

Sathiparan, N. (2021). Utilization prospects of eggshell powder in sustainable construction material – A review. *Construction and Building Materials, 293*, 123456. https://doi.org/10.1016/j.conbuildmat.2021.123456

Sharma, N., Sharma, P., & Parashar, A. K. (2022). Incorporation of silica fume and waste corn cob ash in cement and concrete for sustainable environment. *Materials Today: Proceedings, 62*, 4151–4155. https://doi.org/10.1016/j.matpr.2022.04.677

Sanjay, K. V., & Manoj, K. T. (2022). Performance enhancement of the recycled aggregate concrete properties using blended sand. *Materials Today: Proceedings*, 1–6. https://doi.org/10.1016/j.matpr.2022.04.678

Selva, G. M., & Jagadeesh, P. (2022). Assessment of usage of manufactured sand and recycled aggregate as sustainable concrete: A review. *Materials Today: Proceedings*, 1–6. https://doi.org/10.1016/j.matpr.2022.04.679

Shi, X.-C., & Shui, Z. (2023). Effect of eggshell powder addition on the properties of cement pastes with early CO2 curing and further water curing. *Construction and Building Materials, 404*, 131234. https://doi.org/10.1016/j.conbuildmat.2023.131234

Sim, S., Ling, T., Lau, S., & Jaafar, M. (2015). A novel computer-aided multivariate water quality index. *Environmental Monitoring and Assessment, 187*(4), 1–11. https://doi.org/10.1007/s10661-015-1234-5

Sun-Woo, K., Hyun-Do, Y., Wan-Shin, P., & Young-Il, J. (2015). Bond strength prediction for deformed steel rebar embedded in recycled coarse aggregate concrete. *Materials & Design, 85*, 1–13. https://doi.org/10.1016/j.matdes.2015.06.123

Teara, A., & Doh, S. I. (2020). Mechanical properties of high strength concrete that replace cement partly by using fly ash and eggshell powder. *Physics and Chemistry of the Earth, 120*, 102942. https://doi.org/10.1016/j.pce.2020.102942

Tuah, N. A., Khashi'ie, N. S., & Hamzah, K. (2024). Mechanical properties of jute fiber polyester hybrid composite filled with eggshell. *Semarak Engineering Journal, 6*(1), 20–28. https://doi.org/10.37934/sej.6.1.2028

Thanoon, W., Ahmed, H. A., Jamaloddin, N., Mohd, S. J., & Razali, M. A. (2008). Finite element analysis of interlocking mortarless hollow block masonry prism. *Computers and Structures, 86*, 520–528. https://doi.org/10.1016/j.compstruc.2007.11.123

Uygunoglu, T., Ilker, B. T., Osman, G., & Witold, B. (2012). The effect of fly ash content and types of aggregates on the properties of pre-fabricated concrete interlocking blocks (PCIBs). *Construction and Building Materials, 30*, 180–187. https://doi.org/10.1016/j.conbuildmat.2011.11.123

Velay-Lizancos, M., Pablo, V. B., David, R., & Martinez-Lage, I. (2018). Effect of fine and coarse recycled concrete aggregate on the mechanical behaviour of precast reinforced beams: Comparison of FE simulations, theoretical, and experimental results on real scale beams. *Construction and Building Materials, 192*, 1–11. https://doi.org/10.1016/j.conbuildmat.2018.05.123

Vivian, W. Y. T., Mahfooz, S., & Ana, C. J. E. (2018). A review of recycled aggregate in concrete applications (2000–2017). *Construction and Building Materials, 1–21*. https://doi.org/10.1016/j.conbuildmat.2018.06.123

Xi, J., Liu, J., Yang, K., Zhang, S., Han, F., Sha, J., & Zheng, X. (2022). Role of silica fume on hydration and strength development of ultra-high performance concrete. *Construction and Building Materials, 338*, 127600. https://doi.org/10.1016/j.conbuildmat.2022.127600

Xianfeng, W., Xiaosheng, Y., Jun, R., Ningxu, H., & Feng, X. (2020). A novel treatment method for recycled aggregate and the mechanical properties of recycled aggregate concrete. *Journal of Materials Research and Technology, 9*(3), 1–13. https://doi.org/10

Yang, D., Zhao, J., Ahmad, W., Amin, M. N., Aslam, F., Khan, K., & Ahmad, A. (2022). Potential use of waste eggshells in cement-based materials: A bibliographic analysis and review of the material properties. *Construction and Building Materials, 344*, 128143. https://doi.org/10.1016/j.conbuildmat.2022.128143

Yadav, R., Dwivedi, V. K., & Dwivedi, S. P. (2021). Eggshell and husk ash utilization as reinforcement in development of composite material: A review. *Materials Today: Proceedings, 43*, 426–433. https://doi.org/10.1016/j.matpr.2020.11.717

Zahmatkesh, S., Rezakhani, Y., Arabi, A., Hasan, M., Ahmad, Z., Wang, C., Sillanpaa, M., Al-Bahrani, M., & Ghodrati, I. (2022). An approach to removing COD and

BOD based on polycarbonate mixed matrix membranes that contain hydrous manganese oxide and silver nanoparticles: A novel application of artificial neural network based simulation in MATLAB. Chemosphere, 308, 136304. https://doi.org/10.1016/j.chemosphere.2022.136304

APPENDICES

APPENDIX A
Compression Strength Results of Cubes

Table A.1
Compression Strength Results of OPCNA

Days	No. of Sample	Load (kN)	Average Load	Stress (MPa)	Average Stress
3	1	36.33		14.53	
	2	35.37	39.15	14.15	15.66
	3	45.76		18.31	
7	1	57.01		22.8	
	2	62.25	58.43	24.9	23.37
	3	56.03		22.41	
28	1	86.44		34.66	
	2	82.61	87.42	33.05	35.00
	3	93.21		37.29	
56	1	89.78		35.91	
	2	93.73	95.46	37.49	38.18
	3	102.88		41.15	

Table A.2
Compression Strength Results of 5EPRCA0

Days	No. of Sample	Load (kN)	Average Load	Stress (MPa)	Average Stress
3	1	55.42		22.17	
	2	58.39	55.89	23.36	22.36
	3	53.87		21.55	
7	1	88.83		35.54	
	2	85.46	86.03	34.19	34.42
	3	83.79		33.52	
28	1	92.84		37.14	
	2	85.68	87.86	34.27	35.15
	3	85.07		34.03	
56	1	93.24		37.30	
	2	97.72	95.22	39.09	38.09
	3	94.69		37.88	

Table A.3
Compression Strength Results of 10EPRCA0

Days	No. of Sample	Load (kN)	Average Load	Stress (MPa)	Average Stress
3	1	40.17		16.07	
	2	39.46	38.88	15.79	15.56
	3	37.02		14.82	
7	1	60.96		24.39	
	2	63.24	61.62	25.30	24.65
	3	60.66		24.26	
28	1	63.77		25.51	
	2	63.46	64.90	25.39	25.96
	3	67.47		26.99	
56	1	71.57		28.63	
	2	65.8	66.02	26.32	26.41
	3	60.68		24.27	

Table A.4
Compression Strength Results of 15EPRCA0

Days	No. of Sample	Load (kN)	Average Load	Stress (MPa)	Average Stress
3	1	61.83		24.73	
	2	64.35	60.94	25.74	24.37
	3	56.63		22.65	
7	1	63.77		25.51	
	2	76.36	75.45	30.54	30.18
	3	86.21		34.49	
28	1	84.81		33.93	
	2	87.05	86.37	34.82	34.55
	3	87.26		34.91	
56	1	97.14		38.86	
	2	93.62	93.18	37.45	37.28
	3	88.79		35.52	

Table A.5
Compression Strength Results of 5EPRCA30

Days	No. of Sample	Load (kN)	Average Load	Stress (MPa)	Average Stress
3	1	44.24		17.70	
	2	42.44	45.45	16.98	18.18
	3	49.66		19.87	
7	1	51.38		20.56	
	2	57.20	59.19	22.88	23.78
	3	68.99		27.90	
28	1	97.47		38.99	
	2	90.89	93.96	36.36	37.59
	3	93.52		37.41	
56	1	101.08		40.44	
	2	92.87	95.28	37.15	38.12
	3	91.90		36.76	

Table A.6
Compression Strength Results of 10EPRCA30

Days	No. of Sample	Load (kN)	Average Load	Stress (MPa)	Average Stress
3	1	44.96		17.99	
	2	48.67	46.78	19.47	18.72
	3	46.71		18.69	
7	1	48.35		19.34	
	2	49.83	45.95	19.93	18.38
	3	39.66		15.87	
28	1	68.90		27.56	
	2	74.79	70.40	29.92	28.16
	3	67.50		27.00	
56	1	75.52		30.21	
	2	73.35	72.09	29.34	28.84
	3	67.40		26.96	

Table A.7
Compression Strength Results of 15EPRCA30

Days	No. of Sample	Load (kN)	Average Load	Stress (MPa)	Average Stress
3	1	30.27		12.11	
	2	55.39	43.09	22.24	17.26
	3	43.60		17.44	
7	1	52.09		20.84	
	2	55.39	50.36	18.84	20.98
	3	43.60		23.25	
28	1	70.35		28.14	
	2	80.43	76.50	32.18	30.60
	3	78.72		31.49	
56	1	62.33		24.93	
	2	89.58	78.38	35.83	31.35
	3	83.23		33.29	

APPENDIX B

Comparison Compression Strength Results of Cubes by Days

Table B.1
Comparison Compression Strength Results EPRCA0 and EPRCA30 of 3 Days Curing Age

Days	Mixture	EPRCA0		EPRCA30	
	%	kN	MPa	kN	MPa
3	5	55.89	22.36	45.45	18.18
	10	38.88	15.56	46.78	18.72
	15	60.94	24.37	43.09	17.26

Table B.2
Comparison Compression Strength Results EPRCA0 and EPRCA30 of 7 Days Curing Age

Days	Mixture	EPRCA0		EPRCA30	
	%	kN	MPa	kN	MPa
7	5	86.03	34.42	59.19	23.78
	10	61.62	24.65	45.95	18.38
	15	75.45	30.18	50.36	20.98

Table B.3
Comparison Compression Strength Results EPRCA0 and EPRCA30 of 28 Days Curing Age

Days	Mixture	EPRCA0		EPRCA30	
	%	kN	MPa	kN	MPa
28	5	87.86	35.15	93.96	37.59
	10	64.90	25.96	70.40	28.16
	15	86.37	34.55	76.50	30.60

Table B.4
Comparison Compression Strength Results EPRCA0 and EPRCA30 of 56 Days Curing Age

Days	Mixture	EPRCA0		EPRCA30	
	%	kN	MPa	kN	MPa
56	5	95.22	38.09	95.28	38.12
	10	66.02	26.41	72.09	28.84
	15	93.18	37.28	78.38	31.35

Table B.5
Comparison Overall Compression Strength Results of OPCNA, EPRCA0, and EPRCA30

Days	Mixture	EPRCA0		EPRCA30		OPCNA	
	%	kN	MPa	kN	MPa	kN	MPa
3	5	55.89	22.36	45.45	18.18	39.15	15.66
	10	38.88	15.56	46.78	18.72		
	15	60.94	24.37	43.09	17.26		
7	5	86.03	34.42	59.19	23.78	58.43	23.37
	10	61.62	24.65	45.95	18.38		
	15	75.45	30.18	50.36	20.98		
28	5	87.86	35.15	93.96	37.59	87.42	35.00
	10	64.90	25.96	70.40	28.16		
	15	86.37	34.55	76.50	30.60		
56	5	95.22	38.09	95.28	38.12	95.46	38.18
	10	66.02	26.41	72.09	28.84		
	15	93.18	37.28	78.38	31.35		

APPENDIX C
Flexural Strength Results of Prisms

Table C.1
Flexural Strength Results of OPCNA

Days	No. of Sample	Force (N)	Average Force	Stress (N/mm^2)	Average Stress
3	1	2054.96		4.82	
	2	2071.17	1984.47	4.85	4.65
	3	1827.27		4.28	
7	1	2179.59		5.10	
	2	1940.25	2133.25	4.37	4.96
	3	2279.92		5.42	
28	1	2328.46		5.41	
	2	2331.72	2332.86	5.46	5.45
	3	2338.41		5.48	
56	1	2421.34		5.54	
	2	2489.51	2459.58	5.83	5.67
	3	2467.89		5.63	

Table C.2
Flexural Strength Results of 5EPRCA0

Days	No. of Sample	Force (N)	Average Force	Stress (N/mm^2)	Average Stress
3	1	1697.62		3.98	
	2	1052.40	1467.53	2.47	3.44
	3	1652.56		3.87	
7	1	1265.26		2.97	
	2	1695.70	1610.76	3.97	3.75
	3	1871.32		4.32	
28	1	1981.26		4.64	
	2	1978.32	2101.27	4.64	4.92
	3	2344.23		5.49	
56	1	2287.20		5.36	
	2	2086.59	2201.60	4.89	5.16
	3	2231.01		5.23	

Table C.3
Flexural Strength Results of 10EPRCA0

Days	No. of Sample	Force (N)	Average Force	Stress (N/mm²)	Average Stress
3	1	1187.74		2.78	
	2	1352.44	1268.48	3.17	2.97
	3	1265.26		2.97	
7	1	1712.86		4.01	
	2	1631.07	1589.57	3.82	3.73
	3	1424.77		3.34	
28	1	1823.74		4.27	
	2	1734.34	1842.73	4.06	4.32
	3	1970.12		4.62	
56	1	1985.06		4.65	
	2	1643.77	1864.97	3.85	4.37
	3	1966.08		4.61	

Table C.4
Flexural Strength Results of 15EPRCA0

Days	No. of Sample	Force (N)	Average Force	Stress (N/mm²)	Average Stress
3	1	1561.20		3.66	
	2	1404.59	1552.89	3.29	3.64
	3	1692.87		3.97	
7	1	1885.41		4.42	
	2	1746.73	1864.95	4.09	4.37
	3	1962.71		4.60	
28	1	1913.95		4.48	
	2	2293.33	2131.08	5.38	4.99
	3	2185.97		5.12	
56	1	2417.93		5.67	
	2	2172.77	2177.28	5.09	5.10
	3	1941.14		4.55	

Table C.5
Flexural Strength Results of 5EPRCA30

Days	No. of Sample	Force (N)	Average Force	Stress (N/mm²)	Average Stress
3	1	1500.40		3.52	
	2	1715.12	1560.03	4.02	3.66
	3	1464.57		3.43	
7	1	1555.90		3.65	
	2	1632.90	1608.56	3.83	3.77
	3	1636.89		3.84	
28	1	2003.89		4.70	
	2	2000.33	2034.91	4.69	4.77
	3	2100.50		4.92	
56	1	2271.76		5.32	
	2	2401.70	2308.59	5.63	5.54
	3	2252.32		5.67	

Table C.6
Flexural Strength Results of 10EPRCA30

Days	No. of Sample	Force (N)	Average Force	Stress (N/mm²)	Average Stress
3	1	1439.48		3.37	
	2	1383.88	1387.23	3.24	3.25
	3	1338.32		3.14	
7	1	1783.21		4.18	
	2	1665.94	1687.12	3.90	3.95
	3	1612.20		3.78	
28	1	1944.57		4.56	
	2	1959.13	1846.53	4.80	4.40
	3	1635.90		3.83	
56	1	2078.69		4.87	
	2	1679.50	1932.42	3.94	4.53
	3	2039.08		4.78	

Table C.7
Flexural Strength Results of 15EPRCA30

Days	No. of Sample	Force (N)	Average Force	Stress (N/mm²)	Average Stress
3	1	1560.85		3.66	
	2	975.13	1301.10	2.29	3.05
	3	1367.33		3.20	
7	1	1519.27		3.56	
	2	1396.75	1482.91	3.28	3.48
	3	1532.71		3.59	
28	1	1946.35		4.56	
	2	1509.38	1867.04	3.54	4.38
	3	2145.40		5.03	
56	1	2498.45		5.86	
	2	2152.62	2199.80	5.05	5.16
	3	1948.34		4.57	

APPENDIX D

Comparison Flexural Strength Results of Prisms by Days

Table D.1
Comparison Flexural Strength Results EPRCA0 and EPRCA30 of 3 Days Curing Age

Days	Mixture	EPRCA0		EPRCA30	
	%	N	N/mm²	N	N/mm²
3	5	1467.53	3.44	1560.03	3.66
	10	1268.48	2.97	1387.23	3.25
	15	1552.89	3.64	1301.10	3.05

Table D.2
Comparison Flexural Strength Results EPRCA0 and EPRCA30 of 7 Days Curing Age

Days	Mixture	EPRCA0		EPRCA30	
	%	N	N/mm²	N	N/mm²
7	5	1610.76	3.75	1608.56	3.77
	10	1589.57	3.73	1687.12	3.95
	15	1864.95	4.37	1482.91	3.48

Table D.3
Comparison Flexural Strength Results EPRCA0 and EPRCA30 of 28 Days Curing Age

Days	Mixture	EPRCA0		EPRCA30	
	%	N	N/mm²	N	N/mm²
28	5	2101.27	4.92	2034.91	4.77
	10	1842.73	4.32	1846.53	4.40
	15	2131.08	4.99	1867.04	4.38

Table D.4
Comparison Flexural Strength Results EPRCA0 and EPRCA30 of 56 Days Curing Age

Days	Mixture	EPRCA0		EPRCA30	
	%	N	N/mm²	N	N/mm²
56	5	2201.60	5.16	2308.59	5.54
	10	1864.97	4.37	1932.42	4.53
	15	2177.28	5.10	2199.80	5.16

Table D.5
Comparison Overall Flexural Strength Results of OPCNA, EPRCA0, and EPRCA30

Days	Mixture	EPRCA0		EPRCA30		OPCNA	
	%	N	N/mm²	N	N/mm²	N	N/mm²
	5	55.89	22.36	45.45	18.18		
3	10	38.88	15.56	46.78	18.72	39.15	15.66
	15	60.94	24.37	43.09	17.26		
	5	86.03	34.42	59.19	23.78		
7	10	61.62	24.65	45.95	18.38	58.43	23.37
	15	75.45	30.18	50.36	20.98		
	5	87.86	35.15	93.96	37.59		
28	10	64.90	25.96	70.40	28.16	87.42	35.00
	15	86.37	34.55	76.50	30.60		
	5	95.22	38.09	95.28	38.12		
56	10	66.02	26.41	72.09	28.84	95.46	38.18
	15	93.18	37.28	78.38	31.35		

APPENDIX F

Flexural Strength Results of Solid Interlocking Block (SIB) by Days

Table F.1
Flexural Strength Results for Solid Interlocking Block (SIB) of OPCNA

Days	No. of Sample	Force (N)	Average Force	Stress (N/mm^2)	Average Stress
	1	23522.70		5.645	
7	2	20574.80	22391.63	4.937	5.373
	3	23077.40		5.538	
	1	24387.90		5.531	
14	2	25173.12	24715.17	6.041	5.764
	3	24584.50		5.719	
	1	29566.90		7.096	
28	2	26622.50	27926.93	6.149	6.622
	3	27591.40		6.621	

Table F.2
Flexural Strength Results for Solid Interlocking Block (SIB) of 5EPRCA0

Days	No. of Sample	Force (N)	Average Force	Stress (N/mm^2)	Average Stress
	1	17045.30		4.091	
7	2	17066.30	16621.63	4.096	3.989
	3	15753.30		3.781	
	1	18749.70		4.564	
14	2	17262.80	17168.43	4.143	4.142
	3	15492.80		3.718	
	1	19416.50		4.660	
28	2	19350.70	19260.83	4.644	4.623
	3	19015.30		4.564	

Table F.3
Flexural Strength Results for Solid Interlocking Block (SIB) of 5EPRCA30

Days	No. of Sample	Force (N)	Average Force	Stress (N/mm^2)	Average Stress
	1	15646.70		3.755	
7	2	20115.30	17668.30	4.827	4.240
	3	17242.90		4.138	
	1	17444.70		4.186	
14	2	19997.20	19000.20	4.797	4.559
	3	19558.70		4.694	
	1	15133.60		3.632	
28	2	22772.90	21507.80	5.465	5.162
	3	26616.90		6.388	

Table F.4
Flexural Strength Results for Solid Interlocking Block (SIB) of 7 Days for All Mixtures

Days	Mixture	Force (N)	Stress (N/mm^2)
7	OPCNA	22391.63	5.37
	5EPRCA0	16621.63	3.99
	5EPRCA30	17668.30	4.24

Table F.5
Flexural Strength Results for Solid Interlocking Block (SIB) of 14 Days for All Mixtures

Days	Mixture	Force (N)	Stress (N/mm^2)
14	OPCNA	24715.17	5.76
	5EPRCA0	17168.43	4.14
	5EPRCA30	19000.20	4.56

Table F.6
Flexural Strength Results for Solid Interlocking Block (SIB) of 28 Days for All Mixtures

Days	Mixture	Force (N)	Stress (N/mm^2)
28	OPCNA	27926.93	6.62
	5EPRCA0	19260.83	4.62
	5EPRCA30	21507.80	5.16

APPENDIX G

Flexural Strength Results of Single Inclined Connection Interlocking Block (SICIB) by Days

Table G.1
Flexural Strength Results for Single Inclined Connection Interlocking Block (SICIB) of OPCNA

Days	No. of Sample	Force (N)	Average Force	Stress (N/mm^2)	Average Stress
7	1	12256.70	11789.00	2.939	2.828
	2	11321.30		2.717	
14	1	11429.40	12431.85	2.743	2.984
	2	13434.30		3.224	
28	1	21261.70	17078.55	5.103	4.099
	2	12895.40		3.095	

Table G.2
Flexural Strength Results for Single Inclined Connection Interlocking Block (SICIB) of 5EPRCA0

Days	No. of Sample	Force (N)	Average Force	Stress (N/mm^2)	Average Stress
7	1	10501.10	10138.30	2.503	2.425
	2	9775.50		2.346	
14	1	11772.70	12235.60	2.825	2.937
	2	12698.50		3.048	
28	1	16853.60	16277.80	4.044	3.906
	2	15702.00		3.768	

Table G.3
Flexural Strength Results for Single Inclined Connection Interlocking Block (SICIB) of 5EPRCA30

Days	No. of Sample	Force (N)	Average Force	Stress (N/mm^2)	Average Stress
7	1	14324.30	13045.35	3.439	3.132
	2	11766.40		2.824	
14	1	14053.00	14936.65	3.373	3.585
	2	15820.30		3.797	
28	1	18040.70	17177.55	4.329	4.122
	2	16314.40		3.915	

Table G.4
Flexural Strength Results for Single Inclined Connection Interlocking Block (SICIB) of 7 Days for All Mixtures

Days	Mixture	Force (N)	Stress (N/mm^2)
7	OPCNA	11789.00	2.83
	5EPRCA0	10138.30	2.42
	5EPRCA30	13045.35	3.13

Table G.5
Flexural Strength Results for Single Inclined Connection Interlocking Block (SICIB) of 14 Days for All Mixtures

Days	Mixture	Force (N)	Stress (N/mm^2)
14	OPCNA	12431.85	2.98
	5EPRCA0	12235.60	2.94
	5EPRCA30	14936.65	3.59

Table G.6
Flexural Strength Results for Single Inclined Connection Interlocking Block (SICIB) of 28 Days for All Mixtures

Days	Mixture	Force (N)	Stress (N/mm^2)
28	OPCNA	17078.55	4.10
	5EPRCA0	16277.80	3.91
	5EPRCA30	17177.55	4.12

APPENDIX H

Flexural Strength Results of Dual Tongue Inclined Interlocking Block (DTIIB) by Days

Table H.1
Flexural Strength Results for Dual Tongue Inclined Interlocking Block (DTIIB) of OPCNA

Days	No. of Sample	Force (N)	Average Force	Stress (N/mm^2)	Average Stress
7	1	9179.88	8754.35	2.203	2.101
	2	8328.82		1.999	
14	1	14479.80	13957.05	3.475	3.350
	2	13434.30		3.224	
28	1	15818.60	16327.05	3.580	3.814
	2	16835.50		4.048	

Table H.2
Flexural Strength Results for Dual Tongue Inclined Interlocking Block (DTIIB) of 5EPRCA0

Days	No. of Sample	Force (N)	Average Force	Stress (N/mm^2)	Average Stress
7	1	10067.10	9768.45	2.416	2.386
	2	9469.80		2.356	
14	1	11237.50	11724.70	2.697	2.822
	2	12211.90		2.946	
28	1	12857.80	14820.75	3.057	3.543
	2	16783.70		4.028	

Table H.3
Flexural Strength Results for Dual Tongue Inclined Interlocking Block (DTIIB) of 5EPRCA30

Days	No. of Sample	Force (N)	Average Force	Stress (N/mm^2)	Average Stress
7	1	9024.56	10642.13	2.165	2.606
	2	12259.70		3.047	
14	1	10245.40	12347.25	2.458	2.913
	2	14449.10		3.369	
28	1	16060.50	16232.30	3.673	3.802
	2	16404.10		3.932	

Table H.4
Flexural Strength Results for Dual Tongue Inclined Interlocking Block (DTIIB) of 7 Days for all mixtures

Days	Mixture	Force (N)	Stress (N/mm^2)
7	OPCNA	8754.35	2.10
	5EPRCA0	9768.45	2.39
	5EPRCA30	10642.13	2.61

Table H.5
Flexural Strength Results for Dual Tongue Inclined Interlocking Block (DTIIB) of 14 Days for all mixtures

Days	Mixture	Force (N)	Stress (N/mm^2)
14	OPCNA	13957.05	3.35
	5EPRCA0	11724.70	2.82
	5EPRCA30	12347.25	2.91

Table H.6
Flexural Strength Results for Dual Tongue Inclined Interlocking Block (DTIIB) of 28 Days for all mixtures

Days	Mixture	Force (N)	Stress (N/mm^2)
28	OPCNA	16327.05	3.81
	5EPRCA0	14820.75	3.54
	5EPRCA30	16232.30	3.80

APPENDIX I

Comparison Flexural Strength Results of Interlocking Block by Days

Table I.1
Comparison Flexural Strength Results for Interlocking Block (IB) of 7 Days for All Mixtures

Days	Mixture	SIB		SICIB		DTIIB	
		N	N/mm²	N	N/mm²	N	N/mm²
7	OPCNA	22391.63	5.37	11789.00	2.83	8754.35	2.10
	5EPRCA0	16621.63	3.99	10138.30	2.42	9768.45	2.39
	5EPRCA30	17668.30	4.24	13045.35	3.13	10642.13	2.61

Table I.2
Comparison Flexural Strength Results for Interlocking Block (IB) of 14 Days for All Mixtures

Days	Mixture	SIB		SICIB		DTIIB	
		N	N/mm²	N	N/mm²	N	N/mm²
14	OPCNA	24715.17	5.76	12431.85	2.98	13957.05	3.35
	5EPRCA0	17168.43	4.14	12235.60	2.94	11724.70	2.82
	5EPRCA30	19000.20	4.56	14936.65	3.59	12347.25	2.91

Table I.3
Comparison Flexural Strength Results for Interlocking Block (IB) of 28 Days for All Mixtures

Days	Mixture	SIB		SICIB		DTIIB	
		N	N/mm²	N	N/mm²	N	N/mm²
28	OPCNA	27926.93	6.62	17078.55	4.10	16327.05	3.81
	5EPRCA0	19260.83	4.62	16277.80	3.91	14820.75	3.54
	5EPRCA30	21507.80	5.16	17177.55	4.12	16232.30	3.80

Table I.4
Comparison Flexural Strength Results for Interlocking Block (IB) for all mixtures

Days	Mixture	SIB		SICIB		DTIIB	
		N	N/mm²	N	N	N/mm²	N
7	OPCNA	22391.63	5.37	11789.00	2.83	8754.35	2.10
	5EPRCA0	16621.63	3.99	10138.30	2.42	9768.45	2.39
	5EPRCA30	17668.30	4.24	13045.35	3.13	10642.13	2.61
14	OPCNA	24715.17	5.76	12431.85	2.98	13957.05	3.35
	5EPRCA0	17168.43	4.14	12235.60	2.94	11724.70	2.82
	5EPRCA30	19000.20	4.56	14936.65	3.59	12347.25	2.91
28	OPCNA	27926.93	6.62	17078.55	4.10	16327.05	3.81
	5EPRCA0	19260.83	4.62	16277.80	3.91	14820.75	3.54
	5EPRCA30	21507.80	5.16	17177.55	4.12	16232.30	3.80

APPENDIX J

1.1 Crack SIB

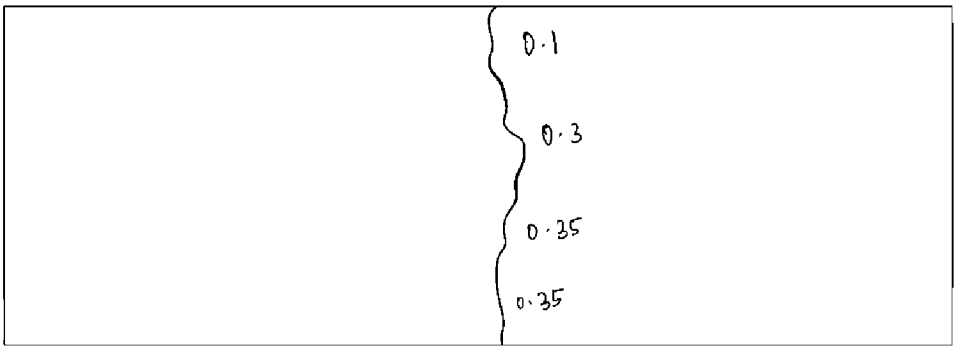

Figure J.1 Crack Pattern of 7 Days OPCNA

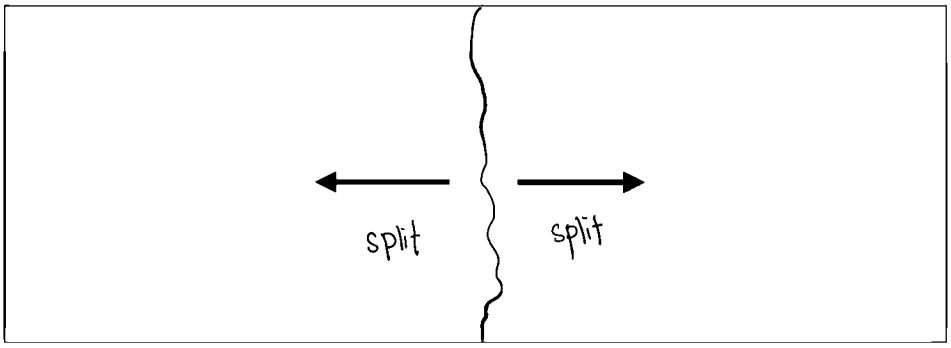

Figure J.2 Crack Pattern of 14 Days OPCNA

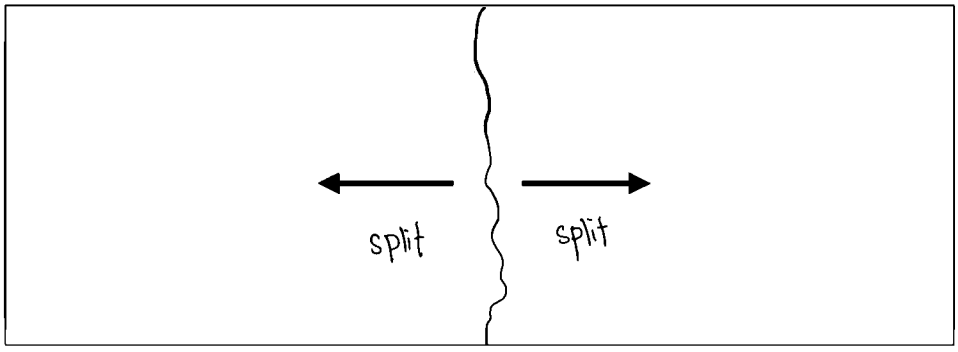

Figure J.3 Crack Pattern of 28 Days OPCNA

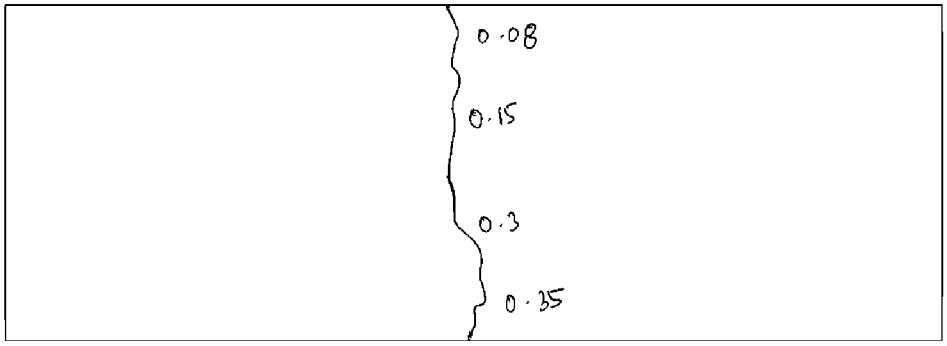

Figure J.4 Crack Pattern of 7 Days 5EPRCA0

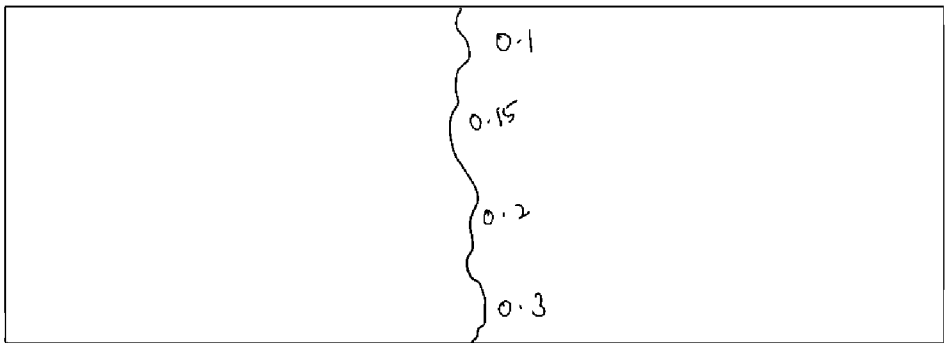

Figure J.5 Crack Pattern of 14 Days 5EPRCA0

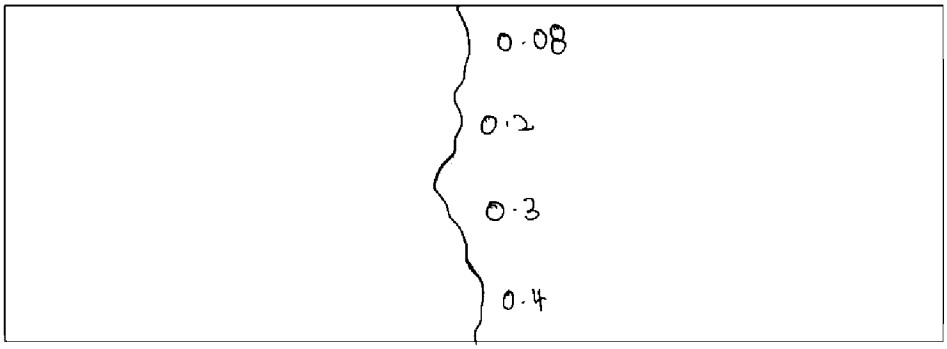

Figure J.6 Crack Pattern of 28 Days 5EPRCA0

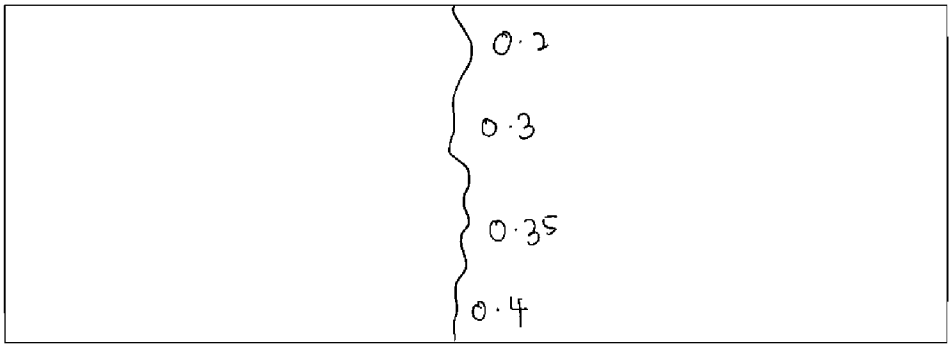

Figure J.7 Crack Pattern of 7 Days 5EPRCA30

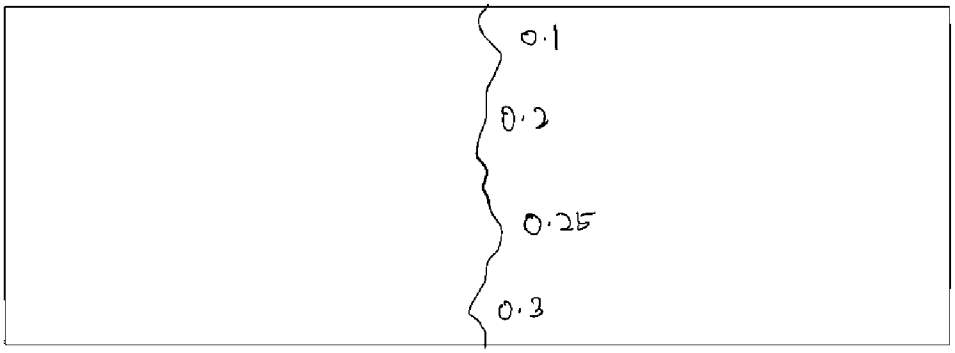

Figure J.8 Crack Pattern of 14 Days 5EPRCA30

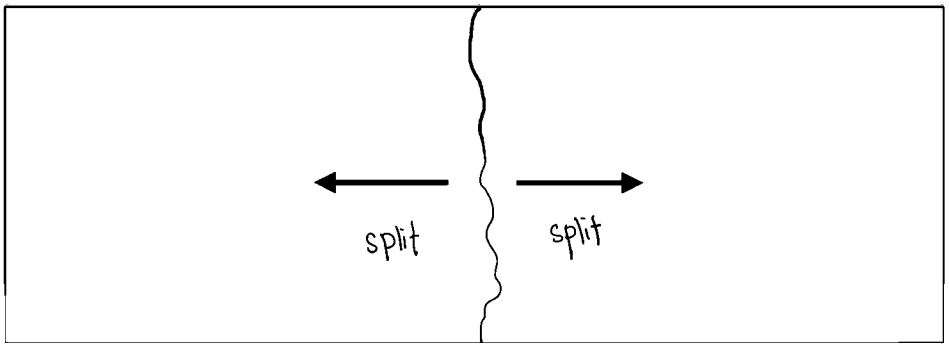

Figure J.9 Crack Pattern of 28 Days 5EPRCA0

1.2 Crack SICIB

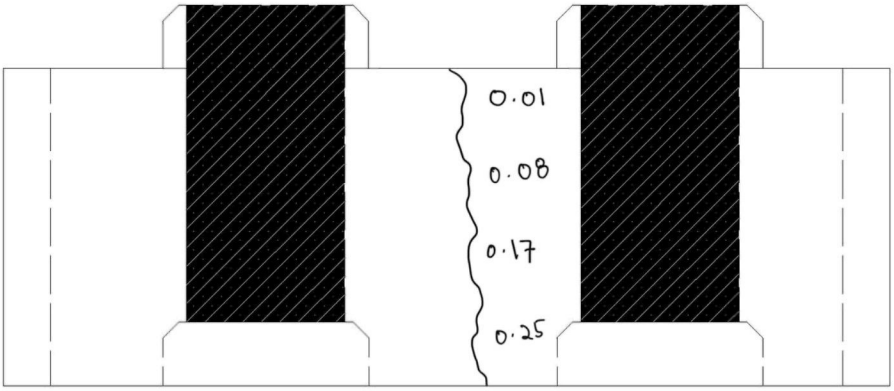

Figure J.10 Crack Pattern of 7 Days OPCNA

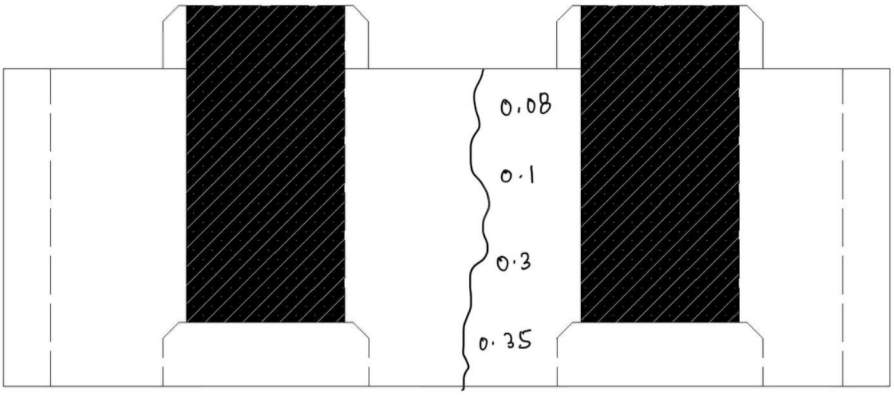

Figure J.11 Crack Pattern of 14 Days OPCNA

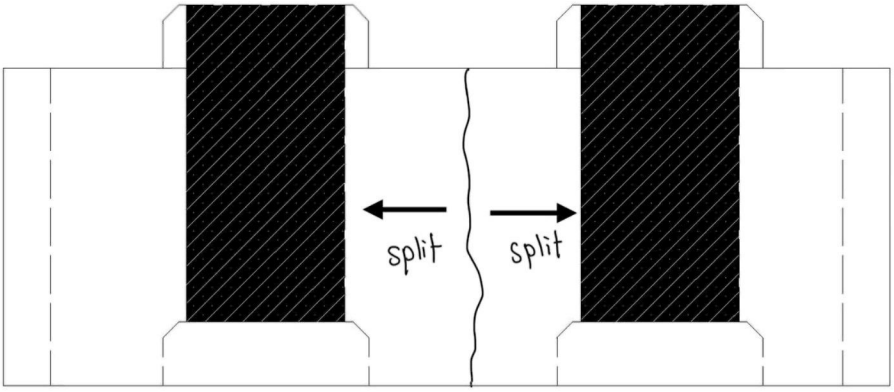

Figure J.12 Crack Pattern of 28 Days OPCNA

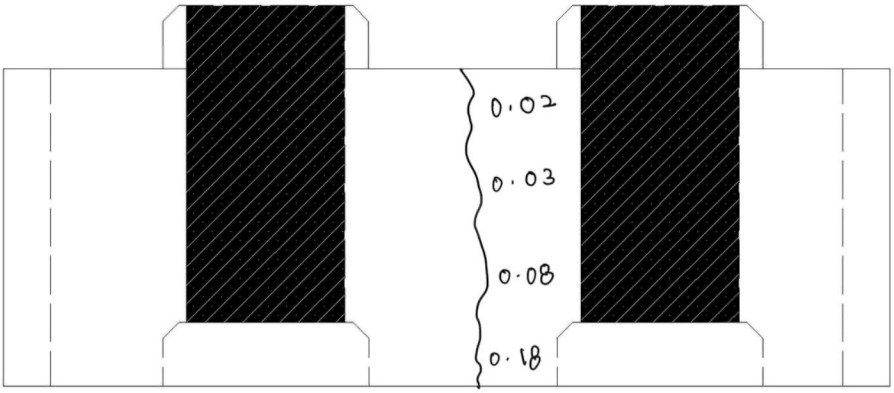

Figure J.13 Crack Pattern of 7 Days 5EPRCA0

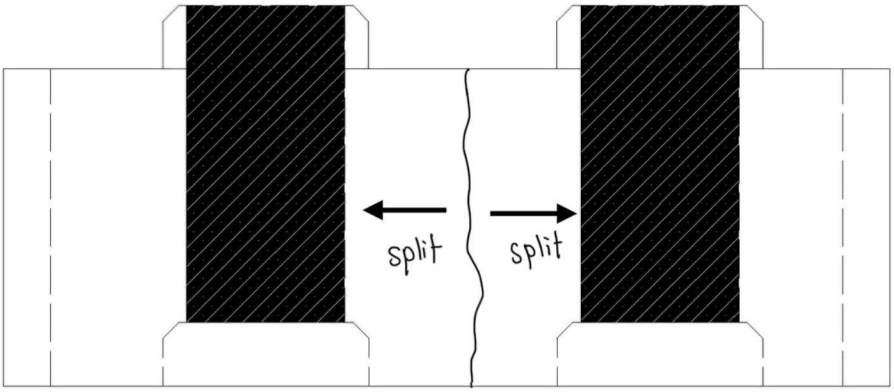

Figure J.14 Crack Pattern of 14 Days 5EPRCA0

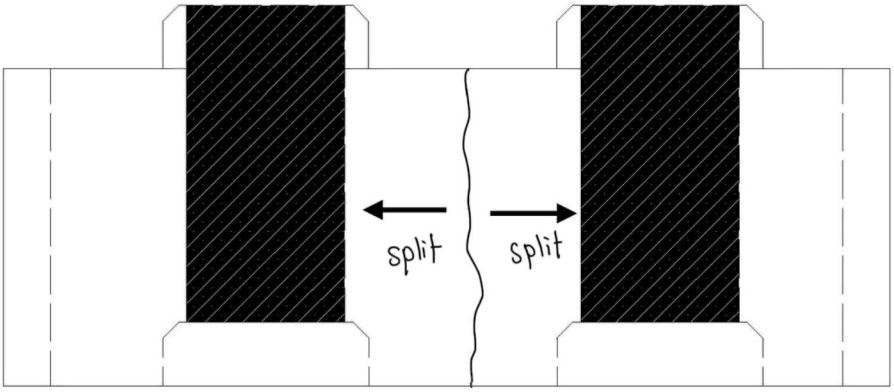

Figure J.15 Crack Pattern of 28 Days 5EPRCA0

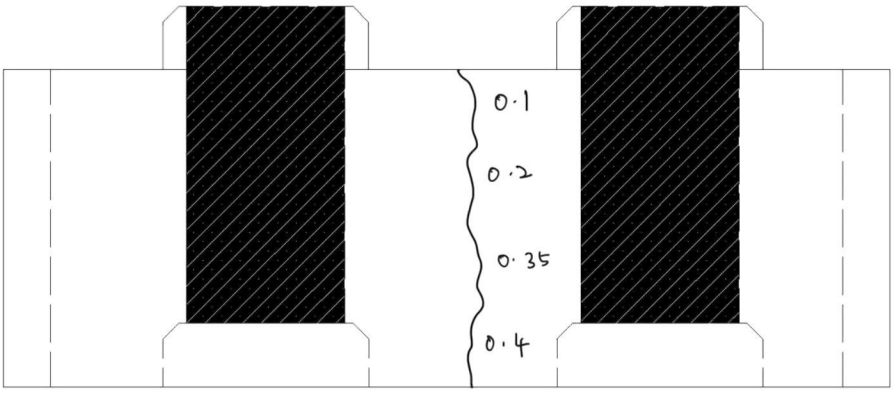

Figure J.16 Crack Pattern of 7 Days 5EPRCA30

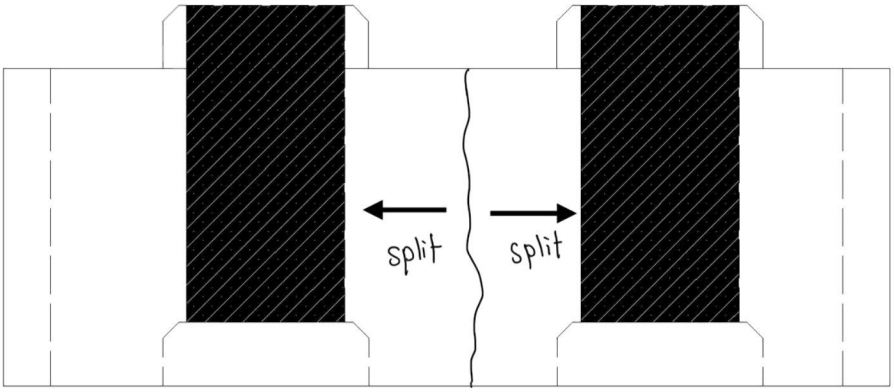

Figure J.17 Crack Pattern of 14 Days 5EPRCA30

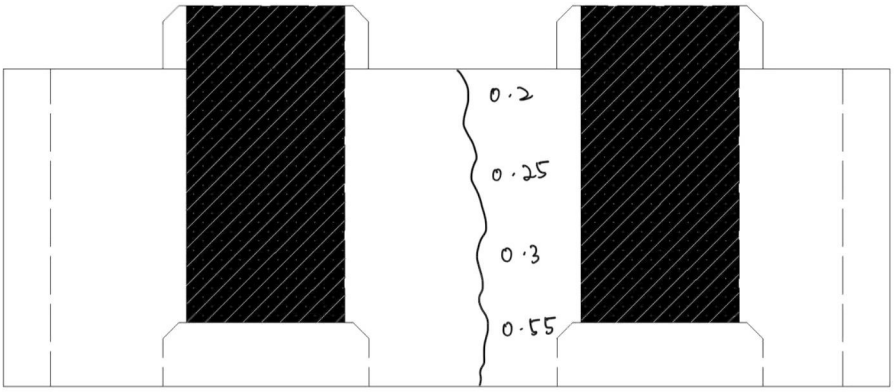

Figure J.18 Crack Pattern of 28 Days 5EPRCA0

1.3 Crack DTIIB

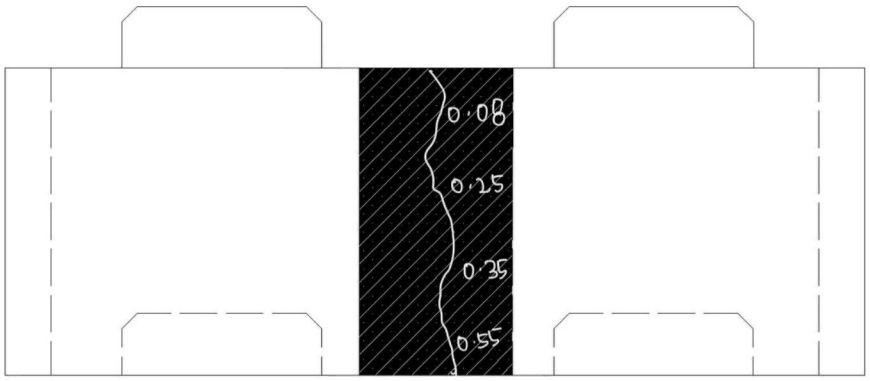

Figure J.19 Crack Pattern of 7 Days OPCNA

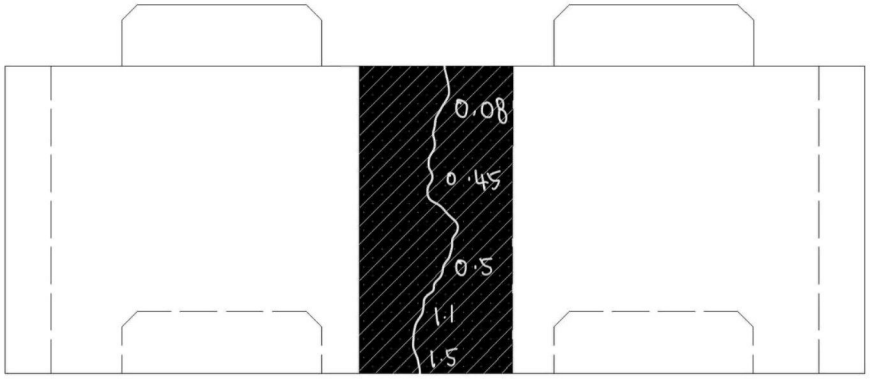

Figure J.20 Crack Pattern of 14 Days OPCNA

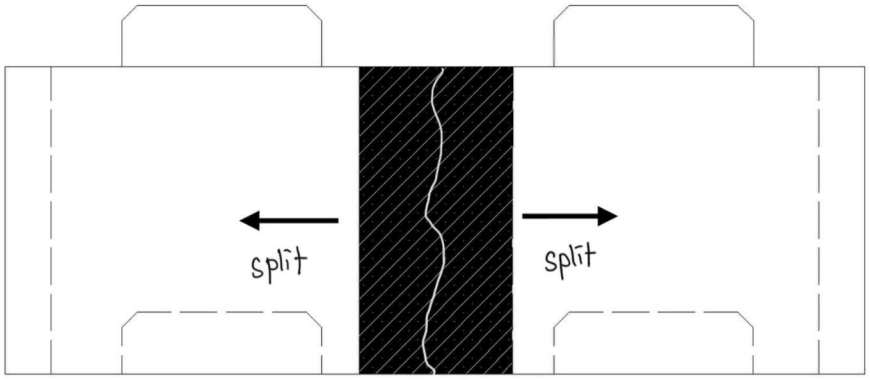

Figure J.21 Crack Pattern of 28 Days OPCNA

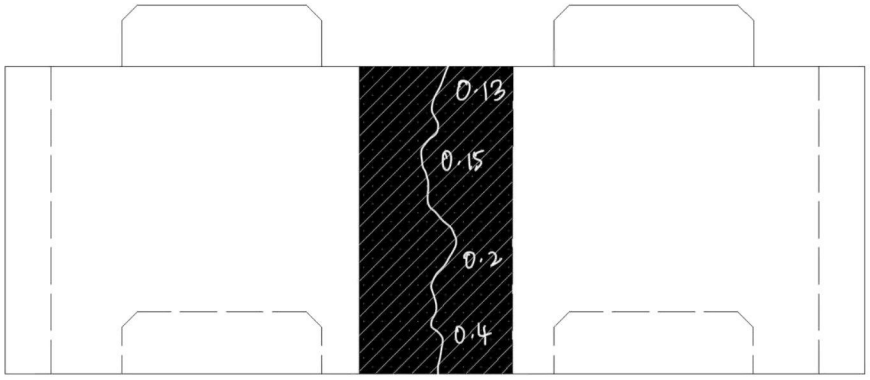

Figure J.22 Crack Pattern of 7 Days 5EPRCA0

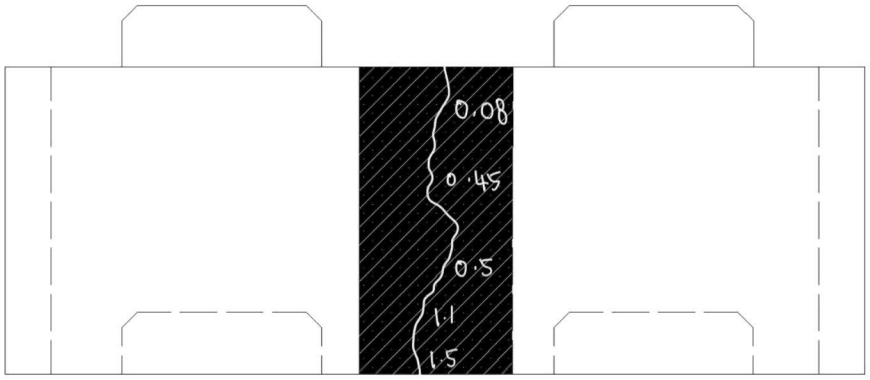

Figure J.23 Crack Pattern of 14 Days 5EPRCA0

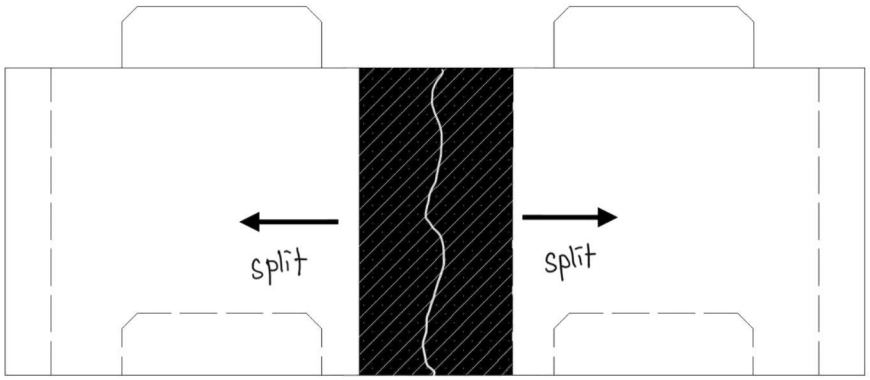

Figure J.24 Crack Pattern of 28 Days 5EPRCA0

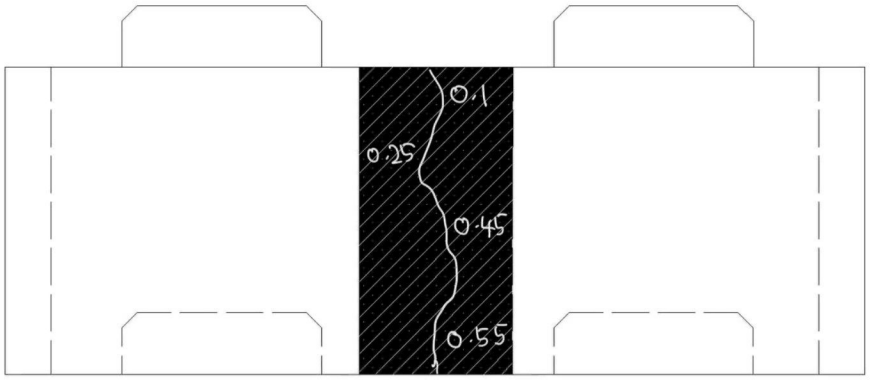

Figure J.25 Crack Pattern of 7 Days 5EPRCA30

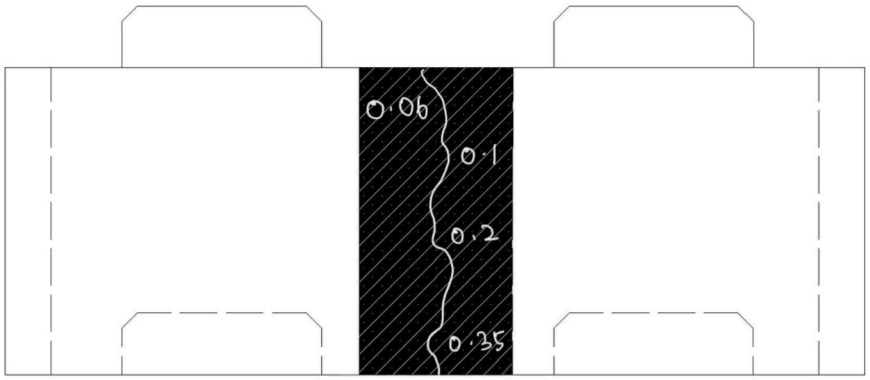

Figure J.26 Crack Pattern of 14 Days 5EPRCA30

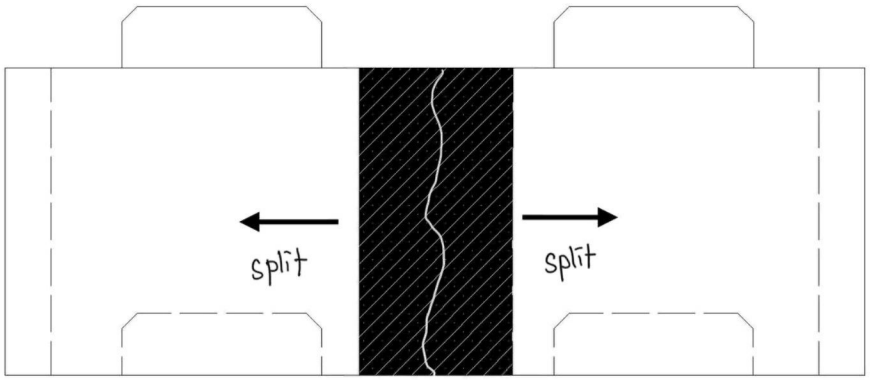

Figure J.27 Crack Pattern of 28 Days 5EPRCA0

APPENDIX K

1.4 RANGE R AND MSE FOR MORTAR

Table K.1
ANN R^2 Range for Different Application Area

Application Area	ANN R^2 Range	Notes
Concrete strength	> 0.80	Good correlation in SCC prediction study (ouci.dntb.gov.ua)
Water distribution systems	~0.96–0.98	High predictive performance in fluid modelling
Pavement subgrade	Validated with 70/15/15 split; $R^2 \approx$ 0.6 (improved from linear)	Training halts on validation plateau
Seepage in canals	≈ 0.997	Excellent accuracy in hydraulics applications
SFRC structural properties	Metrics favour GA training	R, R^2 used to identify optimal algorithms

Table K.2
Good R/R^2 Range for Mortar Strength Range (MPa)

Mortar Strength Range (MPa)	Good R / R^2 Range	Notes
0–10	R: 0.85 – 0.95 R^2: 0.72 – 0.90	Higher relative accuracy expected due to narrow target range
10–50	R: 0.90 – 0.98 R^2: 0.81 – 0.96	Moderate strength range, good correlation achievable
50–100	R: 0.88 – 0.97 R^2: 0.77 – 0.94	Slight drop in accuracy due to more variability
>100	R: 0.85 – 0.95 R^2: 0.72 – 0.90	Large scale can cause more prediction spread

Table K.3
Good MSE Range for Mortar Strength Range (MPa)

Mortar Strength Range (MPa)	Good MSE Range	Notes
0–10	0.01 – 0.1	Low values are expected due to small target range
10–50	0.1 – 1.0	Depends on data quality and noise
50–100	1.0 – 5.0	Still acceptable if R^2 is high
>100	2.0 – 10+	MSE increases naturally with scale

1.5 ANN for Cube OPCNA

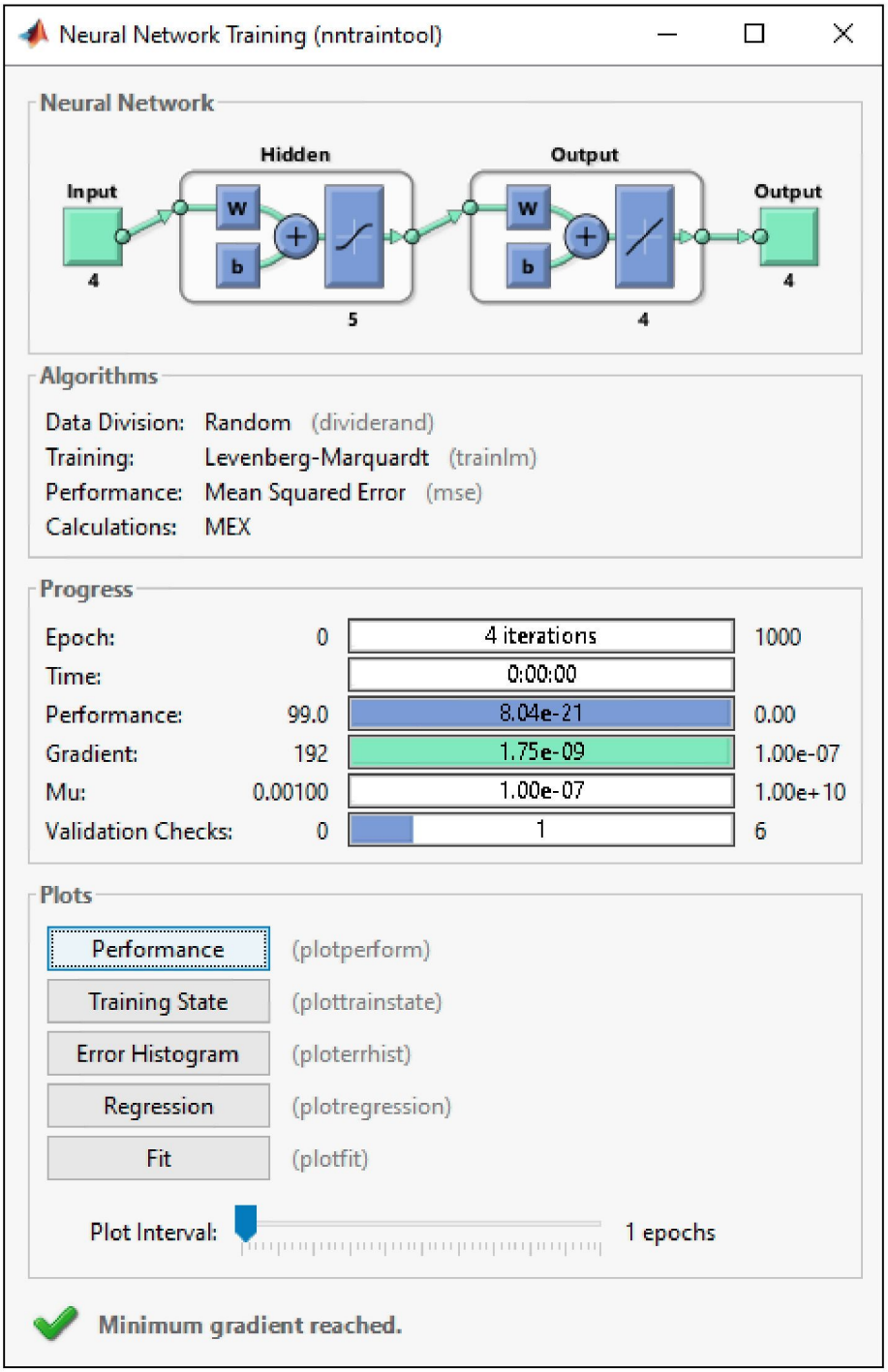

Figure K.1 Neural Network Training (nntraintool) of Cube OPCNA

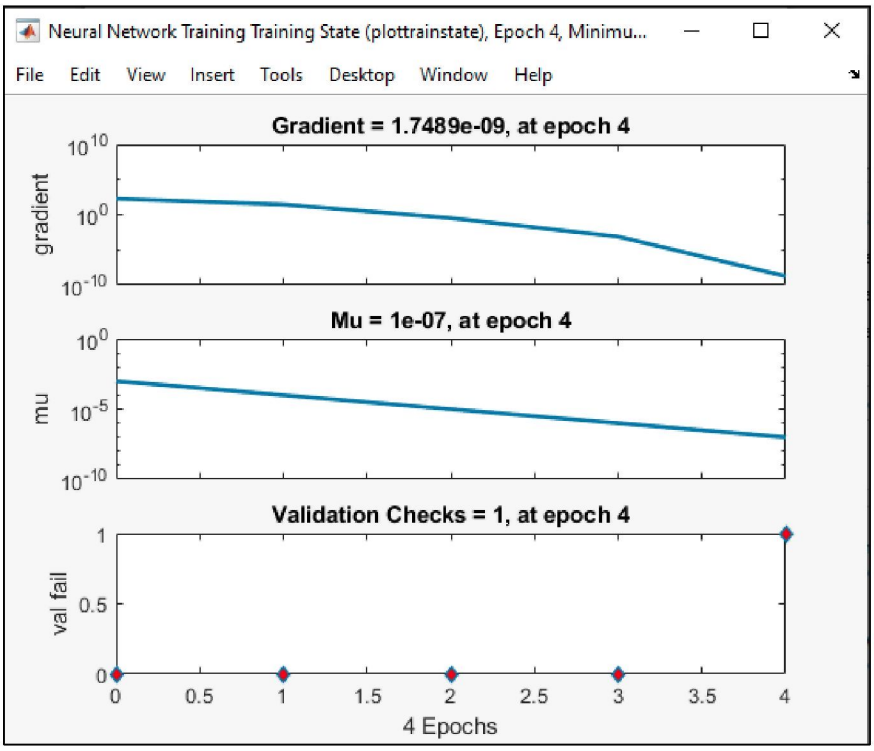

Figure K.2 Plot Training State of Cube OPCNA

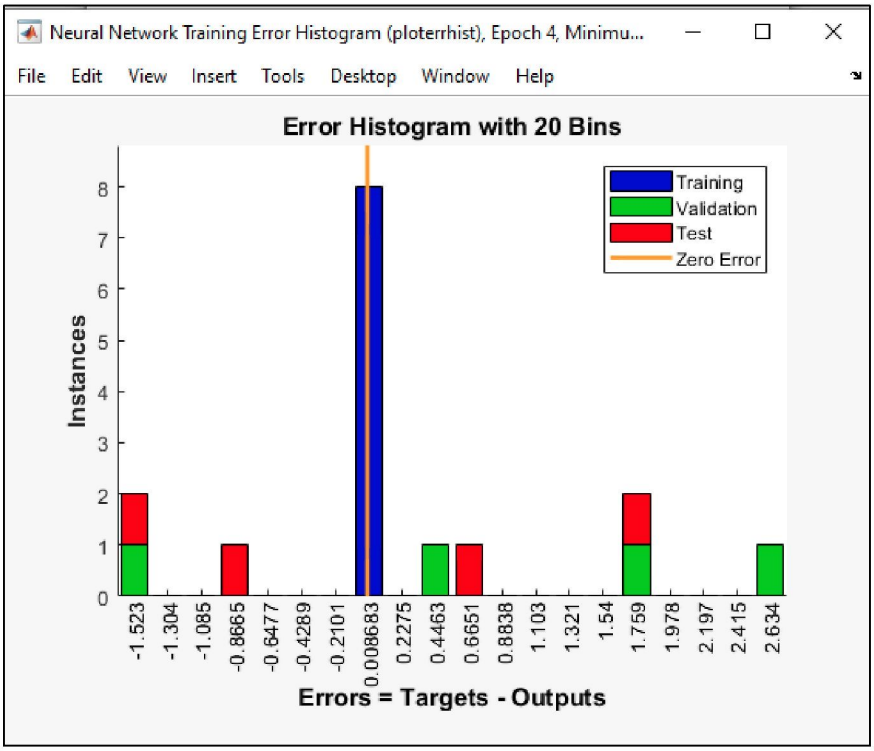

Figure K.3 Plot Error Histogram of Cube OPCNA

1.6 ANN for Cube 5EPRCA30

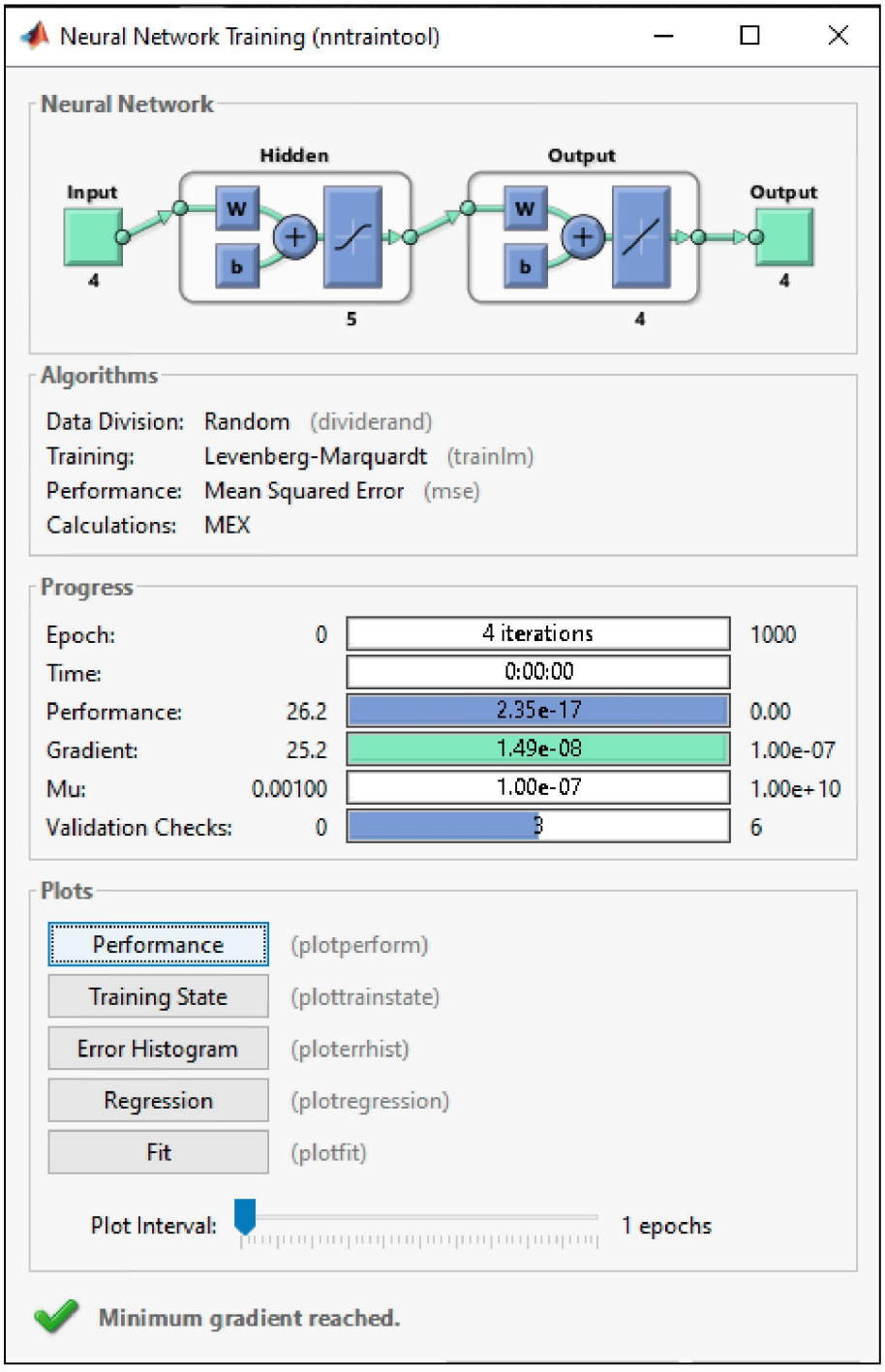

Figure K.4 Neural Network Training (nntraintool) of Cube 5EPRCA30

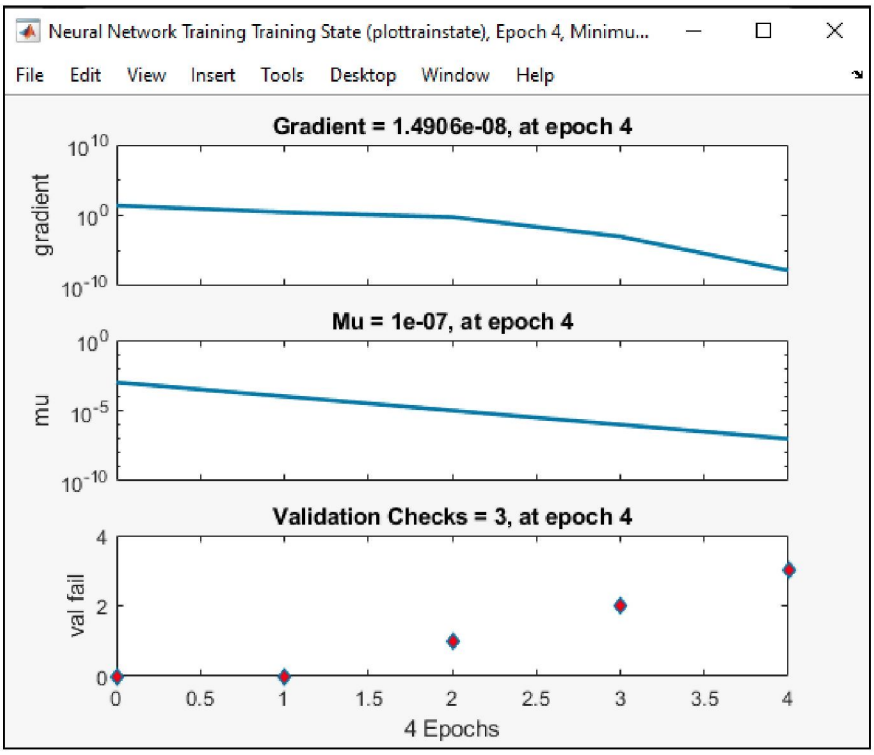

Figure K.5 Plot Training State of Cube 5EPRCA30

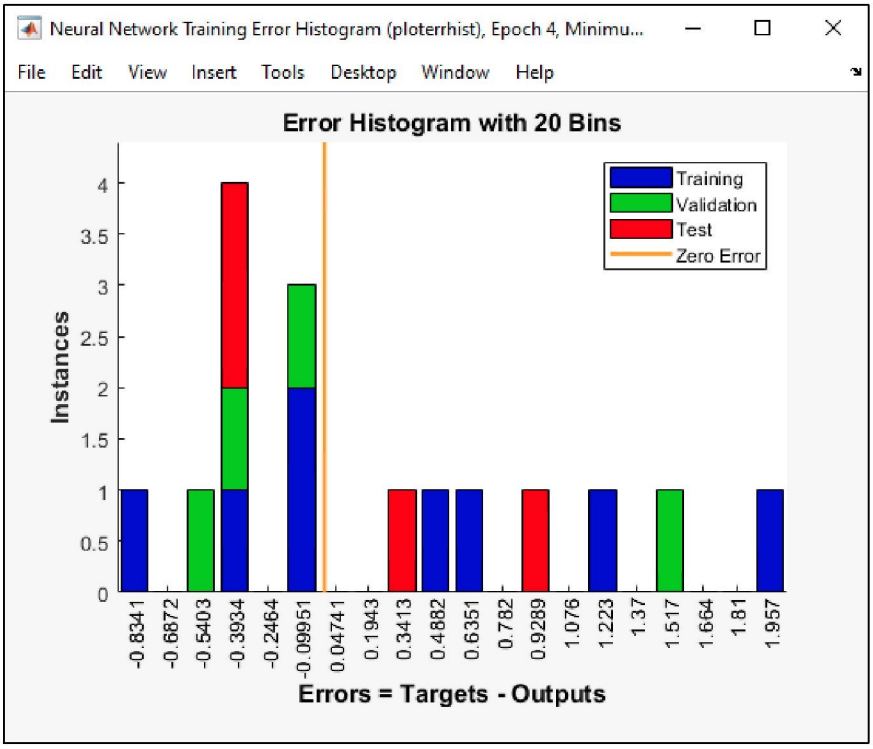

Figure K.6 Plot Error Histogram of Cube 5EPRCA30

1.7 ANN for Prism OPCNA

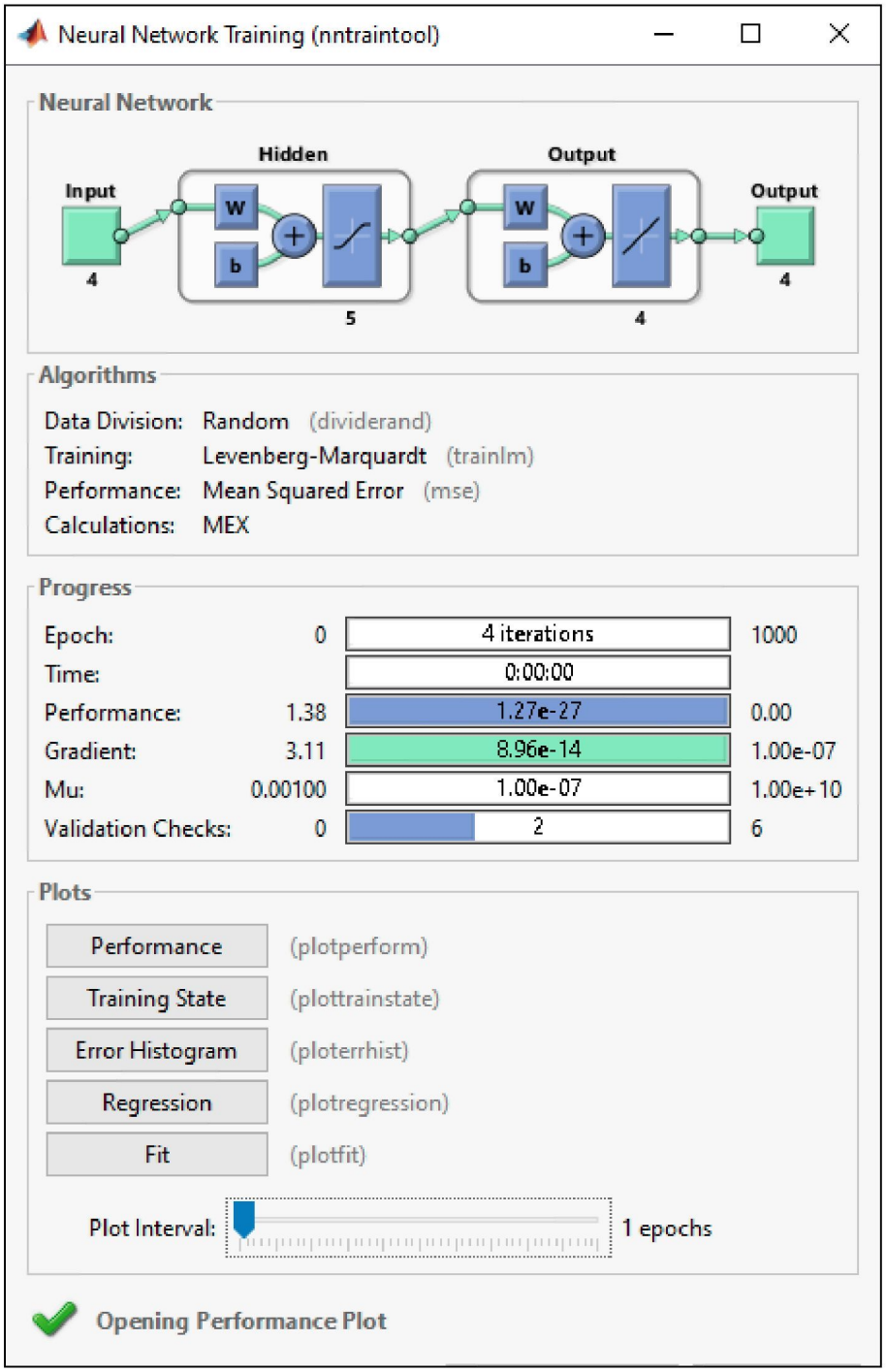

Figure K.7 Neural Network Training (nntraintool) of Prism OPCNA

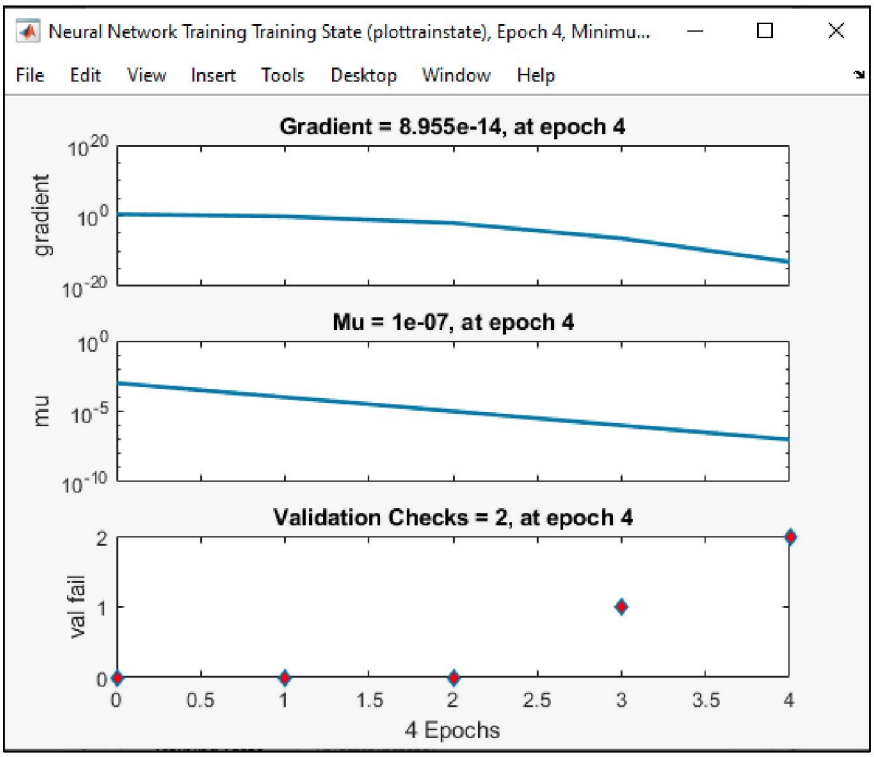

Figure K.8 Plot Training State of Prism OPCNA

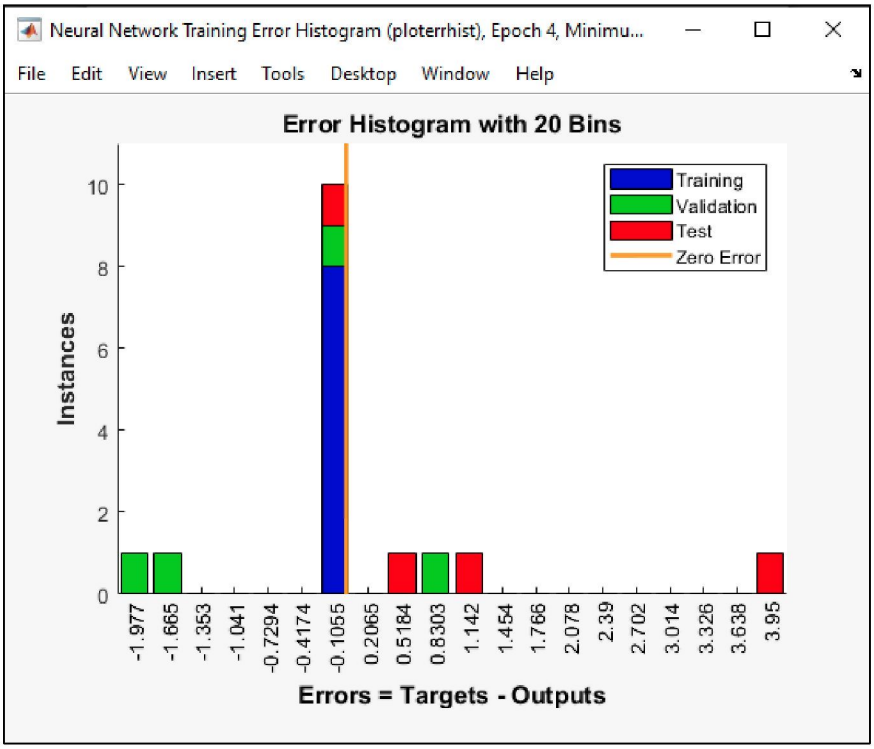

Figure K.9 Plot Error Histogram of Prism OPCNA

1.8 ANN for Prism 5EPRCA30

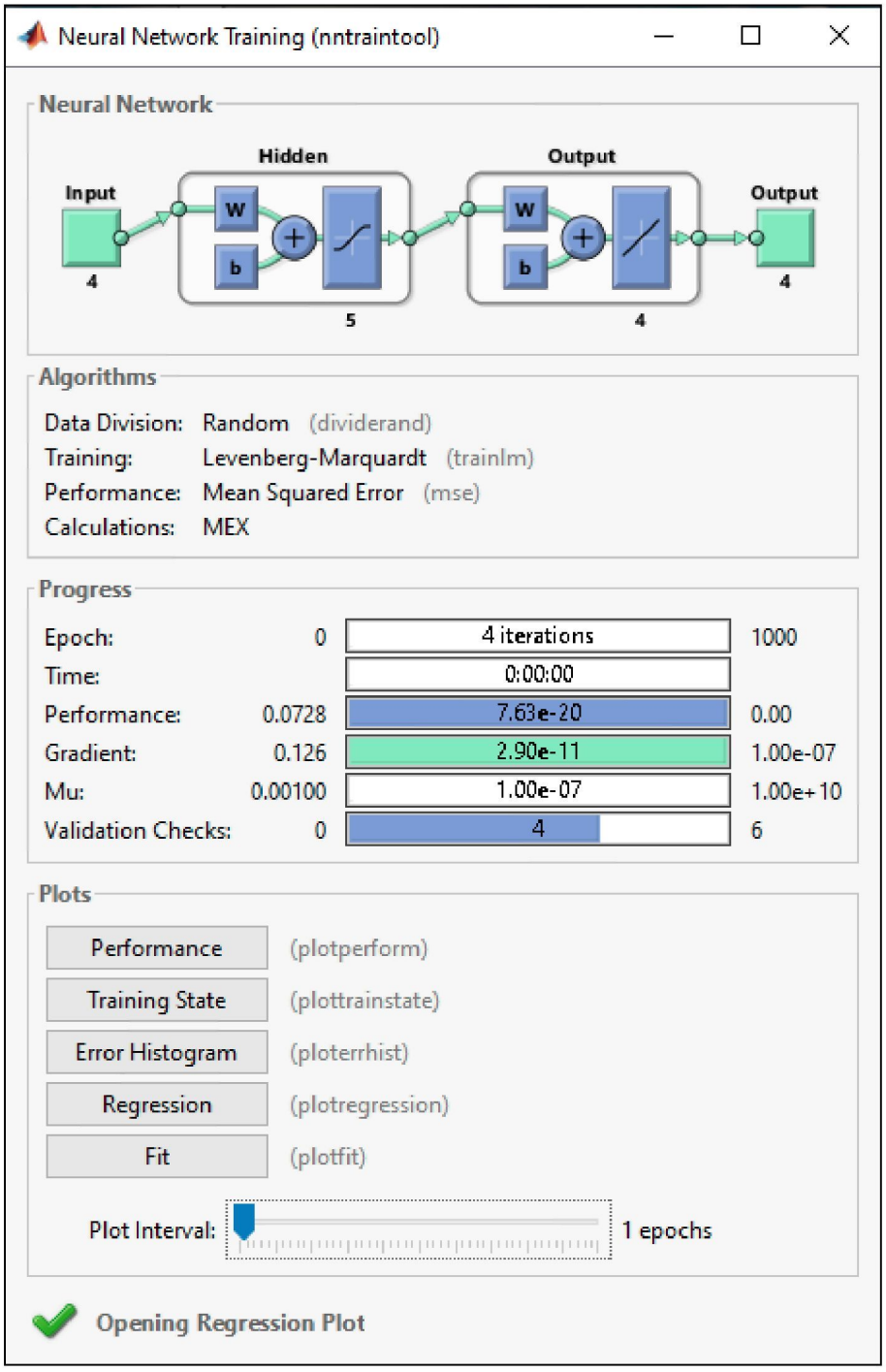

Figure K.10 Neural Network Training (nntraintool) of Prism 5EPRCA30

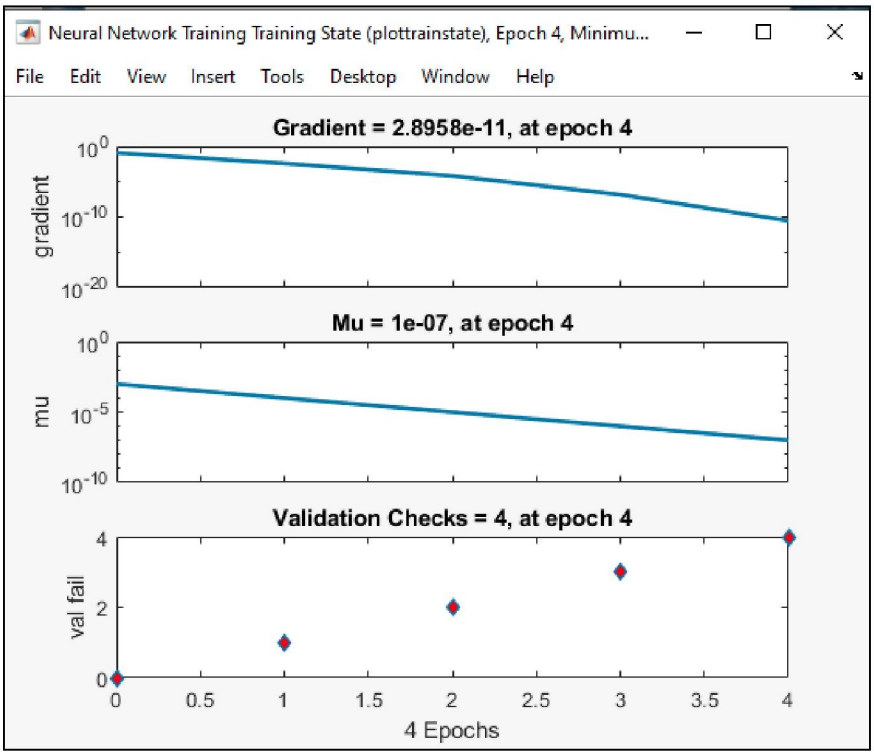

Figure K.11 Plot Training State of Prism 5EPRCA30

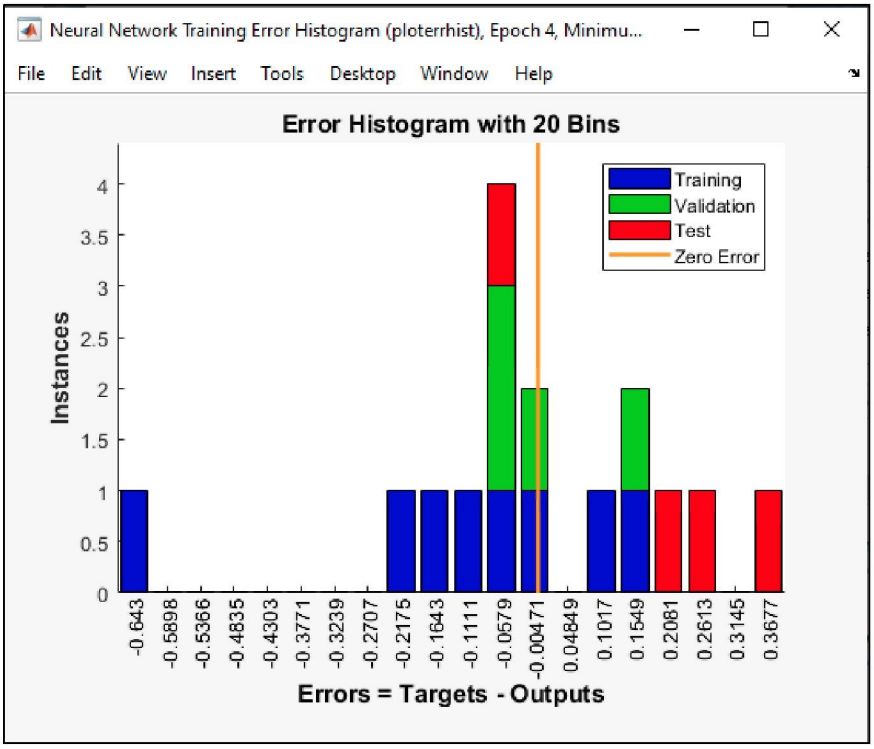

Figure K.12 Plot Error Histogram of Prism 5EPRCA30

1.9 ANN for SIB OPCNA

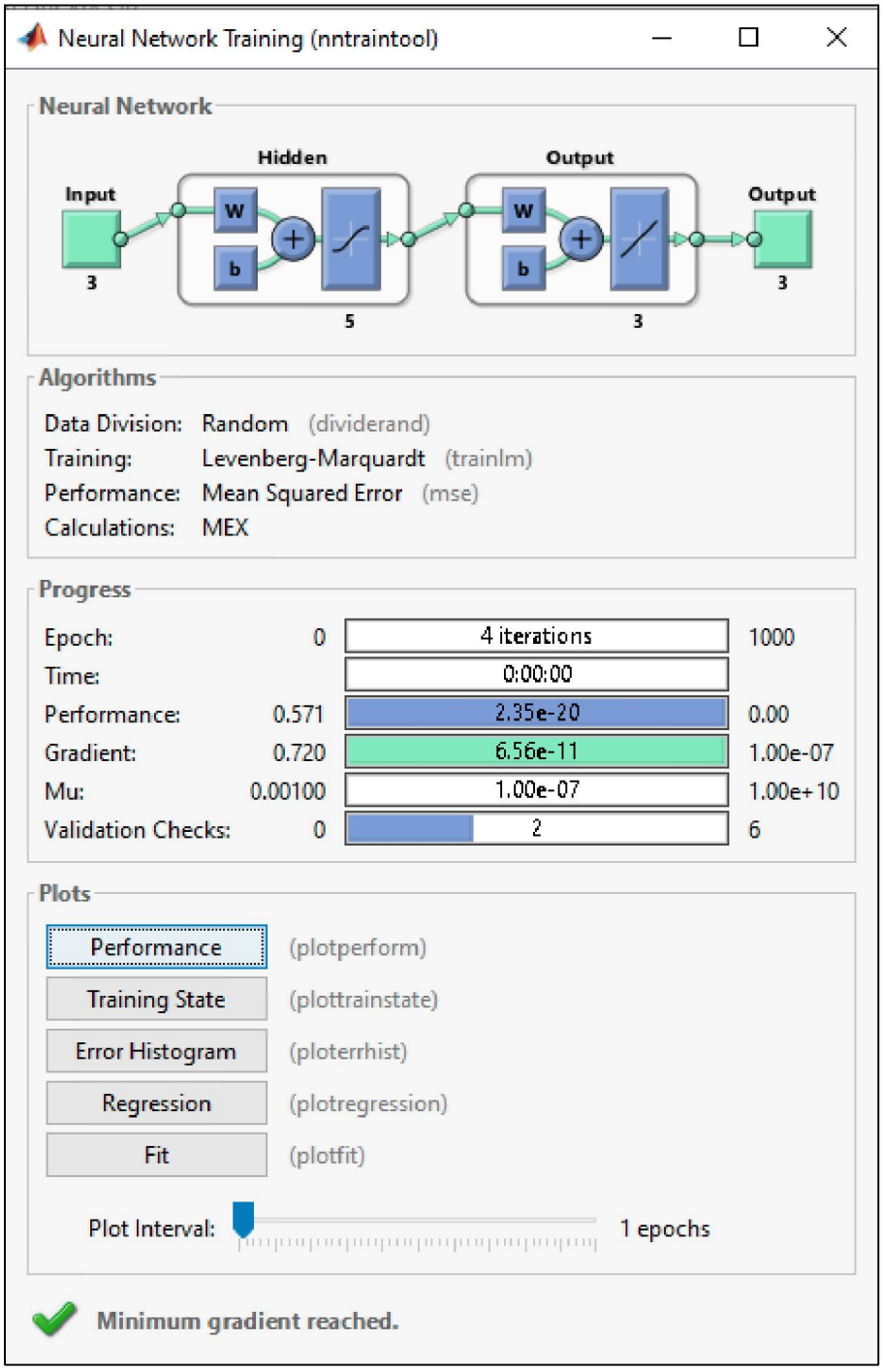

Figure K.13 Neural Network Training (nntraintool) of SIB OPCNA

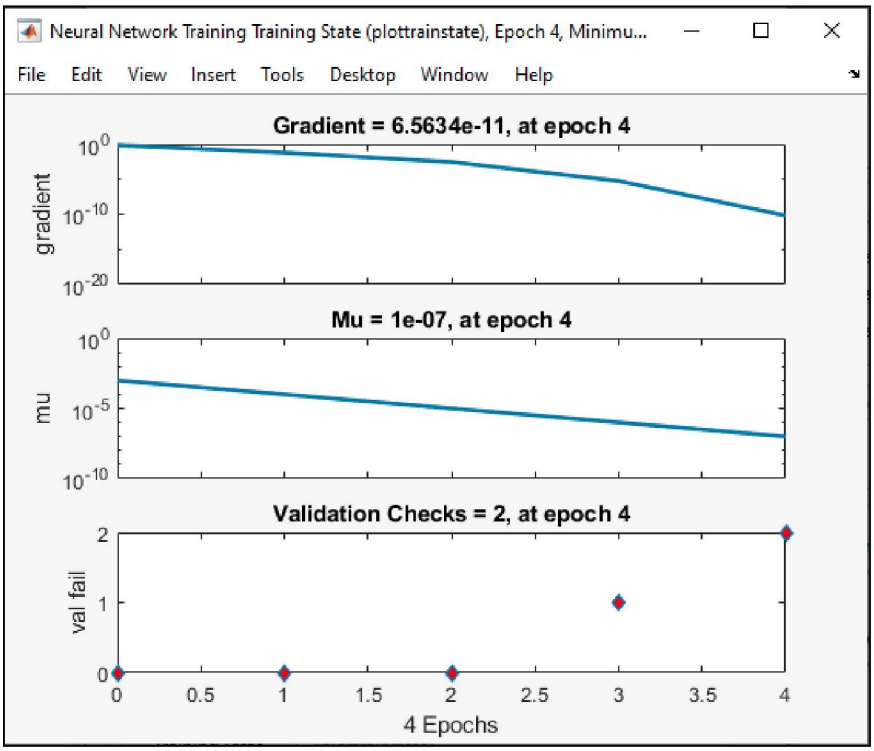

Figure K.14 Plot Training State of SIB OPCNA

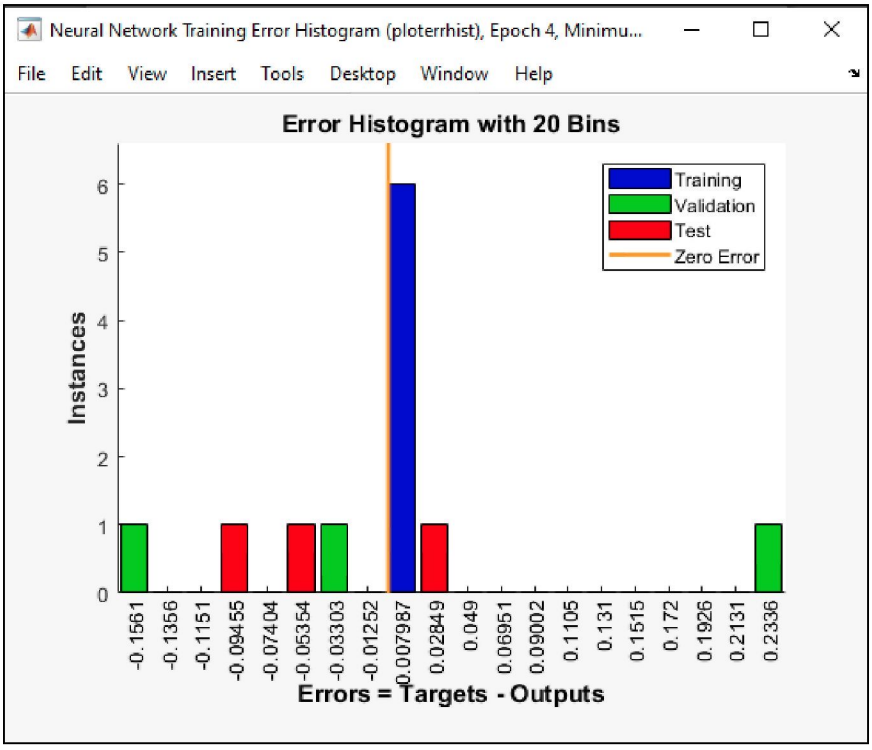

Figure K.15 Plot Error Histogram of SIB OPCNA

1.10 ANN for SIB 5EPRCA30

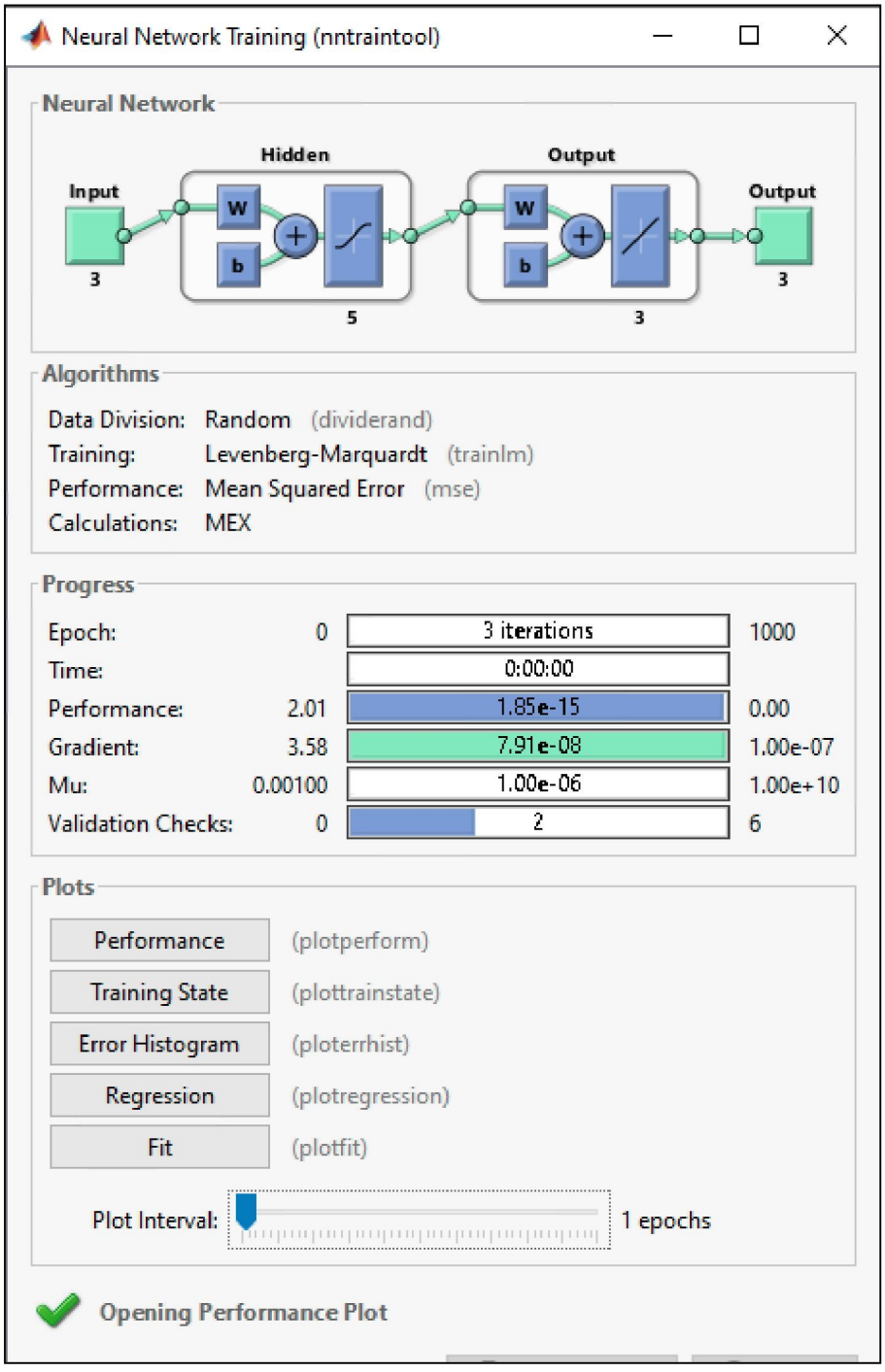

Figure K.16 Neural Network Training (nntraintool) of SIB 5EPRCA30

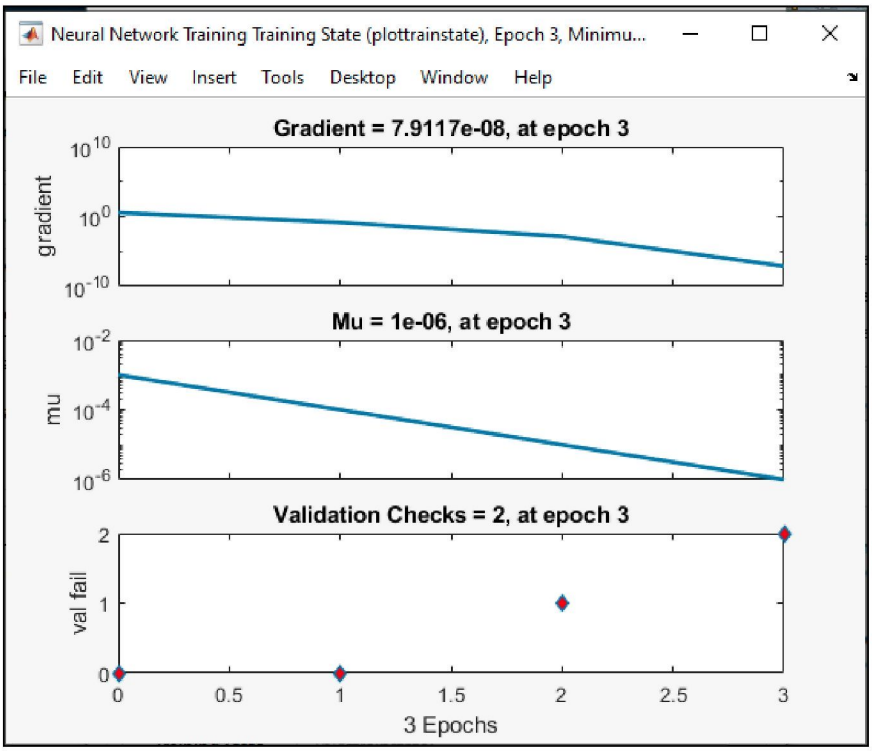

Figure K.17 Plot Training State of SIB 5EPRCA30

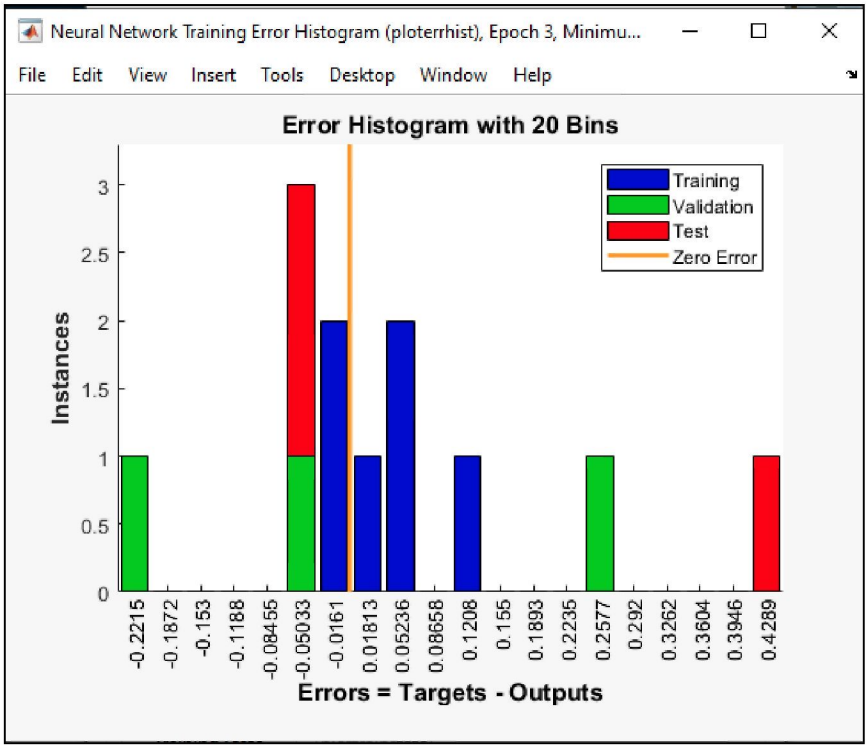

Figure K.18 Plot Error Histogram of SIB 5EPRCA30

1.11 ANN for SICIB OPCNA

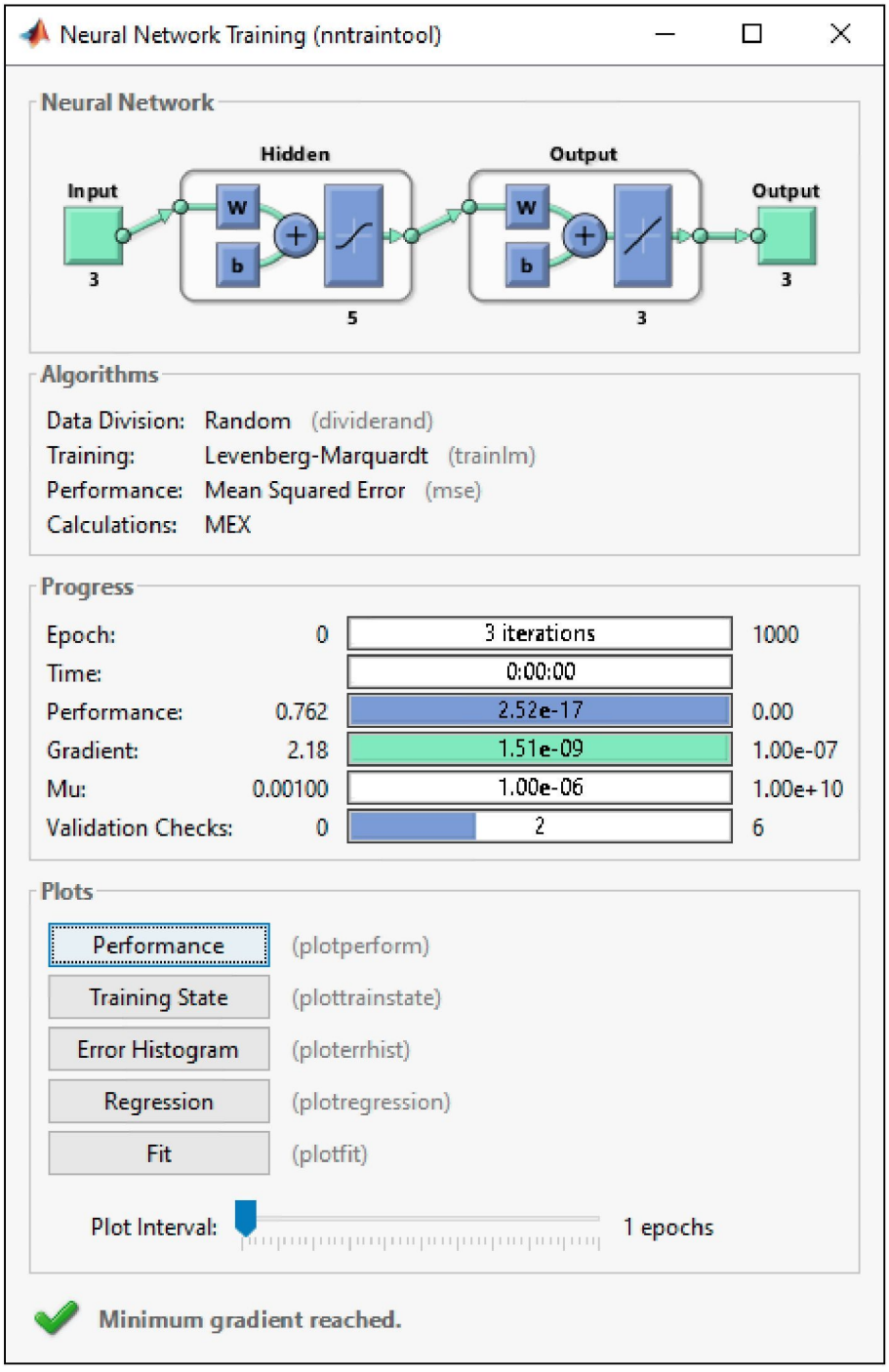

Figure K.19 Neural Network Training (nntraintool) of SICIB OPCNA

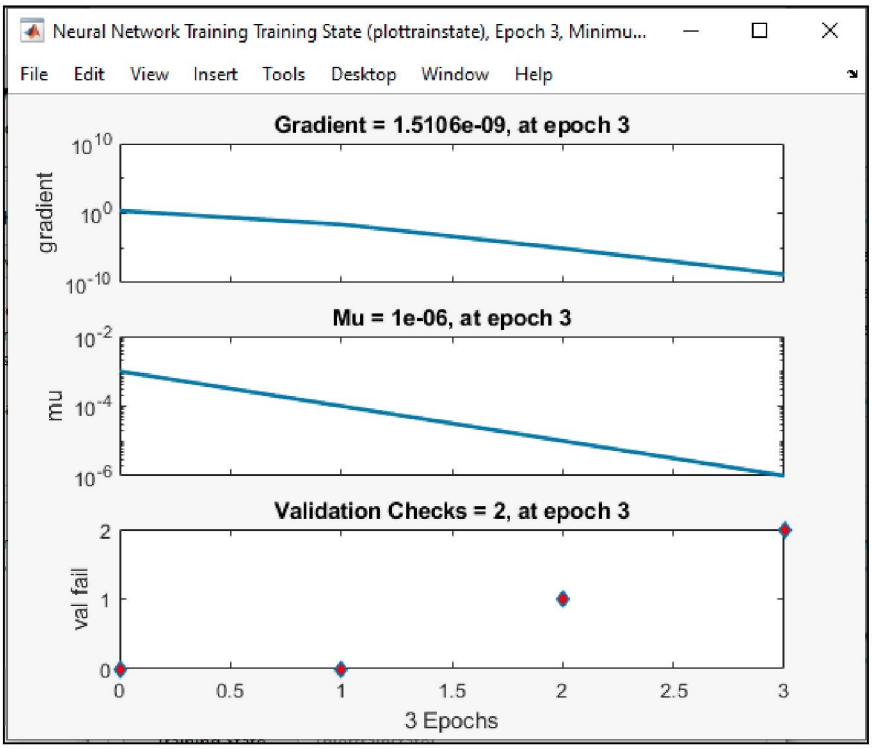

Figure K.20 Plot Training State of SICIB OPCNA

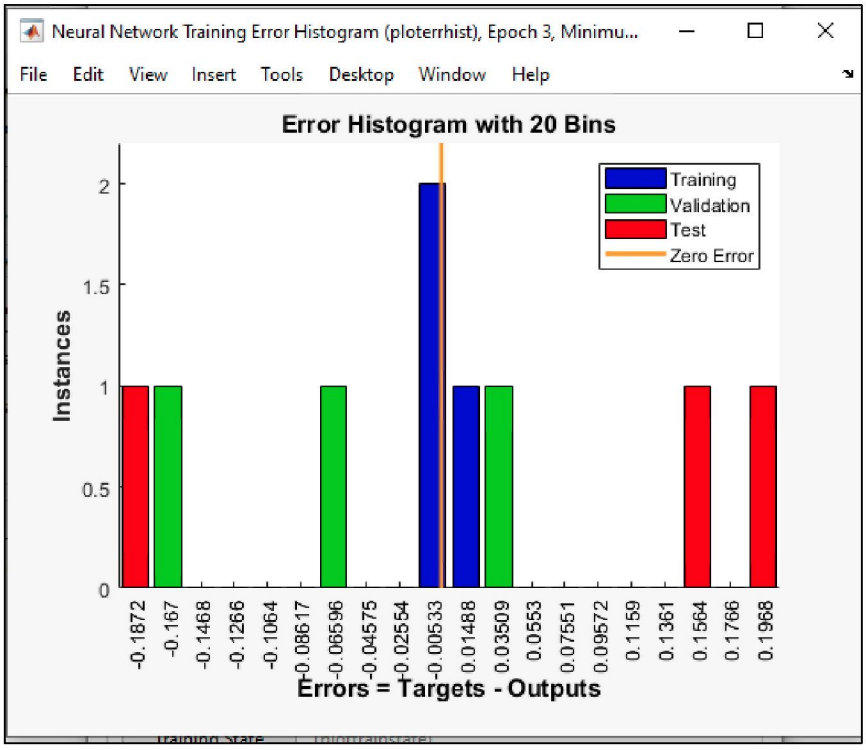

Figure K.21 Plot Error Histogram of SICIB OPCNA

1.12 ANN for SICIB 5EPRCA30

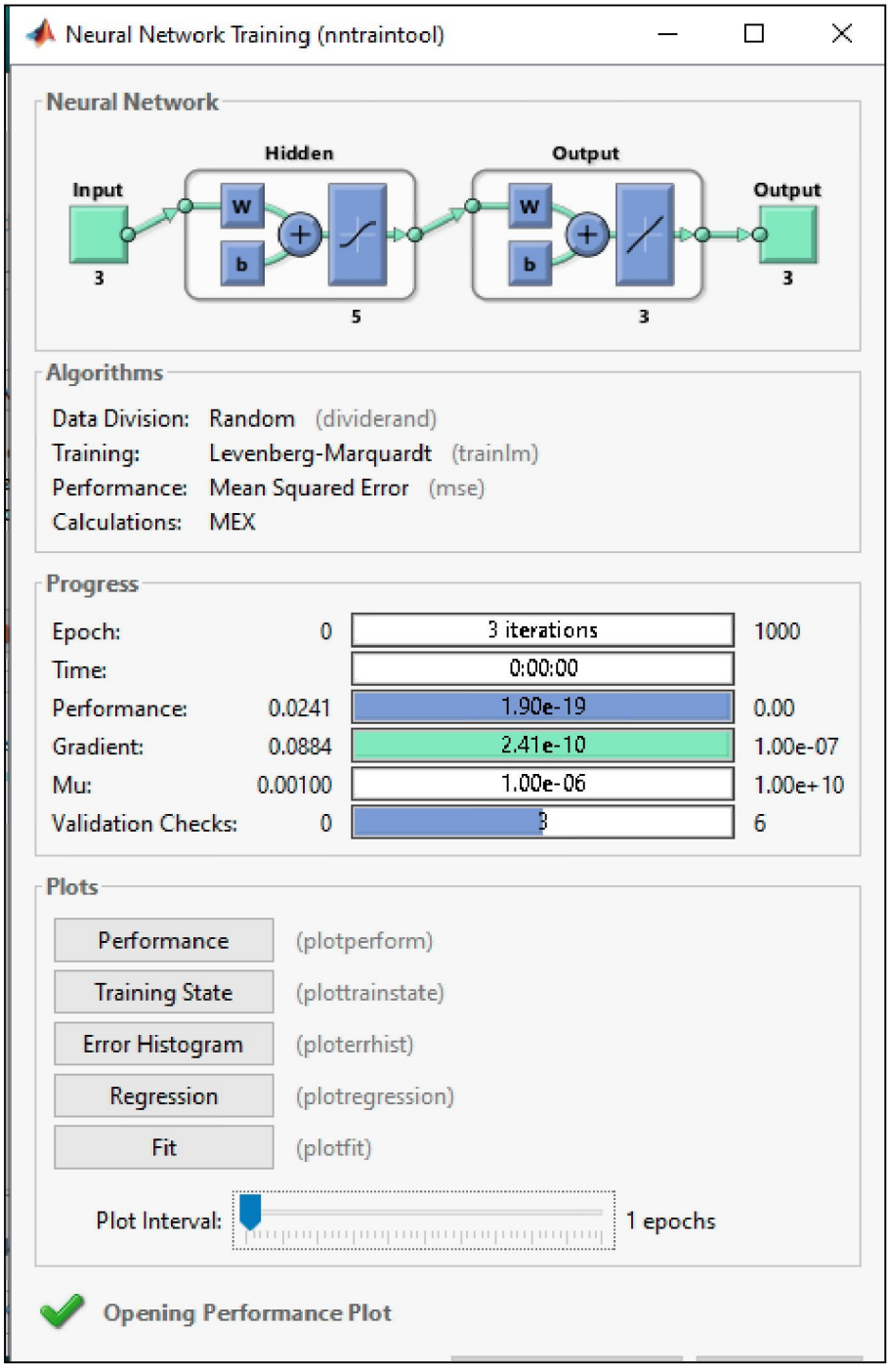

Figure K.22 Neural Network Training (nntraintool) of SICIB 5EPRCA30

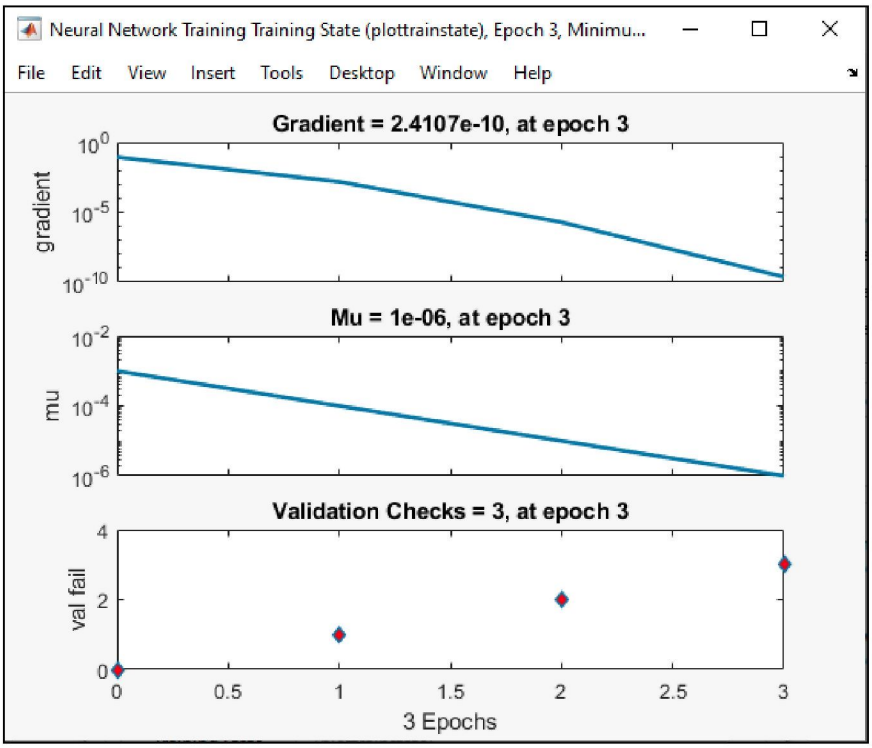

Figure K.23 Plot Training State of SICIB 5EPRCA30

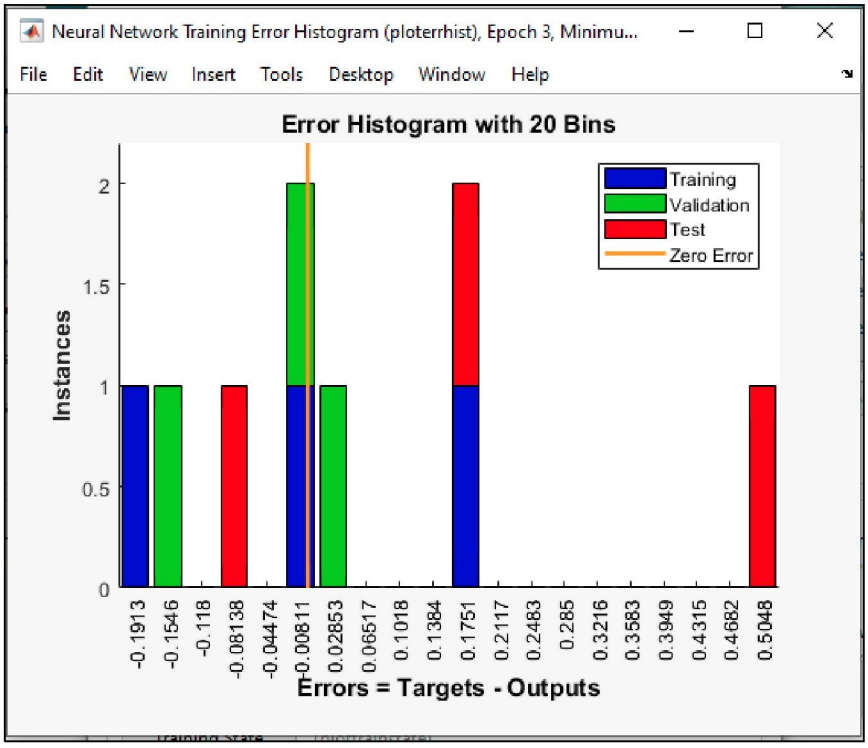

Figure K.24 Plot Error Histogram of SICIB 5EPRCA30

1.13 ANN for DTIIB OPCNA

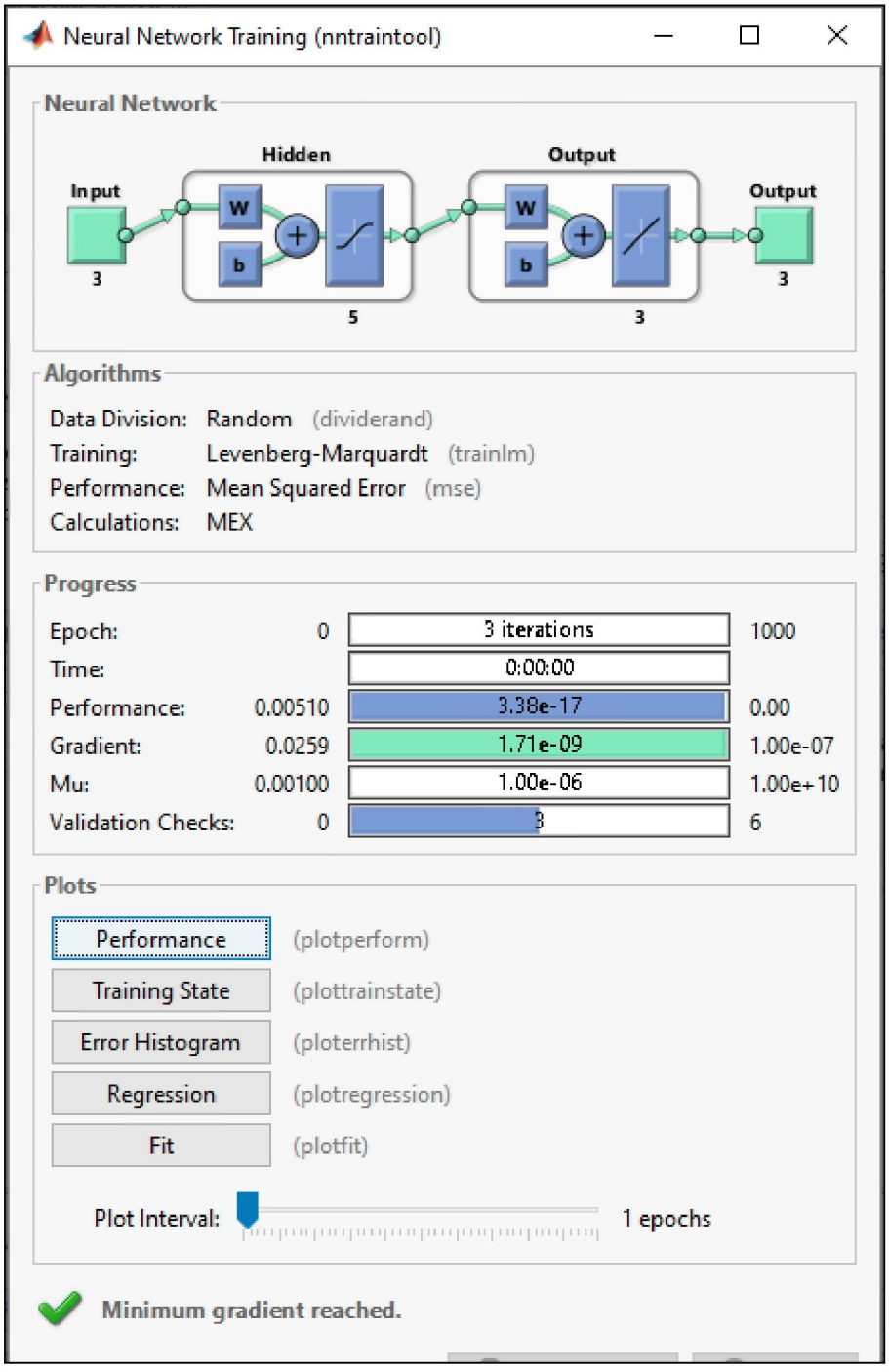

Figure K.25 Neural Network Training (nntraintool) of DTIIB OPCNA

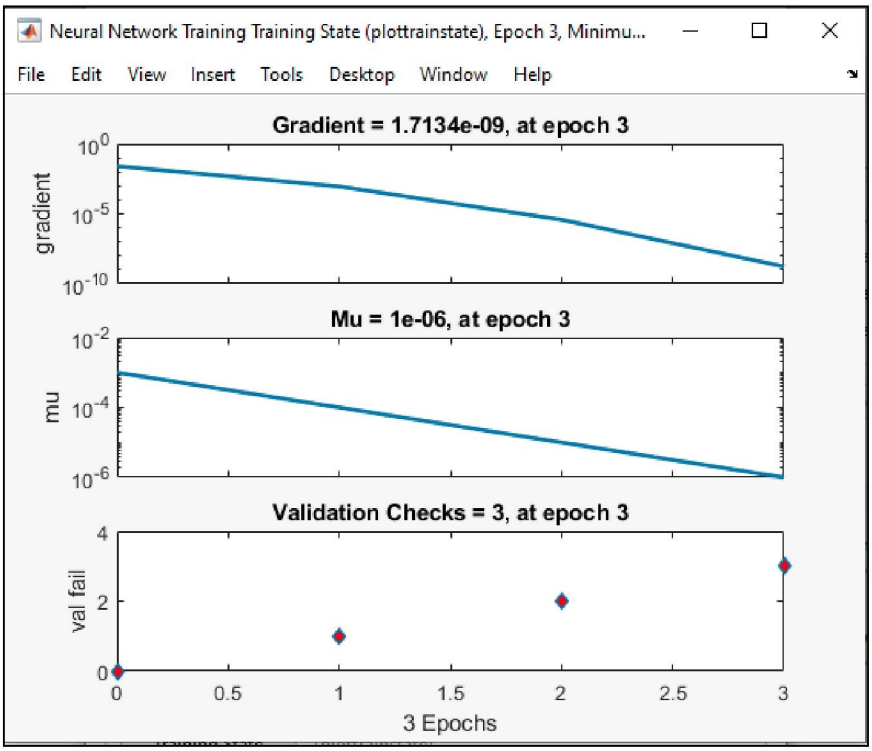

Figure K.26 Plot Training State of DTIIB OPCNA

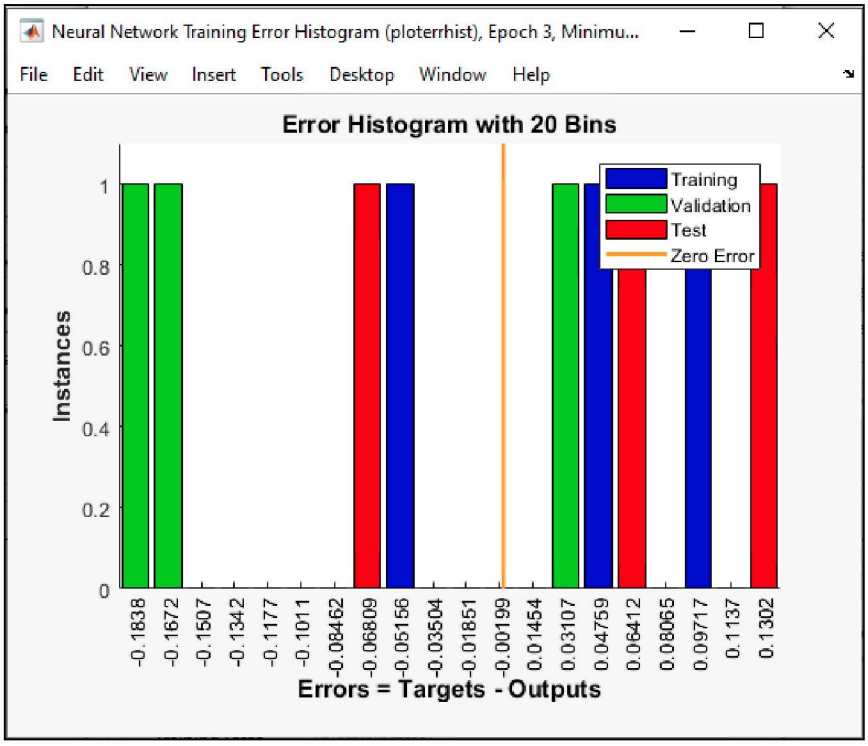

Figure K.27 Plot Error Histogram of DTIIB OPCNA

1.14 ANN for DTIIB 5EPRCA30

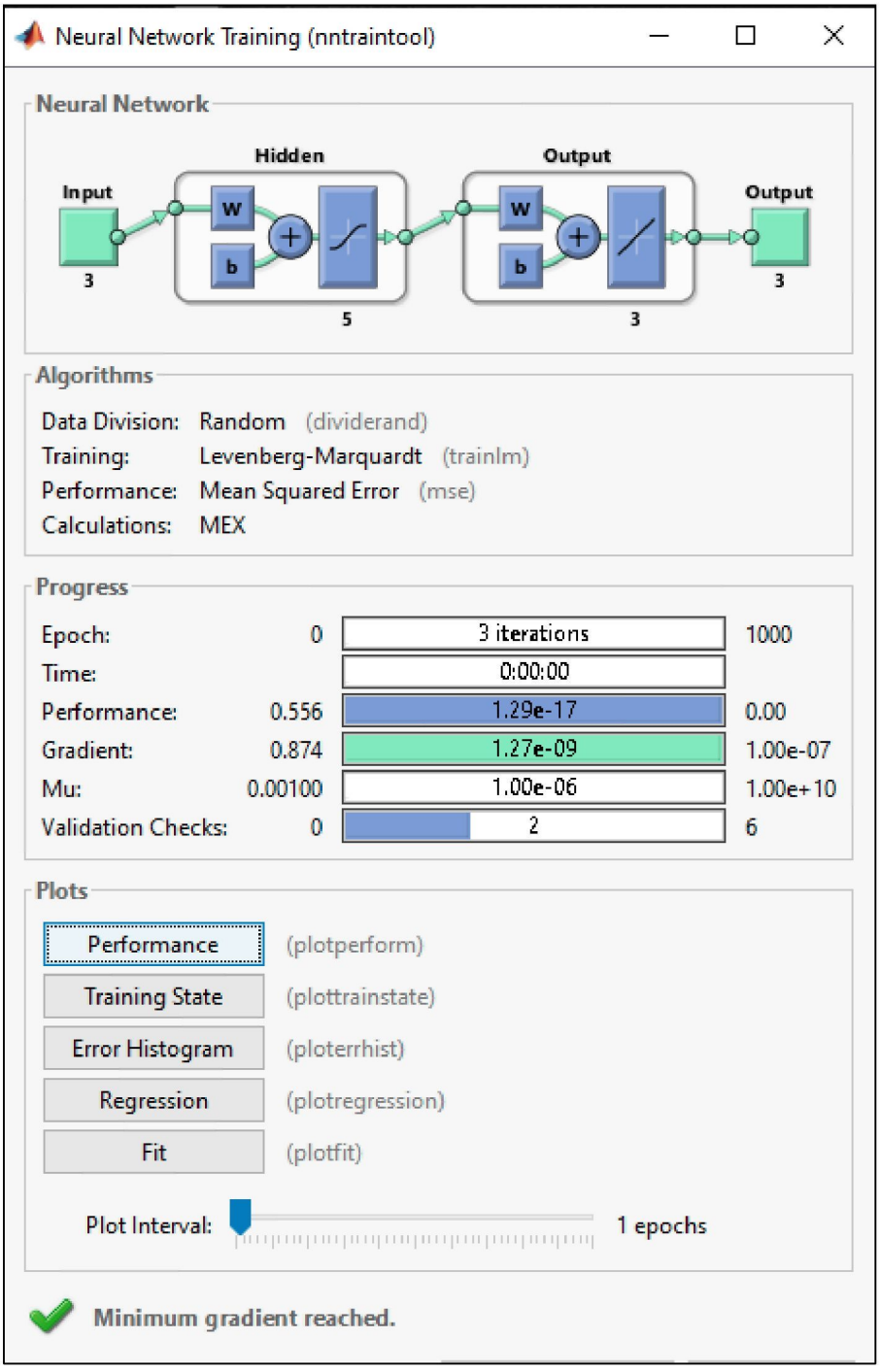

Figure K.28 Neural Network Training (nntraintool) of DTIIB 5EPRCA30

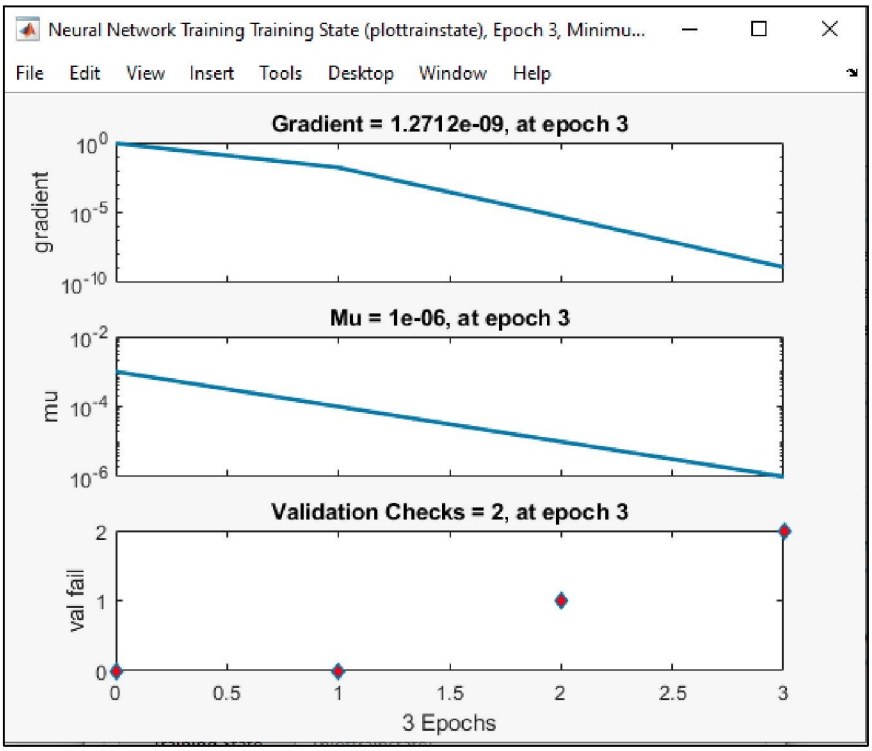

Figure K.29 Plot Training State of DTIIB 5EPRCA30

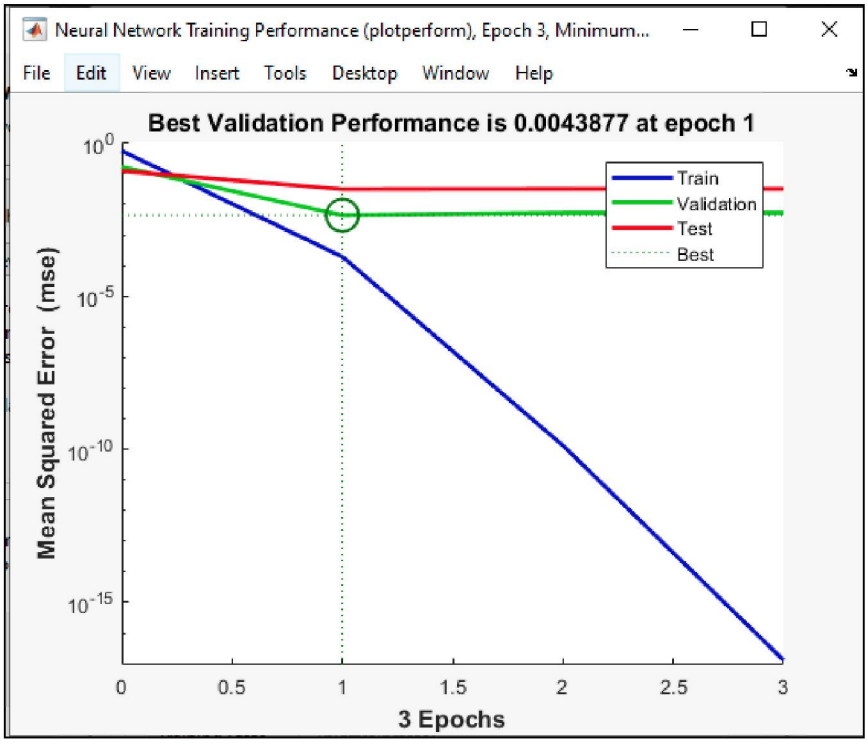

Figure K.30 Plot Error Histogram of DTIIB 5EPRCA30

APPENDIX L
Statistics in Malaysia

Figure L.1 The News of Population Growth in Malaysia.
(Source: Website Malaysia.com, https://www.malaysianow.com/news/2023/07/31/malaysias-population-to-grow-2-1-in-2023, 2023)

Figure L.2 The Pattern of Total Population in Malaysia.
(Source: Website OpenDOSM, Department of Statistics Malaysia, https://open.dosm.gov.my/dashboard/population, 2024)

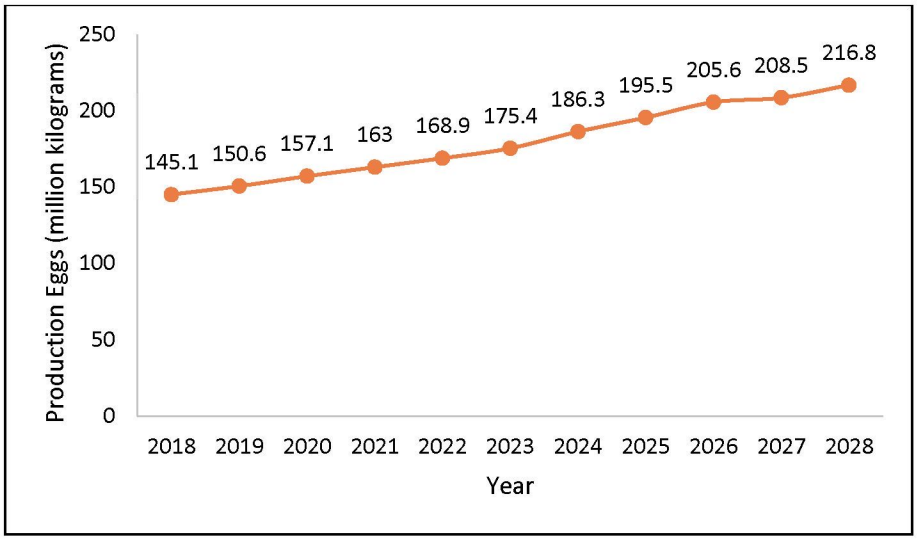

Figure L.3 The Pattern of Production Eggs in Malaysia.
(Source: Statista Market Insights, Eggs - Malaysia | Statista Market Forecast, 2023)

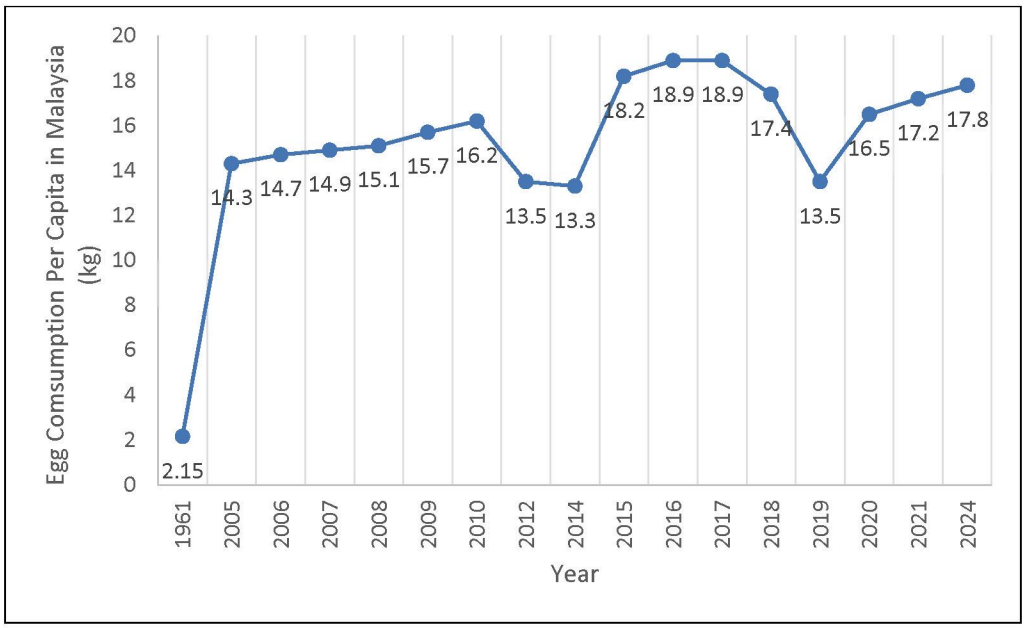

Figure L.4 The Pattern of Eggs Consumption Per Capita in Malaysia.
(Source: Statista Market Insights, Eggs - Malaysia | Statista Market Forecast, 2023, and Ahmad et al., 2013)

APPENDIX M
Previous Research

M.1 Previous Research of Structure Element Containing Eggshell Powder

Author/s	Title	Materials	Replaced	Add. Materials	Percentage	Analysis Outcome
Murthi & Poongodi (2023)	Investigation of The Impact of Eggshell Powder Blended Mortar on Brick Masonry Compressive Strength	Eggshell powder 90um	Cement	-	5%, 10%, 15%, 20%	1. Compressive strength (MPa) highest is 5%, then drop for 7, 28 & 56 days. 2. 7 d – 8 MPa, 28 d – 10 MPa, 56 d – 12 MPa 3. So, the higher percent of ESP replacement, the lower of compressive strength 4. The longest curing age, the higher of compressive strength value. 5. Workability – flow table value is ESP 10% (120mm) the higher then followed by ESP 5%. Then the others.
Nandhini & Karthikeyan (2021)	Effective Utilization of Waste Eggshell Powder in Cement Mortar	Eggshell powder	Cement	-	0% - 20% (5% interval)	1. Workability – 10% highest (128 mm) 2. Compressive strength – 10% highest (7d – 35 N/mm² and 28d – 50 N/mm²) 3. Limit from 0% to 10% replacement of ESP in cement to maintain the strength

Author/s	Title	Materials	Replaced	Add. Materials	Percentage	Analysis Outcome
Kumar & Vasanthi (2022)	Characterization of Paver Blocks Using Eggshell Powder	Eggshell powder	Fine Aggregate	-	0% - 50% (10% interval)	1. The mixture had mix with coarse aggregate too. 2. The density of 30% ESP gave greater density than the other. 3. Compressive strength also the 30% is the higher of 14 (32MPa) & 28 days (40MPa) 4. Splitting tensile strength also 30% the higher (4.5 N/mm²) 5. Flexural strength – 30% higher (almost 8N/mm²) 6. Water absorption – 30% (4%), the highest 50% (6%) 7. Because ESP absorb extra water content than the sand
Nanlan et al. (2023)	Sustainable Strategy of Eggshell Waste Usage in Cementitious Composites: An Integral Testing and Computational Study for Compressive Behaviour in Aggressive Environment	Eggshell powder	Cement / Sand	Superplasticizer, & Silica fume	0% - 15% (2.5% interval)	1. Particle distribution – ESP almost similar with the cement 2. 5% ESP got highest in compressive strength either replace in cement 3. 7.5% ESP got highest in compressive strength either replace in sand

Author/s	Title	Materials	Replaced	Add. Materials	Percentage	Analysis Outcome
Amin et al. (2022)	Testing and Modelling Methods to Experiment The Flexural Performance of Cement Mortar Modified With Eggshell Powder	Eggshell powder	Cement / Fine Aggregate	Silica fume, & superplasticizer	5% - 25% (5% interval)	1. ESP passing similar as cement 2. Flexural strength achieved 5.6MPa with mixture of 5% ESP in cement with SF 20%. 3. FA contained with ESP 7.5% and SF 20% is the highest with 5.8 MPa.
Nandhini & Karthikeyan (2022)	Sustainable and Greener Concrete Production by Utilizing Waste Eggshell Powder as Cementitious Material – A Review	Eggshell powder	Cement	various	Comparison % in review	1. The chemical composition compared to cement shows CaO at 93.2%, SiO2 at approximately 0.24%, MgO at 0.85%, and P2O5 at 0.47%. 2. The high proportion of PES in lightweight concrete reduces the density of the resulting concrete due to PES's lower specific gravity. 3. Workability increased significantly, with a limit of 20%, resulting in a slump test range of 65 to 75 mm. 4. The optimum performance was observed at 5% PES usage, which was 16.8% higher than that of the control concrete. 5. The study concluded that utilizing 5–10% PES as a cementitious blend leads to better compressive strength compared to the reference mix.

Author/s	Title	Materials	Replaced	Add. Materials	Percentage	Analysis Outcome
Murthi et al. (2022)	Effect of Eggshell Powder on Structural and Durability Properties of High Strength Green Concrete for Sustainability: A Critical Review	Eggshell powder	Cement	-	0% - 25% (5% interval)	1. The research findings clearly demonstrated that the chemical composition of ESP closely resembles that of limestone powder, suggesting its potential as a substitute for cement. 2. Strength was higher in 15% for both testing (compression n flexural) 3. Water absorption increasing due to higher percentage of ESP 4. The incorporation of ESP in concrete resulted in a reduced average carbonation depth. 5. The ideal replacement level of cement with ESP is determined to be between 5% and 10%, maintaining the mechanical properties of the concrete.
Teara & Ing (2020)	Mechanical Properties of High Strength Concrete That Replace Cement Partly by Using Fly Ash	Eggshell powder, burned eggshell powder	Cement	Fly ash, & superplasticizer	5%, 10%	1. Have coarse aggregates 2. Chemical analysis of cement contain are same with ESP

	and Eggshell Powder					3. Mixture 3 of 20% FA and 10% ESP have the same workability slump test as natural content resources with 80mm 4. Mixture 4 with 30% FA and 5% ESP getting 75 mm slump test and the highest of the compressive strength (3,7,14,28,90) – 70 MPa 5. Flexural strength the highest is mixture 4 with almost 7 MPa. 6. Ultrasonic pulse velocity – mixture 4 (4.82 km/sec) 7. So, cement replace with 5% ESP and 30% or 40% FA can be beneficial for high grade concrete.
Shi & Shui (2023)	Effect of Eggshell Powder Addition on The Properties of Cement Pastes With Early CO_2 Curing and Further Water Curing	Eggshell powder	Cement	-	0% - 20% (5% interval)	1. Replacement of ESP cause dropping the compressive strength but not give obvious different when in matured curing age in 28 days 2. The ideal percent is 5% 3. The high concentration of CaCO3 in ESP resulted in an increased CO_2 uptake in carbonated samples as the percentage of ESP replacement rose. 4. Early CO_2 curing led to a reduction in pore size, which facilitated the development of strength at early ages. 5. Hydration levels increased with 5% and 10% ESP replacement, while a 20% replacement showed reduced hydration at 28 days.

	6. The porosity of cement pastes with ESP replacement significantly decreased, attributed to the filling effect of ESP.

Author/s	Title	Materials	Replaced	Add. Materials	Percentage	Analysis Outcome
Karthikeyan & Dhinakaran (2017)	Influence of Ultrafine TiO_2 and Silica Fume on Performance of Unreinforced and Fiber Reinforced Concrete	Silica fume	cement	Ultra-fine TiO_2, steel fibre, & superplasticiser	0% - 15% (5% interval)	1. 10% SF registered as the highest values of compressive strength, and flexural strength 2. Also, it was a lower sorption coefficient as supposed in an inverse proportionality.
Liu et al. (2020)	Mechanical and Fracture Properties of Ultra-high Performance Geopolymer Concrete: Effects of Steel Fiber and Silica Fume	Silica fume	cement	Slag, steel fibre, & fly ash	5%, 10%, 20%, 30%	1. With 10% SF, the workability be improved but, it turned to decreasing when additions of 20% - 30% SF. 2. The mechanical and fracture properties of UHPGC improved as the dosage of silica fume exceeded 10%, resulting in a better bonding characteristic between the matrix and fibres.
Chen et al. (2022)	Effect of Silica Fume and Fly Ash on Properties of Mortar Reinforced with Recycled-Polypropylene	Silica fume	cement	Recycled Polypropylene plastic	0%, 4%, 7%, 10%, 13%, 15%	1. 10% SF jotted as the highest values of compressive strength, and flexural strength compared to other SF percentages 2. Also, compared to the control, the mortar contain 10% SF had more compact structure and had some smaller cracks.

Author/s	Title	Materials	Replaced	Add. Materials	Percentage	Analysis Outcome
Amin et al. (2022)	Effect of Ferrosilicon and Silica Fume on Mechanical, Durability, and Microstructure Characteristics of Ultra High-performance Concrete	Silica fume	cement	Steel fibre	0% - 25% (5% interval)	1. For compressive strength and flexural strength, they got the 20% SF the highest values. 2. As reason, the steel fibres mitigated the failure behaviour of prisms under the flexural test and resolved the brittle behaviour of UPHC
Habibi et al. (2021)	RSM-based Evaluation of Mechanical and Durability Properties of Recycled Aggregate Concrete Containing GGFS and Silica Fume	Silica fume	cement	Ground-granulated blast-furnace slag (GGBFS), & recycled concrete aggregate (RCA)	1.94%, 8.06%, 5%, 10%	1. SF had a positive effect on the compressive strength of RCA at all curing ages, due to the pozzolanic activity and filling effect of its particles. 2. For instance, the use of 5% and 10% SF leads to increase the compressive strength by 3.5% and 7%, respectively.
Ali et al. (2021)	Effect of Waste Electronic Plastic and Silica Fume on Mechanical Properties and Thermal Performance of Concrete	Silica fume	cement	Plastic aggregate (PA), & Plasticiser	0%, 10%, 15%, 20%	1. 20% SF-PA were used in the production of concrete showed a 4% decrease in compressive strength compared with the reference concrete. 2. 10% SF-PA was the highest values in mechanical properties as compared with the other percentages

Sharma et al. (2022)	Incorporation of Silica Fume and Waste Corn Cob Ash in Cement and Concrete for Sustainable Environment	Silica fume	cement	Waste corn cob ash, (WCCA)	0% - 15% (5% interval)	1. The combination of corn cob ash and SF effect the reduction of slump test when it's exceeded 10% of combination, that reduces to achieved workability. 2. 10% SF-WCCA beneficial the mechanical properties once OPC be replaced because in the mixture can help to increase the long-term durability of the concrete.

M.2 Previous Research of Structure Element Containing Recycled Concrete Aggregate

Author/s	Title	Specimen	Materials	Testing	Percentage	Analysis Outcome
Garge & Shrivastava (2022)	A Review on Utilization of Recycled Concrete Aggregates (RCA) And Ceramic Fines in Mortar Application	1. Fresh Mortar 2. Hardened Mortar	RCA & 40% Ceramic	1. Compressive Strength 2. Flexural Strength 3. Adhesive Strength 4. Bond Strength	0% - 25% (5% interval)	1. Compressive strength (MPa) was the right strength in used up 20% till 25%. 2. The longest curing age, the higher of compressive strength value. 3. Flexural strength also getting the same higher strength of 25% RCA replacement of fine aggregates.
Rezaei et al. (2023)	Mechanical Features and Durability of Concrete Incorporating Recycled Coarse Aggregate and Nano-Silica: Experimental Study, Prediction, and Optimization	Concrete	RCA & nano-silica (in cement)	1. Flexural Strength 2. Compressive Strength 3. Water Absorption	0% - 100% (25% interval)	1. Flexural strength was 3.88 MPa at 28 days that replacing NA with 25% RCA. 2. The strength is the highest value compared with the others percentage replaced. 3. Compressive strength of sample 25% RCA have increasing strength from early ages until 90 days, that 42.5 MPa that in different 1.3 MPa with control sample. 4. Water absorption also the lowest of the replaces percentages of RCA.

Author/s	Title	Specimen	Materials	Testing	Percentage	Analysis Outcome
Rifa et al. (2023)	A Systematic Comparison of Performance of Recycled Concrete Fine Aggregates with Other Alternative Fine Aggregates: An Approach to Find A Sustainable Alternative to River Sand	1. Hardened Mortar 2. Concrete	RCA	1. Slump test 2. Flexural Strength 3. Compressive Strength 4. Water Absorption 5. Carbonation	0% - 100% (10% interval)	1. Compressive strength increased around 6.2% by replacing natural sand with 30% RCA. 2. Further increasing replacement declined the compressive strength to achieved the target should be. 3. For natural sand replacement levels of 30% and 100% with RCFA, the average carbonation depth is 40% and 110% higher than that of control concrete, respectively. 4. Replacing natural sand with 70–80% RCA slightly reduced concrete's flexural strength. 5. A 25% RCA replacement led to a strength of 16.5 MPa, which is 2.25 MPa higher than the control (14.25 MPa). 6. The highest flexural strength recorded was 19.5 MPa at 50% RCA replacement.
Khoshkenari et al. (2014)	The Role of 0 – 2 mm Fine Recycled Concrete Aggregate on The Compressive and Splitting Tensile Strengths of Recycled Concrete Aggregate Concrete	RC Beam	RCA (fine and coarse aggregates), superplasticizer & 10% silica fume (in cement)	1. Flexural Strength 2. Compressive Strength 3. Water Absorption	0%, 10%, 16%, 20%, 30%, 40%, 50%	1. The amount of recycled concrete aggregate (RCA) used in a mix affects the overall quality of the concrete. 2. Research shows that replacing up to 50% of natural aggregates with RCA can still produce concrete suitable for structural use.

						3. Additional studies confirm that RCA can be used in high-strength, durable, and high-performance concrete. 4. But, due to the lack of bonding between recycled aggregate and cement matrix and also the high water absorption capacity of recycled aggregate can be the factor of lowering strength if the replacement of RCA are too high.
Limbachiya et al. (2012)	Use of Recycled Concrete Aggregate in Fly-ash Concrete	Flexural Test: Beam (100 mm X 100 mm X 500 mm); Compressive Test: Cube (100 mm)	RCA	1. Compressive strength 4. Flexural strength	0%, 30%, 50%, 100%	1. Compressive strength for RCA 30% had achieved the C30 design strength at mature curing ages that 28 days, then strength keep increasing once the curing ages increasing. 2. RCA 30% in flexural strength had overlapped control sample strength that almost 5 MPa. 3. As the replacement RCA increasing to 50% and 100%, the strength reducing to almost 4 MPa. 4. Thus, 30% has been set as the optimum level for RCA replacement.

Author/s	Title	Specimen	Materials	Testing	Percentage	Analysis Outcome
Zhang et al. (2024)	Mechanical Properties and Early-age Shrinkage of Ultra-high Performance Concrete Mortar with Recycled Fine Aggregate	UHPC mortar Size: (70.7 X 70.7 X 70.7 mm^3) and (40 X 40 X 160 mm^3)	RCA, superplasticizer & silica fume, quartz powder (in cement)	1. Flowability 2. Compressive Strength 3. Water Absorption	0% - 100% (25% interval)	1. The RCA 25% in flowability is lower than the other percentages as the higher the RCA replaced, the higher the flowability because the RCA is low moisture content that might absorb free water during mixture process. 2. Thus, compressive strength be higher after control sample as the workability is controllability. 3. Porosity of the RCA 25% is the closer with the control sample. 4. Studies suggests that the excessive water from RCA 50% might negatively affect the porosity

M.3 Previous Research of Design Interlocking Block

Author/s	Title	Name	Design	F. Strength	Problem
Aswad et al. (2022)	A Systematic Review Study on Different Kinds of Interlocking Concrete Blocks Designs and Properties	Thai Interlock Brick System: ISSB Origin: (Thailand)	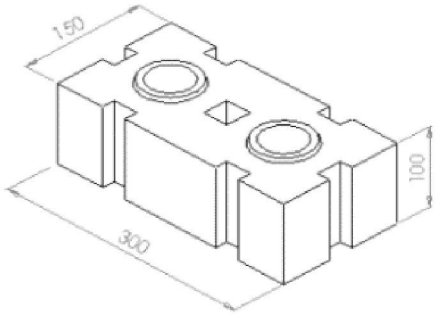	2 – 2.3 MPa	The way the blocks lock together is not very strong because the knobs and holes are too small (less than 5mm). To make it stronger, you might need to add something on the surface or fill the holes with a special material and put extra support if necessary. Material: RHA, OPC, Soil, Water Size: (300mm x 150mm x 100mm)
Surwade & Kamal (2023)	Exploring the Potential of Hydraform Interlocking Block as a Building Material for Masonry Construction	SOLBRIC Interlock Brick System: Hydraform Origin: (South Africa)	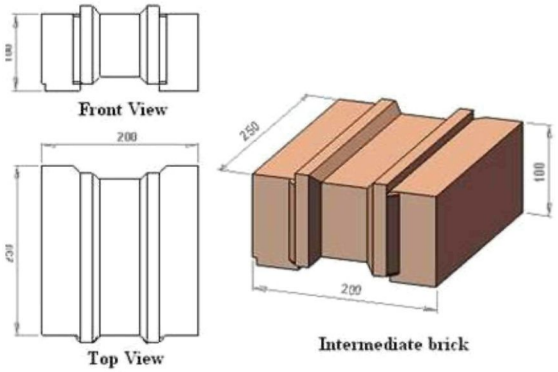	1.5 MPa	The shape of the interlocking block provides small horizontal spaces between the courses and has a flat internal surface, also externally a pointed joint surface from the chamfered of bricks on one side. It is seems like easy to use, but there have no connecting features as it has small thickness (< 15mm) of vertical and horizontal tongues that have questionable due to the material used (soil stabilised with cement that is brittle in nature). Material: OPC, Soil, Water Size: (250mm x 200mm x 100mm)

Author/s	Title	Name	Design	F. Strength	Problem
Al-Fakih et al. (2022)	Experimental Investigation of Dry-bed Joints in Rubberized Concrete Interlocking Masonry	Rubberized Concrete Interlocking Brick ISSB System Origin: (Thailand)	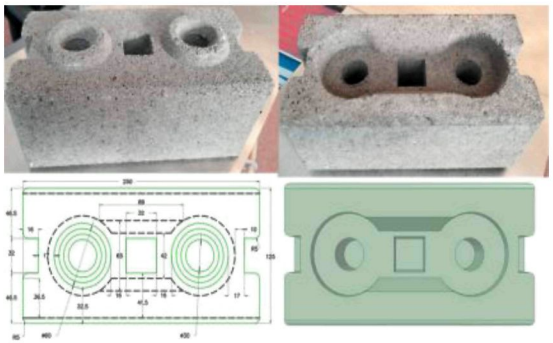 Top face Bottom face	2.23 MPa	The block is the innovation from the Thai interlocking block in early 1980s. The block interlocked with a tongue and grooved features at the sides and top and bottom. The size and material were changed to give a new upbringing from the previous block. The imperfect geometric lead to irregular load percolation between course, so causing localized stress concentrations and resulting the cracks. Material: OPC, FA, NA, Crumb rubber, Water Size: (250 mm x 105 mm x 125 mm).
Ameer et al. (2021)	The Performance of Interlocking Compressed Earth Brick Units in Terms of Compressive Strength	Conventional Malaysian Interlocking Brick System: ICEB System Origin: (Malaysia)	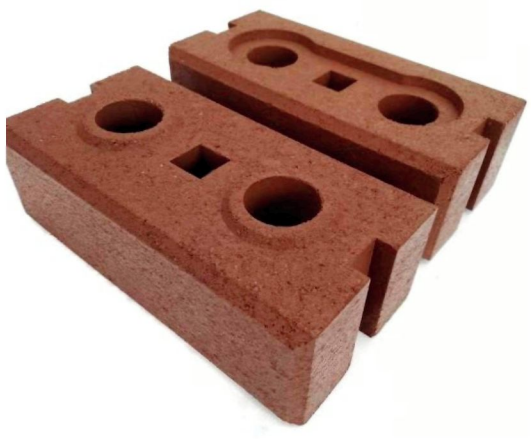	1.2 – 2.2 MPa	Without mortar, these bricks fit together nicely and are simple to construct. However, if they are not shielded from dampness and rain, they deteriorate, crack, and draw insects. Additionally, they can be challenging to replace once installed and don't come in a wide variety of styles. Material: OPC, Laterite Soil, NA Water Size: (280 mm x 100 mm x 125 mm)

Author/s	Title	Name	Design	F. Strength	Problem
Al-Fakih et al. (2018)	Development of Interlocking Masonry Bricks and Its' Structural Behaviour: A Review Paper	Hydraform Interlock Brick System: Hydraform Origin: (South Africa)	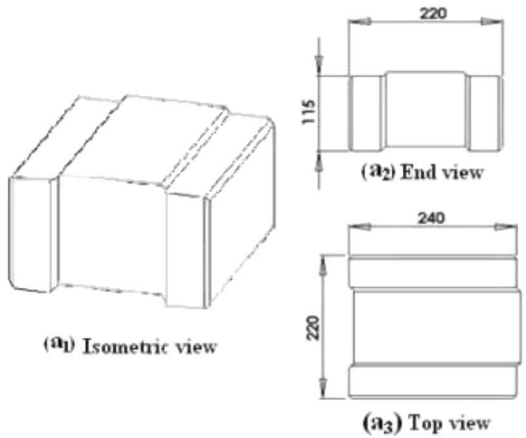	1.7 – 2.5 MPa	The block interlocked with a tongue and grooved joint at the sides and top and bottom. It can be free to slide along the course horizontally, when be pushed along to achieve tighter perpends (vertical joints). The width and weight (massiveness) of the Hydraform blocks, rather than the locking mechanism, provide solidity to the wall constructed from them. Material: OPC, NA, FA, Soil Water Size: (240 mm x 220 mm x 115 mm)
Kintingu (2009)	Design of Interlocking Bricks for Enhanced Wall Construction Flexibility, Alignment Accuracy and Load Bearing	Bamba Interlocking Brick System: Bamba Origin: (South Africa)	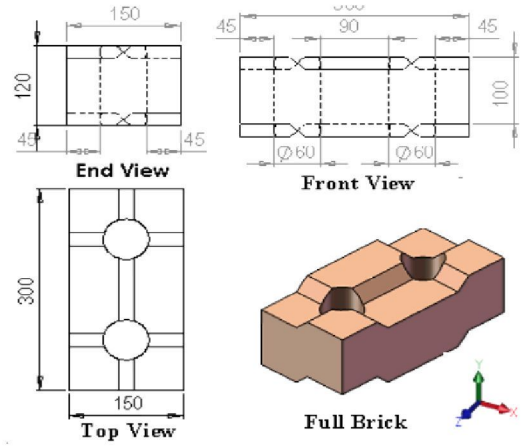	1.5 – 2 MPa	Even though the shape can result in a rigid construction, brick flaws are exceedingly tough to fix. The technology is unsuitable for application in underdeveloped nations since it necessitates precise machinery and advanced soil selection expertise to guarantee consistent production. In addition, because of its intricate construction and poor 37 accuracy in size and shape, it takes a lot of effort to shave and shimmy brick imperfections. Material: OPC, Soil, Water Size: (300 mm x 150 mm x 120 mm)

M.4 Previous Research of Prediction Studies by using ANN

Author/s	Title	Theme	Objective	ML Problem Type	ANN Framework	Performance Metrics
Sipos˘ et al. (2017)	Model for Mix Design of Brick Aggregate Concrete Based on Neural Network Modelling	Concrete Mix Design Modelling	Predicting compressive strength of RAC mixes	Regression	DNN	1. MAE 2. RMSE 3. MAPE 4. R
Akkurt et al. (2003)	The Use of GA-ANNs in The Modelling of Compressive Strength of Cement Mortar	Cement Properties Modelling	Predicting compressive strength of cement mortar under standard curing conditions	Regression	MLPNN	1. Average 2. Error % 3. Emax
Duan et al. (2013)	Using Artificial Neural Networks for Predicting The Elastic Modulus of Recycled Aggregate Concrete	RAC Properties Modelling	Predicting elastic modulus of RAC	Regression	MLPNN	1. RMSE 2. R^2 3. MAPE
Golafshani et al. (2012)	Prediction of Bond Strength of Spliced Steel Bars in Concrete Using Artificial Neural Network and Fuzzy Logic	Bond Strength Modelling	Predicting bond strength of spliced steel bars in concrete	Regression	MLPNN	1. MAE 2. MAPE 3. RMSE 4. R^2 5. R
Sanad & Saka (2001)	Prediction of Ultimate Shear Strength of	Beams Strength Modelling	Predicting ultimate shear strength of reinforced concrete	Regression	MLPNN	Error %

	Reinforced-Concrete Deep Beams Using Neural Networks		deep beams			
Chen et al. (2024)	Maximum Displacement Prediction Model for Steel Beams with Hexagonal Web Openings Under Impact Loading Based on Artificial Neural Networks	Steel Beam Properties Modelling	Predicting steel beam maximum displacement under impact loading	Regression	MLPNN	1. MSE 2. MAE 3. R^2 4. RRMSE 5. Error%

AUTHOR'S PROFILE

Nur Syahirah Binti Othman obtained Bachelor of Engineering (Hons) Civil (Infrastructure) in 2023 from School of Civil Engineering, Universiti Teknologi MARA, Cawangan, Pulau Pinang. She had experience as an intern student at UEM Edgenta Propel Berhad for a degree internship in 2022. She completed her diploma in civil engineering in 2020 from the School of Civil Engineering, Universiti Teknologi MARA, Cawangan Johor, in 2020. She attended Amona Infra Care Sdn Bhd for a diploma internship in 2020. She pursues her academic in Master of Science (Civil Engineering) at School of Civil Engineering, Universiti Teknologi MARA, Cawangan, Pulau Pinang. Now, in 2024, she is working on her master thesis in title Flexural interlocking Block with replacement waste materials. Throughout her academic and professional journey, she has actively participated in various prestigious platforms. To begin with, she joined the *International Conference on Civil Engineering & Technology (CIVENTECH 2023)* held online, followed by her involvement in the *4th International Conference on Science, Engineering, and Technology (ICSET2024)* at Hemangini Hotel, Bandung, Indonesia. In addition, she competed in innovation contests such as the *Penang International Invention, Innovation, and Design (PIID 2023)* and the *Johor International Innovation Invention Competition and Symposium (JIIICaS 2024)*, both of which earned her silver medals. Moreover, she served twice as a panelist for master's coursework presentations in the subject *FIE707 – Infrastructural Damage Assessment*. Not only that, she contributed as a paper reviewer for the *International Symposium on Sustainable Engineering Education & Accreditation (iS2E2A 2024)* and the *Global Conference on Social*

Science, Education and Technology 2025 (GoSET2025). On top of that, she auditioned for *Innovathon Musim 3*, a reality TV program aired on Astro, during its physical selection round held at *UiTM Alor Gajah, Melaka*. Although she successfully advanced to the second round, she did not proceed further in the competition. Nevertheless, her consistent involvement reflects a strong commitment to academic excellence, innovation, and public engagement.

LIST OF PUBLICATION:

Othman, N. S., Md Nor, N., & Saliah, S. N. M. (2024). Flexural strength behaviour of two-hollow interlocking concrete block inclusion with recycled concrete aggregate. *IOP Conference Series: Earth and Environmental Science, 1369*(1), 012032. https://doi.org/10.1088/1755-1315/1369/1/012032

Othman, N. S., Md Nor, N., Saliah, S. N. M. & Md Nujid, M. (2025). Strength Performance of Two-Hollow Interlocking Concrete Block Inclusion with Recycled Concrete Aggregate as a Replacement of Natural Fine Aggregate. *Jurnal Kejuruteraan, 37*(3). DOI: 10.17576/jkukm-2025-37(3)-03

Othman, N. S., Md Nor, N., Saliah, S. N. M. & Md Nujid, M., & Setiawan, A. F. (2026), A Bibliographic Analysis and Review of The Chemical Properties in Concrete: Eggshell Powder and Silica Fume, *Journal of Advanced Research in Micro and Nano Engineering, 42 (1)*: 124-139 ARMNE_V42_N1_P124_139.pdf

Othman, N. S., Md Nor, N., Saliah, S. N. M., Osman, M. R., & Kamal Din, N. A. (2024). EPRCA Interlocking Block, *Johor International Innovation Invention Competition and Symposium 2024 (JIIICaS 2024),* JIIICAS2024_Version 2 BOOKLET.pdf

Othman, N. S., Md Nor, N., & Saliah, S. N. M. (2024), Flexural Strength Behaviour of Prism Mortar with Eggshell Powder and Silica Fume as Cement Replacement Partially, *Proceedings of the 2nd Conference on Engineering Durability (MyCED 2024),* CED2024 BOOKLET Proceeding.pdf

Kamal Din, N. A., Othman, N. S., Md Nor, N., & Mat Saliah, S. N. (2024), Analysis of Compressive Strength of Harden Mortar Containing Eggshell Powder as

Partial Cement Replacement, *Proceedings of the 2nd Conference on Engineering Durability (MyCED 2024),* CED2024 BOOKLET Proceeding.pdf

Osman, M. R., Mat Saliah, S. N., Othman, N. S., & Md Nor, N.(2024), Determination of the Strength of Single Inclined Connection Recycled Concrete Cube Interlocking Block, *Proceedings of the 2nd Conference on Engineering Durability (MyCED 2024),* CED2024 BOOKLET Proceeding.pdf

Mohd Saufi, M. A. F., Mat Saliah, S. N., Othman, N. S., & Md Nor, N.(2024), The Feasibility of Dredging Material as Sand Replacement through Preliminary Strength Testing of Concrete Cubes and Prisms, *Proceedings of the 2nd Conference on Engineering Durability (MyCED 2024),* CED2024 BOOKLET Proceeding.pdf

UNIVERSITI TEKNOLOGI MARA

PERPUSTAKAAN TUN ABDUL RAZAK
BAHAGIAN SUMBER RUJUKAN UNIVERSITI (BSRU)

BORANG PENYERAHAN BAHAN HARTA INTELEK UiTM

UiTM's Intellectual Property Submission Form

Nama *(Name)* : NUR SYAHIRAH BINTI OTHMAN

No. Telefon(Pejabat/Hp) : *Telephone No.(Office / handphone)*

Fakulti/Pusat Akademik/Bahagian : *Faculty / Academic Centres / Department* KOLEJ PENGAJIAN KEJURUTERAAN

E-mel *(E-mail)* : 2023267672@student.uitm.edu.my

Tarikh *(Date)* : 17-03-2026

Pihak Fakulti / Pusat Akademik / Bahagian / Saya bersetuju bahawa dokumen dan tajuk yang disenaraikan untuk dimasukkan ke dalam Repositori Institusi UiTM.
The Faculty / Academic Centres / Department / I agree that the document and titles listed below to be placed in the UiTM Institutional Repository.

JENIS BAHAN (Sila nyatakan) : *Types of Material (Please specify)* Thesis / Theses

Types of Material: Article / Book / Theses / Bulletin / Seminar / Image / Entrepreneurship / Student Project / Research Report / Industrial Training / Annual Report / Manual / Oral History / Exam Paper / Speech / Dataset / Audio / Video / Others

MAKLUMAT BAHAN ***(Information of Materials)*:**

Bil. *No*	JUDUL BAHAN *Title*	HARDCOPY (✓)	SOFTCOPY (✓)
1.	Development and Mechanical Evaluation of Interlocking Blocks Incorporting Eggshell Powder and Recycled Concrete Aggregate	✔	✔

* Sila sediakan lampiran sekiranya ruangan yang disediakan tidak mencukupi *(Please provide attachment if necessary)*

TUJUAN PENYERAHAN BAHAN (Sila tandakan √):

Purpose (Please mark √):

1. **Bahan untuk dimuat naik ke dalam Repositori Institusi UiTM.** ✔
   (Materials for uploading into the UiTM Institutional Repository (UiTM IR)):
   Fakulti / Pusat Akademik / Bahagian / Saya perlu memastikan bahawa setiap dokumen telah dibuat semakan terlebih dahulu dan tidak mengandungi sebarang maklumat sulit sebelum diserahkan kepada pihak PTAR.
   The Faculty / Academic Centres / Department must ensure that each document has been reviewed in advance and does not contain any confidential information before being submitted to PTAR.
2. **Bahan mengandungi maklumat TERHAD yang telah ditentukan oleh organisasi / badan di mana penyelidikan dijalankan:**.
   (Materials consisting of RESTRICTED information which has been determined by the organisation/body where the research was conducted):
   Sila nyatakan tarikh tamat embargo (jika ada):
   (Please indicate the embargo expiry date (if any)):
   Embargo expiry date: Day: Month: Year:
   Nota: Embargo Expiry Date adalah tarikh tamat tempoh yang ditetapkan oleh penulis di mana pada atau selepas tarikh ini, bahan tersebut akan dipaparkan secara langsung di Repositori Institusi UiTM dan ianya boleh diakses.
   Note: Embargo Expiry Date is the date that an author or a publisher imposed embargo expires. On and after this date, this document will be accessible in UiTM Institutional Repository.
3. **Bahan boleh diakses secara teks penuh dan terbuka.** ✔
   (Materials can be accessed in full text via open access).
4. **Bahan dipinjamkan sementara untuk tujuan pendigitalan dan akan dikembalikan semula kepada pemilik.** ✔
   (Materials are on temporary loan for digitization and will be returned to the owner).

Pemberitahuan: Jika Repositori Institusi UiTM menerima bukti pelanggaran hak cipta, bahan yang berkaitan akan dikeluarkan serta-merta.
(Notification: If UiTM Institutional Repository receives proof of copyright violation, the relevant item will be removed immediately).

PERAKUAN :
Declaration:
Saya / kami akan bertanggungjawab ke atas bahan yang diserahkan untuk pendigitalan dan muat naik ke dalam Repositori Institusi UiTM.
I / we will be responsible for the materials submitted for digitization and uploaded into UiTM Institutional Repository.

Tandatangan Pemohon
Applicant Signature
Tarikh *(Date)*: 17/03/2026

DR SOFFIAN NOOR MAT SALIAH
Senior Lecturer
Faculty of Civil Engineering
Universiti Teknologi MARA Cawangan Pulau Pinang

Tandatangan dan Cop Ketua Jabatan / Bahagian / Penyelia
Head of Division / Department / Supervisor Signature and stamp
Tarikh *(Date)*: 17 March 2026

UNTUK KEGUNAAN PEJABAT *(For office use)*

DITERIMA OLEH / *Received By* :
TANDATANGAN / *Signature* :
TARIKH *(Date)*:

DISAHKAN OLEH / *Certified By* :
TANDATANGAN / *Signature* :
TARIKH *(Date)*: